NAPL Recovery Using CO_2-Supersaturated Water Injection: Distribution of the CO_2 Gas Phase

by

Cynthia Doughty

A thesis
presented to the University of Waterloo
in fulfillment of the
thesis requirement for the degree of
Master of Science
in
Earth Sciences

Waterloo, Ontario, Canada, 2006

I hereby declare that I am the sole author of this thesis. This is a true copy of the thesis, including any required final revisions, as accepted by my examiners.

I understand that my thesis may be made electronically available to the public.

Abstract

Gas inFusion™ is a novel remedial technology that dissolves CO_2 into water under pressure for NAPL recovery. As the supersaturated liquid flows through the porous medium gas evolution occurs in situ as the system returns to thermodynamic equilibrium. The evolution of gas bubbles leads to NAPL recovery by two mechanisms: 1) volatilization and 2) mobilization by the NAPL spreading in a film around the rising bubbles. Laboratory experiments by Li demonstrated that injecting the supersaturated water into a porous medium minimized the buoyancy driven flow of gas and the fingering phenomena that limit typical gas sparging. The distribution of carbon dioxide at partial pressures (p_{CO2}) above the applicable hydrostatic pressure and the evolved gas phase were determined in two field experiments conducted in the relatively homogeneous fine to medium sand at CFB Borden. First, CO_2-supersaturated water was injected into a single point located approximately 4 metres below ground surface. Then this injection was repeated with pumping of two nearby wells to see if the lateral distribution of CO_2 gas could be controlled hydraulically. Groundwater monitoring of p_{CO2} above the hydrostatic pressure and geophysical surveys (neutron measurements, surface ground penetrating radar (GPR), and cross-borehole GPR) to find zones of induced gas content were supported by hydraulic monitoring and physical observations of gas bubble distribution at the water table.

Based on the results of these tests, enhanced CO_2 levels above the hydrostatic pressure were observed up to 5.5-7.0 m from the injection point and the gas phase up to ~5.3 m. It was not possible to determine the impact hydraulic control had on the lateral distribution of CO_2 due to problems with the experiment. The distribution of the gas phase was heterogeneous with CO_2 gas pockets forming below low permeability layers, as evidenced by surface GPR, permeameter tests, and grain size analyses. These gas pockets accumulated until sufficient pressure built up to overcome the displacement pressure of these lower permeability layers. At this point there is evidence of CO_2 breakthrough in the cross-borehole GPR data and physical observations of gas bubbles at the water table. These observations are consistent with previous investigations, which indicate that although the Borden aquifer is homogeneous, distinct horizontal layering is present with sufficient variations in permeability/displacement pressure to trap and cause some lateral spreading of a gas phase. The evidence of channeling and the impact of heterogeneities on gas distribution are consistent with air sparging studies.

Acknowledgements

I would like to thank my thesis supervisor Dr. Jim Barker and my committee members Dr. Neil Thomson and Dr. Tony Endres for their guidance and support for this project.

I would like to thank the partners of inVentures Technologies Incorporated (iTi), John Archibald, Craig Glassford and Jim Snider for giving me the opportunity to test a new remedial technology. I would also like to thank Tom Li and Wade Campbell for the technical support they provided for the setup of these experiments.

I would like to acknowledge the American Petroleum Institute (API), the Natural Science and Engineering Research Council (NSERC) of Canada, the Canadian Foundation for Innovation (CFI), the Ontario Innovation Trust, inVentures Technologies, Water & Earth Science Associates, and C3 Environmental Limited for their financial support.

I would also like to thank Scott Piggott for collecting and processing the geophysics data, Claudia Naas for her invaluable help setting up and operating the experiments, Maryanne vanderGriendt for analyzing the groundwater samples, and Bob Ingleton and Paul Johnson for installing the monitoring network. The field support provided by Cory Steelman, Leif Nelson, Alex Oiffer, Michelle Fraser, and Rasheeda Byer-Coward are also much appreciated.

I wish to thank my friends and colleagues for their encouragement and support. I would specifically like to thank my colleagues, Scott MacMillin, Mike Brother, Bill Soukup, and Jeff Caputi. I am also grateful to Derek Brunner for the Williams sessions. And I give special thanks to Adrian Thorne for always being available to assist me. :)

Finally, I would like to thank my family, Dan Doughty, Susan Doughty, Rosey Godin, Chris Godin, and Madison Godin, for their encouragement and support.

Table of Contents

List of Tables

List of Figures

Chapter 1
Introduction and Background

1.1 Air Sparging

Air sparging is a technology commonly used for treatment of source zones and dissolved groundwater plumes. It involves the injection of air into an aquifer to volatilize contaminants and, in some cases, supply oxygen for aerobic biodegradation. According to Leeson et al (2002), the three most significant factors affecting air sparging performance are:

- The air distribution in the target treatment zone;
- The distribution (location and concentration) of contaminants relative to the air distribution, and
- The contaminant characteristics (composition and chemical properties).

1.1.1 Air Distribution

A number of researchers have performed various flow visualization and flow characterization experiments to provide insight into air distributions and how they are affected by geology and process conditions (e.g., flow rate, injection pressure, pulsing).

Ji et al (1993) conducted two-dimensional (2-D) flow visualization experiments to observe the air distribution beneath the water table and the impact of particle size, stratigraphy, and air injection flow rate on the air distribution. As illustrated on Figure 1.1, homogeneous media resulted in symmetric channel flow about the vertical axis through the injection point; whereas, heterogeneous media resulted in non-symmetric channel flow due to minor variations within the bead mixture. Figure 1.2 demonstrates the effects of flow rate changes on the air distribution in a homogeneous medium. At a low air injection rate, air flowed vertically through the medium in a few distinct air channels. As the airflow rate was increased, the density and number of continuous air channels increased while the size of the channels remained relatively constant.

The results from the 2-D laboratory experiments performed by Ji et al (1993) are consistent with field-scale flow visualization studies. Leeson et al (1995) reported a small zone of influence (ZOI) around the injection point, ranging from 1.2 to 4.9 m, with little effect on the size caused by increasing the flow rate. However, the density of channeling increased as the injection rate increased. Lundegard and LaBrecque (1998) used cross-borehole electrical resistance tomography (ERT) to image changes in water content due to increases in air saturation at a homogeneous and a heterogeneous site. For the homogeneous site, consisting of dune sand, the region of airflow was approximately symmetric about the sparge well with a radius of ~ 2.5 m. Conversely, the heterogeneous site, consisting of glacial till, had a more complex air distribution pattern with a major

April 26, 2006

Cynthia Doughty
University of Waterloo
200 University Avenue West
Waterloo, Ontario N2L 3G1

Dear Ms. Doughty:

You have permission to reprint Figures 1.1 and 1.2 from an article in *Ground Water Monitoring & Remediation*. In the text, there must be the following citation as well as a credit line:

The citation should read:
Ji W., Dahmani A., Ahlfeld D.P., Lin J.D., and E. Hill III 1993. Laboratory Study of Air Sparging: Air Flow Visualization. *Ground Water Monitoring and Remediation* 23, no. 4: 115-126.

The credit line for the figures should read:
"Reprinted from *Ground Water Monitoring & Remediation* with permission of the National Ground Well Association. Copyright 1993."

Please feel free to contact me if I can be of any further assistance.

Thad Plumley

Thad Plumley
Director of Publications
National Ground Water Association

horizontal component. Based on the more complex pattern, a meaningful radius of influence (ROI) was not definable for the heterogeneous site. The importance of porous media heterogeneities were confirmed by studies performed by Semer et al (1998), Reddy and Adams (2001), and Tomlinson et al (2003). Lundegard and LaBrecque (1995) demonstrated that conventional monitoring data, such as water table mounding, soil gas pressure, soil gas composition and tracer gas response, provided an ambiguous indication of the region of air flow.

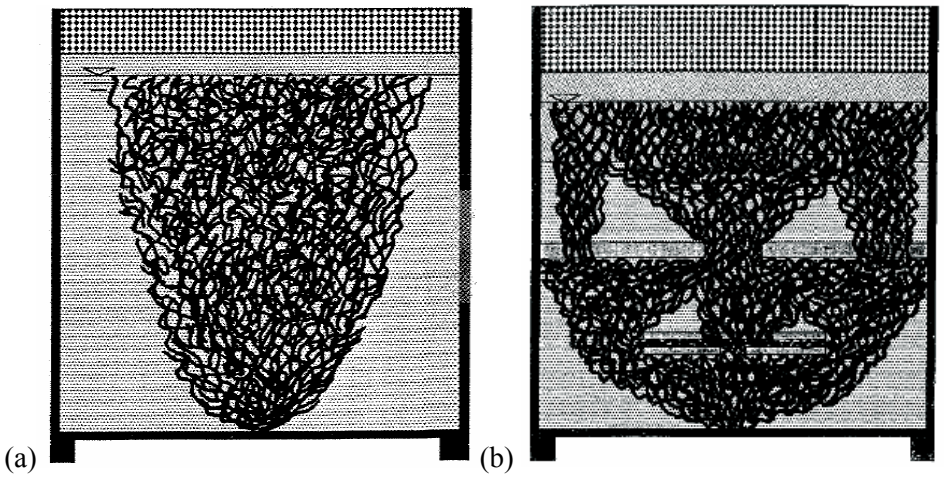

Figure 1.1 - Drawing of air channels at high air injection rate (a) uniform bead medium and (b) stratified medium (Ji et al, 1993). Reprinted from *Ground Water Monitoring & Remediation* with permission of the National Ground Water Association. Copyright 1993.

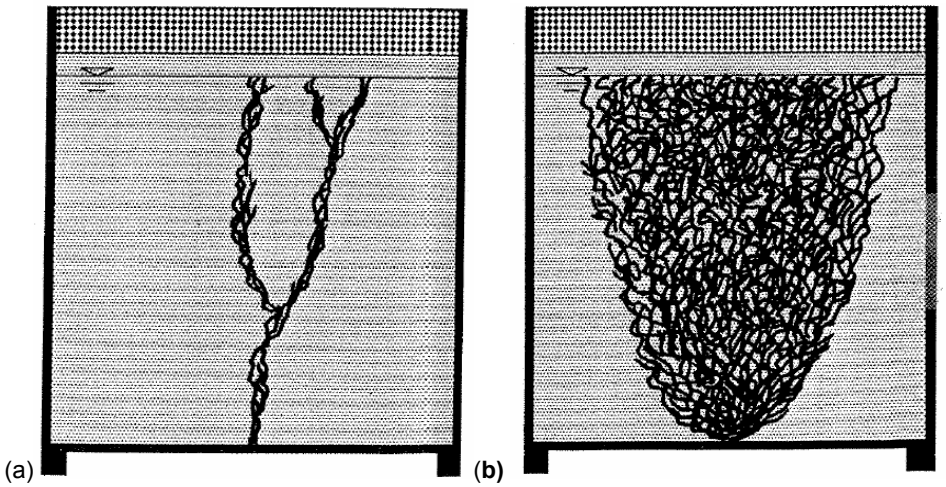

Figure 1.2 – Drawing of air channels in 0.75 mm uniform bead medium (a) low air injection rate and (b) high air injection rate (Ji et al, 1993). Reprinted from *Ground Water Monitoring & Remediation* with permission of the National Ground Water Association. Copyright 1993.

1.1.2 Contaminant Removal

In addition to the significance of air distribution, the location and concentration of contaminants relative to the air distribution is another important factor affecting air sparging performance. A typical conceptual model developed by Ahlfeld et al (1994) to understand contaminant removal during air sparging and discussed within Leeson (2002) indicates that:

- Air flow generally occurs in small continuous air channels;
- Removal processes for contaminants within air channels are similar to soil vapor extraction (Johnson et al, 1990) and bioventing (Leeson and Hinchee, 1996); and
- Removal processes for contaminants located in water-saturated regions outside the air channels are liquid-phase mass-transfer limited (Johnson et al, 2001).

Within the air channels, the contaminant removal processes occurring are due to volatilization. Accordingly, initial volatilization removal rates for both source and dissolved phase treatment areas can be calculated. On the other hand, the contaminant removal occurring outside the air channels is not as well understood. Previously, it was speculated that air sparging performance was limited by diffusion; thus, a significant reduction in contaminants would only occur in areas where the contaminants directly contacted the air channels. However, based on air sparging case studies, including Bass et al (2000), it appears that significant contaminant removal occurs outside of the air channels (Johnson et al, 2001). The removal of contaminants outside of the air channels may be accounted for by water evaporation into the air channels, which may result in significant advection of dissolved contaminants towards the air channels (Unger et al, 1995 and Johnson, 1998).

Although significant contaminant reduction is possible with air channeling, more efficient removal would occur with higher gas saturation. To address this issue, an alternative remedial technology that also utilizes volatilization to recover residual NAPLs and dissolved phase-contaminants has been developed. The principles of this process are discussed in Section 1.2 and the results of laboratory experiments using this technology are provided in Section 1.3.

1.2 Gas inFusion™ Principles

The Gas inFusion™ (GI) generator dissolves gas into flowing water at elevated pressures. The gas-water interface for mass-transfer is provided by thousands of hydrophobic micro-hollow fibres (Figure 1.3) located around a perforated pipe. Water flows into and radially out of the perforated pipe, contacting thousands of gas filled micro-hollow fibres, which provide 7.2 m^2 of mass transfer contact surface area. The hydrophobic nature of the fibres prevents water from entering them. The pressure of the system is determined by the pressure of the water supply.

If gas is dissolved into water at an elevated pressure and then reduced to atmospheric pressure, the water will have a supersaturated concentration of gas. A solution is supersaturated if the dissolved gas concentration exceeds the maximum thermodynamically stable concentration at a given

temperature and pressure. When a supersaturated liquid is injected into a porous medium, bubble nucleation (i.e. gas evolution) will occur in situ as the system returns to thermodynamic equilibrium. In situ gas evolution should result in the appearance of a gas phase in places within the pore network where capillary forces would otherwise not permit. In situ gas evolution causes a decrease in the water relative permeability, which redirects the flow of supersaturated water (and subsequent gas evolution) to less permeable zones. The redirection of water flow should provide a more homogeneous distribution of the gas phase (Li, 2004). A schematic of the conceptual design of the SWI process is seen in Figure 1.4.

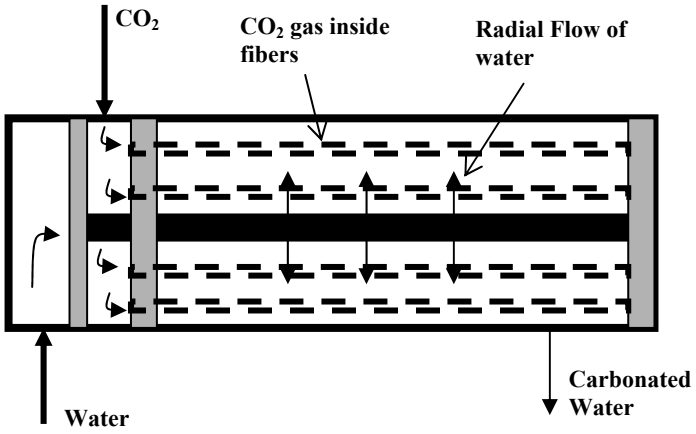

Figure 1.3 – Schematic of Gas inFusion operation (Li, 2004).

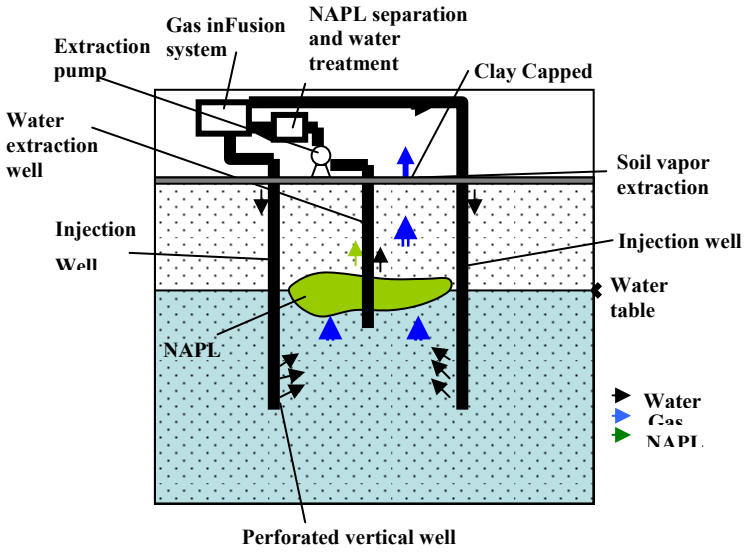

Figure 1.4 – Conceptual design of supersaturated water injection (SWI) NAPL recovery process (Li, 2004).

1.3 Laboratory Experiments

Laboratory experiments were performed by Li (2004) to demonstrate the effectiveness of NAPL recovery from a water saturated porous medium by supersaturated water injection. These included pore scale and 2-D gas evolution experiments, as well as, macroscopic experiments to recover residual LNAPL (hexane and octane) from a sand packed glass column.

1.3.1 Gas Distribution in a Two-Dimensional Flow System

A 2-D gas evolution experiment was performed to visualize gas evolution in the porous medium. Figure 1.5 is a schematic of the 125 cm box designed to visualize and measure gas flow in the upward direction.

The transient gas evolution period with a GI operating pressure of 220 kilopascal (kPa) [32 pounds per square inch (psi)] and flow rate of 120 cm^3/min is depicted on Figure 1.6. The advancement of the gas front in the porous medium is shown as a lighter gray in the photos and is annotated with a black line to aid in the visualization. Gas evolves over the entire length of the box (125 cm) in ~ 60 minutes. It appears to evolve uniformly as a front with apparent higher gas saturation closer to the injection well. The actual gas saturation was not measured.

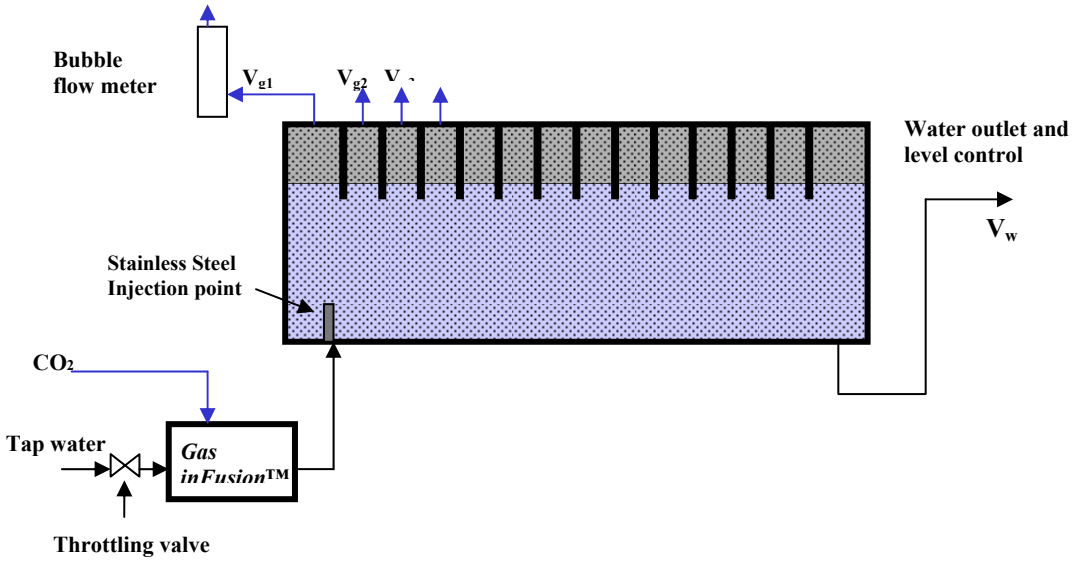

Figure 1.5 – Flow diagram of the gas evolution experiment (Li, 2004).

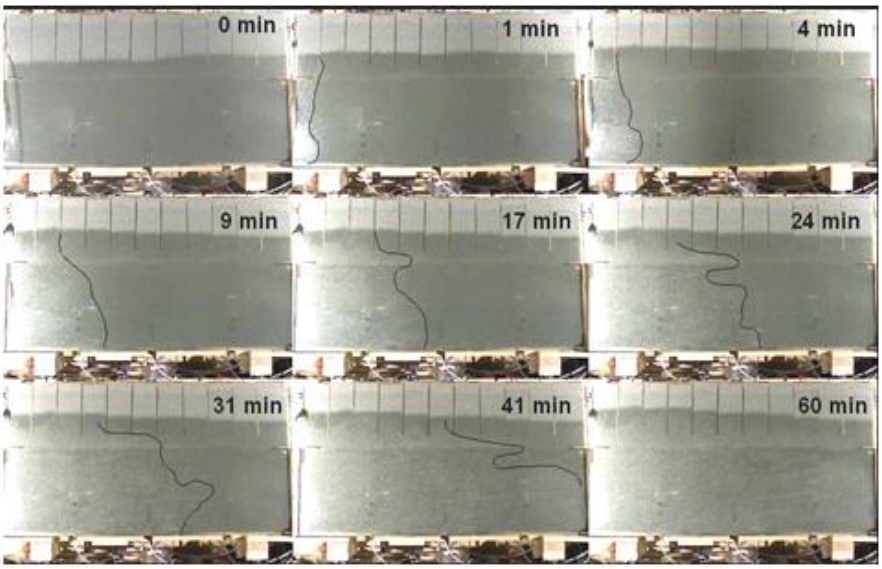

Figure 1.6 – Gas evolution in a porous medium over time during the transient period (Li, 2004)

To determine the affect of heterogeneities on gas distribution, a similar 2-D experiment was performed in a smaller rectangular box with two horizontal metal plates used to simulate impermeable layers. Figure 1.7 demonstrates that early in the experiment gas evolved and rose as free gas in channels. These gas pathways diverted themselves around the impermeable layers; however, as supersaturated water injection continued the heterogeneities appeared to have no effect on the gas distribution.

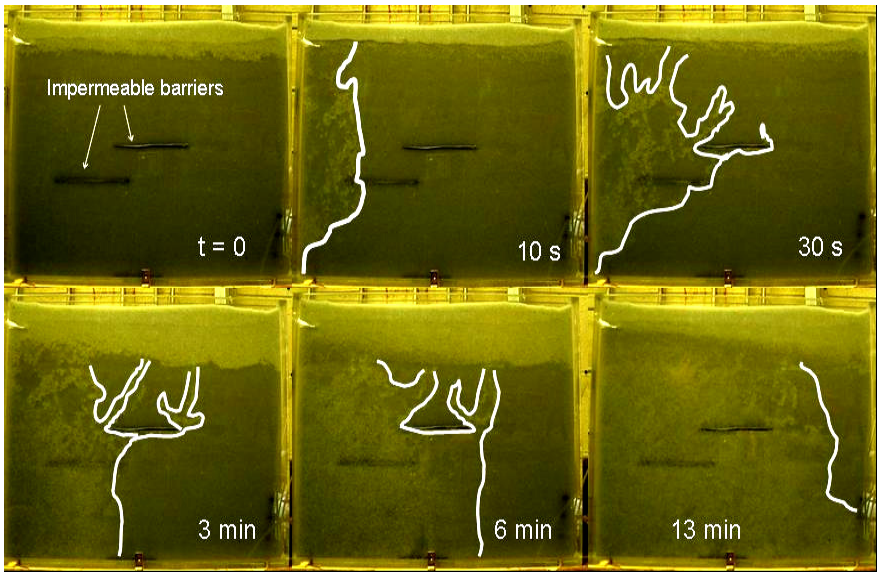

Figure 1.7 – Gas evolution profiles in the heterogeneous porous medium at various times. The solid line outlines the area with the evolved gas phase (Li, 2004).

1.3.2 Contaminant Removal in a Column

A glass column containing uniform medium sized sand contaminated with residual phase NAPL was remediated using the Gas inFusion™ generator. Figure 1.8 depicts the experimental setup. During the initial stages of the experiment, mobilization of NAPL was observed, which was not anticipated to be a recovery method. Volatilization was assumed to be the main mechanism for NAPL recovery.

A chromatograph was used to analysis the VOCs in the gaseous stream and within the recovered NAPL. NAPL constituents were detected in the gas stream according to their volatility with hexane, the more volatile component, occurring in the effluent gas earlier in the experiment. Hexane and octane were both present in the gas stream during the latter stages of the experiment. Table 1.1 depicts the amount of hexane and octane recovered by each mechanism (i.e., volatilization and mobilization), in addition to the portion unaccounted for during the experiment. The unaccounted for portion may be due to a number of factors, including:

- Loss of NAPL from the bottom of the gas-liquid separator;
- Sorption to the sand particles; and
- Uncertainty in the gas chromatograph measurements for both vapor and free phase NAPL.

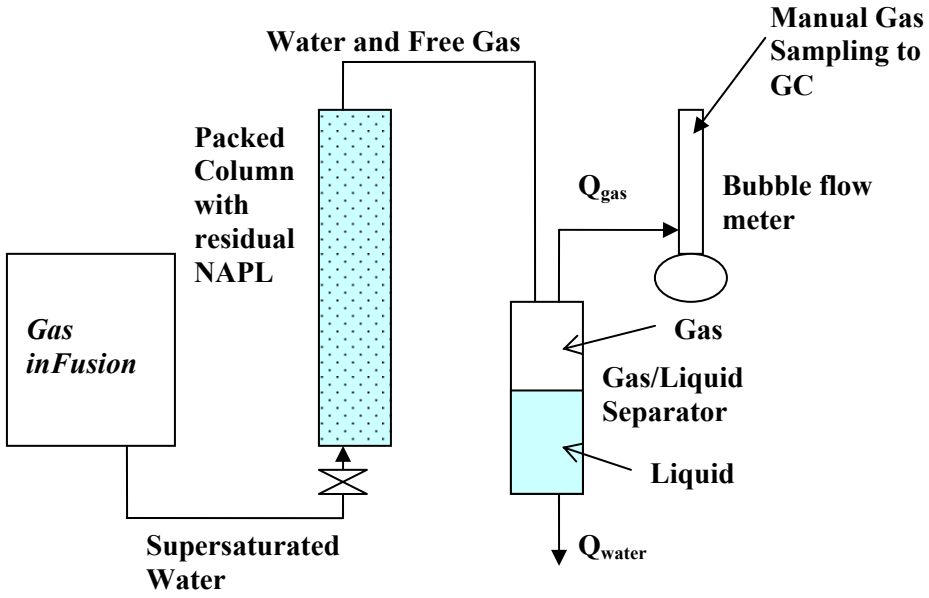

Figure 1.8 – Experimental set-up of NAPL recovery in a packed column (Li, 2004).

Table 1.1 – Mass balance of NAPL recovery experiment (Li, 2004).

	Hexane	Octane
Initial	**33.6 g**	**17.4 g**
Removed by volatilization	19.2 g	5.7 g
Removed by mobilization	3.2 g	3.5 g
Measured removal	**22.4 g**	**9.2 g**
Residual NAPL after experiment	1.2 g	2.3 g
% NAPL unaccounted for	**29.8 %**	**33.1%**

1.4 Project Objective

Based on the results of Li's laboratory experiments, a 3-D field experiment was implemented to determine the gas saturation and to provide a "zone-of-influence" for designing a field-scale NAPL recovery experiment. The experiment was performed under both passive and active conditions, with active conditions being achieved by extraction of groundwater from two wells. The hydraulic control experiment was performed to determine if the "zone-of-influence" obtained in the passive scenario could be increased laterally.

1.5 Site Description

The gas distribution experiments were performed in an inactive sand quarry at Canadian Forces Base Borden near Alliston, Ontario. The aquifer, which is comprised of a homogeneous, clean, well-sorted, fine to medium-grained sand, extends approximately 9-11 metres below ground surface (m bgs). Although the aquifer is relatively homogeneous, distinct bedding features are present. The layering is primarily horizontal and parallel; however, some cross-bedding and convolute bedding have been observed. The aquifer is underlain by a thick silty clay deposit (Mackay et al, 1986).

Chapter 2
Methods and Procedures

2.1 Injection Point Testing

A number of injection point designs were tested in the laboratory to obtain the back pressure and flow rate sought for the two (2) field experiments. The initial field design required 400 kPa (58 psi) and 5 litres per minute (lpm) with later design revisions calling for ~58 psi at 8 lpm. The laboratory experiment used a 40 L plastic garbage can filled with water from a laboratory sink using ~16 mm (5/8-inch or 5/8") inner diameter (ID) garden hose (Figure 2.1). The garbage can was connected to a high-pressure multi-stage centrifugal pump (Goulds Model 5GBC0514-60) with ~16 mm (5/8") ID braided polyvinylchloride (PVC) tubing. The outlet of the pump was equipped with a T-pipe fitting. The T-pipe fitting was used to split the flow between the injection point and the water by-pass. The injection point pressure and flow rate were controlled via a flow control valve located between the T-pipe fitting and the GI generators. The water by-pass was constructed of ~25 mm (1.0") ID PVC tubing. Injection points were constructed of ~12.5 mm (1/2") ID schedule 40 PVC with either factory made slots (0.010 inches) or holes drilled using various sizes of drill bits. Pre-slotted PVC had inconsistent slot sizes; thus, it was not possible to obtain a representative pressure and flow rate based on the number of slots. The size of the holes and the number of holes were varied to obtain the required flow rate and pressure. Each injection point design was tested to obtain the possible range of flow rates and pressures. In Appendix A, Table A.1 presents a summary of all injection point designs tested with their pressure and flow rate ranges.

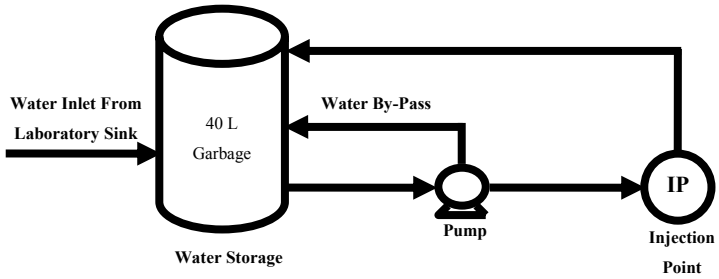

Figure 2.1 – Flow diagram of laboratory experiment to test injection point designs.

2.2 Field Test Site Installations

To evaluate the in situ evolution of carbon dioxide (CO_2) gas from the injection of CO_2-supersaturated water at the centrally located injection point, a network comprised of monitoring wells and geophysical access tubes was installed within the study area. Extraction wells were installed for the hydraulic control experiment.

2.2.1 Injection Point Installations

Based on the results attained from the laboratory experiments, three injection points (IP-1 through IP-3) were initially installed within the study area (Figure 2.2). Each of these injection points was installed to a nominal depth of 4 m (~13 feet or ft) bgs and is described as follows:

- Injection Point IP-1 – is located in the middle of the 12-m x 12-m (39.4-ft x 39.4-ft) study site. This point is constructed of 12.5 mm (1/2") ID schedule 40 PVC pipe with a well screen consisting of 4-1.2 mm (3/64") holes.
- Injection Point IP-2 – is located 0.5 m north of IP-1. It is constructed of 12.5 mm (1/2") ID schedule 40 PVC pipe with a well screen consisting of 8-0.79 mm (1/32") holes.
- Injection Point IP-3 – is located 0.5 m south of IP-1 and is constructed of 12.5 mm (1/2") ID schedule 40 PVC pipe with a well screen consisting of 10-0.79 (1/32") holes.

After installation of the injection points, aquifer restrictions on the screened area caused flow rates to decrease by ~ 40 percent. As a result, a fourth injection point (IP-4) was installed with the design accounting for the flow rate reduction caused by the aquifer, as well as, the increased flow rate (~8 lpm) required for the field experiments. This injection point is described as follows:

- Injection Point IP-4 – is located 0.25 m (0.82 ft) south of IP-1. It is constructed of a 12.5 mm (1/2") ID schedule 40 PVC pipe well screen with 19-0.79 mm (1/32") holes and 25 mm (1") ID PVC well riser.

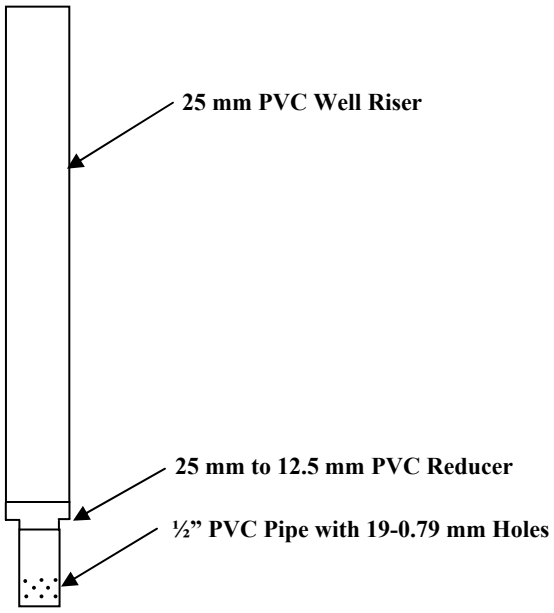

Boreholes for IP-1 through IP-3 were drilled using a direct-push technique with a hydraulic hammer where a ~ 60 mm (2.4") outer diameter (OD) steel rod was advanced to depth. The PVC pipe was inserted into the steel rod and the rod was pulled out allowing the aquifer material to collapse around the PVC pipe. IP-4 was installed using a direct-push technique with a pneumatic handheld hammer where an ~ 60 mm (2.4") OD casing was advanced to depth. The PVC pipe was inserted into the casing and Borden sand was placed by hand within the annulus as the steel casing was withdrawn. Sand was installed within the annulus to minimize carbon dioxide (CO_2)-supersaturated water from escaping along the annular space of the injection point.

Based on the revised design requirements and the reduced flow rates caused by the aquifer, IP-1 and IP-2 were filled by hand with Borden sand, as they did not meet the design requirements and may behave as conduits for the evolved CO_2 gas. Although IP-3 did not meet the design requirements for flow rate, it was kept as a backup injection point should problems develop with IP-4.

2.2.2 Geophysical Access Tubes

Eighteen geophysical access tubes (GP-1 through GP-18) constructed of ~ 50 mm (2") ID schedule 40 PVC pipe were installed approximately 0.75 to 5.8 m (2.5 to 19 ft) from IP-4 (Figure 2.2). Each access tube was sealed along the joints connecting sections of PVC pipe and along the cap on the bottom of the pipe. Access tubes were installed using a jetting technique where a ~ 90 mm (3.5") OD casing was hammered to a nominal depth of 5 m (16.4 ft) then the casing interior was flushed with water. PVC pipe was inserted into the steel casing then filled with water before removing the casing, allowing the aquifer material to collapse around the pipe. Once the aquifer material had collapsed sufficiently around the PVC pipe to prevent it from moving up within the borehole, the water was pumped from the access tube. Grouts and seals were not placed around the access tubes to minimize interference during geophysical testing. Two of the access tubes (GP-2 and GP-13) installed with the jetting technique were manually filled with aquifer material and replaced due to damage caused during installation. GP-2 and GP-13 were re-installed using hollow-stem auger techniques where a ~200 mm (8") OD hollow-stem auger was advanced to a nominal depth of 5 m (16.4 ft), prior to flushing the auger interior with water. PVC pipe was inserted into the auger, filled with water, and then the auger was removed, as aquifer material was placed by hand within the annulus. Water was completely removed from the PVC pipe after it was secured at the installation depth. The total depths of the access tubes ranged from 4.89 to 5.30 m (16.04 to 17.39 ft) bgs.

2.2.3 Monitoring Wells

Twelve monitoring well couplets (MW-1 through MW-12) consisting of one shallow and one deep well, designated as S and D, respectively, were installed approximately 2.0 to 5.6 m (6.6 to 18.4 ft) from IP-4 (Figure 2.2). The nominal depths of the monitoring wells were 2.5 m (8.2 ft) bgs and 4.0 m (13.1 ft) bgs. Of the twelve well couplets, ten were constructed of ~ 25 mm (1") ID schedule 40 PVC with a 0.15 m well screen. The remaining two were constructed of ~ 50 mm ID schedule 40 PVC with a 0.15 m (0.5 ft) well screen (MW-2 and MW-6). Boreholes for each monitoring well were drilled using a jetting technique where an ~ 65 mm (2.5") OD or ~ 90 mm (3.5") OD steel casing was

advanced to depth before the interior was flushed with water. The PVC well was placed into the casing before pulling the casing, allowing the aquifer material to collapse around the well.

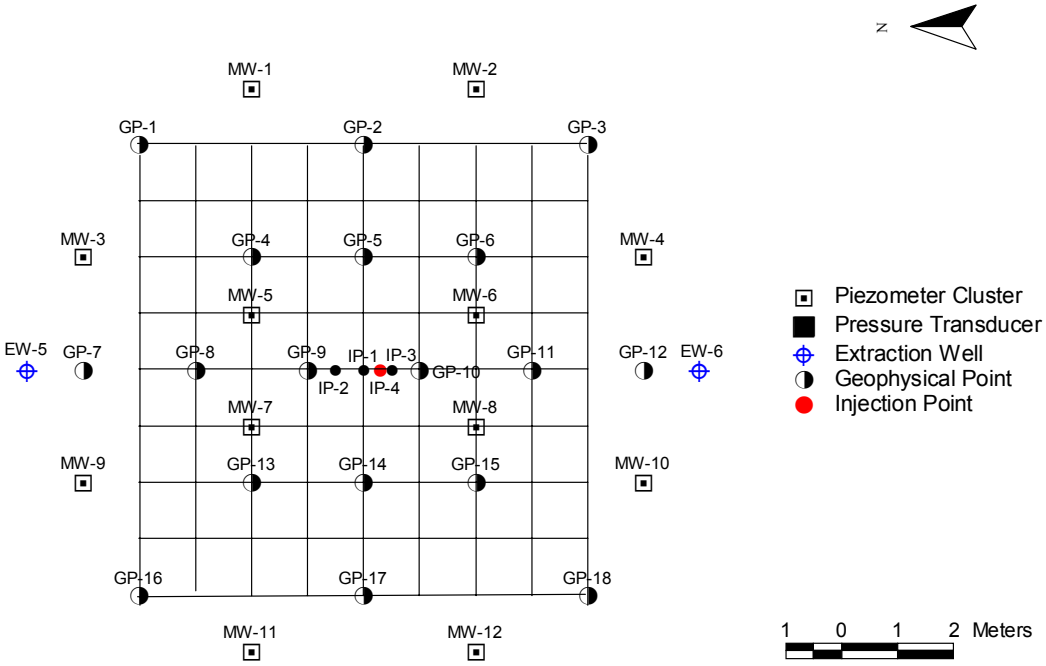

Figure 2.2 – Schematic of study site layout.

2.2.4 Extraction Wells

One extraction well constructed of ~ 25 mm (1") ID schedule 40 PVC with a 1.0 m (3.3 ft) well screen was installed at each of the four corners of the study area (EW-1 through EW-4). Each of these boreholes was advanced using a jetting technique where a ~ 65 mm (2.5") OD steel casing was advanced to a nominal depth of 4.5 m (14.8 ft) bgs before flushing the interior with water. The PVC well was placed within the casing prior to pulling the steel casing, permitting the aquifer material to collapse around the pipe. Based on changes to the design of the hydraulic control experiment, two additional extraction wells (EW-5 and EW-6) were installed ~ 6 m (19.7) north and south of IP-4, respectively (Figure 2.2). These wells were constructed of ~ 50 mm (2") ID schedule 40 PVC with a 1.0 m (3.3 ft) well screen. They were advanced using hollow-stem auger drilling techniques where an ~ 200 mm (8") OD hollow-stem auger was advanced to a nominal depth of 4.5 m (14.8 ft) before flushing the casing interior with water. PVC pipe was inserted into the casing, filled with water, and then the casing was removed as aquifer material was placed in the annular space. All water was pumped from the PVC pipe once it was anchored at the installation depth.

2.3 Experimental Setup

Carbonated water was injected into IP-4 located in the center of the 12-m x 12-m (39.4-ft x 39.4-ft) study area, as shown in Figure 2.2. The injection point was connected via ~ 12.5 mm (1/2") ID braided PVC tubing equipped with a T-pipe fitting to two in parallel Gas inFusion™ (GI) generators. Each GI generator received CO_2 from the gas tank via ~ 12.5 mm (1/2") ID braided PVC tubing equipped with a T-pipe fitting. Similarly, water was supplied to each GI generator from a high-pressure multi-stage centrifugal pump connected with ~ 25 mm (1") ID braided PVC tubing outfitted with a T-pipe fitting. The outlet of the pump was equipped with another T-pipe fitting to permit the division of flow between the GI generators and the water by-pass. The GI generator side of the T-pipe fitting was equipped with a flow control valve that restricted the injection point pressure and flow rate. The tubing connected to the GI generators for the water by-pass was constructed of ~ 25 mm (1") ID PVC tubing. The inlet of the pump was attached with ~ 25 mm (1") ID braided PVC tubing to the water tank, which received water from two to three upgradient ~ 200 mm (8") ID wells. Four 0-100 psi (0-690 kPa) pressure gauges were used to measure fluid pressure between the pump and the injection point, including one (1) between the pump and GI generators, one on each of the two GI generators, and one immediately upgradient of the injection point. The water flow rate was monitored with a 0-20 lpm flow meter located immediately downgradient of the pump and before the first pressure gauge. For the hydraulic control experiment, water was extracted from two extraction wells (EW-5 and EW-6) using a ~ 50 mm (2") submersible pump (Grundfos Redi-Flo2), which directed flow to the water tank. A block diagram of the experiment is shown in Figure 2.3. Specific details regarding operation of the two experiments are provided in Sections 3.2 and 4.2.

2.4 Monitoring Data

Groundwater monitoring of enhanced CO_2 levels and geophysical surveys (neutron measurements, surface ground penetrating radar (GPR), and cross-borehole GPR) to find induced gas content were supported by hydraulic monitoring and physical observations of gas bubble distribution at the water table.

2.4.1 Process Data

During the experiments, the following process data were monitored and recorded:

- Date and time;
- Water flow rate (lpm);
- Pump pressure (psi);
- GI generator pressures (psi);
- IP back pressure (psi);
- CO_2 gas tank pressures (psi);

- CO_2 gas flow rates;
- Extraction pumps frequency (Hz) and flow rates (lpm), if applicable; and
- Problems encountered.

Process data readings are provided in Appendix B.

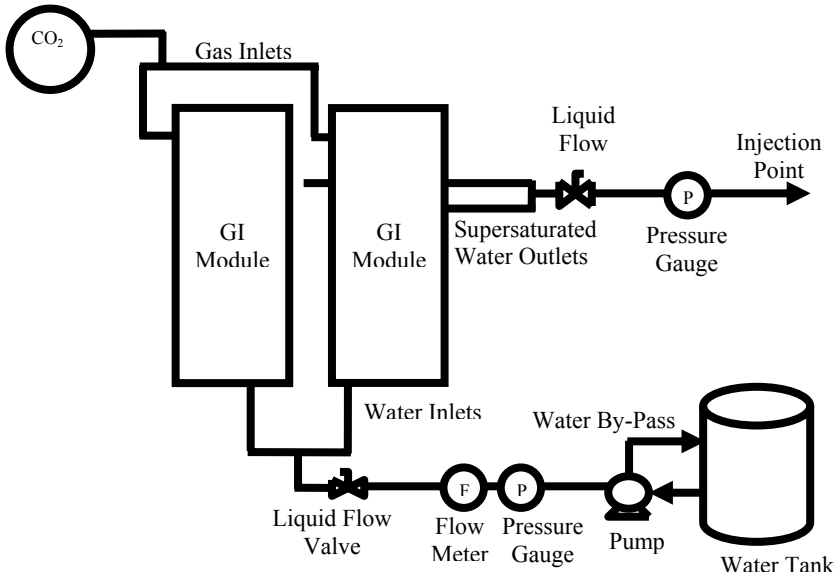

Figure 2.3 – Flow diagram of the GI experiment without hydraulic control.

2.4.2 Groundwater Quality Samples

Prior to sample collection, each well was purged of three well volumes to remove stagnant water from the well bore. Well purging in each well was accomplished by using a peristaltic pump and ~ 6 mm ID polyethylene tubing. Each well was sampled through the pump discharge. The groundwater was monitored in the field for pH and gas pressure and analyzed in the laboratory for total inorganic carbon.

2.4.2.1 Field Parameters

Prior to groundwater sample collection, whenever possible, pH and total gas pressure were measured in each well. Calibration problems and availability of a pH probe made measurements during each sampling event impossible. pH was measured using an Orion 290A pH meter and gas pressure was measured using a Tensionometer 300E (Alpha Designs Ltd). The tensionometer measures the total

pressure of all dissolved gases present within the groundwater. Table 2.1 presents the groundwater sampling dates and relevant field parameters measured.

Table 2.1 – Field Parameters Collection Schedule

Sampling Date	Day	pH	Total Gas Pressure (mm Hg)	Experiment
May 5, 2005	Background	No	No	Background.
May 12, 2005	2	No	Yes	No hydraulic control.
May 16, 2005	6	No	Yes	
May 20, 2005	10	No	Yes	
May 24, 2005	14	No	Yes	
May 27, 2005	17	Yes	Yes	
May 30, 2005	20	Yes	Yes	
June 2, 2005	23	Yes	Yes	
June 21, 2005	Between	No	Yes	Between experiments (19 days).
June 23, 2005	2	No	Yes	With hydraulic control.
June 27, 2005	6	No	Yes	
June 28, 2005	7	No	Yes	
June 30, 2005	9	No	Yes	
July 7, 2005	16	No	Yes	

2.4.2.2 Aqueous Carbon Dioxide Concentrations

Changes in dissolved CO_2 concentrations were measured by analyzing groundwater samples to determine the presence of zones of increased gas content. This was accomplished by collecting 20 ml aqueous samples in a 60 ml plastic syringe, without headspace, and sealed with either a double luer connector or a rubber stoppered needle tip. In the laboratory, each syringe was fitted with a double luer connector and acidified with 0.5 ml of a 4N sulfuric acid solution. Approximately 30 ml of pre-purified helium was added via the valve, as the syringe was held upright, until the plunger reached the 50 ml graduation. Each sample was shaken and allowed to equilibrate for several hours at room temperature prior to extracting a 6 ml aliquot of the gaseous phase. The gas sample was injected (overfilled) into a 2 ml gas sample loop. A valve switch introduced the sample into the carrier gas stream of a GOW-MAC (Series 350GP) gas chromatograph equipped with a thermal conductivity detector (TCD). Peak areas were measured by a HP3380A integrator.

Calibration was by external standard method, using commercially obtained certified gaseous standards in the expected range of the collected samples. Carbon dioxide standards consisted of 0.5%, 10%, 25%, 50%, and 100% carbon dioxide and air at 0.03% carbon dioxide. When the

chromatogram of the standard gas mixture was obtained, the peak area was subjected to linear regression analysis and the resultant equation was used to determine the unknown gas sample concentrations. At least three samples of carbon dioxide (at five concentrations) were run prior to the analysis of unknown samples and also after every ten unknown samples to ensure the gas chromatogram was operating in a consistent manner. Sample peak areas were measured and the concentration of gaseous carbon dioxide was determined using the linear regression equation. Aqueous concentrations were calculated from the gaseous concentration using the Ideal Gas Law and solubility coefficients (Oswald Coefficient).

The groundwater sampling schedule is presented on Table 2.2 and the results are discussed in Section 3.3.

Table 2.2 – Groundwater Sampling Schedule

Sampling Date	Day	Number of Samples (per event)	Experiment
May 5, 2005	Background	26	Background.
May 12, 2005	2	26	No hydraulic control.
May 16, 2005	6	26	
May 20, 2005	10	26	
May 24, 2005	14	26	
May 27, 2005	17	26	
May 30, 2005	20	26	
June 2, 2005	23	26	
June 21, 2005	Between	26	Between experiments (19 days).
June 23, 2005	2	26	With hydraulic control.
June 27, 2005	6	26	
June 28, 2005	7	26	
June 30, 2005	9	26	
July 7, 2005	16	26	

2.4.3 Hydraulic Monitoring

A Solinst Reelogger Model 2001 datalogging system equipped with a 22 mm diameter in-line sensor was installed in two monitoring well couplets (MW-2 and MW-6) and two extraction wells (EW-5 and EW-6). These dataloggers were used to monitor changes in water levels. In the shallow monitoring wells (MW-2S and MW-6S), the in-line sensor was installed 2.0 m below the top of casing (TOC). The in-line sensors were installed 3.5 m below the TOC in the deep monitoring wells (MW-2D and MW-6D) and 4.0 m below the TOC in the extraction wells. These wells are located

approximately 2.5 to 6.2 m from IP-4. Water levels were monitored between May 8, 2005 and August 1, 2005; however, the dataloggers in four wells (MW-2S, MW-6S, MW-6D, and EW-5) were removed between June 3, 2005 and June 20, 2005, as they were required for another experiment.

2.4.4 Geophysical Surveys

Surface GPR, cross-borehole GPR, and neutron measurements surveys were performed within the study area to detect changes in water content caused by the introduction of a CO_2 gas phase.

2.4.4.1 Ground Penetration Radar

GPR is a geophysical technique that uses high-frequency electromagnetic (EM) energy to acquire subsurface information. It detects changes in EM properties (e.g., dielectric permittivity, electrical conductivity, and magnetic permeability) that are a function of many natural conditions such as soil and rock material, water content, voids, fractures, intrusions, and bulk density as well as man-made objects. Data are normally acquired using antennas placed on the ground surface or in boreholes.

2.4.4.1.1 Surface GPR

Surface GPR radiates short pulses of high-frequency EM energy downward into the ground from a transmitting antenna located on the surface. The EM wave propagates in the ground at a velocity that is primarily a function of the relative dielectric permittivity of subsurface materials. A portion of the wave is reflected back to the receiving antenna when it encounters subsurface electrical discontinuities, while the rest of the energy continues to penetrate deeper.

The depth to buried layers or objects is proportional to the time it takes the EM wave to travel from the transmitter antenna to the target and back again to the receiver antenna. This time is dependent on the dielectric properties of the media through which the radar pulse travels. In most cases this is primarily influenced by moisture content since water has a very high dielectric constant (80) compared to most dry geologic materials (4 to 8) (Kearey & Brooks, 1991). Greater depth penetration can be achieved with lower frequency antennas, but they have poorer spatial resolution compared with higher frequency antennas. The resolution of radar reflections can be improved by increasing the frequency of the radar waves transmitted into the ground; however, there is a trade-off between increased resolution and depth of penetration.

Surface GPR surveys were performed using a pulseEKKO 100 GPR system (Sensors & Software Inc.) with 200 MHz antennas and a 400 V transmitter. A step size of 0.1 m was used between readings in 2004 and 0.05 m in 2005. The antenna separation, which is the distance between the centres of the transmitter and receiver antennas, was 0.5 m. The survey schedule is presented in Table 2.3.

The locations of the surface GPR lines from the initial background survey (May 7, 2004) are provided on Figure 2.4, while Figures E.5 and E.10 in Appendix E depict the orientations of the lines for the other survey dates. The results are presented in Section 3.5.1.

Table 2.3 – Surface GPR Survey Schedule

Survey Date	Day	Number of Survey Lines	Experiment
May 7, 2004	Background	6	Background prior to installations of access tubes & monitoring wells.
October 9, 2004	Background	6	Background subsequent to installations and prior to experiments.
April 21, 2005	Background	2	Background.
May 19, 2005 May 30, 2005	9 20	2 2	No hydraulic control.
June 17, 2005	Between	2	Between experiments (15 days).
July 6, 2005	15	2	With hydraulic control.

Data Analysis

Surface GPR reflection profile data were processed and plotted using pulseEKKO V4.22 (Sensors & Software Inc.). The processing of the data required the application of a gain function to make the attenuated GPR reflections more visible. The GPR wave strength decreases with depth because of the attenuating effect of spherical spreading of the wave front and the exponential ohmic dissipation of energy. A gain function increases the amplitudes of the reflections on each wave by applying a mathematical multiplicative factor. The two most common types of gain functions are Automatic Gain Control (AGC) and Spreading and Exponential Compensation (SEC).

The AGC equalizes all signals by applying a gain function that is inversely proportional to the signal strength. This results in the loss of relative amplitude information; however, it tends to balance the signal strength across the section. Because of the equalization of all signals, AGC data can not be used to estimate the strength of any particular reflector relative to other reflectors. This type of gain is useful for defining continuity of reflection events across the section. The AGC function requires the user to specify an upper gain limit to prevent the gain in zones of extremely low signal strength from becoming too large.

The SEC attempts to compensate for the attenuating effect of spherical spreading of the wave front and the exponential ohmic dissipation of energy. It applies the same gain to every trace regardless of signal strength; thereby, preserving relative amplitude and strength information for different reflectors. This gain is a composite of linear and exponential time gains (i.e. the gain value increases with time down the trace according to a mathematical relationship that is a composite of a linear and

exponential function of time). The user specifies an attenuation factor (in dB/m) that describes how quickly the wave is attenuated as it travels through the ground (i.e. how quickly the gain function increases with time). A maximum gain is specified so that the gain function does not become too large because a large gain value at late times on the trace where there may not be a visible reflection signal, will unduly magnify signal noise. A start value (i.e. the value of the gain function at time 0 ns) must be specified. It is typically set to 1 (i.e. a multiplying factor of 1 and no gain at 0 ns). Each GPR reflection profile was plotted using a SEC gain, with the maximum gain set to 3000, attenuation set to 2.7 dB/m, and a start value of 1. The resultant GPR reflection profiles showed major reflections prominently while preserving the relative strength of different reflectors.

Trace-to-trace and down-the-trace averaging filters were applied to the data. A trace-to-trace averaging filter replaces each trace with the average of that trace and at least one neighbouring trace (i.e. a horizontal running average filter). This type of filtering tends to enhance the appearance of flat lying reflectors while suppressing dipping reflectors and random noise. A trace-to-trace filter of 2 (i.e. each plotted trace was the average of two neighboring traces) was applied to all data. This small filter was selected to avoid excessive suppression of dipping reflectors while still suppressing some random noise. A down-the-trace averaging filter replaces each point along the trace as the average of a number of points within a window centred about the point. The window width (i.e. number of points) must be specified. This type of filter tends to suppress random noise along each trace. A window width of 2 points was used (Piggott, 2006).

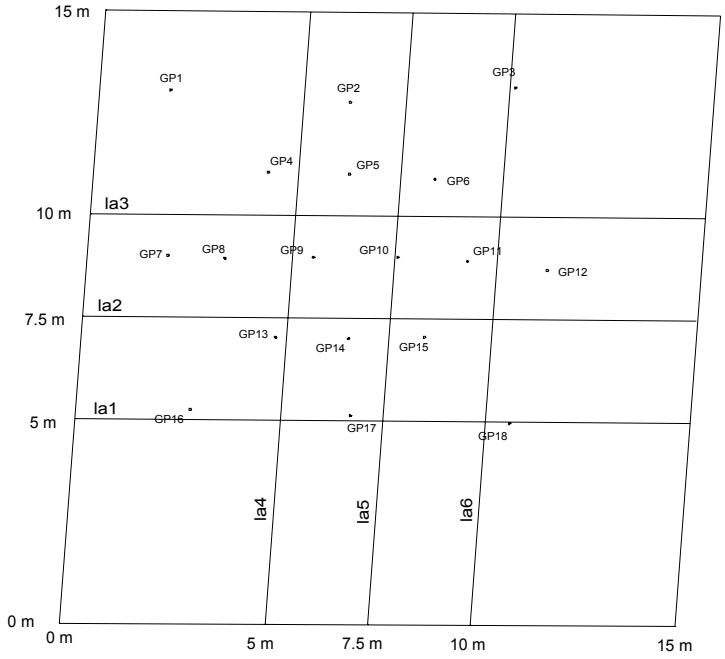

Figure 2.4 – Diagram of May 7, 2004 surface GPR survey lines relative to GP access tubes.

2.4.4.1.2 Cross-borehole GPR

Borehole GPR images subsurface physical properties between boreholes by measuring the time and amplitude of radar waves traveling from one borehole to another. These two measurements are used to determine the velocity and attenuation of the material between boreholes, which in turn can be used to obtain a measure of water content and estimate electrical conductivity, respectively.

In this instance, the method was used to determine the water content between boreholes. The average velocity (V) of the EM wave was determined by measuring the travel time of the wave between a transmitter in one borehole and a receiver in another borehole a known distance apart. The calculated average velocity and the velocity of the EM wave in free space (c) were used to determine the dielectric permittivity (K) between the boreholes using

$$K = \frac{c^2}{V^2} \qquad \textbf{Equation 2.1}$$

The dielectric permittivity was used to calculate the volumetric water content (θ) using the empirical relationship developed by Topp et al. (1980):

$$\theta = -5.3\times10^{-2} + 2.92\times10^{-2}K - 5.5\times10^{-4}K^2 + 4.3\times10^{-6}K^3 \qquad \textbf{Equation 2.2}$$

Topp et al. contend that this relationship can be used to determine water content in soil independent of soil properties (i.e., type, density, temperature; and soluble salt content), within a water content error of approximately 0.013 over the complete range of water contents.

Borehole GPR data were acquired using a pulseEKKO 100 GPR system with 200 MHz antennas and a 400 V transmitter. For these experiments, the GPR trace stored to disk was an average of 32 individual traces collected rapidly in a process known as stacking. The stack number selected was the largest that could be used while still completing the surveys in the allotted time. A higher number of stacks takes longer to collect but improves the signal to noise ratio. The data were collected using two acquisition modes – zero offset profile (ZOP) and multiple offset gather (MOG) (2.5). The separations between the access tube pairs, designated as GPs, used for the borehole GPR measurements ranged from approximately 1.4 m to 4.5 m.

In the ZOP acquisition mode, radar traces were recorded with the transmitter and receiver at identical positions in their respective access tubes, as shown in Figure 2.5. These radar traces provided a one-dimensional (1-D) profile along the length of the boreholes, which indicates the average water content between corresponding points in the access tube pair. A series of 34 to 37 positions were recorded per access tube pair, while both antennas were moved downward using a step size of 0.125 m. The profiles extend from 0.50 m to between 4.625 and 5.000 m bgs. ZOP water

content profiles were acquired primarily between the access tube pairs shown in Figure 2.6 on the dates indicated on Table F.1 located in Appendix F.

ZOP Data Analysis

All borehole GPR data were initially processed with PICKER (Sensors & Software Inc.), a data picking software program. PICKER allows the user to select and record the time on each GPR trace that corresponds to the arrival of the transmitted pulse at the receiver, referred to as the first break. The selection of the first break for each GPR trace allows the travel time of each wave from transmitter to receiver to be determined.

The options selected in PICKER for the automatic first break picking were a 19-point smoothing filter with a 20% negative edge of the first arrival pulse. The negative edge chosen corresponds to a first break selection that is at least 20% of the maximum amplitude for a specific GPR trace. A smaller negative edge may be selected; however, experience indicates that this may result in noise being selected as the first break.

The first break times obtained from each ZOP calibration file were used to recalculate the time-zero points for the downhole ZOP data. The ZOP calibration determines the travel time in air of the radar wave between the transmitter and receiver a known distance apart (i.e. the distance between an access tube pair), which allows for correction of the subsequent downhole ZOP traces for the curcumas path from the computer to the transmitter. After the calibration of the ZOP data, the travel time of each wave from transmitter to receiver was determined, this was used to calculate the velocity and water content using equations 2.1 and 2.2, for each of the 34 to 37 antenna positions between access tube pairs.

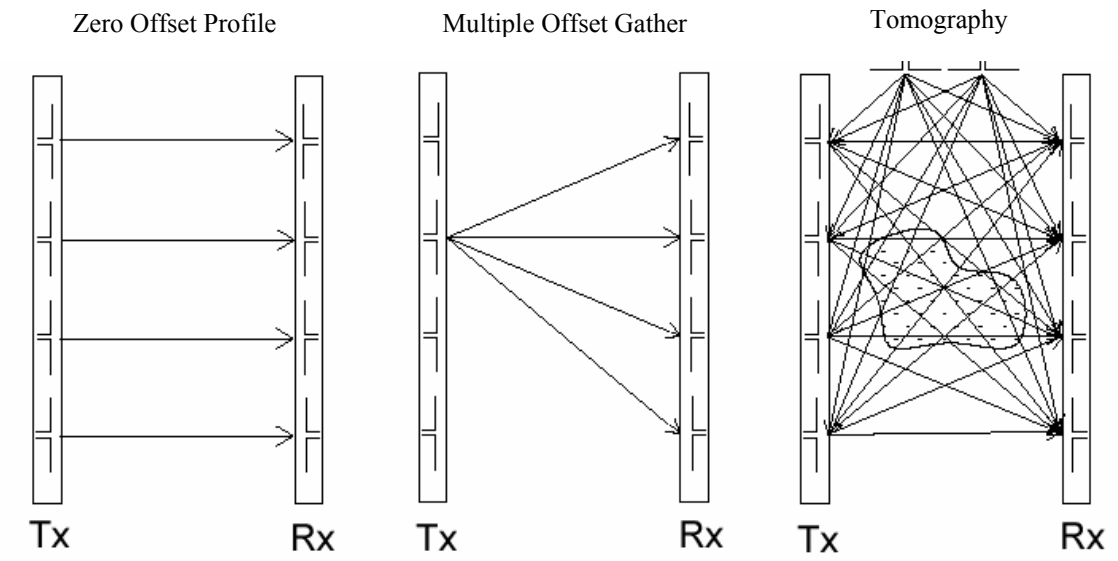

Figure 2.5 – Borehole radar data acquisition modes showing typical ray path patterns between transmitter (Tx) and receiver (Rx) positions (Piggott, 2003).

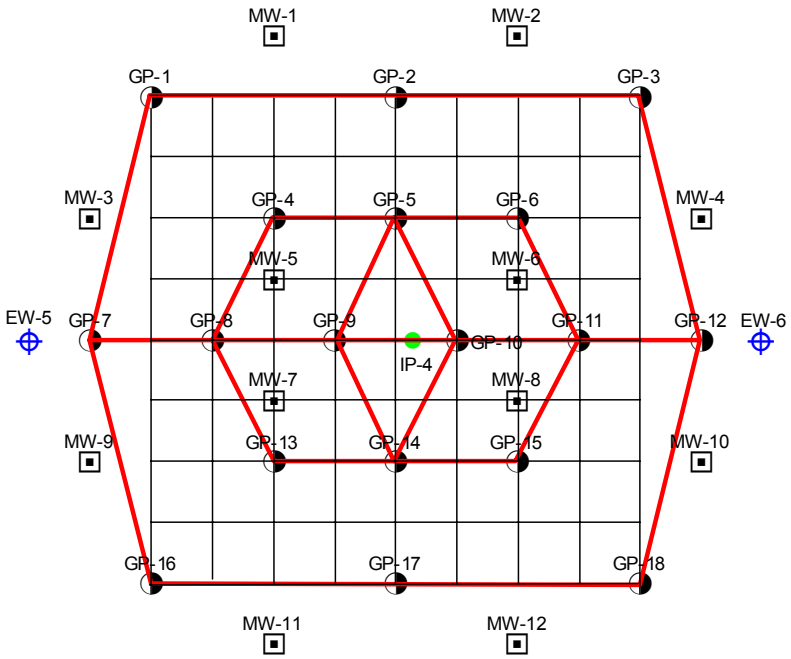

Figure 2.6 – Diagram showing primary geophysical access tube pairs used for ZOP acquisition mode.

2.4.4.1.2.1 Multiple Offset Gather (MOG)

The MOG acquisition mode was used to generate a 2-D image of the water content in the plane between an access tube pair. In this mode, the transmitter antenna was fixed at a given position in an access tube while the receiver antenna was moved along the second access tube using a step size of 0.25 m. Radar traces were collected at 15 to 16 receiver positions between 1.00 m and ~ 4.50 to 4.75 m bgs. This process was repeated for each of the 15 to 16 transmitter positions located 0.25 m apart from 1.00 m to ~ 4.50 to 4.75 m bgs. The complete set of 225 to 256 radar traces were required to produce a tomogram of the average water content between the access tube pair. A diagram of this acquisition mode is provided in Figure 2.5. MOG 2-D water content images were acquired from the access tube pair locations provided on Figure 2.7 for the survey dates presented on Table 2.4.

MOG Data Analysis

Each MOG file contains the data for a single transmitter position and all 15 to 16 receiver positions (i.e. one multiple offset gather). Due to the relatively long duration of a MOG survey, there is the potential for drift of the time-zero point of the GPR traces. Therefore, the first break time for each zero-offset MOG trace was shifted to correspond with the relatively quickly collected, relatively drift free, equivalent ZOP trace. All traces within the MOG were shifted by an identical amount. This process was repeated for each of the 15 to 16 transmitter positions (i.e. MOGs) required to produce a tomogram of average water content between an access tube pair.

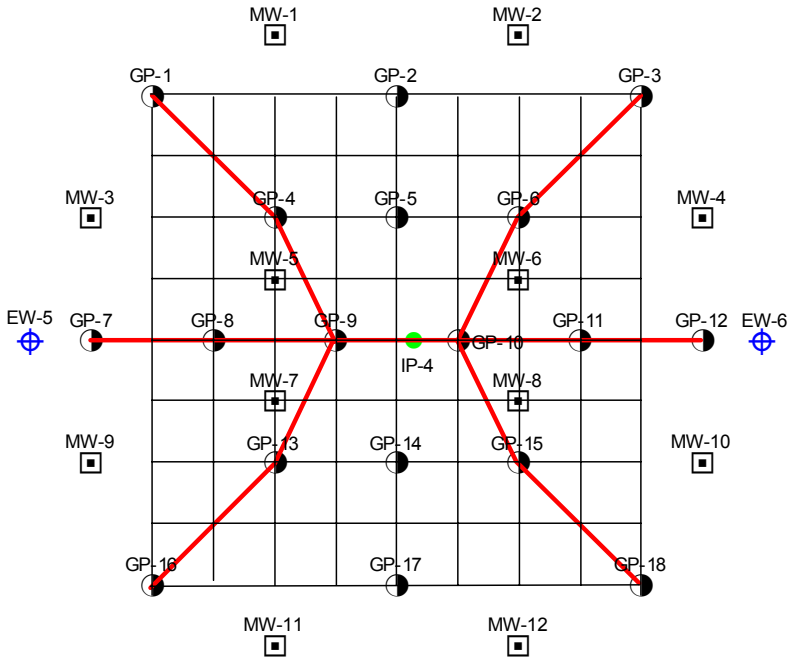

Figure 2.7 – Diagram showing geophysical access tube pairs used for MOG acquisition mode.

The complete set of 15 to 16 MOG files, corrected for time-zero drift were merged using the EKKO_IMAGE V1.0 program (Sensors & Software Inc.). The merged file was inputted into the picker program for automatic first break selection. Atypical automatic picks were rejected manually in PICKER.

The acceptable travel times from PICKER were processed with the EKKO_IMAGE program, which incorporates the straight ray processing component of the MIGRATOM tomographic modeling program (Jackson and Tweeton, 1993). In this tomographic inversion process, a 0.25 m by 0.23 to 0.28 m cell size was used, resulting in a 17 cell by 38 cell area. A consistent vertical cell size of 0.25 m corresponding to the MOG step size was used; however, the horizontal step size was variable as it was dependent on the distance between an access tube pair. The output from the MIGRATOM tomographic process is the water content distribution (one water content for each 0.25 by 0.23 to 0.28 m cell). These water contents were obtained by MIGRATOM using equations 2.1 and 2.2. The numerical water content distribution data were interpolated and plotted, using TRANSFORM V3.4 (Fortner Software LLC), to generate a 2-D contoured image of the water content in the plane between an access tube pair (Piggott, 2003).

2.4.4.2 Neutron Measurements

Neutron measurements use high-energy (fast) neutrons to measure soil moisture content by determining the hydrogen containing material present within the soil. These fast neutrons are released from a neutron source located within the probe containing radioactive americium-241 (^{241}Am) and

non-radioactive beryllium (Be). ^{241}Am releases both alpha particles and photons. The photons are irrelevant to the operation of the gauge; whereas the alpha particles are responsible for the process that initiates the neutron emission. These alphas strike the Be and cause it to release high-energy neutrons in all directions. These high-energy neutrons penetrate the medium around the borehole and lose energy primarily through elastic collisions with the similar sized nuclei of hydrogen atoms. Neutrons that lose energy become slow neutrons or "thermalized" neutrons. Thermal neutrons are detected by a Helium-3 (He^3) gas filled chamber that measures the count rate of thermal neutrons in counts per second (cps). The number obtained from the counting device is used in a computation to obtain soil moisture content. Neutron measurements were performed using the Campbell Pacific Nuclear (CPN) International, Inc. Model 503DR Hydroprobe and the Comprobe Inc. Dual Spaced Neutron Probe Model 1836.

Table 2.4 – MOG Survey Schedule

Survey Date	Number of Pairs	Experiment
May 5, 2005	12	Background.
June 15, 2005	12	Between experiments (13 days).
July 4, 2005	12	With hydraulic control.

2.4.4.2.1 CPN Model 503 DR Hydroprobe

The 503 DR probe has a 50-millicurie (mCi) ^{241}Am-Be source with one He^3 detector located 0.1 m from the neutron source. Based on the distance between the source and detector, the vertical resolution of the tool is estimated to be 0.1 m with a radial distance of investigation of approximately 0.13 m, assuming a water content of 0.35. This measurement radius (~ 0.13 m) is approximately three times the borehole radius (0.025 m) plus estimated disturbed annular zone around the borehole from access tube installations (~ 0.015 m). Thus, the relatively small variation in the measurement radius and borehole radius may have some impact on the neutron measurements results. Neutron profiling was performed along the length of the access tube to a nominal depth of 5 m (actual depths ranged from 4.683 to 5.008 m bgs) with a vertical sampling interval of 0.15 m. The CPN probe provided a measured neutron count per 16 seconds (s) that was used in a computation to obtain soil moisture content (Equation 2.3).

$$\theta = \left(\frac{Measured\ Count}{Standard\ Count} \right) \times A + B \qquad \textbf{Equation 2.3}$$

where θ = volumetric water content,

Measured Count = downhole neutron count,

Standard Count = background neutron count for probe,

A = calibration constant, and

B = calibration constant.

The standard count for the probe was obtained by averaging seventeen measurements of the hydrogen in the wax located in the shield of the hydroprobe, which resulted in a standard count of 7372. The calibration constants A and B were determined using the CPN factory calibration coefficients for 2" aluminum casings with the schedule 40 PVC shielding factor (0.6). A and B were found to be 31.2550 and -1.8388 percent water by volume, respectively. The resultant calculated water contents are discussed in Section 3.5.3. The sampling frequency for the CPN probe is provided in Table 2.5.

Table 2.5 – CPN Neutron Measurements Schedule

Survey Date	Day	Number of GPs	GP IDs
May 6, 2005	Background	11	4 to 12; 14 to 15
May 12, 2005	2	15	3 to 12; 14 to 18
May 16, 2005	6	8	1 to 2; 5; 8 to 11; 14
May 24, 2005	14	2	9; 15
June 2, 2005	23	2	10; 14

2.4.4.2.2 Comprobe Model 1836 Dual Spaced Neutron Probe

The Comprobe tool contains a 3-curie (Ci) ^{241}Am-Be source with two He^3 detectors, spaced 0.343 m and 0.569 m above the neutron source. The vertical resolution of this tool is estimated to be 0.569 m based on the source-far receiver separation and the radial penetration depth is approximately 0.3 m (Ellis, 1987). Unlike the 503DR hydroprobe, formation disturbance should have a minimal effect on the neutron logging as the measurement radius of this tool (0.3 m) is large relative to the borehole radius (0.025 m) plus estimated disturbed annular zone around the borehole from access tube installations (~ 0.015 m). Neutron profiling was performed at a 0.25 m step size along the length of

the access tube. The neutron tool provided a measured count rate that was calibrated using a linear relationship with volumetric water content (θ) given by

$$\theta = m \log N + b \qquad \text{Equation 2.4}$$

Where θ = volumetric water content,

N = measured count rate,

m = calibration constant, and

b = calibration constant.

The calibration constant m was obtained from Tomlinson et al (2003). Tomlinson determined the slope (-0.510) by measuring the neutron count rate within the unsaturated and saturated zone in PVC cased holes located within the sand pit at Borden and compared the results to water content values determined from borehole GPR surveys. Calibration constant b was not provided by Tomlinson since only the slope is required to calculate water content change during sparging. The average porosity (40%) obtained from borehole GPR surveys was used to convert the water content measurements to their equivalent CO_2 gas saturation.

Dual spaced neutron probe surveys were performed twice during the hydraulic control experiment, including once at the end of the experiment with hydraulic control and once after the experiment was completed to obtain background data. The end of experiment data was collected on July 7, 2005, 16 days after injections began for the hydraulic control experiment. No pre-injection surveys were performed; therefore, background measurements were obtained after an acceptable length of time had passed for evolved CO_2 gas to dissipate. These background readings were taken on August 26, 2005, approximately 7 weeks after the hydraulic control experiment was stopped.

2.4.4.2.3 Neutron Probe Comparisons

Both of the neutron tools employed measure water content by determining the amount of hydrogen present; however, there are some differences between these tools. They are as follows:

- Vertical Resolution
  - 503 DR – 0.1 m
  - Dual Spaced Neutron Probe – 0.569m
- Penetration Depth
  - 503 DR – ~ 0.13 m because of the low emission source (50-mCi ^{241}Am-Be source)
  - Dual Spaced Neutron Probe – ~ 0.3 m because of the higher emission source (3-Ci ^{241}Am-Be source)

- Count Rate/Water Content
    - 503 DR – A higher water content results in a higher count rate because hydrogen (water) present near the probe slows the neutrons closer to the source, which is detected almost immediately by the receiver located only __ m from the source.
    - Dual Spaced Neutron Probe – A higher water content causes a lower count rate because the thermalized neutrons have to travel some distance to be detected by the receiver. If the water content is high, the neutrons get slowed down more quickly and most will not make it to the receiver.

2.4.5 Physical Observations

To physically observe CO_2 gas distribution at the water table, four excavations of the vadose zone to the water table were performed prior to shutting down the experiment with hydraulic control. The water table was located ~ 1 m bgs. The locations of these excavations are depicted on Figure 2.8 and the observations are discussed in Section 4.0.

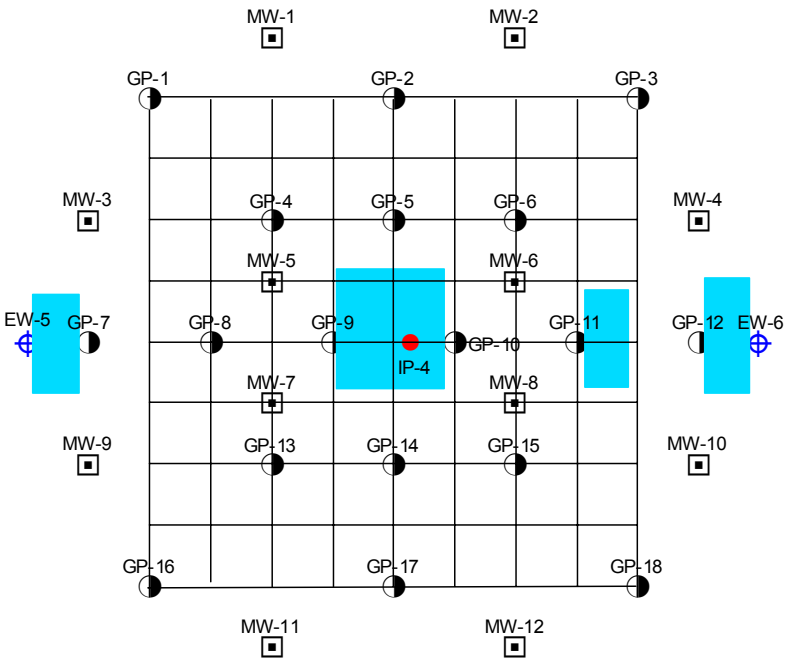

Figure 2.8 – Schematic of approximate locations of excavations to water table for physical observations of CO2 gas distribution.

2.4.6 Hydraulic Conductivity Tests

Six borings (B-1 to B-6) were advanced to provide soil samples for hydraulic conductivity tests, including falling-head permeameter tests and grain size distributions. These tests were performed to determine if experimental observations were attributable to heterogeneities within the aquifer. Although the Borden aquifer is considered to be homogeneous from a hydraulic perspective, previous studies indicate that heterogeneities are present (Thomson, 2004 and Tomlinson et al, 2003).

2.4.6.1 Falling-Head Permeameter Tests

Falling-head permeameter tests were performed on six to thirteen soil samples selected from each of the six soil borings (B-1 to B-6) advanced within the study area. The following procedure was used

- Select a 5-cm portion of soil from the core and insert into the permeameter apparatus.
- Record the thickness of the soil sample.
- Pass carbon dioxide through the soil sample to remove trapped air.
- Introduce deaerated water at a very slow rate into the sample chamber.
- Record the time for the head within the tube to fall between two points (H_0 to H_1).
- Repeat procedure a minimum of three times for each sample.
- Calculate the hydraulic conductivity using (Freeze and Cherry, 1979)

$$K = \frac{aL}{At}\ln\left(\frac{H_0}{H_1}\right) \qquad \textbf{Equation 2.5}$$

Where K = hydraulic conductivity

a = cross-sectional area of tube

L = thickness of the soil sample

A = cross-sectional area of the soil sample cylinder

t = time for the water head to fall from H_0 to H_1

H_0 = initial head

H_1 = final head

- Determine geometric mean of the hydraulic conductivities from each test to obtain a representative value for the sample.

The hydraulic conductivities calculated from the falling-head permeameter tests are provided in Section 5.

2.4.6.2 Grain Size Distribution

In addition to the falling-head permeameter tests performed to determine hydraulic conductivity, grain-size distributions were determined for six to twelve samples collected from three of the soil cores (B-2, B-3, and B-6). Each 5 cm sample, located between ~ 2 and 4 m bgs, was air-dried prior to passing it through a set of eleven sieves. The sieves selected were 1.000-mm (No. 18), 0.500-mm (No. 35), 0.250-mm (No. 60), 0.180-mm (No. 80), 0.150-mm (No. 100), 0.125-mm (No. 120), 0.106-mm (No. 140), 0.090-mm (No. 170), 0.075-mm (No. 200), 0.063-mm (No. 230), and 0.032-mm (No. 450). The mass retained on the selected series of sieves was recorded. Grain size distribution cumulative curves were prepared for each sample. The hydraulic conductivity of each of these samples was determined from the Hazen empirical relationship (Fetter 1994):.

$$K = C(d_{10})^2 \qquad \textbf{Equation 2.6}$$

where K = hydraulic conductivity (cm/s)

C = coefficient that factors in the characteristics of the material

d_{10} = effective grain-size diameter (cm)

For the medium-grained, well sorted Borden sand, a coefficient (C) of 100 was selected from the table presented in Section 4.4.3 of Fetter (1994). The grain size cumulative distribution curves and the derived hydraulic conductivities are presented in Section 5.0.

Chapter 3
Passive Injection of Carbonated Water

3.1 Scope

To evaluate in situ gas evolution, CO_2-supersaturated water was injected into a porous medium in a 3-D field experiment. A ZOI was estimated using geophysical tools and groundwater monitoring for CO_2 partial pressures above the applicable hydrostatic pressure.

3.2 Process Data

Passive injection of carbonated water occurred over 23 days. However, injection of CO_2-supersaturated water was intermittent due to problems with operation of the experiment. The experiment ended once geophysical data showed no additional increase in the ZOI. Table 3.1 shows the dates and times of experimental shutdowns relative to the start of the experiment (Day 0). The stop time of each injection cessation was obtained from the hydraulic monitoring data discussed in Section 3.4. Additional process data are provided in Table B.1 in Appendix B.

3.3 Groundwater Quality Samples

Groundwater quality samples were collected according to the procedures presented in Section 2.4.1. The field measurements and laboratory results are provided below.

3.3.1 Field Parameters

pH and total gas pressure were measured in the field prior to submitting groundwater samples for laboratory analysis of CO_2. These field parameters primarily provided an immediate method to assess areas with increased CO_2 gas content. pH measurements along with laboratory determined CO_2 concentrations were also used to calculate CO_2 partial pressures for each groundwater sample.

3.3.1.1 pH

Log pH versus CO_2 concentrations in site groundwater are depicted on Figure 3.1. A linear regression was employed to model the inverse relationship between log pH and CO_2 concentrations. As noted on Figure 3.1, when modeled using a linear function, the log pH versus CO_2 concentrations exhibit a high correlation ($R^2 = 0.7149$). The derived analytical model ($y = -2E\text{-}05x + 0.8568$) was used to estimate the log pH for each sample when field pH data were unavailable. The pH data, both measured and calculated, were used with CO_2 concentration data to calculate CO_2 partial pressures for each sample (Section 3.3.2).

Table 3.1 – Select Process Data Showing Experiment Problems

Day	Time	Note
0	14:05	Started injection.
2	3:30	Ran out of CO_2.
2	9:45	Restarted.
4	20:45	Problem with CO_2 tanks.
5	9:45	Restarted.
15	6:00	Ran out of H_2O.
15	20:15	Restarted.
16	18:00	Ran out of CO_2.
17	9:00	Restarted.
18	2:45	Problem with CO_2 gauge.
19	13:10	Restarted.
20	12:20	Redeveloped IP-4 due to flow rate decrease.
20	12:45	Restarted.
23	5:30	First experiment finished.

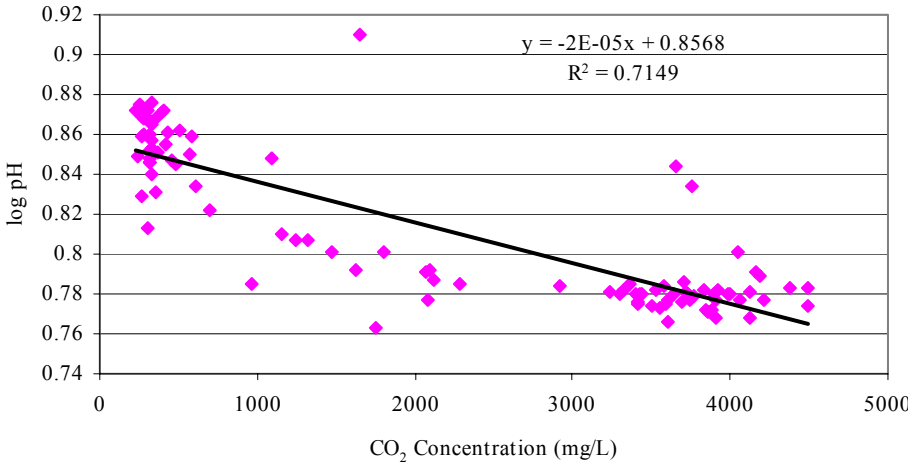

Figure 3.1 – Log pH versus aqueous CO_2 concentrations.

3.3.1.2 Total Gas Pressure

A power function was used to evaluate the relationship between total gas pressures and CO_2 concentrations in Site groundwater as it provided the best-fit to the data, as presented in Figure 3.2. When modeled using this function, the total gas pressure versus CO_2 concentration exhibits a high correlation ($R^2 = 0.7048$). Field readings for total gas pressure provide only an estimate of areas with enhanced CO_2, as in situ measurements were impractical due to the larger diameter of the tensionometer relative to most of the monitoring wells. This approximation is evident in the scattered data points present on Figure 3.2. Negative total gas pressures were not included in the correlation because these values were below the calibrated "zero" value. Before measuring total gas pressure the probe was reset to zero using the atmospheric total gas pressure measured at the ground surface.

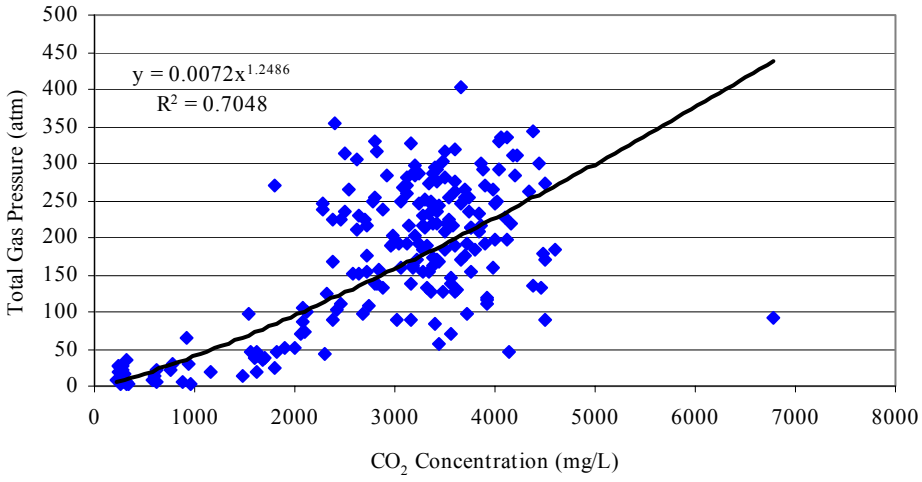

Figure 3.2 – Total gas pressure versus aqueous CO_2 concentrations.

3.3.2 Aqueous Carbon Dioxide

The groundwater samples were analyzed in accordance with the procedure presented in Section 2.4.2.2 to determine the aqueous concentration of CO_2. Each of these CO_2 concentrations was transformed into a CO_2 partial pressure (p_{CO2}) for comparison with the applicable hydrostatic pressure. If a groundwater sample collected at atmospheric pressure had a CO_2 partial pressure above the applicable hydrostatic pressure at depth, the in situ groundwater at that location was supersaturated with CO_2 and in situ gas evolution was possible.

3.3.2.1 Carbon Dioxide Partial Pressure Calculations

Laboratory determined CO_2 concentrations in mg/L were transformed into mol/L using the CO_2 molecular mass (44 g/mol). They are related by

$$CO_2(mol/L) = CO_2(mg/L) \times \frac{mol}{44g} \times \frac{1g}{1000mg}$$ **Equation 3.1**

CO_3^{2-} is neglected in the carbonate equilibria as the pH is < 8. The applicable mass reactions are:

$TIC = H_2CO_3 + HCO_3^-$ **Equation 3.2**

where TIC = Total Inorganic Carbon

CO_2 (g) + $H_2O = H_2CO_3$ **Equation 3.3**

$H_2CO_3 = H^+ + HCO_3^-$ **Equation 3.4**

From Freeze & Cherry (1979) (equations 3.18 and 3.31), we obtain the relation

$$K_{CO_2} = \frac{[H_2CO_3]}{p_{CO_2}}$$ **Equation 3.5**

and

$$K_{H_2CO_3} = \frac{[H^+][HCO_3^-]}{[H_2CO_3]}$$ **Equation 3.6**

If we assume a temperature of 10°C and use the equilibrium constants presented on Table 3.7 in Freeze & Cherry (1979), $K_{CO_2} = 10^{-1.27}$ and $K_{H_2CO_3} = 10^{-6.47}$.

Rearranging equation 3.5 and substituting the equilibrium constant for K_{CO_2}, we obtain

$$P_{CO_2} = \frac{[H_2CO_3]}{10^{-1.27}}$$ **Equation 3.7**

Rearranging equation 3.6 and substituting the equilibrium constant for $K_{H_2CO_3}$, we get

$$[H_2CO_3] = \frac{[H^+][HCO_3^-]}{10^{-6.47}}$$ **Equation 3.8**

Substituting equation 3.8 into equation 3.7 yields

$$P_{CO_2} = \frac{[H^+][HCO_3^-]}{10^{-7.74}}$$ **Equation 3.9**

Rearranging the mass reaction in equation 3.2 gives

$$[HCO_3^-] = [TICO_2] - [H_2CO_3]$$ **Equation 3.10**

Substituting equation 3.10 into equation 3.9 yields

$$p_{CO_2} = \left(\frac{[TICO_2][H^+]}{10^{-7.74}}\right) - \left(\frac{[H_2CO_3][H^+]}{10^{-7.74}}\right)$$ **Equation 3.11**

Rearranging equation 3.7 gives

$$[H_2CO_3] = p_{CO_2} \times 10^{-1.27}$$ **Equation 3.12**

Substituting equation 3.12 into equation 3.11 yields

$$p_{CO_2} = \left(\frac{[TICO_2][H^+]}{10^{-7.74}} \right) - \left(\frac{p_{CO_2} \times [H+] \times 10^{-1.27}}{10^{-7.74}} \right) \qquad \textbf{Equation 3.13}$$

Collecting p_{CO_2} terms in equation 3.13 gives

$$p_{CO_2} \left(1 + \frac{[H^+] \times 10^{-1.27}}{10^{-7.74}} \right) = \left(\frac{[TICO_2][H^+]}{10^{-7.74}} \right) \qquad \textbf{Equation 3.14}$$

Solving for p_{CO_2} yields

$$p_{CO_2} = \frac{[TICO_2][H^+]}{10^{-7.74} + [H^+] \times 10^{-1.27}} \qquad \textbf{Equation 3.15}$$

To calculate p_{CO_2} measured/estimated values of $[TICO_2]$ and $[H^+]$ (pH = -log [H]) were substituted into Equation 3.15. If field pH data were unavailable, pH values were estimated using the derived analytical model obtained using a linear regression model to describe the relationship between log pH and CO_2 concentrations (Section 3.3.1.1). This analytical model resulted in an R^2 value of 0.71, which indicates how closely the estimated values for the trendline correspond to the actual data. An R^2 of <1 is indicative of a relationship that does not completely correlate. Hence, a degree of uncertainty is introduced with the estimated pH values, which is further propagated in the calculated p_{CO_2} values. The p_{CO_2} results are summarized in Table C.1 presented in Appendix C.

3.3.2.2 Hydrostatic Pressure Calculations

CO_2-partial pressures along with the hydrostatic pressures for the shallow and deep monitoring wells were used to locate groundwater zones supersaturated with CO_2 gas. To calculate the hydrostatic pressures, the water temperature and depth to the water table were assumed to be 10°C and 1.0 m bgs, respectively. Shallow and deep monitoring wells, with total depths of approximately 2.5 and 4.0 m bgs, were determined to have gauge pressures of 1.5 m H_2O and 3.0 m H_2O, respectively. Each gauge pressure was converted into an absolute pressure using

$$\text{Abs. Pressure (atm)} = \text{Gauge Pressure (m } H_2O) \times \frac{1\text{ atm}}{10.33\text{ m } H_2O} + 1\text{ atm} \qquad \textbf{Equation 3.16}$$

The hydrostatic pressures for the shallow and deep monitoring wells are 1.145 atm and 1.290 atm, respectively.

3.3.2.3 Comparison of CO_2 Partial Pressures to Hydrostatic Pressures

Computed p_{CO2} values for each monitoring well were compared to the applicable hydrostatic pressure. If p_{CO2} were above the applicable hydrostatic pressure, dissolved CO_2 levels (at a specific monitoring point location) are at supersaturated concentrations, suggesting that CO_2-charged water has the potential to nucleate (form) bubbles in situ.

Monitoring wells screened at ~ 4.0 m bgs (i.e., deep), corresponding to the depth of injection, provided little to no indication of potential to release additional induced CO_2 gas. P_{CO2} for MW-3D and each of the deep wells located 2 – 2.5 m from IP-4 are provided on Figure 3.3. Each of the nearby deep wells had p_{CO2} above the hydrostatic pressure ~ 6 days after injection began. After Day 6, p_{CO2} values within these wells were typically below the hydrostatic pressure. MW-3D (~ 5 m north of IP-4) had potential for CO_2 gas nucleation between 14 and 20 days after commencement of injection. The other deep monitoring wells located 5 – 5.5 m from IP-4 had no evidence of nucleated bubbles, as shown on Figure C.1 located in Appendix C.

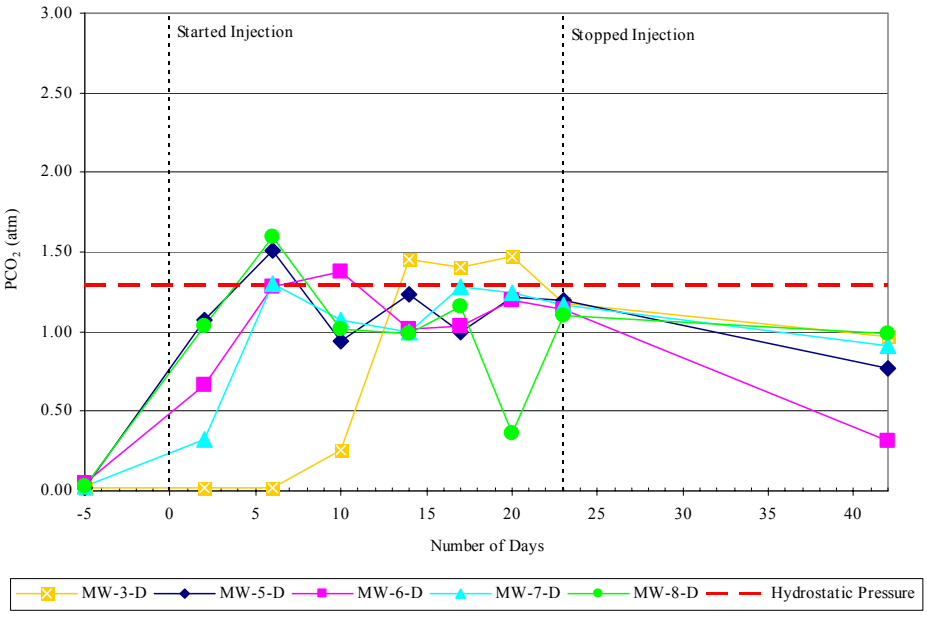

Figure 3.3 – Deep monitoring wells located ~ 2 – 2.5 m from IP-4, with the exception of MW-3D (~ 5.5 m from IP-4), with p_{CO2} above the hydrostatic pressure.

Similarly, shallow monitoring wells located in close proximity to the injection point (~ 2.0 – 2.5 m) suggest the presence of nucleated bubbles 6 days after initiation of the experiment (Figure 3.4). However, the p_{CO2} values indicate that these wells do not consistently have the potential to nucleate bubbles. This lack of consistent response may be due, at least in part, to intermittent injection of CO_2-superaturated water. The shallow wells, located ~ 5.0 – 5.5 m from the injection point, initially indicated potential for bubble formation 14 to 20 days after injection began (Figure 3.4). This nucleation was first evident southwest of the injection point, followed by north, and then northwest of the injection point. None of these wells consistently indicated CO_2 partial pressures above the hydrostatic pressure. The remainder of the shallow wells located further away from IP-4 showed no potential to nucleate CO_2 gas bubbles.

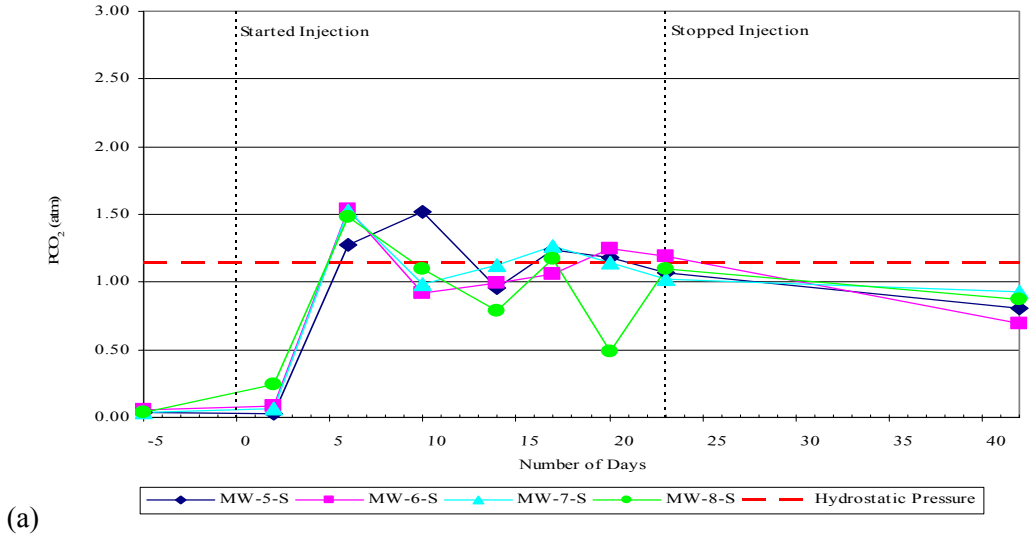

(a)

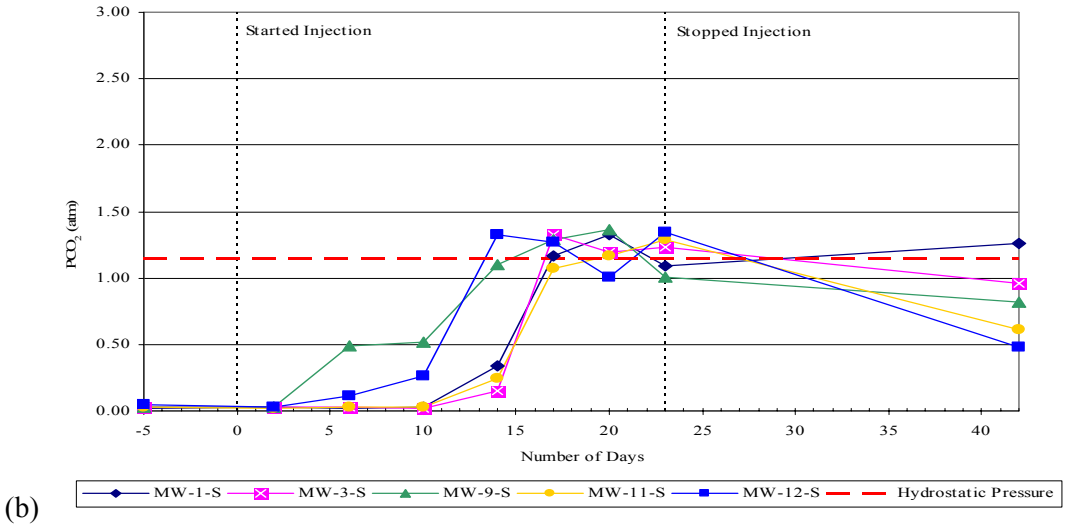

(b)

Figure 3.4 – Shallow monitoring wells located (a) ~ 2 – 2.5 m and (b) ~ 5 – 5.5 m from IP-4 with p_{CO2} above the hydrostatic pressure.

3.3.2.4 CO_2 Gas Distribution

The p_{CO2} time series plots presented in Section 3.3.2.3 were contoured for horizontal slices at 2.5 and 4.0 m bgs using Surfer V.8 (Golden Software, Inc.). These slices correspond to the depths of the shallow and deep monitoring wells, respectively. Slices were prepared for each depth 2, 6, 17, 20, and 23 days after initiation of CO_2-supersaturated water injection. P_{CO2} below the hydrostatic pressure, suggesting no CO_2 gas phase, are shown in blue; whereas exceedances of the hydrostatic pressure are shown in colors ranging from green to red. These exceedances indicate potential for CO_2 gas formation rather than presence of CO_2 gas.

Two days after initiation of injection there was no evidence of potential CO_2 gas formation (Figure 3.5). By Day 6, an elliptical area around IP-4, both at 2.5 and 4.0 m bgs, suggested bubble nucleation was possible at a radial distance of 2 to 2.5 m (Figure 3.6). 17 days into the experiment at the injection depth, CO_2 gas formation was possible in an isolated area north of IP-4, along the northern limit of the study area (Figure 3.7). As we move up vertically to 2.5 m bgs, uniform p_{CO2} both north and west of IP-4, with the exception of the area near MW-11, indicated widespread areas for likely CO_2 gas evolution up to ~ 5 to 5.5 m from the point of injection. At Day 20 the distribution of areas with the potential for CO_2 gas formation at 4.0 m bgs is similar to Day 17 (Figure 3.8). At 2.5 m bgs, CO_2 gas formation is likely in a less laterally extensive area, being limited to the northern limit of the study area. Subsequently, CO_2 gas formation is not evident at 4.0 m bgs. As we move up vertically to 2.5 m bgs, the areal distribution based on potential for CO_2 gas evolution was less extensive laterally with two (2) separate areas, including an isolated area along the northern limit of the study site (previously identified in the deep interval) and an area west of IP-4 (Figure 3.9). This western area is in agreement with borehole GPR data, which indicated CO_2 gas broke through the confining layer located ~ 3 to 3.5 m bgs by Day 23 after initiation of injection. This is discussed in greater detail in Section 3.5.2.

Evaluation of p_{CO2} over time suggests that the radial distance of supersaturated water from the point of injection was at least 2 to 2.5 m at the depth of injection. This corresponds with the radial distance from IP-4 where CO_2 levels decreased below the saturation point. As carbonated water moves further away from the injection point, p_{CO2} are below the hydrostatic pressure until the water ascends. At this point, the hydrostatic pressure decreases, thereby permitting additional release of CO_2 gas until thermodynamic equilibrium is attained again. This is demonstrated in, Figure 3.10 which depicts the maximum possible CO_2 concentration at a given pH is higher in the deeper wells (4.0 m bgs) than the shallower wells (2.5 m bgs). This is consistent with the ability of the carbonated water to release additional CO_2 as the water ascends. Groundwater data indicated irregular release of CO_2 gas at shallower depths during operation of the experiment, which may be attributable, at least in part, to the intermittent injection of carbonated water. However, areas north and west of the point of injection generally have more potential for bubble nucleation.

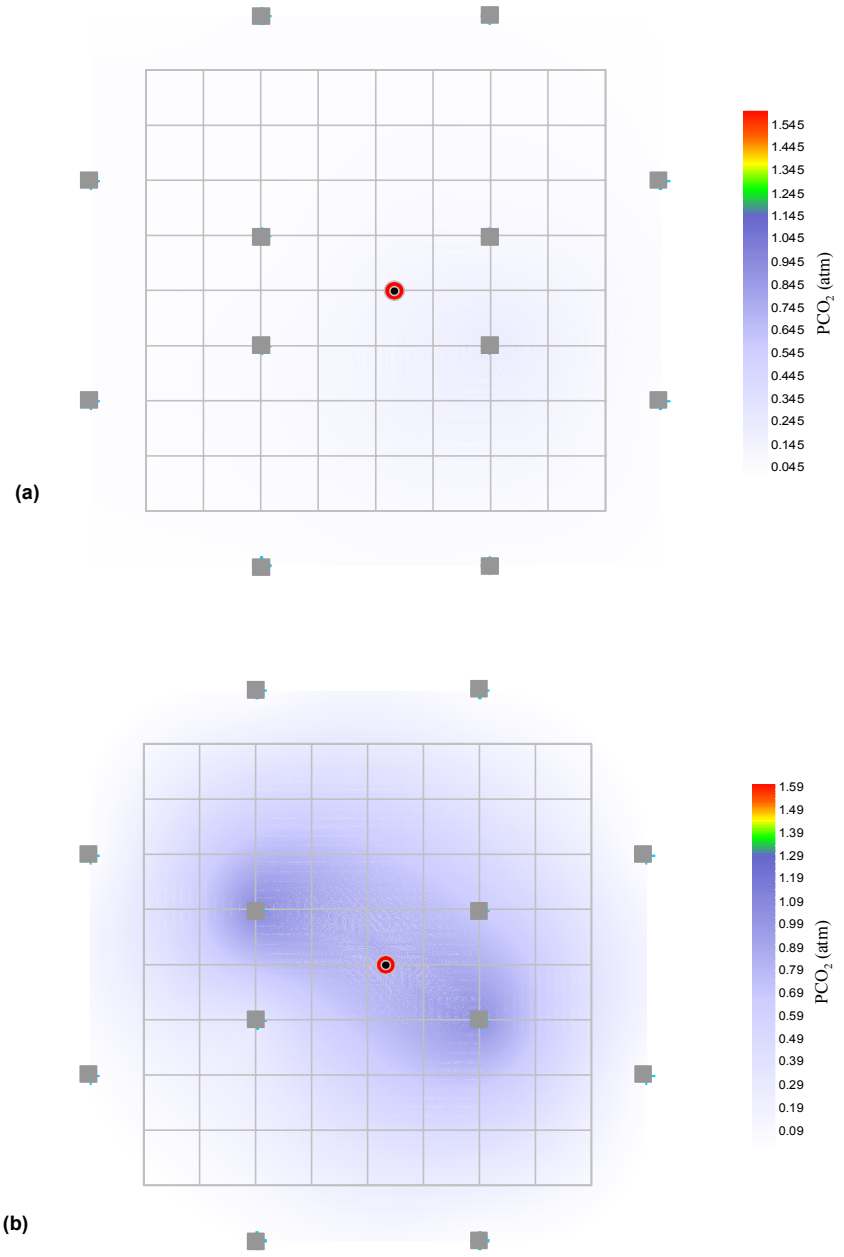

Figure 3.5 – Horizontal slices of estimated CO_2 gas distribution from p_{CO2} measurements, *2 days* after commencing the experiment without hydraulic control, at two depths: a) 2.5 m bgs and b) 4 m bgs (depth of injection). The (■) symbol indicates a monitoring well location. The applicable hydrostatic pressures are 1.145 atm and 1.290 atm for the shallow and deep depths, respectively. P_{CO2} measurements above these values indicate potential CO_2 gas evolution.

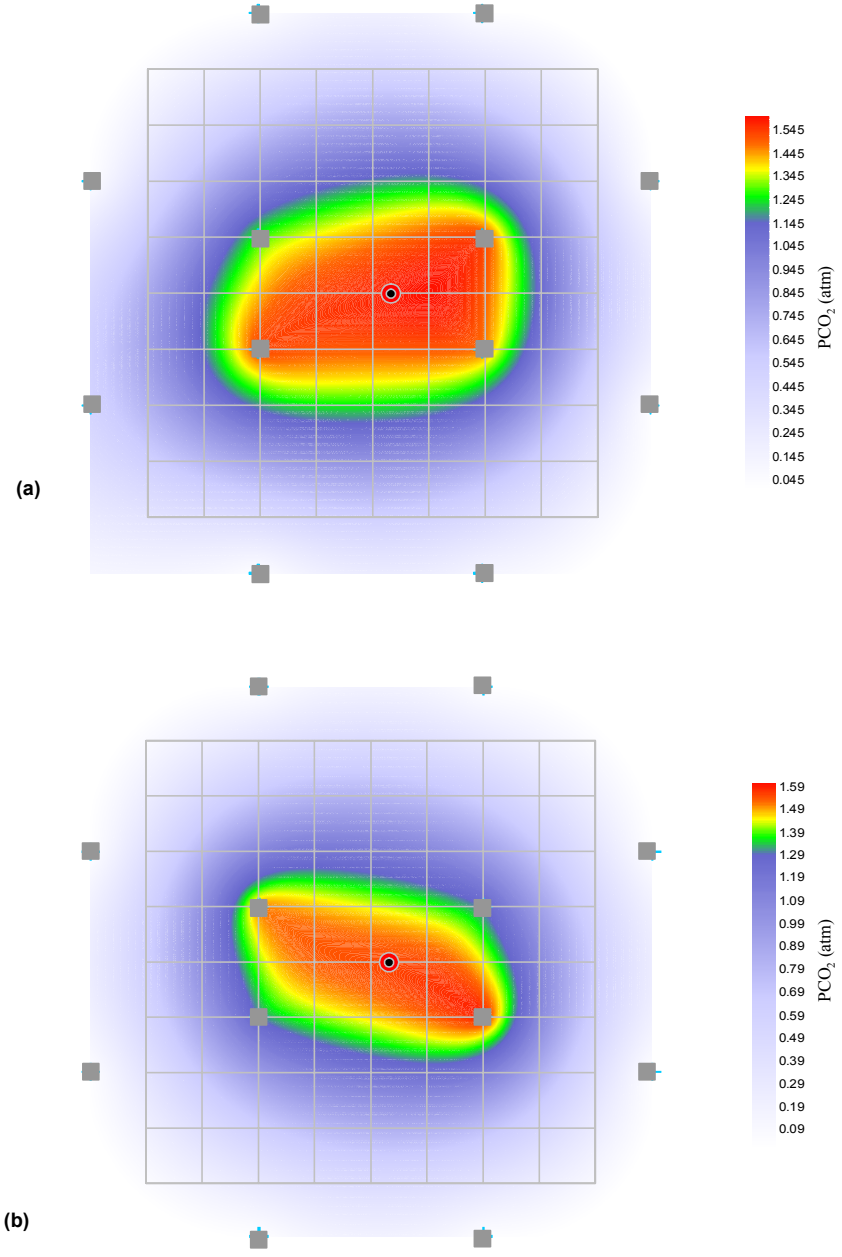

Figure 3.6– Horizontal slices of estimated CO_2 gas distribution from p_{CO2} measurements, *6 days* after commencing the experiment without hydraulic control, at two depths: a) 2.5 m bgs and b) 4 m bgs (depth of injection). The (■) symbol indicates a monitoring well location. The applicable hydrostatic pressures are 1.145 atm and 1.290 atm for the shallow and deep depths, respectively. P_{CO2} measurements above these values indicate potential CO_2 gas evolution.

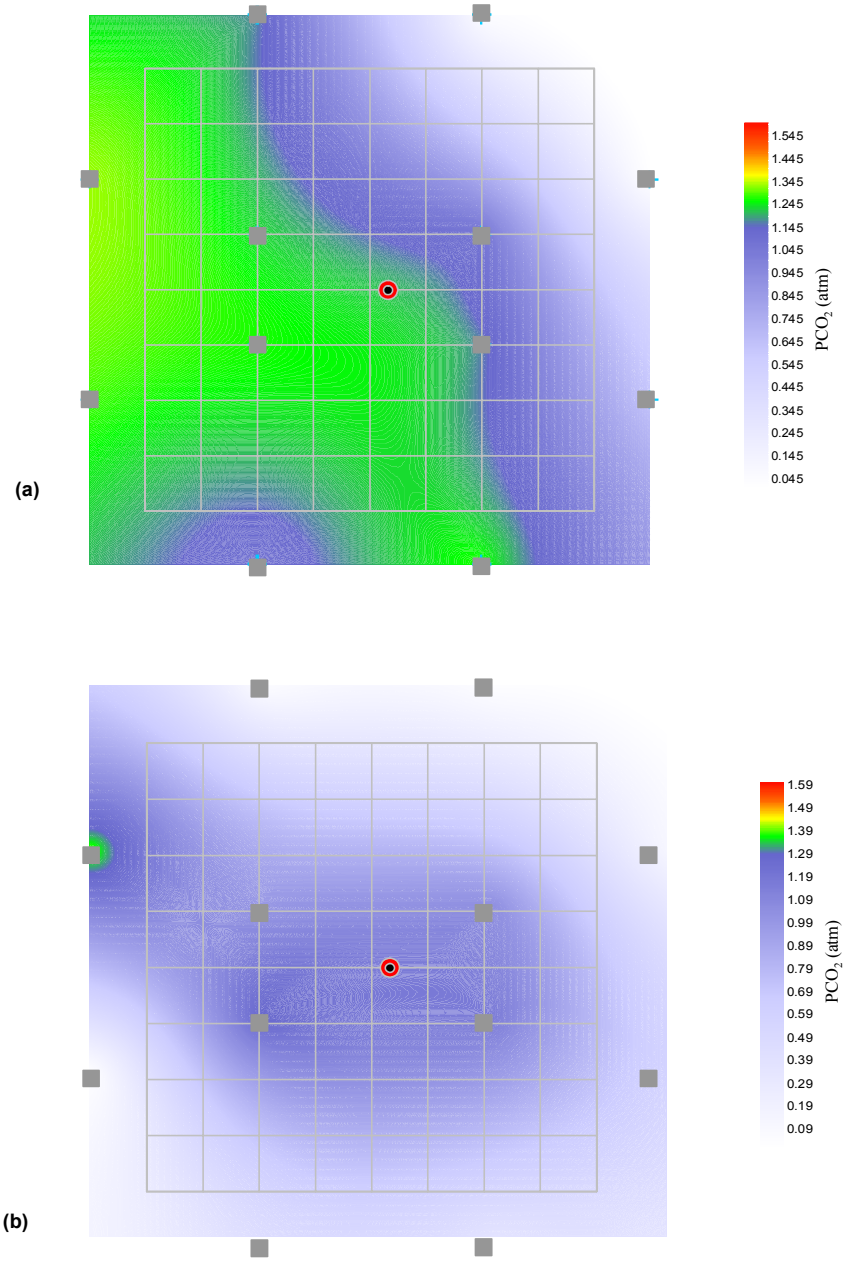

Figure 3.7 – Horizontal slices of estimated CO_2 gas distribution from p_{CO2} measurements, *17 days* after commencing the experiment without hydraulic control, at two depths: a) 2.5 m bgs and b) 4 m bgs (depth of injection). The (■) symbol indicates a monitoring well location. The applicable hydrostatic pressures are 1.145 atm and 1.290 atm for the shallow and deep depths, respectively. P_{CO2} measurements above these values indicate potential CO_2 gas evolution.

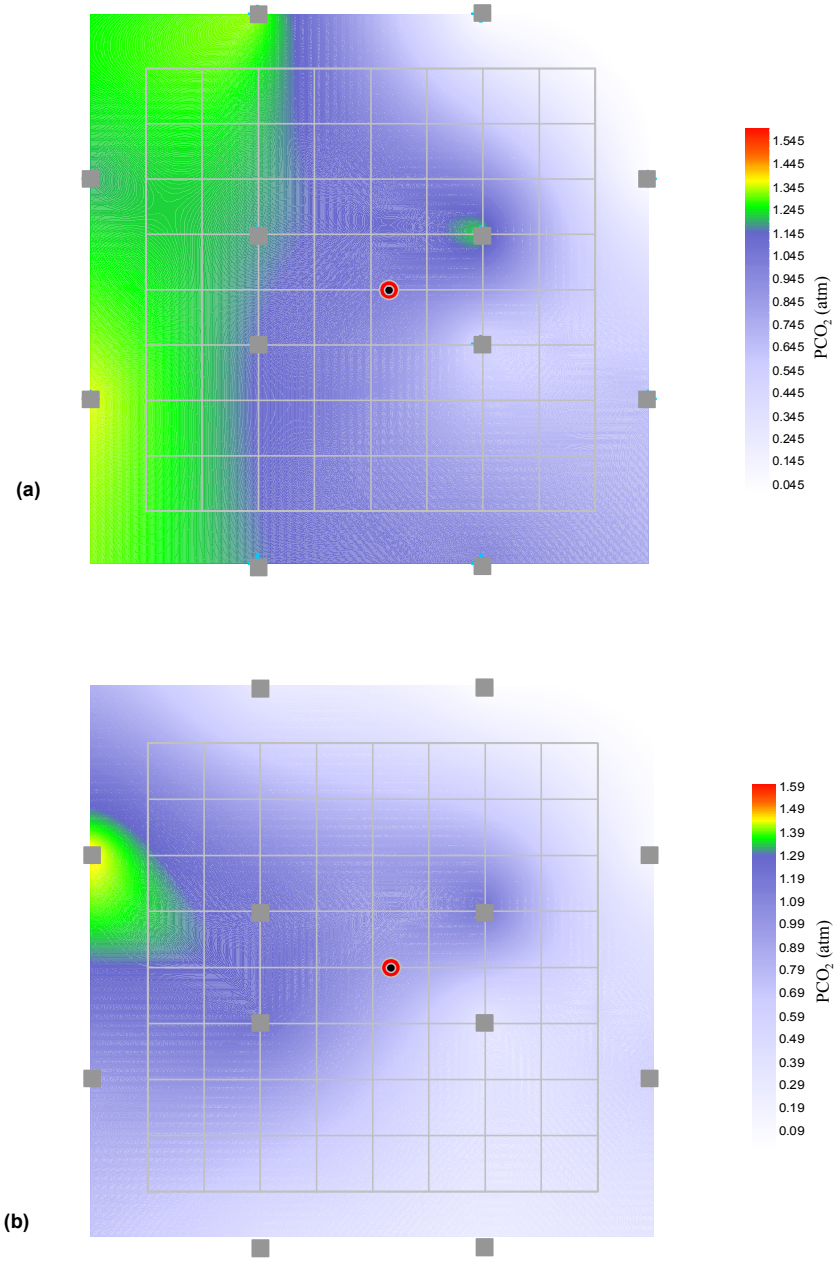

Figure 3.8 – Horizontal slices of estimated CO_2 gas distribution from p_{CO2} measurements, *20 days* after commencing the experiment without hydraulic control, at two depths: a) 2.5 m bgs and b) 4 m bgs (depth of injection). The (■) symbol indicates a monitoring well location. The applicable hydrostatic pressures are 1.145 atm and 1.290 atm for the shallow and deep depths, respectively. P_{CO2} measurements above these values indicate potential CO_2 gas evolution.

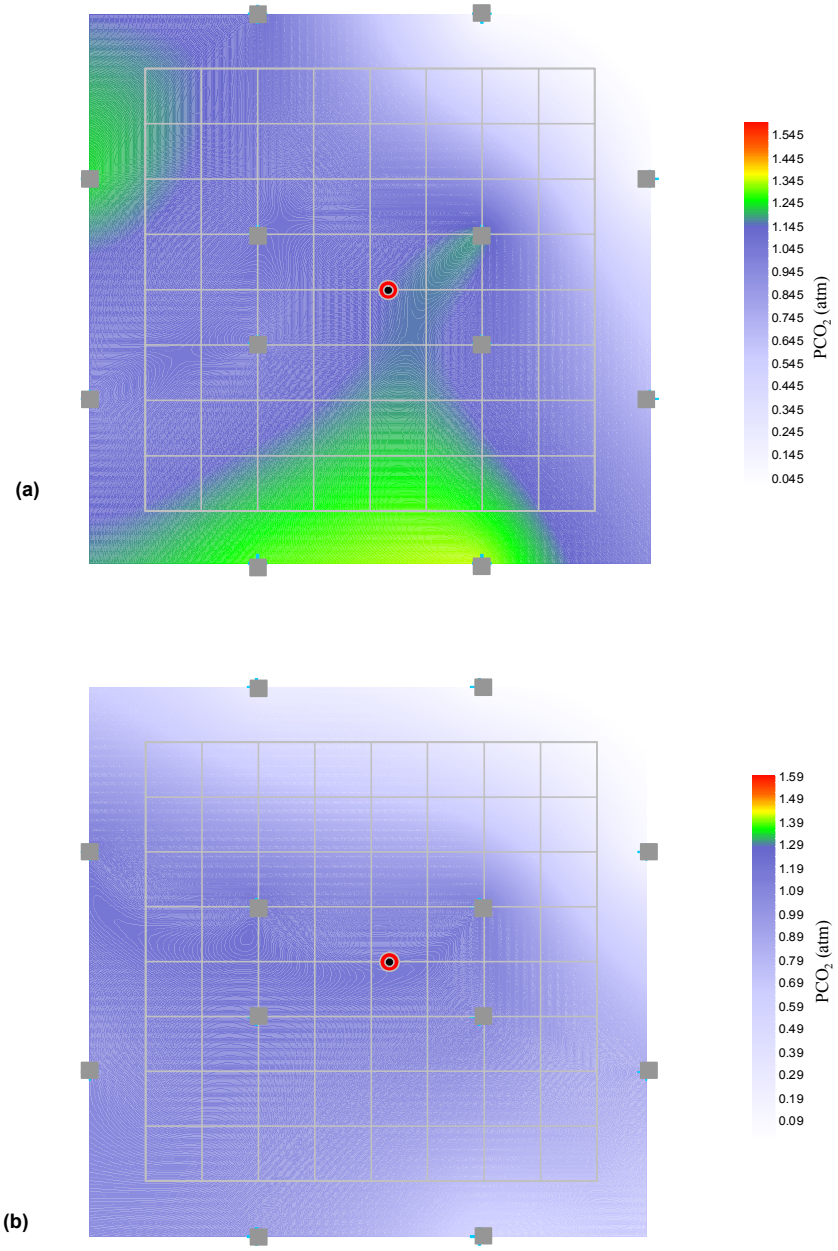

Figure 3.9 – Horizontal slices of estimated CO_2 gas distribution from p_{CO2} measurements, *23 days* after commencing the experiment without hydraulic control, at two depths: a) 2.5 m bgs and b) 4 m bgs (depth of injection). The (■) symbol indicates a monitoring well location. The applicable hydrostatic pressures are 1.145 atm and 1.290 atm for the shallow and deep depths, respectively. P_{CO2} measurements above these values indicate potential CO_2 gas evolution.

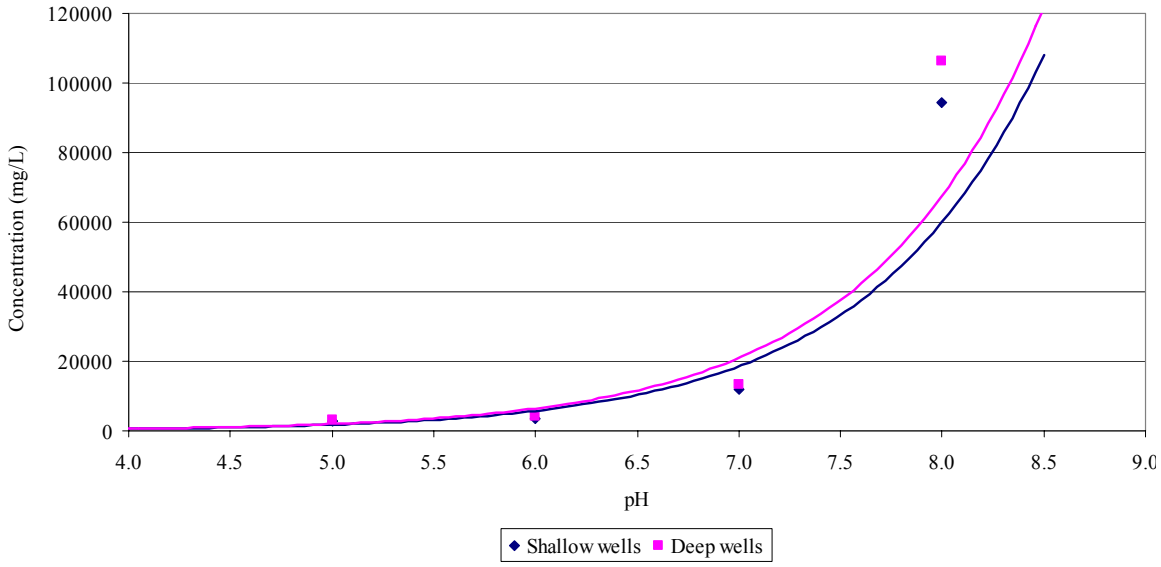

Figure 3.10 – Maximum concentration of CO_2 dissolved in groundwater at specific pH values for shallow and deep wells. Concentrations above these levels are thermodynamically unstable. Deep wells have larger hydrostatic pressures and are therefore able to dissolve more CO_2.

3.4 Hydraulic Monitoring

A 96 period moving average was used to smooth out the sinusoidal pattern evident in the hydraulic monitoring data (Figure 3.11). This pattern was caused by barometric changes over a 24-hour period. By removing the influences of barometric pressure it was possible to identify changes in head due to the experiment.

Each monitoring well experienced a sudden increase in head due to the initiation of water injection (Day 0). During CO_2-charged water injection, heads in couplet MW-6 (royal blue and cyan on Figure 3.11) are similar with small downward gradients typically present. The head in couplet MW-2 (orange and magenta on Figure 3.11) is normally higher in the shallow (orange) monitoring well (i.e., strong downward gradient), which may be due to a lower permeability peat layer present between the screened intervals. This layer is discussed in detail in Section 5.0. Experiment shutdowns that were due to difficulties with continual injection are visible in the hydraulic monitoring data and were used to determine the duration of each shutdown.

3.5 Geophysical Surveys

The University of Waterloo Environmental Geophysics Facility performed and processed the geophysical surveys in accordance with the procedure presented in Section 2.4.4 to determine the presence of CO_2 gas.

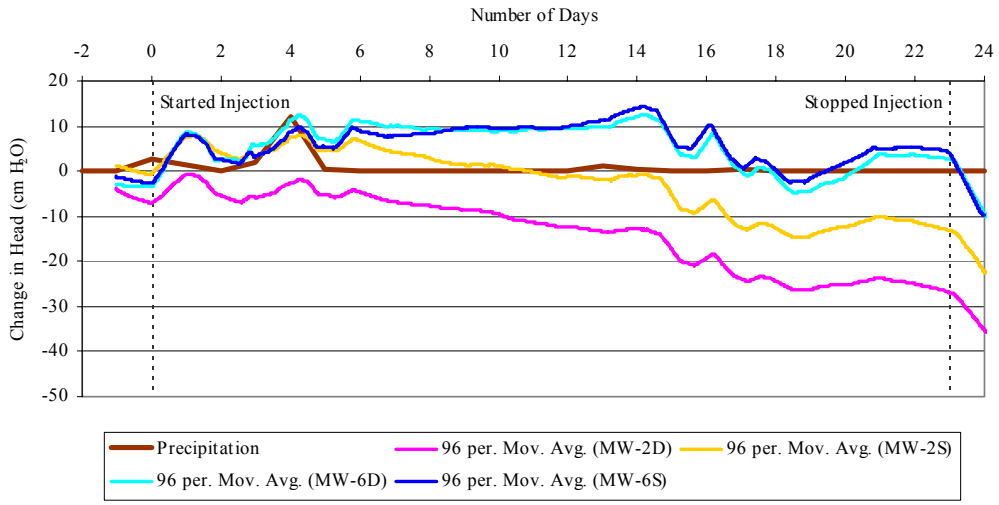

Figure 3.11 – Hydraulic monitoring data for experiment without hydraulic control.

3.5.1 Surface GPR Results

GPR reflections profiles, which show the cross-sectional image produced from the reflections below the survey line, were plotted with each trace downward as a function of time and/or depth. Each trace was plotted side by side horizontally according to position from left to right. The initial background surface GPR survey line 1a1 (near the western limit of the study area) performed prior to the monitoring network installations, indicates fairly homogeneous lithology, with some cross-bedding, down to ~ 3.0 m bgs. At 3.5 m bgs, there is a strong reflection representing a change in water content (Figure 3.12), due to a significant stratigraphic boundary. Below this interface, the radar stratigraphy consists of horizontal bedding. This is consistent with borehole GPR and hydraulic conductivity data. These data are discussed in greater detail in Sections 3.5.3 and 5.0, respectively.

The reflection present at 3.5 m bgs near the western limit of the study area is also evident 2.5 m east (near GP-13 to GP-15) of line 1a1, but disappears by 5 m (near the main line of the access tubes). This reflection is absent in the perpendicular survey lines (east to west).

Background data acquired subsequent to the installation of the monitoring points shows interference from the PVC monitoring points in each of the survey lines. This is substantiated with the peaks present near the ground surface at the access tube locations and the attenuated data with depth (Figure 3.13).

The orientation of the survey lines relative to the GP access tubes was adjusted prior to injection to minimize interference from the geophysical access tubes (Figure E.10 in Appendix E). These survey lines ran diagonally across the study area from west to east. Reflections evident prior to injection were attenuated during the experiment, with most of the reflectors being nearly absent by the end of the experiment (Figure 3.14). The reason for this attenuation is unknown.

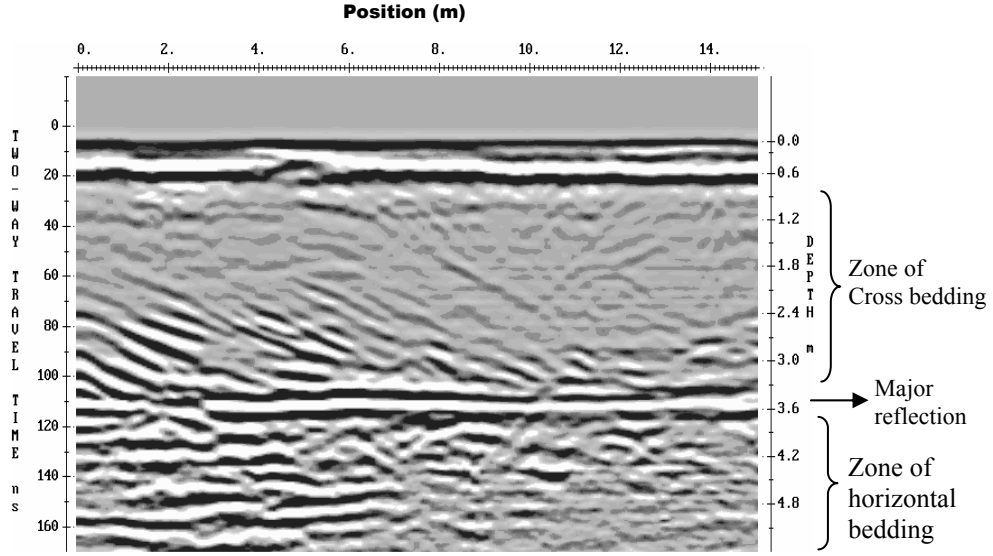

Figure 3.12 – Ground penetrating radar survey at 200 MHz for line 1a1 (near access tubes GP-16 to GP-18) prior to geophysical access tube installations. A spherical spreading, exponential compensation (SEC) gain function (maximum gain 3000 and attenuation 2.7 db/min) was used to process the GPR data.

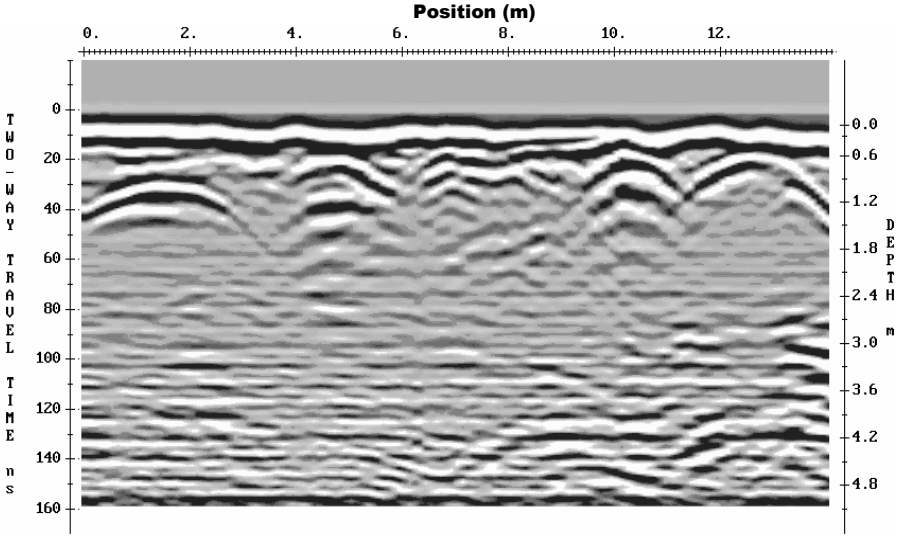

Figure 3.13 – Ground penetrating radar survey at 200 MHz for line 1b2 (near access tubes GP-7 to GP-12) subsequent to geophysical access tube installations, but prior to injection of CO_2-supersaturated water. A SEC gain function (maximum gain 500 and attenuation 2.7 db/min) was used to process the GPR data.

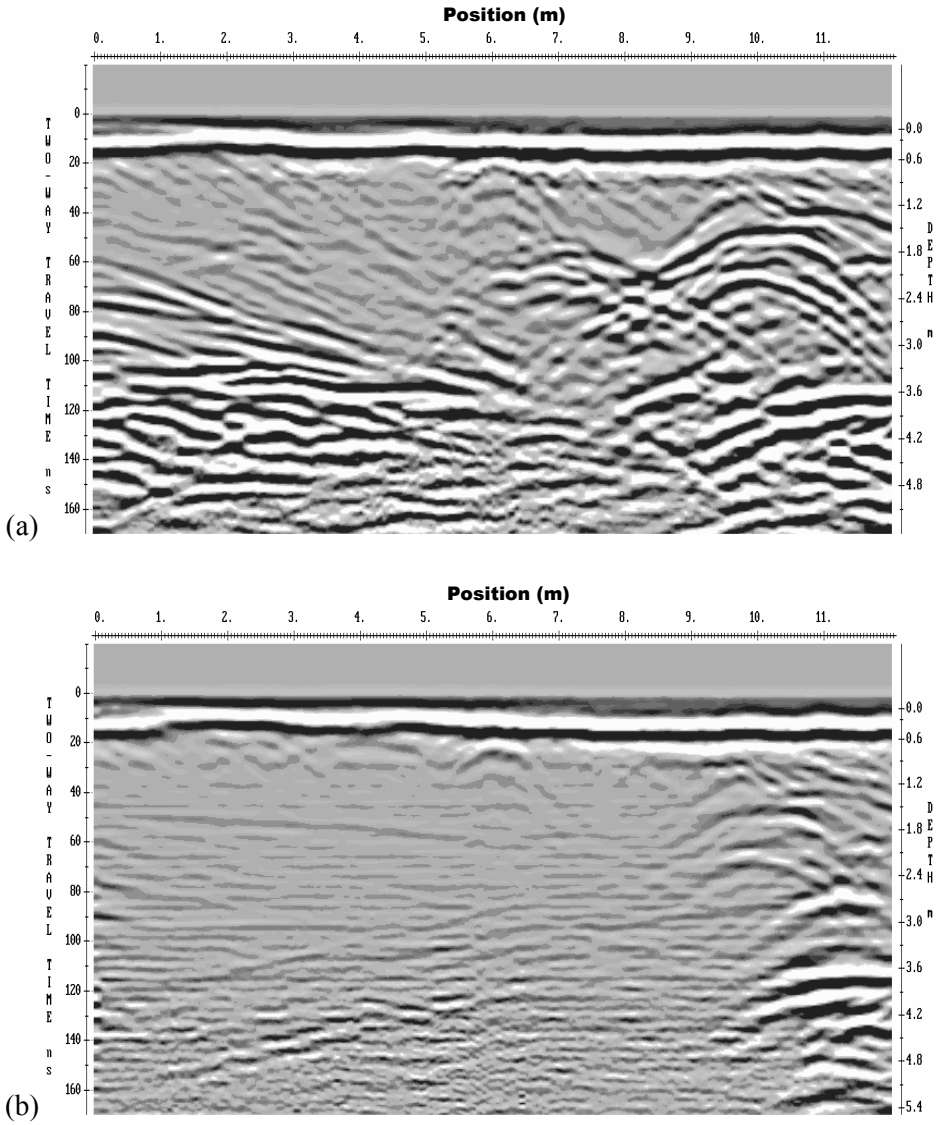

Figure 3.14 – Ground penetrating radar survey at 200 MHz for line 1 (diagonal from near GP-16 to GP-3) showing attenuation of reflections between (a) April 21, 2005 (before injection) and (b) May 30, 2005 (20 days after initiation of injection). A SEC gain function (maximum gain 3000 and attenuation 2.7 db/min) was used to process the GPR data.

3.5.2 Cross-borehole GPR Results

3.5.2.1 Zero-Offset Profile Results

ZOP water content profiles provide an indication of natural water content variations within the study area, indicating the presence of CO_2 gas.

3.5.2.1.1 Initial Water Contents

Background ZOP surveys were performed on 37 access tube pairs, prior to initiation of the injection experiments to establish initial water content conditions. The water content values measured between access tube pairs, 0.5 m below the average water table depth of 1.0 m bgs (1.5 m bgs), varied between approximately 0.376 and 0.482, with an average water content of 0.425. Background water contents for access tube pairs that included GP-2 or GP-13 were not included in the range or average water content because each of these locations was damaged during their installation. Although the absolute water content values for GP-2 and GP-13 are probably not accurate, changes in water content over time from in situ CO_2 gas evolution should still be evident. Representative background water content profiles are provided in Figure 3.15. Irregular water content profiles were investigated further by coring and subsequent hydraulic conductivity testing of soil samples. The results are discussed in Section 5.0.

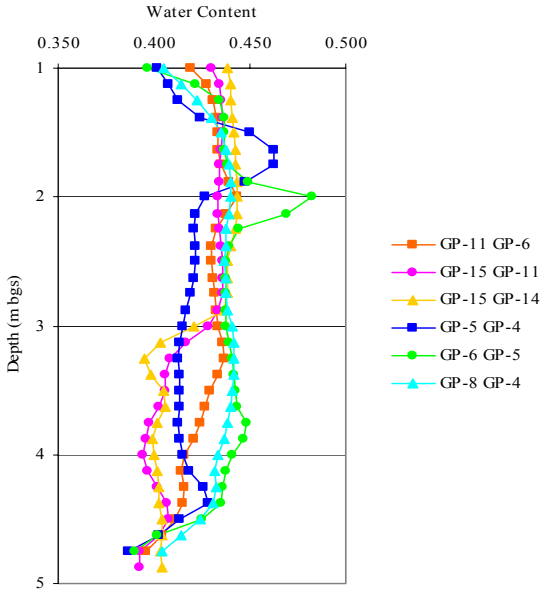

Figure 3.15 – Representative background ZOP water content profiles.

3.5.2.1.2 CO_2 gas Distribution

Water content variations over time due to in situ CO_2 gas evolution were determined for each ZOP profile by taking the difference between the background water content profile and the profiles measured during injection of the CO_2-supersaturated water. These profiles show a decrease in water content (i.e. increase in gas content) as negative while an increase is positive. The resulting water content change profiles suggest the presence of trapped CO_2 gas beneath a barrier on the western side of the Site. The maximum accumulation occurred at ~ 3 – 3.5 m bgs, 6 days after injection commenced. In Figure 3.16 trapped CO_2 gas pockets are shown as sharp peaks indicating an abrupt increase in gas content (i.e. decrease in water content) below the trapping layer. Collapse of this CO_2

gas pocket was clearly evident 23 days after injection began (Figure 3.16) by the smaller size of the peak indicating less gas content. P_{CO2} data for the same day indicate supersaturated concentrations above the trapping layer, which may be due to the collapse of the gas pocket.

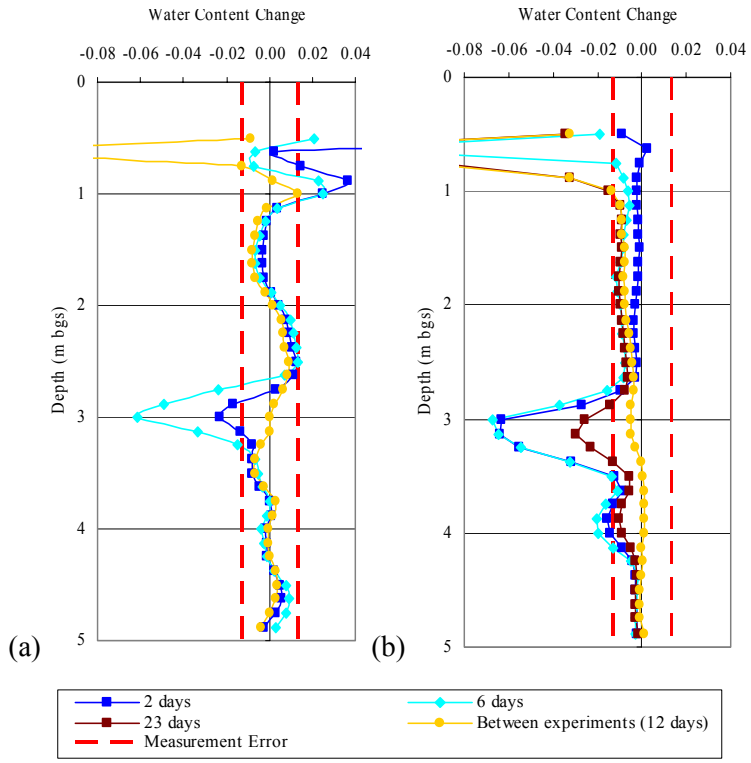

Figure 3.16 – Water content change profiles from ZOP borehole GPR data showing the maximum water content changes. (a) GP-17/GP-14, (b) GP-14/GP-9.

The water content change profiles were converted into CO_2 gas saturation profiles by dividing the differenced profiles by the porosity profile (i.e., initial water content profiles). The CO_2 gas saturation profiles were contoured for horizontal slices at 2.5 m bgs, 3.0 m bgs, and 4.0 m bgs using Surfer V.8. The depths of the horizontal slices were selected to correspond to 1) the depth of the shallow monitoring wells, as well as being above the confining layer causing the accumulation of CO_2 gas, 2) the maximum amount of CO_2 trapped, and 3) the depth of injection, respectively. Each of these horizontal slices was prepared for 2, 6, and 23 days after injection began to demonstrate CO_2 gas distribution with time. At 2 days, the CO_2 gas distribution inferred from the ZOP data indicated low CO_2 gas saturation at 4.0 m bgs over a laterally extensive area with a spherical high extending 2 – 2.5 m from IP-4 to the west (Figure 3.17). The maximum CO_2 gas content was 9.4%. As we move vertically up to 3.0 m, the distribution is not as laterally extensive, being confined to the western side of the study site. The distribution area is larger, with a more elongated spherical shape extending to and beyond the western limit. The maximum CO_2 gas content was ~14.5%, which corresponds with

the approximate depth of the trapping layer evident on the water content change profiles. At 2.5 m bgs, the CO_2 gas distribution is laterally limited with uniform levels asymmetric around the injection point, extending 0.5 to 2.5 m from IP-4. The maximum CO_2 gas content at this depth is ~1.2%.

By 6 days after injection began at 4 m bgs (Figure 3.19c), the CO_2 gas distribution is less extensive laterally on the eastern side of the site. The maximum CO_2 gas saturation, at 6 days, is 15.3% at 3 m bgs. The size and maximum CO_2 gas content of the spherical area is similar to that observed 2 days after injection began. At 3.0 m bgs (Figure 3.19b), the distribution remains limited to the western portion of the site. However, the spherical area has expanded and is more parabolic in shape, extending to and past the western edge of the study area. As we move up vertically to 2.5 m bgs (Figure 3.19a), the distribution remains laterally limited and asymmetric around the injection point; however, the radial distance varies from 1.0 to 2.0 m from IP-4.

On Day 23 of the experiment, the CO_2 distribution is not as extensive at 4 m bgs and is uniform with the absence of the spherical high gas content previously present (Figure 3.19c). The maximum distance from IP-4 is at least 3.0 m. Similarly at 3.0 m bgs (Figure 3.20b), CO_2 gas content is uniform with no evidence of the previously present parabolic shaped gas high. CO_2 gas is present at least 4.0 m from IP-4. At 2.5 m bgs, CO_2 gas distribution remains asymmetric around the injection point; however, it is more extensive with the long-axis now extending to and beyond the southwestern edge of the study area (Figure 3.20a). The general gas distribution suggests collapse of the deeper accumulation of CO_2 gas and upward migration. The maximum CO_2 gas saturation at 23 days is 5.9% at 3 m bgs between geophysical access tube pair GP-14/GP-9.

3.5.2.2 Multiple-Offset Gather

CO_2-saturation images inferred from the borehole GPR data using the MOG acquisition mode provide an indication of water content variations within the study area resulting from the presence of CO_2 gas.

Background water content values measured between access tube pairs, 0.5 m below the approximate average water table depth of 1.0 m bgs (1.5 m bgs), varied between approximately 0.369 and 0.473, with an average water content of 0.422. This value is comparable with the average water content (0.425) obtained with the ZOP acquisition mode. These background water contents were interpolated and plotted using TRANSFORM to generate 2-D contoured images of the water content in the plane through the main line of the study area (Appendix G).

However, the MOG acquisition mode was not used to obtain borehole GPR data during injection; therefore, no CO_2 gas distribution information is available for this method.

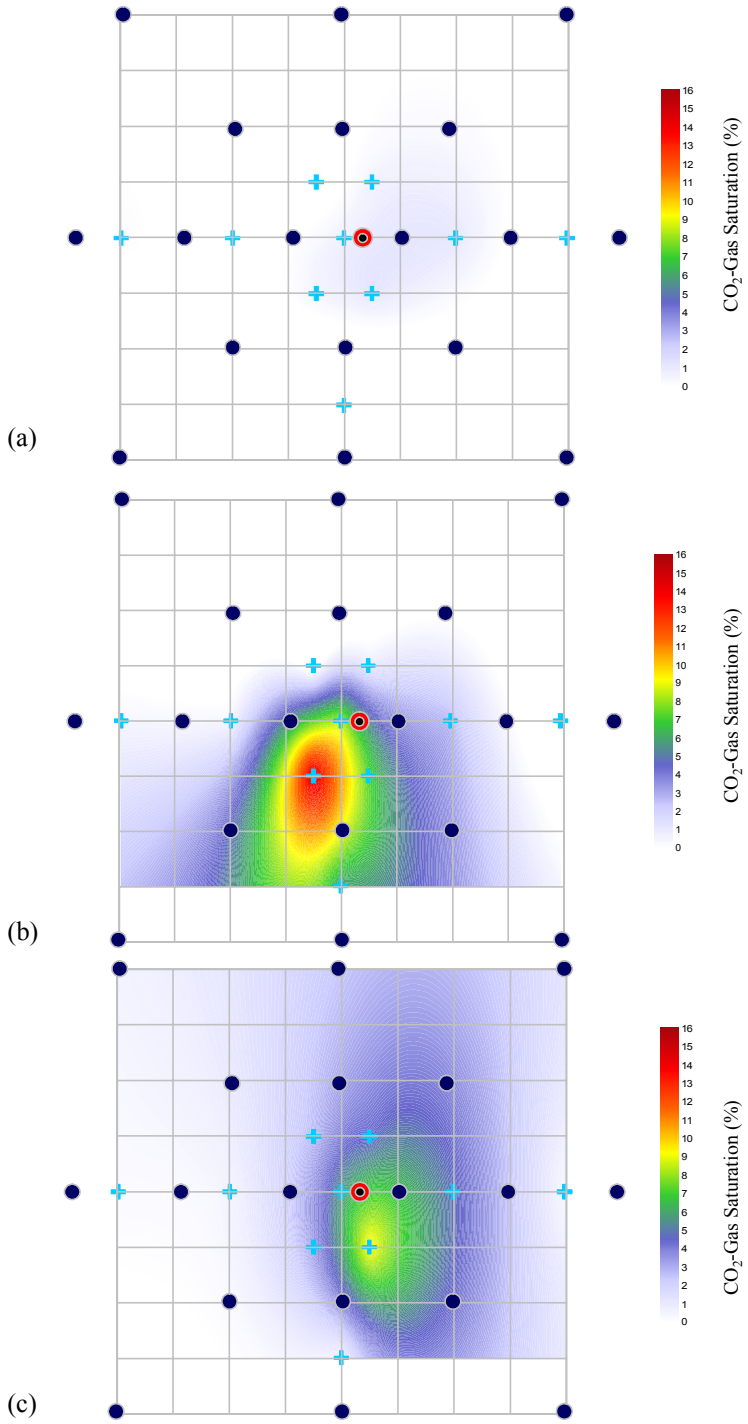

Figure 3.17 – Horizontal slices of estimated CO_2 gas distribution from ZOP borehole GPR measurements, 2 days after commencing experiment the without hydraulic control at three depths: a) 2.5 m bgs; b) 3.0 m bgs; and c) 4 m bgs (depth of injection). The (+) symbol indicates the mid-point between access tube pairs where GPR data were collected.

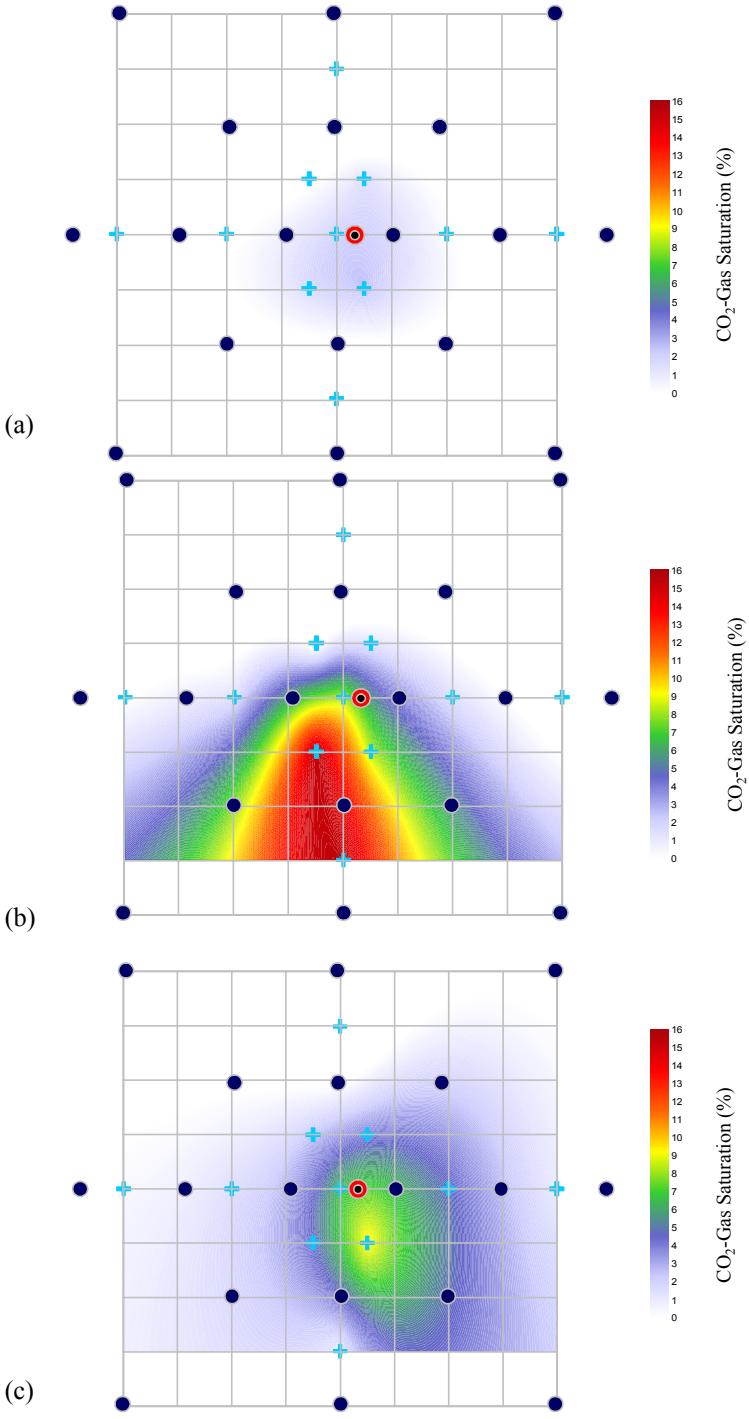

Figure 3.18 – Horizontal slices of estimated CO_2 gas saturation distribution from ZOP borehole GPR measurements, 6 days after commencing the experiment without hydraulic control at three depths: a) 2.5 m bgs; b) 3.0 m bgs; and c) 4 m bgs (depth of injection). The (+) symbol indicates the mid-point between access tube pairs where GPR data were collected.

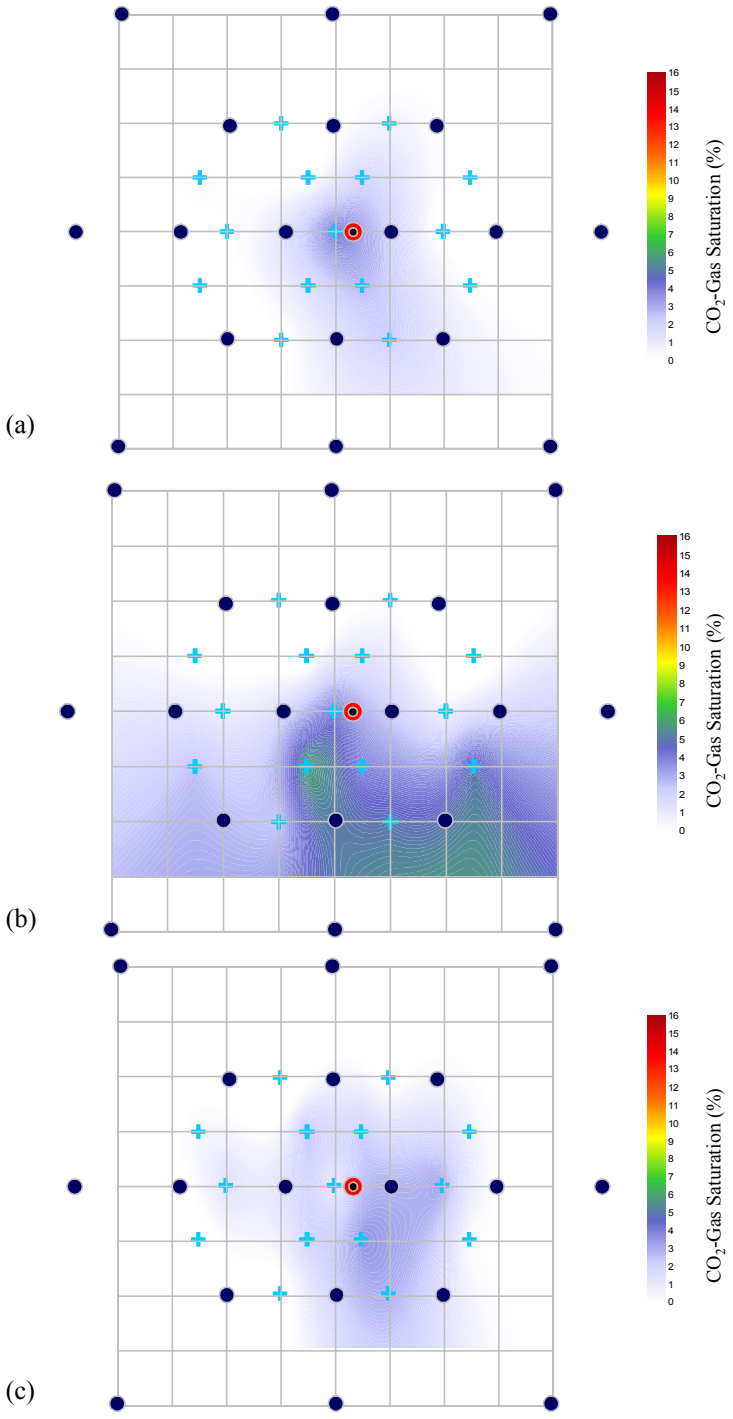

Figure 3.19 – Horizontal slices of estimated CO_2 gas distribution from ZOP borehole GPR measurements, 23 days after commencing the experiment without hydraulic control at three depths: a) 2.5 m bgs; b) 3.0 m bgs; and c) 4 m bgs (depth of injection). The (+) symbol indicates the mid-point between access tube pairs where GPR data were collected.

3.5.3 Neutron Measurements - CPN Model 503DR Hydroprobe

Neutron measurements water content profiles are another method for evaluating background water content variations within the study area and the presence of CO_2 gas.

3.5.3.1 Background Water Contents

Background neutron measurements was performed in 11 of the geophysical access tubes prior to initiation of the injection experiments to establish background water content conditions 0.5 m below the approximate average water table depth of 1.0 m bgs (1.5 m bgs). These background water content values were between 0.330 and 0.426, with an average water content of 0.350. These values are less than the average water contents obtained from the ZOP and MOG measurements. This difference is attributable, in part, to the different methods used to obtain these water contents. Although the background water content values may not be accurate, changes in water content over time due to in situ CO_2 gas evolution should still be evident and comparable to the ZOP determined values.

3.5.3.2 CO_2 Gas Distribution

Water content variations over time were obtained for each neutron measurement profile by taking the difference between the background water content profile and the profiles measured during injection of the CO_2-supersaturated water. These profiles show a decrease in water content (i.e. increase in gas content) as negative, while an increase is positive. The largest water content change is similar to that obtained from the ZOP survey method; however, there are significant differences between the results for the two methods. According to the ZOP method, access tube pair GP-10/GP-9 had the maximum water content change at 3.13 m bgs on both Day 2 and 6 after injection started. In contrast, the neutron measurements show a similar magnitude of change at 3.45 m bgs, on Day 2 after initiation of injection (Figure 3.20). These differences may be partially attributable to the nature (size/shape/volume) of the zones of influence measured by the two methods. The CPN tool measures only close to the access tube (~0.13 m radius), while GPR measures the plane between the access tube pair.

The water content change profiles were converted into CO_2 gas saturation profiles by dividing the water content change profiles by the porosity profile (i.e., background water content profile). The CO_2 gas saturation profiles were contoured for a cross-section through the main line of access tubes (GP-7 through GP-12) for Day 2 after the injection commenced. These plots further demonstrate the discrepancies between the ZOP and neutron measurements. The ZOP mode measurements were plotted as the midpoint between the access tube pair; whereas neutron measurements were plotted at the access tube location. Plotting the ZOP data as the midpoint neglects the fact that it is an ellipsoidal volume of soil that is measured with each ZOP ray path. The ZOP data indicate a larger area of influence around the injection point compared to the CPN data which may be due to the presence of more CO_2 gas between the access tube pairs. The small change in CO_2-saturation near the access tube in Figure 3.22b using the CPN tool may not be detected by the borehole GPR because the GPR method averages the water content over a much larger area. Another consideration is the

amount of scatter present in most of the CPN measurements and the fact that the measurements were not as repeatable as the borehole GPR data. The lack repeatable for the neutron measurements makes them less reliable than the borehole GPR data.

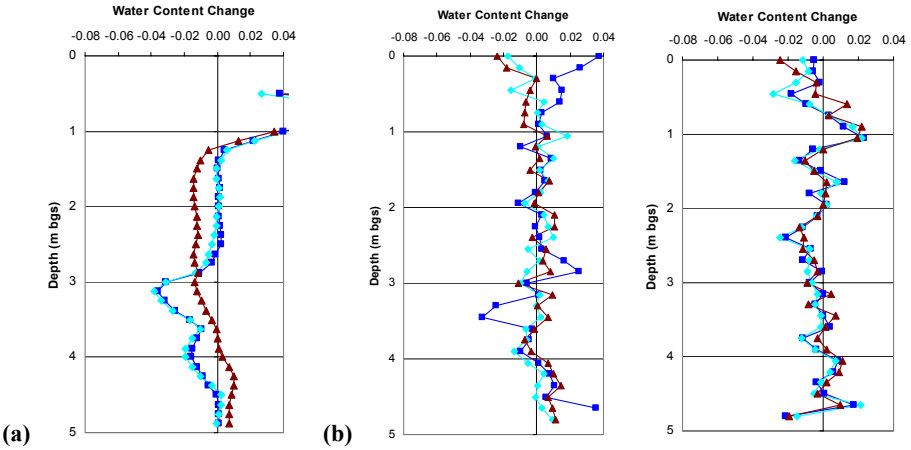

Figure 3.20 – Comparison of change in water content for cross-borehole GPR (ZOP) and CPN neutron measurements. (a) ZOP mode for GP-10/GP-9, (b) CPN for GP-9 and GP-10.

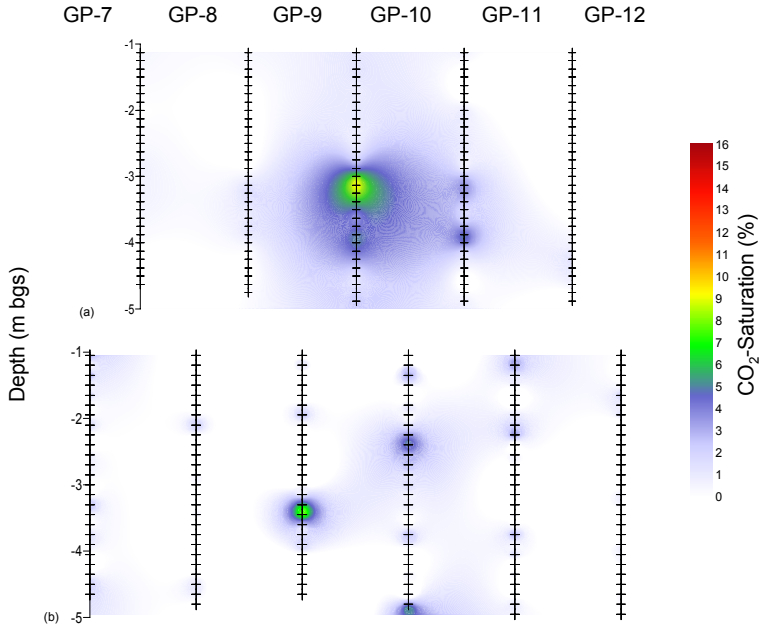

Figure 3.21 – Cross-sections of estimated CO_2 gas distribution 2 days after commencing experiment from (a) ZOP borehole GPR measurements; b) neutron measurements. The (+) symbol in (a) indicates the mid-point between access tube pairs where GPR data were collected and in (b) indicates an access tube location where CPN data were collected.

Chapter 4

Injection of Carbonated Water with Hydraulic Control

4.1 Scope

To determine the influence of pumping on the lateral distribution of evolved CO_2 gas, water was extracted from two wells while simultaneously injecting CO_2-supersaturated water at one injection point. Similar to the passive injection experiment, a ZOI was estimated using geophysical tools and groundwater monitoring for CO_2.

4.2 Process Data

Process data are summarized in Table B.2 in Appendix B. Injection of carbonated water with hydraulic control occurred over 17 days. However, problems were evident during implementation of the experiment and were subsequently observed in the data evaluated. During the experiment, less CO_2 gas appeared to be dissolving in the water, although the pressure and flow rate of water and CO_2 were consistent with the passive injection experiment. This apparent decrease in CO_2 dissolution was corroborated by the results of the data evaluation, which indicated no impact on the lateral distribution of evolved CO_2 gas as a result of pumping.

4.3 Groundwater Quality Samples

Groundwater quality samples were collected and analyzed in accordance with the procedure described in Section 2.4.1. Each CO_2 concentration (in mg/L) was converted to a CO_2 partial pressure using the method discussed in Section 3.3.2.1. The resultant p_{CO2} were compared to the applicable hydrostatic pressures and the findings are discussed below.

4.3.1 Comparison of CO_2 Partial Pressures to Hydrostatic Pressures

Each of the shallow and deep wells located ~ 2 – 2.5 m from IP-4 had p_{CO2} below the applicable hydrostatic pressure for the duration of the experiment (Figure 4.1). These p_{CO2} are indicative of no potential to nucleate bubbles in situ.

In contrast, the passive injection experiment suggested induced CO_2 gas at least 2 to 2.5 m from IP-4 at the depth of injection (4.0 m bgs) and out to 5 – 5.5 m at a shallower depth (2.5 m bgs). Active injection was expected to at least produce a similar ZOI. The data and field observation that less CO_2 gas was being dissolved in the water by the GI generator are consistent with a smaller ZOI.

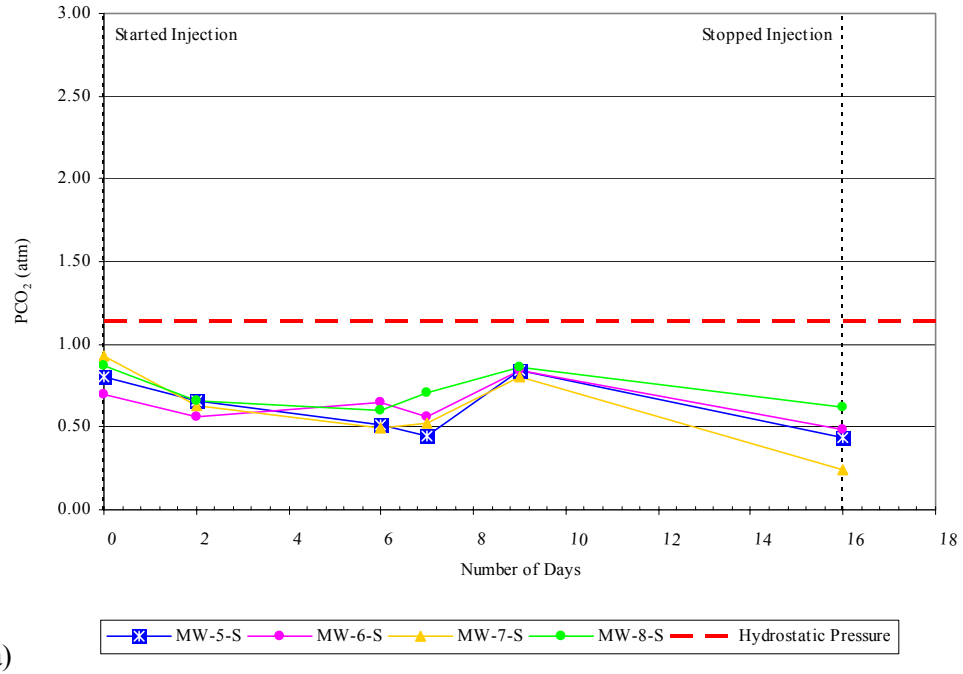

(a)

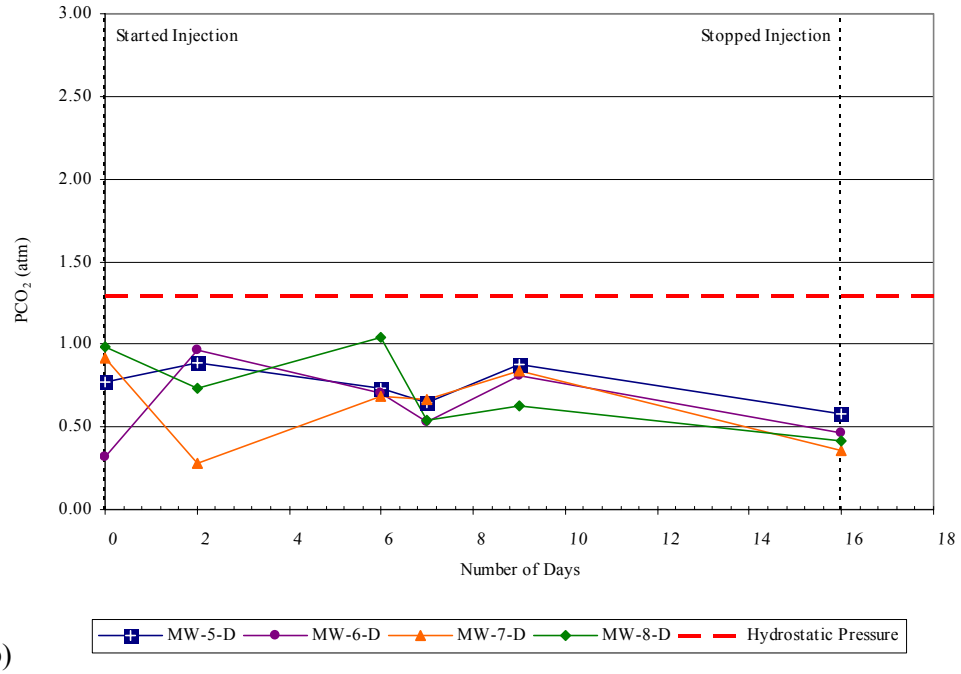

(b)

Figure 4.1 – P_{CO2} in the monitoring wells located ~ 2 – 2.5 m from IP-4 (a) shallow wells screened at 2.5 m bgs and (b) deep wells screened at 4.0 m bgs.

4.3.2 CO_2 gas Distribution

No contour plots were prepared from the p_{CO2} time series plots as all p_{CO2} were below the hydrostatic pressure and would therefore be represented in the same colour.

4.4 Hydraulic Monitoring

As discussed in the passive injection experiment summary, hydraulic monitoring data were ineffective for determining areas of induced CO_2 gas. The hydrographs prepared for this experiment are consistent with the general hydraulic trends discussed in Section 3.4. Figure 4.2 illustrates a small downward gradient at MW-6 and a strong downward gradient at MW-2.

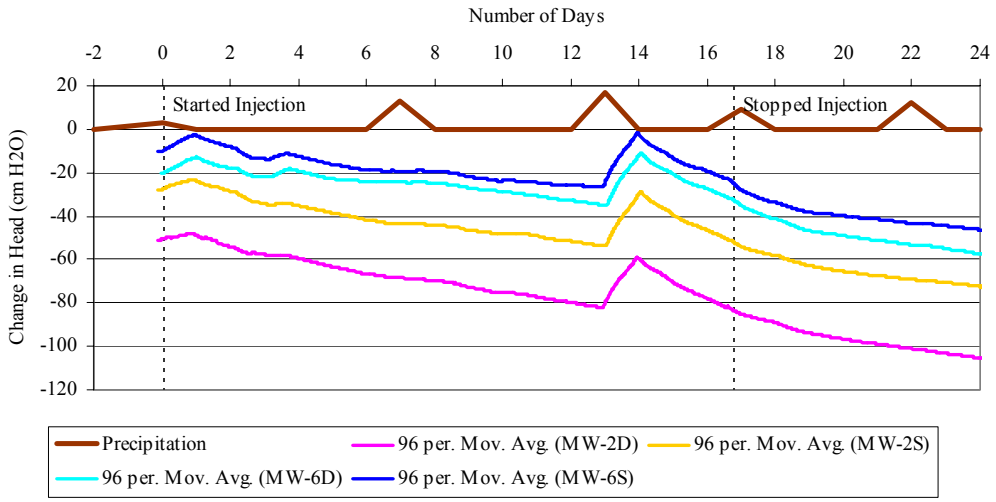

Figure 4.2 – Hydraulic monitoring data for experiment with hydraulic control.

4.5 Geophysical Surveys

4.5.1 Surface GPR Results

During the passive injection experiment, reflections evident prior to injection were attenuated, with most of the reflectors being nearly absent by the end of the experiment. This attenuation of reflections was persistent between the experiments when no injection of carbonated water was occurring and continued throughout the active injection experiment. Figure 4.3 depicts the GPR reflection profiles obtained between the two experiments and 15 days after the initiation of injection. As discussed previously, surface GPR data were ineffective for determining areas of induced CO_2 gas, possibly due to the attenuation of the reflectors.

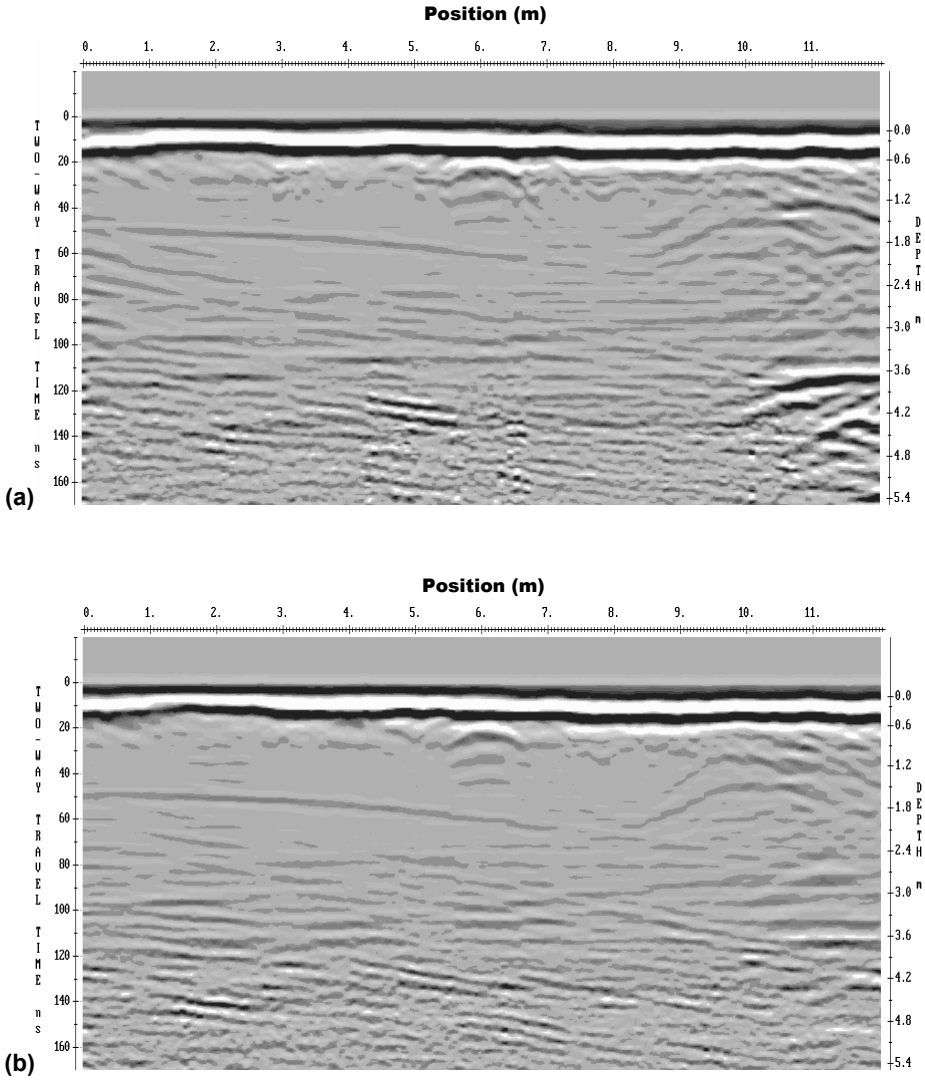

Figure 4.3 – Ground penetrating radar survey at 200 mHz for line 1 (diagonal from near GP-16 to GP-3) showing attenuation of reflections between (a) June 17, 2005 (between experiments) and (b) July 6, 2005 (15 days after initiation of injection). A SEC gain function (maximum gain 3000 and attenuation 2.7 db/min) was used to process the GPR data.

4.5.2 Cross-borehole GPR Results

Cross-borehole GPR data obtained using both the ZOP and MOG acquisition modes were evaluated to provide an indication of water content variations within the study area due to the introduction of CO_2 gas. A decrease in water content suggests the presence of CO_2 gas.

4.5.2.1 Zero-Offset Profile CO_2 gas Distribution

The ZOP profiles were differenced following the method described in Section 3.5.2.2.2 to detect changes in CO_2 gas content induced by the experiment. According to the passive injection experiment, the maximum accumulation of CO_2 gas occurred at ~ 3 – 4 m bgs 6 days after injection began. Similarly, the injection experiment with hydraulic control showed the maximum accumulation at ~ 3 – 4 m bgs 6 days into the experiment. The maximum change in water content observed during the active injection experiment was larger at 4.0 m bgs and smaller at ~ 3.25 m bgs then those seen during the passive injection experiment (Figure 4.4).

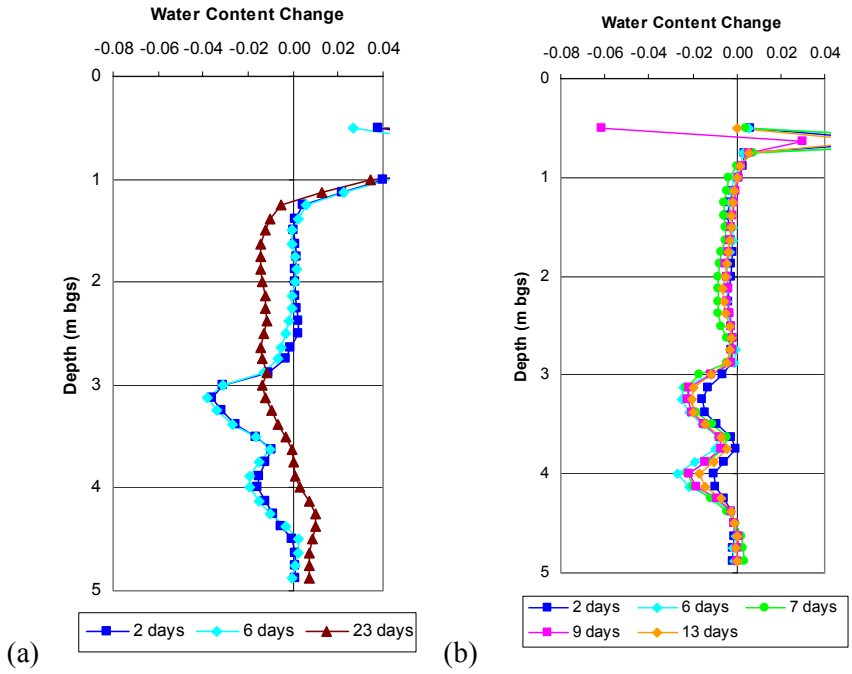

Figure 4.4 – Comparison of change in water content between GP-9 and GP-10 for cross-borehole GPR (ZOP) data from the (a) passive injection experiment and (b) active injection experiment.

The CO_2 gas saturation profiles were contoured for a cross-section between GP-8 and GP-11 for 9 days after injection. The date selected does not correspond with the maximum CO_2 gas accumulation (day 6) observed during the passive injection experiment because the cross-borehole pairs along this orientation were not monitored on day 6. No other orientation provided a comparable depiction of CO_2 gas accumulation on day 6. Figure 4.5 depicts the smaller ZOI observed at day 9 of the active injection experiment compared with the passive injection experiment. However, at day 6 of the active injection experiment, the CO_2 gas saturation distribution was similar to that observed on day 9 of the passive injection experiment (Figure 4.6) (i.e., similar lateral extent). Based on the available data, it appears that pumping had no impact on the lateral distribution of CO_2 gas. This lack of response is likely attributable, at least in part, to less dissolved CO_2 present within the water.

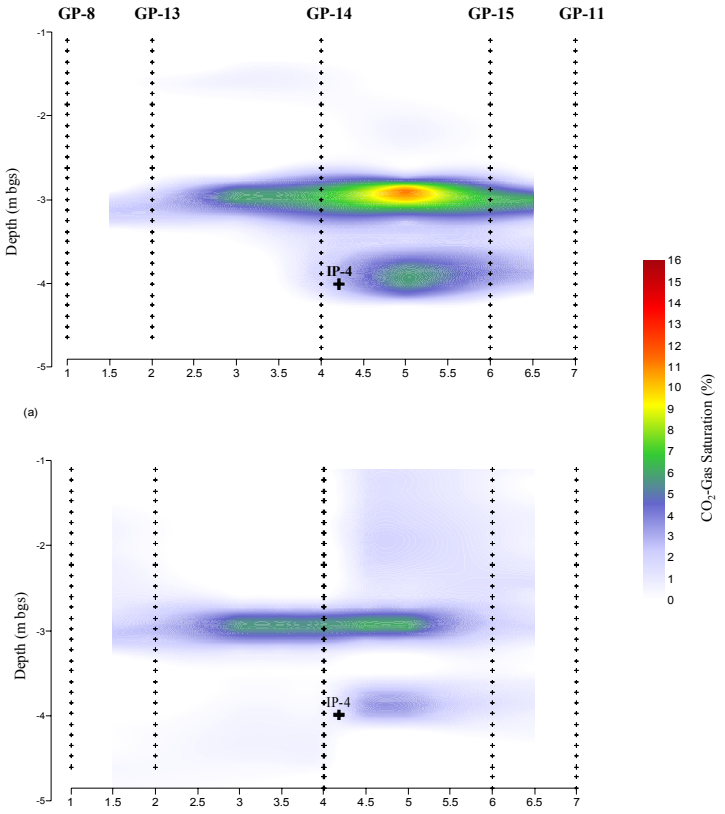

Figure 4.5 – Cross-sections of estimated CO_2 gas distribution, for day 9 after commencing experiment, inferred from cross-borehole GPR (ZOP) data for the (a) passive injection experiment and (b) active injection experiment. The (+) symbol indicates an access tube location where data were collected.

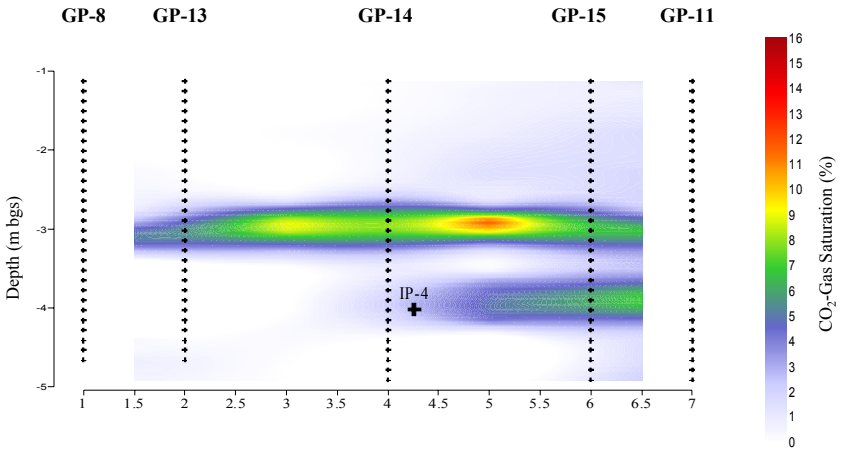

Figure 4.6 – Cross-section of estimated CO_2 gas distribution inferred from cross-borehole GPR (ZOP) data obtained 6 days after commencing active injection experiment. The (+) symbol indicates an access tube location where data were collected.

4.5.2.2 Multiple-Offset Gather CO_2 gas Distribution

CO_2 gas saturation profiles were prepared for the MOG acquisition mode by dividing the water content change profiles (i.e., difference between water content profiles obtained between the two experiments and the induced water content profiles) by the porosity profile (i.e., between experiments background water content profiles). The resultant profiles were contoured for day 13 for a cross-section located through the main line of geophysical access tubes (GP-7 through GP-12). Figure 4.7 illustrates that the CO_2 gas distribution inferred from the MOG data has an area of low CO_2 gas saturation between GP-9 and GP-10, which is consistent with the ZOP data collected on the same date. However, the CO_2 gas saturation was lower with the MOG acquisition mode. This discrepancy is probably due to the measurement differences between these acquisition modes, as discussed in Section 2.4.4.1.2.

No other contour plots were prepared as only one round of MOG data were collected during the active injection experiment. The reason for this was the considerable length of time required to perform a complete set of MOGs for a borehole pair. Thus, this method was only used once steady-state conditions were anticipated. Attainment of steady-state was based on no apparent increase in the area of influence. This condition was determined using the ZOP mode cross-borehole GPR data, as it tended to be the most responsive to changes in water content. It was anticipated that once the area of induced CO_2 gas, inferred from the cross-borehole GPR data (ZOP), was no longer expanding/increasing the area of influence would remain constant. However, the fact that the maximum ZOI was temporary may be attributable to inconsistent amounts of CO_2 gas dissolved within the water. Based on the available data, there is no evidence suggesting that pumping had any impact on the lateral distribution of CO_2 gas.

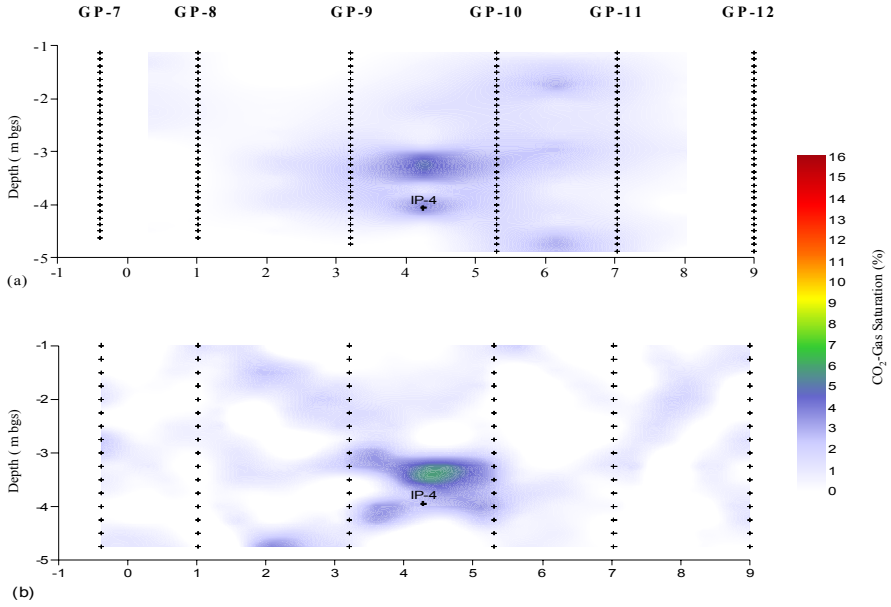

Figure 4.7 – Comparison between (a) ZOP and (b) MOG acquisition modes for the main line of geophysical access tubes 13 days after initiation of injection. The (+) symbol indicates an access tube location where data were collected.

4.5.3 Neutron Logging CO_2 gas Distribution

Given the very limited ability to observe CO_2 gas accumulation during the passive injection experiment using the CPN neutron tool, a neutron probe (Comprobe Model 1836) with a larger radial penetration depth was employed for the active injection experiment. Neutron probe measurements were obtained near the end of the experiment (day 16) when steady state conditions were anticipated. Based on the available data, the contours prepared from the CO_2 gas saturation profiles provided no indication of a response caused by induced CO_2 gas (Figure 4.8). The reason for this lack of response is unknown.

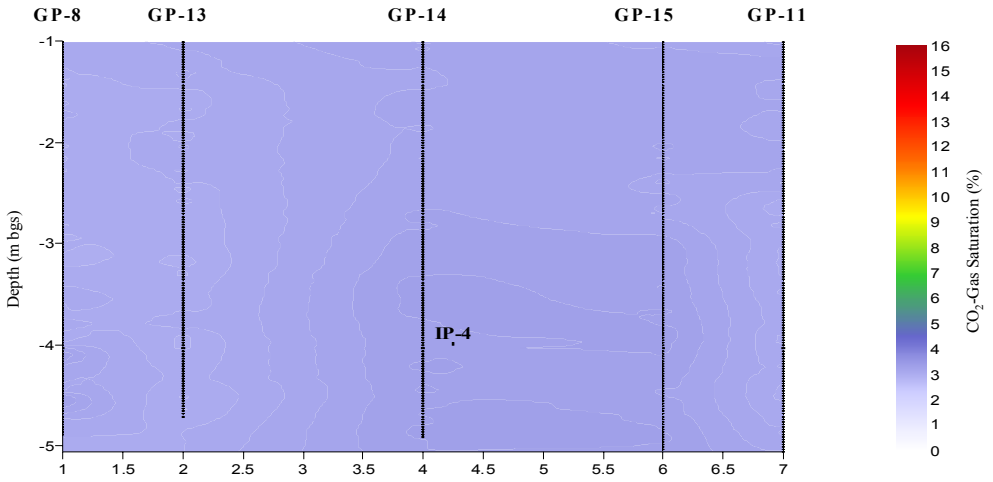

Figure 4.8 – Cross-section of estimated CO_2 gas distribution inferred from neutron logging data obtained 16 days after commencing experiment. The (+) symbol indicates an access tube location where data were collected.

4.6 Physical Observations

The CO_2 gas distribution at the exposed water table was physically observed on day 17 prior to shutting down the active injection experiment. Of the four excavations performed only the one located between GP-9 and GP-10 showed any bubbling. In this excavation, bubbling occurred periodically over the entire exposed area, with the exception of the injection point location, which consistently showed rapid bubbling. This was the result of channeling along the injection point annulus. The CO_2-distribution was observed at the extents of this excavation; thus, the CO_2 gas was assumed to go beyond this excavation. However, it should be noted the excavations located ~ 2 and 4 m on either side of this excavation showed no indication of bubbles. This lack of bubbles is consistent with other observations that suggest a small, laterally limited area of high CO_2 gas saturation between GP-9 and GP-10.

4.7 Summary

The geophysical and CO_2-concentration data evaluated corroborated the field observation suggesting less CO_2 gas was being dissolved during the active injection field experiment. It is not possible to accurately determine if pumping did have any impact on the lateral distribution of CO_2 gas. The limited amount of useable data obtained suggested the absence of any influence from pumping, which was likely attributable to the aforementioned problem associated with dissolving CO_2 gas. The reason for the decrease is unknown, and it is uncertain whether this decrease was the only reason for the failure of the experiment. There are several reasons that may individually or collectively explain the problem with CO_2 gas dissolution, including the following:

- Less CO_2 gas was dissolved due to higher temperatures. The average temperate increased by 10˚C between the two experiments (Figure 4.9).
- The water used contained more sediment. This observation was made during the experiment; however, it is unknown if this caused any damage to the fibres present within the Gas inFusion™ generators.
- Problem(s) with the Gas inFusion™ generators used to dissolve the CO_2 gas, which may be simply due to the turbid water mentioned above. There was no other indication of possible problems with the GI generators.

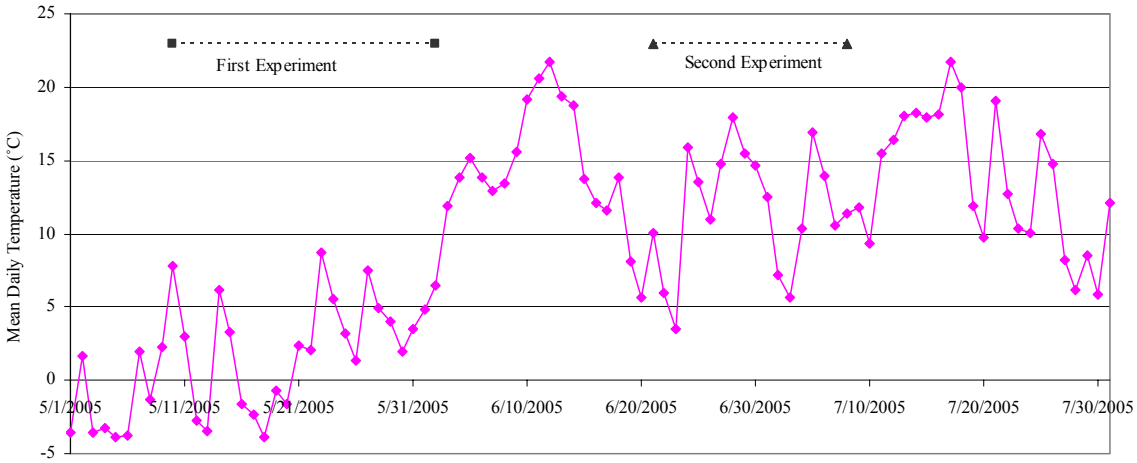

Figure 4.9 – Mean daily temperatures obtained for Borden AWOS, Ontario (Environment Canada website)

Chapter 5

Controls on Gas Accumulation

5.1 Soil Borings

Soil boring locations were selected in an attempt to correlate cross-borehole GPR observations with the presence of heterogeneities. Hydraulic conductivity tests were performed on soil samples obtained from these borings. Figure 5.1 depicts the locations of the six borings relative to the access tubes and wells.

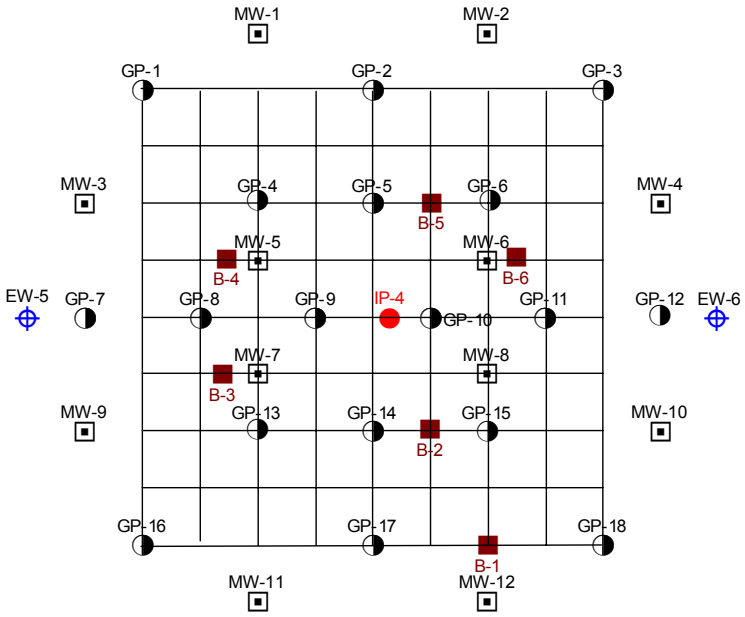

Figure 5.1 – Boring locations (B-1 to B-6) relative to geophysical access tubes and wells.

The locations chosen included areas with apparent trapped CO_2 gas pockets and areas that showed no significant water content changes due to CO_2 gas evolution, but showed significant variations in background water content. Figure 5.2a shows trapped CO_2 gas at 3.0 and 4.0 m bgs between access tubes GP-14 and GP-15, which was selected as the location of boring B-2. Conversely, Figure 5.2b shows an abrupt increase in water content at 2.0 m bgs between access tubes GP-5 and GP-6 (corresponding to boring location B-5), which is not associated with any apparent change in water content due to induced CO_2 gas.

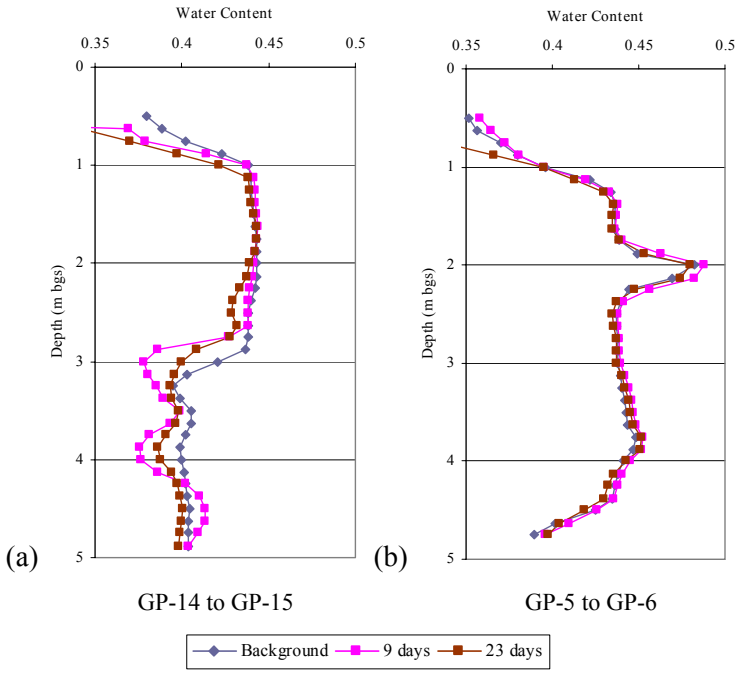

Figure 5.2 – Variations in water content observed on cross-borehole GPR (ZOP mode) profiles with (a) representing an area suggesting trapping of CO_2 gas and (b) depicting an abrupt change in water content that may explain the absence of CO_2 gas.

5.2 Hydraulic Conductivity Tests

Hydraulic conductivity tests, including falling-head permeameter tests and grain size distributions were performed in accordance with the procedures described in Sections 2.4.6.1 and 2.4.6.2, respectively.

5.2.1 Falling-Head Permeameter Results

Hydraulic conductivity profiles based on the results of the falling-head permeameter tests were prepared to determine variations with depth. On these profiles the hydraulic conductivity on the x-axis increases to the left, which corresponds with the direction showing higher gas saturations on the water content change profiles. Therefore, a lower permeability layer would be represented by a peak increasing towards the right. Figure 5.3 depicts the falling-head permeameter hydraulic conductivity profiles for each of the soil borings.

Figure 5.3a shows lower permeable layers at 2.4 to 2.7 m bgs, 3.0 m bgs, and 3.5 m bgs in borings B-2, B-3 and B-6. Each of these lower permeable layers at B-2 had CO_2 gas accumulated, based on the ZOP profiles (Figure 5.4), within higher permeable layers located beneath these low permeability layers. On the other hand, only one of these lower permeable layers (~ 2.6 m bgs) at B-3 was associated with the trapped gas observed at GP-13/GP-8 (Figure 5.5). Although lower permeability

layers were also present in boring B-6, there was no evidence of CO_2 gas accumulation beneath them (Figure 5.6).

Figure 5.3b shows lower permeability layers in boring B-1 (between GP-18 and GP-17) at ~ 1.9, 2.7, and 4.0 m bgs; however, only the heterogeneity evident at ~ 2.7 m bgs corresponded with trapped CO_2 gas based on the ZOP profile data (Figure 5.7). Conversely, the area located between GP-8 and GP-4 (B-4) provided no indication of induced CO_2 gas and the corresponding hydraulic conductivity profile suggested a relatively homogeneous material (Figure 5.8). Boring B-5 was advanced to identify the anomaly shown in Figure 5.2b between GP-6 and GP-5 at ~ 2 m bgs. This anomaly corresponded with a peat layer and provided no indication of trapped CO_2 gas pockets (Figure 5.9). The reason for the increase in water content change in Figure 5.9 at ~ 2 m bgs is unknown. A similar increase in water content was not present within other borings with expected peat layers based on the measured water content profiles.

Each location with trapped CO_2 gas pockets correlated with a lower permeability layer; however, a lower permeability layer was not always associated with trapped CO_2 gas. This correlation suggests that areas with higher CO_2 gas saturation were the result of trapping below lower permeability layers. These variations in permeability were not evident via noticeable physical changes in grain size, but grain-size distributions were performed on a select number of samples to provide an independent evaluation of permeability variations with depth. These results are discussed in Section 5.2.2.

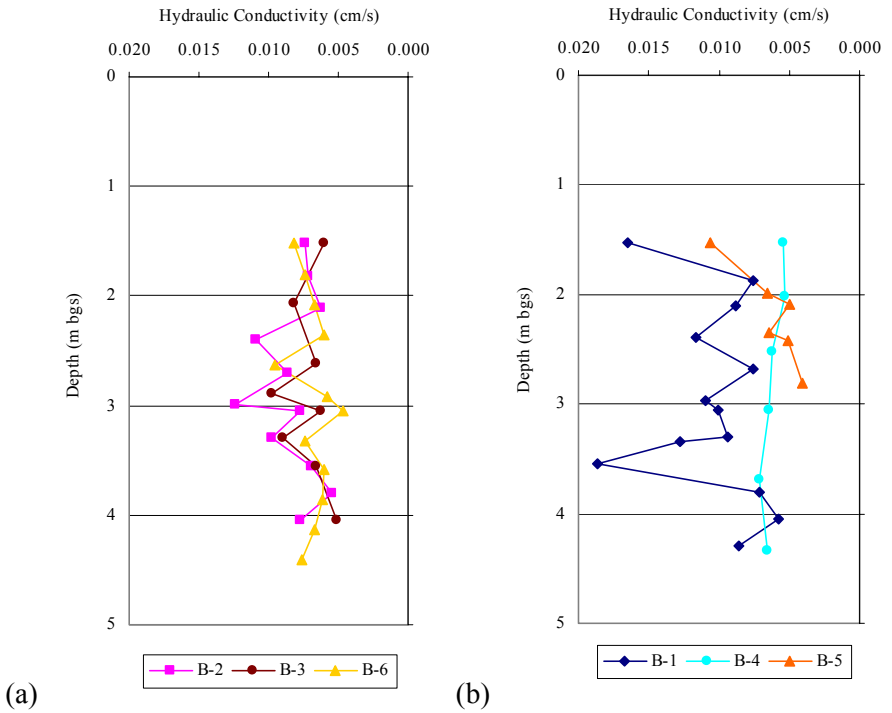

Figure 5.3 – Hydraulic conductivities obtained from falling-head permeameter tests: (a) depicting variations at depths corresponding to trapped CO_2 gas and (b) showing variations at depths that are not necessarily associated with trapped CO_2 gas.

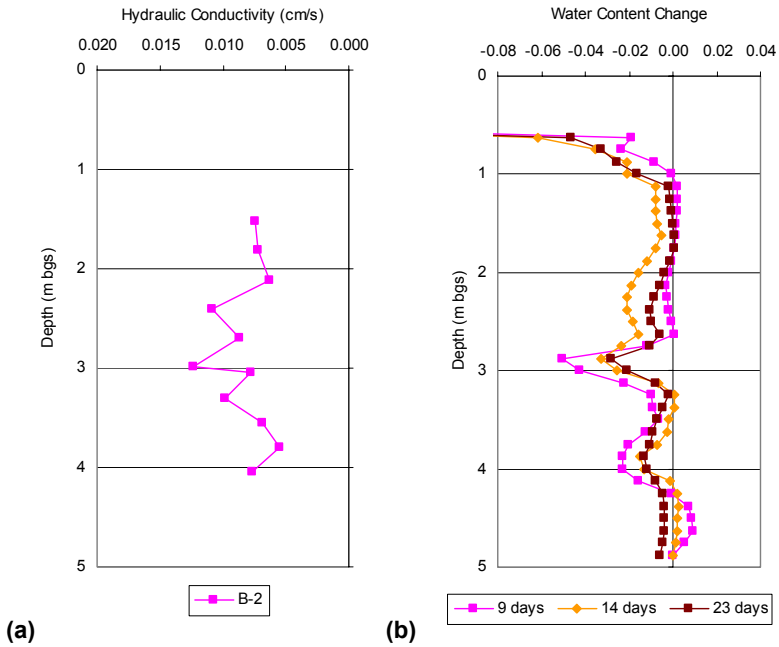

Figure 5.4 – Comparison between GP-15/GP-14 ZOP and boring B-2 results: (a) variations in hydraulic conductivity with depth and (b) increases in CO_2 gas saturation.

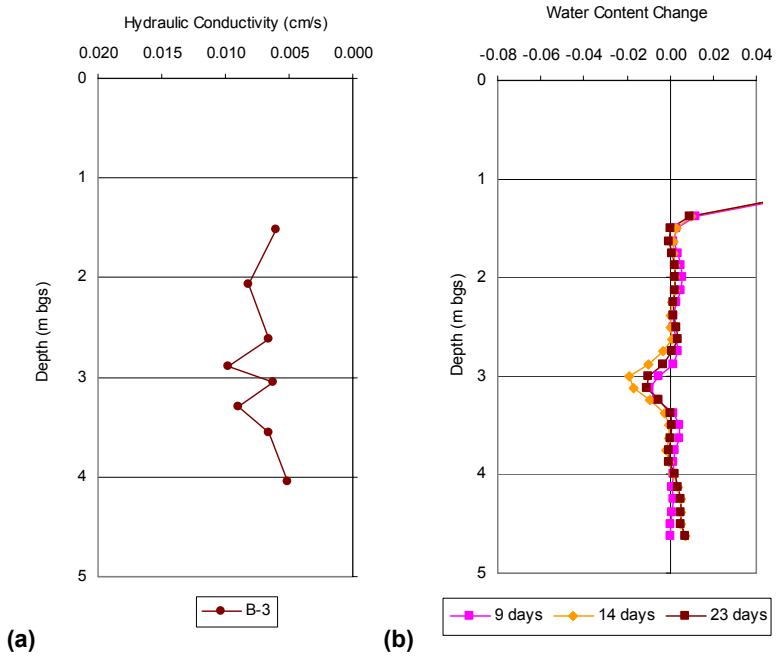

Figure 5.5 – Comparison between GP-13/GP-8 ZOP and boring B-3 results: (a) variations in hydraulic conductivity with depth and (b) increases in CO_2 gas saturation.

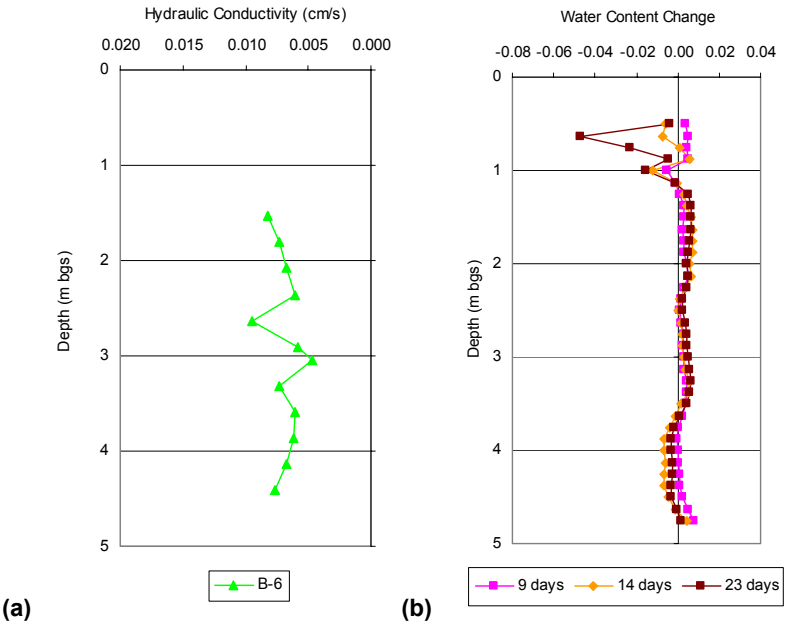

Figure 5.6 – Comparison between GP-11/GP-6 ZOP and boring B-6 results: (a) variations in hydraulic conductivity with depth and (b) increases in CO_2 gas saturation.

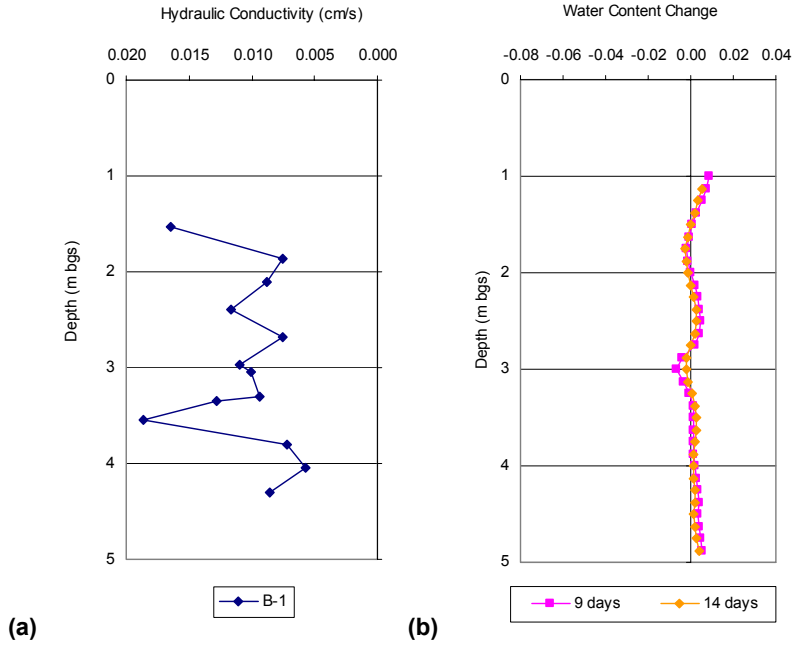

Figure 5.7 – Comparison between GP-18/GP-17 ZOP and boring B-1 results: (a) variations in hydraulic conductivity with depth and (b) increases in CO_2 gas saturation.

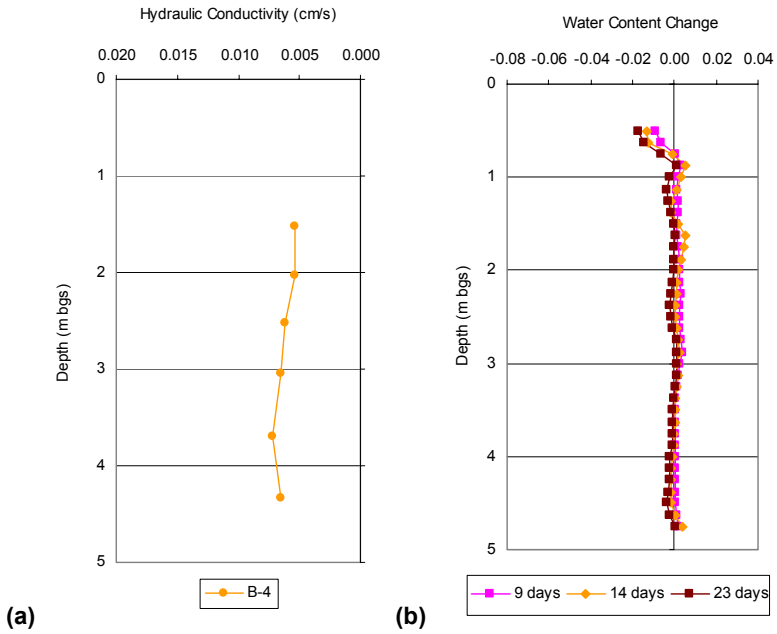

Figure 5.8 – Comparison between GP-8/GP-4 ZOP and boring B-4 results: (a) variations in hydraulic conductivity with depth and (b) increases in CO_2 gas saturation.

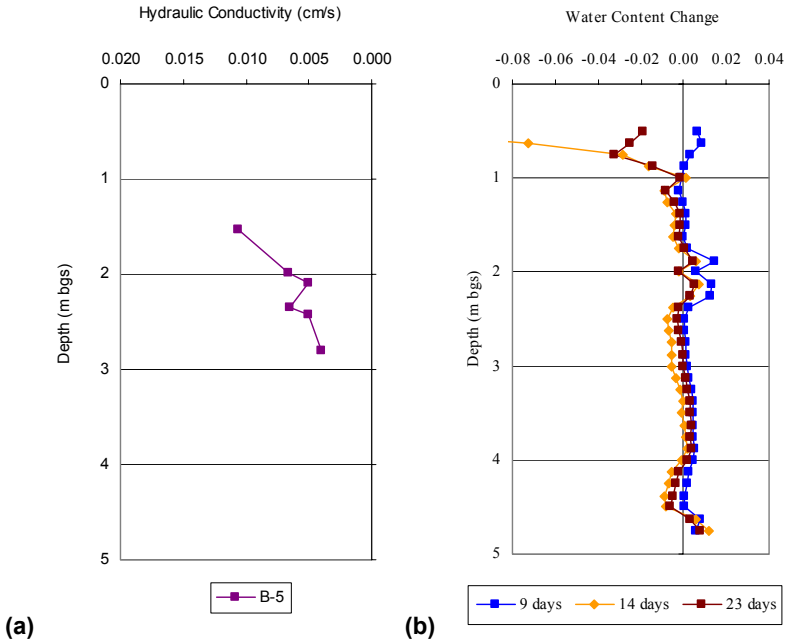

Figure 5.9 – Comparison between GP-6/GP-5 ZOP and boring B-5 results: (a) variations in hydraulic conductivity with depth and (b) increases in CO_2 gas saturation.

5.2.2 Grain-Size Distribution Results

Hydraulic conductivity profiles based on the results of the grain-size distributions were prepared to determine variations with depth at borings B-2, B-3 and B-6. Table 5.1 presents a summary of the geometric mean hydraulic conductivity calculated for each sample analyzed.

Table 5.1 – Summary of Hydraulic Conductivities from Grain Size Distributions

Boring ID	Top Depth (m bgs)	d10 (mm)	K (cm/s)
B-2	2.13	0.08	6.40E-03
B-2	2.75	0.079	6.24E-03
B-2	2.81	0.093	8.65E-03
B-2	2.87	0.097	9.41E-03
B-2	2.93	0.095	9.03E-03
B-2	2.99	0.115	1.32E-02
B-2	3.05	0.113	1.28E-02
B-2	3.1	0.114	1.30E-02
B-2	3.15	0.118	1.39E-02
B-2	3.3	0.115	1.32E-02
B-2	3.55	0.075	5.63E-03
B-2	4.05	0.064	4.10E-03
B-3	2.07	0.108	1.17E-02
B-3	2.62	0.091	8.28E-03
B-3	2.89	0.104	1.08E-02
B-3	3.05	0.094	8.84E-03
B-3	3.3	0.109	1.19E-02
B-3	3.55	0.093	8.65E-03
B-3	4.05	0.097	9.41E-03
B-6	2.08	0.102	1.04E-02
B-6	2.64	0.1	1.00E-02
B-6	2.91	0.096	9.22E-03
B-6	3.05	0.091	8.28E-03
B-6	3.32	0.079	6.24E-03
B-6	4.13	0.064	4.10E-03

The lower permeability layers observed at B-3 based on the falling-head permeameter test results were consistent with the hydraulic conductivities calculated from the grain-size distributions (Figure 5.10b). In contrast, the hydraulic conductivities determined from the grain-size distributions for B-2 and B-6 are generally inconsistent with the hydraulic conductivities determined from the falling-head permeameter tests. These differences may be attributable to the inability of grain-size analyses to account for porosity, pore continuity, and/or packing of soil grains; whereas these soil characteristics are considered by the permeameter analyses. Because of these limitations the hydraulic conductivities associated with the grain-size analyses are generally less accurate then those obtained

from the falling-head permeameter tests. However, the falling-head permeameter tests provided only an approximation of the hydraulic conductivity as the samples analyzed were disturbed and then repacked in the permeameter chamber. Grain-size distribution curves are presented in Appendix I.

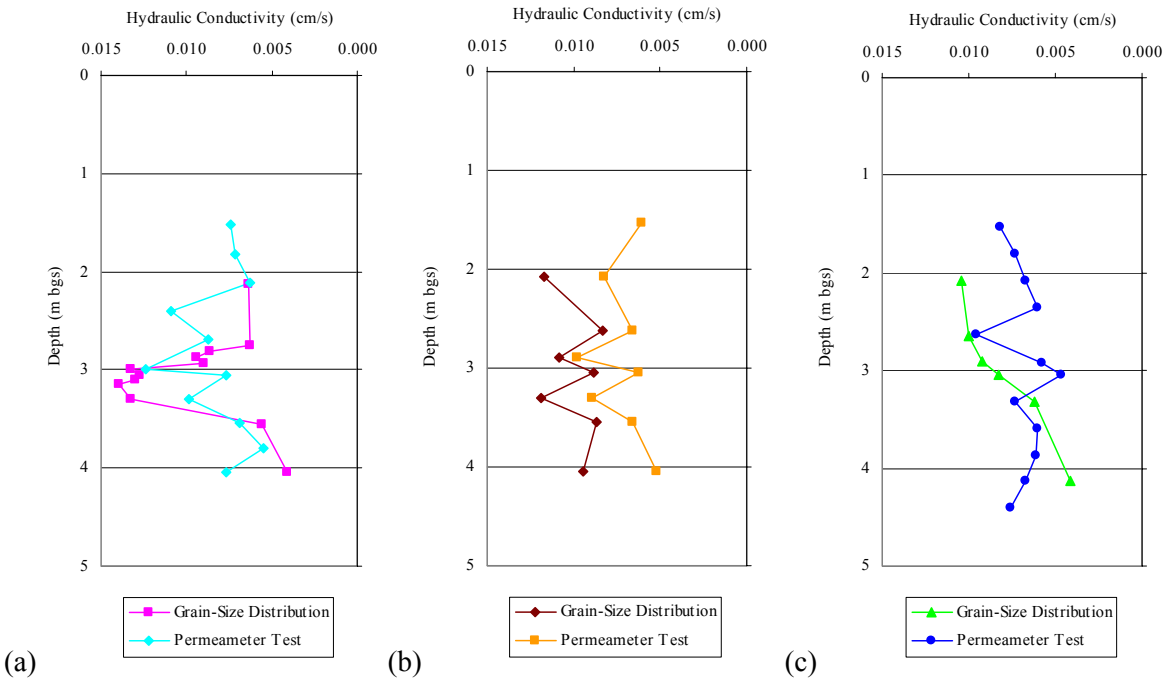

Figure 5.10 – Comparison of hydraulic conductivity profiles for falling-head permeameter and grain-size distribution tests for (a) B-2 located between GP-15 and GP-14, (b) B-3 located between GP-13 and GP-8, and (c) B-6 located between GP-11 and GP-6

5.2.3 Hydraulic Conductivity and Entry Pressure Relationship

Hydraulic conductivities obtained from the falling-head permeameter tests ranged from 1.64 x 10^{-3} cm/s to 3.01 x 10^{-2} cm/s, with a geometric mean of 7.49 x 10^{-3} cm/s, which is consistent with previous investigations of the Borden aquifer. Kueper and Frind (1991) performed falling-head permeameter tests on seven Borden sand samples and obtained hydraulic conductivities between 4.30 x 10^{-3} cm/s and 1.21 x 10^{-2} cm/s. These soil samples were also used to measure tetrachloroethylene-water drainage capillary pressure curves, which are depicted on Figure 5.11 along with the associated hydraulic conductivities. This figure shows that a lower permeability sample has a higher displacement pressure. These variations in permeability/displacement pressure are sufficient to cause build up of the non-wetting fluid beneath a lower-permeability lens until the capillary pressure exceeds the entry pressure into the lens. The build up of the non-wetting fluid causes the injected fluid to spread laterally below the lower-permeable layer. This observation is consistent with the results from the Gas inFusion™ experiments, which indicate that although the Borden aquifer is

ELSEVIER

26 April 2006 Our ref: CT/mm/apr.06.J038

Ms Cynthia Doughty
University of Waterloo
Cdoughty@GeoSyntec.com

Dear Ms Doughty

JOURNAL OF CONTAMINANT HYDROLOGY, *Vol 2, 1991, pp 95-110, Kueper et al, "An overview of..." 1 Figure only*
Vol 67, 2003, pp 113-132, Tomlinson et al, "Air distibution..." Figures 1, 4 & 6 only

As per your letter dated 24 April 2006, we hereby grant you permission to reprint the aforementioned material at no charge **in your thesis** subject to the following conditions:

1. If any part of the material to be used (for example, figures) has appeared in our publication with credit or acknowledgement to another source, permission must also be sought from that source. If such permission is not obtained then that material may not be included in your publication/copies.

2. Suitable acknowledgment to the source must be made, either as a footnote or in a reference list at the end of your publication, as follows:

   "Reprinted from Publication title, Vol number, Author(s), Title of article, Pages No., Copyright (Year), with permission from Elsevier".

3. Reproduction of this material is confined to the purpose for which permission is hereby given.

4. This permission is granted for non-exclusive world **English** rights only. For other languages please reapply separately for each one required. Permission excludes use in an electronic form. Should you have a specific electronic project in mind please reapply for permission.

5. This includes permission for the Library and Archives of Canada to supply single copies, on demand, of the complete thesis. Should your thesis be published commercially, please reapply for permission.

Yours sincerely

C. Truter

Clare Truter
Deputy Rights Manager, S&T

relatively homogeneous, distinct horizontal layering is present with sufficient variations in permeability/displacement pressure to trap and cause some lateral spreading of a gas phase.

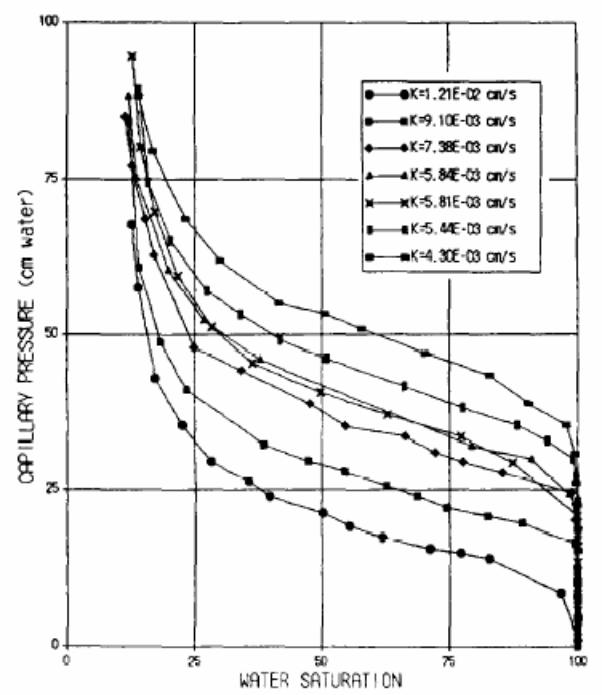

Figure 5.11 – Laboratory measured capillary pressure –saturations curves along with the associated hydraulic conductivities for seven Borden aquifer samples (Kueper and Frind, 1991). Reprinted from *Journal of Contaminant Hydrology* with permission of Elsevier. Copyright 1991.

Chapter 6
Assessment of the Conceptual Model

6.1 Supersaturated Water Flow

Initially as supersaturated water was injected it flowed laterally in a radial direction from the injection point. During continued injection a horizontal component of supersaturated water flow continued to move away from the injection point, while another component of flow moved vertically. The flow of water was controlled by heterogeneities in the porous medium.

Elevated p_{CO_2} data acted as a tracer to evaluate the flow of supersaturated water from the injection point. P_{CO_2} data from 6 days after commencing the experiment without hydraulic control showed p_{CO_2} levels above the hydrostatic pressure radially around the injection point (Figure 3.6). This horizontal component of supersaturated water flow was present for the duration of the experiment, as shown by the presence of elevated CO_2 concentrations at the depth of injection (Figures 3.3 and C.1b). Supersaturated water was first evident at the deep wells located 5 – 5.5 m from the injection point 14 days after injection commenced, with the exception of MW-1D where it was not evident until day 20 and southeast of the injection point (MW-2D and MW-4D) where it was absent for the length of the experiment (Figure C.1b). Although supersaturated water was generally evident radially around the wells at similar times at the depth of injection concentrations in each direction was highly variable, which indicates preferential flow paths.

A vertical component of supersaturated water flow was evident by the presence of supersaturated water at the shallower well in a well couplet at an earlier time than the corresponding deep well. This occurred at locations MW-1, MW-9, and MW-12 (Figures 3.4b and C.1b). The presence of supersaturated water in each shallow well at variable times suggests preferential flow of water.

6.2 Gas Flow

At the depth of injection the CO_2 gas exsolved from the supersaturated water and moved vertically until it encountered a lower permeability layer. When the gas encountered the lower permeability lens some of the gas moved laterally and some of the gas accumulated below the confining layer. The gas below the confining layer continued to accumulate until it built up enough pressure to exceed the entry pressure of the lens. Once the entry pressure was exceeded the gas broke through the lower permeability layer and moved vertically to the ground surface. Although the gas flow was predominately influenced by one laterally extensive lower permeability lens, other less extensive lenses may have contributed to lateral gas flow. Vertical gas flow also occurred along the annular space of the injection point and via the backup injection point (IP-3).

Gas was first evident at the injection point and the backup injection point (IP-3) by the presence of gas bubbles at the ground surface. The bubbles at the injection point were evident in the standing water temporarily present at the injection point as a result of startup testing. In IP-3 the gas bubbles were observed within the well; however, by Day 6 bubbling at IP-3 was no longer evident. Both of these observations of bubbles suggested preferential flow paths. The only other direct evidence of gas flow was the sound and physical observation of bubbling at MW-8 approximately 6-10 days after injection commenced.

Inferred gas flow based on cross-borehole GPR data suggested that at the depth of injection gas exsolved from the supersaturated water as the water moved radially away from the injection point. The exsolved gas moved vertically until a lower permeability layer was encountered. Once the lower permeability layer was encountered some of the gas moved laterally with the predominate direction of flow being to the west of the injection point and some of the gas accumulated beneath the lower permeability lens. The flow continued to be dominated by preferential flow paths for the duration of the experiment. However, there is evidence of breakthrough of the lower permeability lens by Day 23 (Figure 3.19).

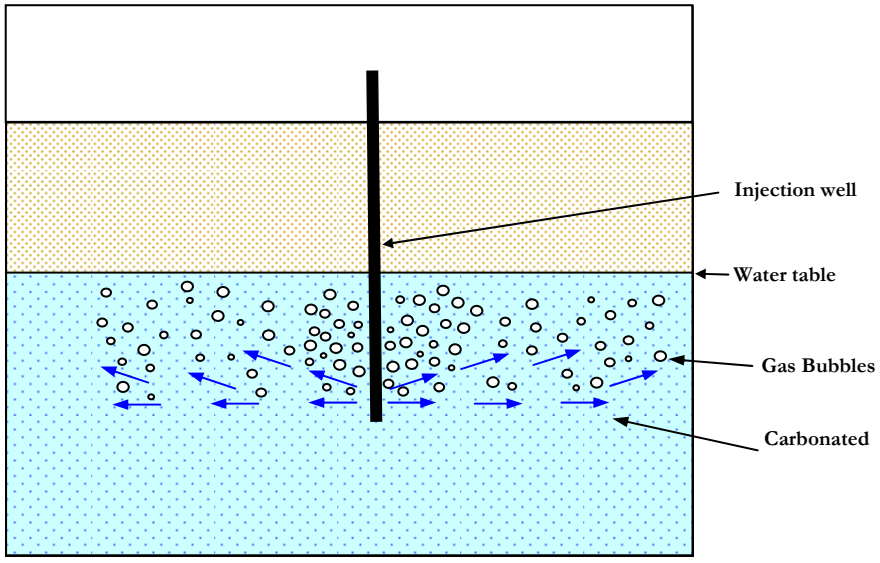

Figure 6.1 – Conceptual model for supersaturated water injection.

ELSEVIER

26 April 2006 Our ref: CT/mm/apr.06.J038

Ms Cynthia Doughty
University of Waterloo
Cdoughty@GeoSyntec.com

Dear Ms Doughty

JOURNAL OF CONTAMINANT HYDROLOGY, *Vol 2, 1991, pp 95-110, Kueper et al, "An overview of..." 1 Figure only*
Vol 67, 2003, pp 113-132, Tomlinson et al, "Air distibution..." Figures 1, 4 & 6 only

As per your letter dated 24 April 2006, we hereby grant you permission to reprint the aforementioned material at no charge **in your thesis** subject to the following conditions:

1. If any part of the material to be used (for example, figures) has appeared in our publication with credit or acknowledgement to another source, permission must also be sought from that source. If such permission is not obtained then that material may not be included in your publication/copies.

2. Suitable acknowledgment to the source must be made, either as a footnote or in a reference list at the end of your publication, as follows:

   "Reprinted from Publication title, Vol number, Author(s), Title of article, Pages No., Copyright (Year), with permission from Elsevier".

3. Reproduction of this material is confined to the purpose for which permission is hereby given.

4. This permission is granted for non-exclusive world **English** rights only. For other languages please reapply separately for each one required. Permission excludes use in an electronic form. Should you have a specific electronic project in mind please reapply for permission.

5. This includes permission for the Library and Archives of Canada to supply single copies, on demand, of the complete thesis. Should your thesis be published commercially, please reapply for permission.

Yours sincerely

C. Truter

Clare Truter
Deputy Rights Manager, S&T

Chapter 7
Comparison Between Air Sparging and Gas inFusion™ ZOI Experiments

7.1 Summary of an In Situ Air Sparging Experiment within the Borden Aquifer

A similar field experiment was conducted within the sand quarry at Borden to assess the air distribution from a single in situ air sparging injection point (Tomlinson et al, 2003). The air distribution was assessed using geophysical surveys (neutron measurements, surface GPR, and cross-borehole GPR), hydraulic monitoring data, physical observations at the exposed water table, and hydraulic testing. The experiment operated until steady state (7 days) was achieved using a flow rate of ~ 200 m^3/day (5 scfm). The locations of the monitoring points relative to the air sparge point are illustrated on Figure 7.1.

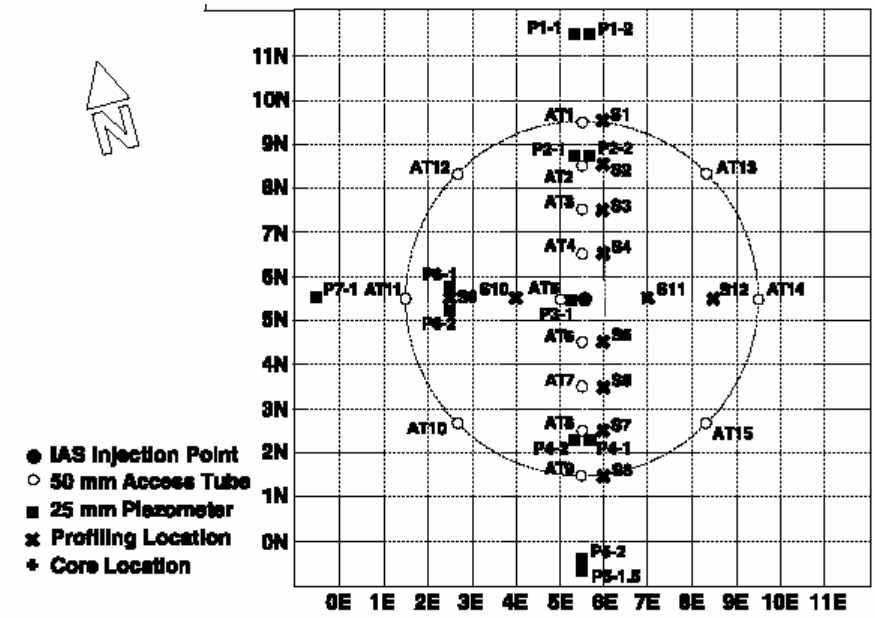

Figure 7.1 – Air sparging study area layout (Tomlinson et al, 2003). Reprinted from the *Journal of Contaminant Hydrology* with permission of Elsevier. Copyright 2003.

The results of this study indicated distinct horizontal layering with vertical permeabilities ranging from 2.5 x 10^{-14} m^2 to 2.1 x 10^{-10} m^2, with a geometric mean of 3.3 x 10^{-12} m^2. This is equivalent to hydraulic conductivities between 1.57 x 10^{-1} cm/s to 1.87 x 10^{-5} cm/s, with a geometric mean of 2.47

x 10^{-3} cm/s, assuming a water temperature of 10˚C. The air sparging hydraulic conductivities are consistent with the geometric mean of the hydraulic conductivities determined from the Gas inFusion™ experiments (7.49 x 10^{-3} cm/s). Surface GPR data suggested that these horizontal layers extended across most of the site. Based on the neutron probe and GPR data, the air distribution was stratified with high air-saturation pockets forming below these lower permeability horizons (Figure 7.2).

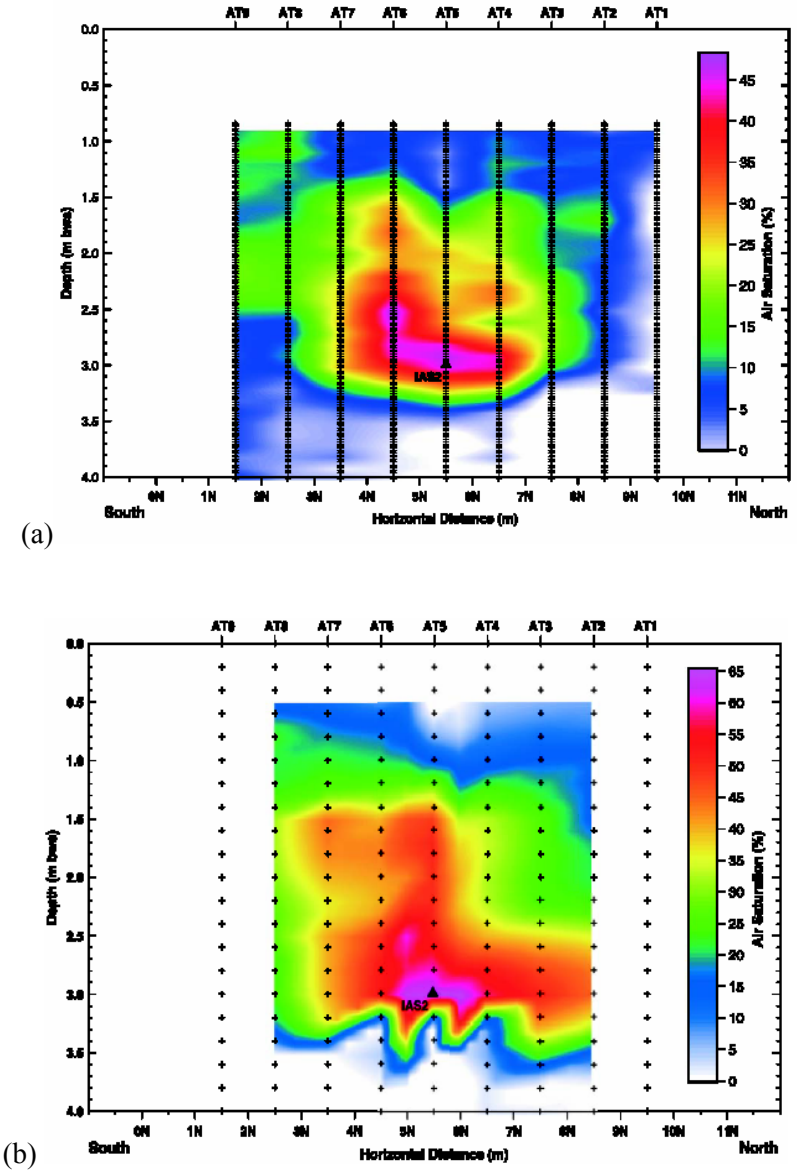

Figure 7.2 – Estimated steady-state air distribution from (a) neutron logging data and (b) borehole GPR measurements conducted between access tube pairs spaced 2 m apart. The (+) indicates the location of data used to construct these distributions (Tomlinson et al, 2003). Reprinted from the *Journal of Contaminant Hydrology* with permission of Elsevier. Copyright 2003.

The estimated steady-state air saturation distributions indicated that air migrated through these lower permeability layers, which included layers at 2.0 and 2.9 m below water surface (bws). This migration was confirmed by the observations of air release at the exposed water table. The air release indicated that the air pressure and hence, capillary pressure, built up beneath the lower permeability layers until the displacement pressure associated with these layers was exceeded or the air found an alternate path through or around these lenses. Geophysical data collected suggested a ROI of elevated levels of air saturation between 15% and 60% within a 2.5 m radius around the sparge point. The ROI represents the radial distance from the sparge point where the air saturation is sufficient for groundwater treatment.

7.2 Comparison Between Gas inFusion™ and Air Sparging Experiments

Table 7.1 provides a comparison of the Gas inFusion™ and air sparging experiments. As noted on this table, air sparging resulted in an higher gas saturation (60%) than Gas inFusion™ (16%), as illustrated on Figure 7.3. However, it should be noted that air sparging introduced approximately 11.5 times more gas (1400 m^3 compared to 122 m^3). As shown on Figure 6.3, the GI experiment had a narrow area of gas saturation sufficient for groundwater treatment (>15%) that extended ~ 3 m from the injection point. The gas saturation in this area was 16%. In comparison, the air sparging experiment had a much larger area of air saturation sufficient for groundwater treatment that extended ~ 2.5 m from the injection point, with air saturations between 15 and 60%. In both experiments the gas extended to and beyond the limits of the study area. At the limits of the air sparging experiment, the gas saturation was ~ 45%, whereas for the GI experiment it was 16%. Based on the gas saturations at the limits of the study area, it is likely that the ROI for gas saturations sufficient for groundwater treatment would be larger for the air sparging experiment compared to the GI experiment. If indirect indicators, such as dissolved carbon dioxide above the applicable hydrostatic pressure, are considered, the area of influence was at least 5.5 – 7.0 m for the Gas inFusion™ experiment. Similar information (i.e., dissolved oxygen) was not collected for the air sparging experiment. Although Lundegard and LaBrecque (1995) demonstrated that conventional air sparging monitoring data, such as water table mounding, soil gas pressure, soil gas composition and tracer gas response, provided an ambiguous indication of the region of air flow.

Tomlinson et al (2003) indicates that for air sparging a gas saturation of >15% is required for groundwater treatment. For the comparison between the two experiments it was assumed that a similar gas saturation (>15%) would be required for groundwater treatment using the GI. Although based on the experiments performed, it is uncertain what minimum gas saturation is necessary for groundwater/source zone treatment using CO_2-supersaturated water injection. The smaller gas-saturation introduced by Gas inFusion™ may be a limiting factor for groundwater/source zone treatment.

The gas-saturation distribution for both technologies was controlled by lower permeability layers. These layers had sufficient variations in permeability/displacement pressure to cause stratification and trapping of higher gas-saturation pockets. The trapped gas-pockets spread laterally beneath the lower

permeability layers until the displacement pressure of the trapping layer was exceeded or until an alternate pathway through or around these layers was found.

Table 7.1 - Comparison of the Gas Infusion™ and Air Sparging Experiments

Parameter	Gas inFusion™	Air Sparging
Length of Time (days)	Initial 6	7 (Steady State)
Total Length of Time Running (days)	5.2	7
Gas	CO_2	Air
Total Volume of Gas (m^3)	122	1400
Total Volume of Water (L)	57,000	No water
Gas Saturation (%)	2-16	15 – 60
Approximate Distance from Injection/Sparge Point [Geophysics] with 0 – 10 % Gas Saturation (m)	> 5.3	> 3
Approximate Distance from Injection/Sparge Point [Geophysics] with 10 – 16 % Gas Saturation (m)	> 3	> 3
Approximate Distance from Injection/Sparge Point [Geophysics] with >16 % Gas Saturation (m)	0	> 2.5
Approximate Distance from Injection/Sparge Point with Potential to Release Gas [Groundwater Data] (m)	≥ 5.5 – 7	No groundwater quality data available.
Impact of Hydraulic Control on Lateral Distribution of Gas Saturation	Unknown	Not tested.

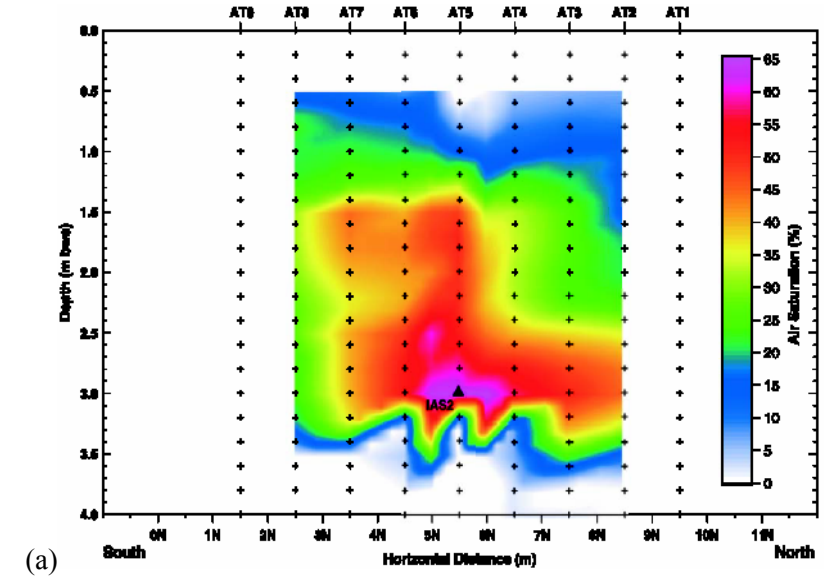

(a)

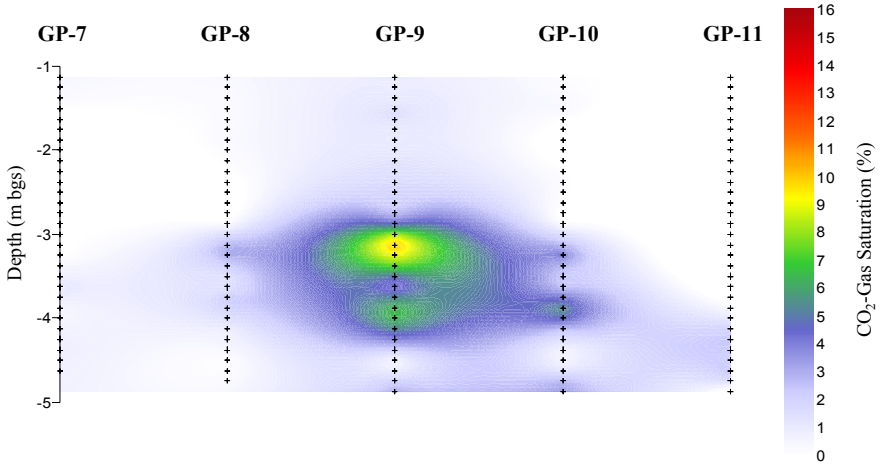

(b)

Figure 7.3 - Estimated steady-state gas-distribution from (a) air sparging (main line cross-section), and (b) Gas inFusion™ (main line cross-section). The (+) indicates the location of data used to construct these distributions (a from Tomlinson et al, 2003). Figure 7.3a is reprinted from the *Journal of Contaminant Hydrology* with permission of Elsevier. Copyright 2003.

Chapter 8
Conclusions and Recommendations

8.1 Conclusions

- The apparent ZOI for sufficient groundwater treatment (i.e., gas saturations > 15%) from air sparging is likely larger than that from CO_2-supersaturated water injection. This conclusion is based on the gas saturations at the limits of the study area. For air sparging, the gas saturation was ~ 45% at ~ 2.5 m from the injection point, while for CO_2-supersaturated water injection the gas saturation was 16% at 3.0 m.
- Channeling of CO_2 gas was evident by the sporadic, periodic nature of the bubbles at the exposed water table, which is consistent with air sparging research.
- Heterogeneities within the porous medium control the gas-saturation distribution for both the Gas inFusion™ and air sparging technologies. In both cases, the displacement pressure of the trapping layer was exceeded or an alternate pathway through or around these layers was found.
- The main mechanism for CO_2 nucleation away from the injection point appears to occur as water flows upward to areas with lower hydrostatic pressure. As the hydrostatic pressure decreases, additional release of CO_2 will occur until thermodynamic equilibrium is attained. This mechanism was evident by more potential to nucleate bubbles, inferred from the p_{CO2} data, at shallower depths above the injection depth.
- Based on the problematic and limited amount of useable data obtained with hydraulic control, which was achieved by extraction from two wells, it is not possible to accurately determine if pumping will have an impact on the lateral distribution of CO_2 gas.

8.2 Recommendations

- Additional field studies are necessary to determine if the low levels of CO_2 gas saturation detected are adequate to efficiently treat contaminated groundwater and source zone areas.
- The injection flow rate and pressure should be studied further to optimize the radial distance and CO_2 gas saturation. Additional GI generators can be connected in sequence to achieve the desired CO_2 gas saturation at a given flow rate and pressure.
- The ability of the Gas inFusion™ generator to introduce high levels of dissolved gas over a large area should be studied for enhanced natural attenuation applications.
- The injection point design should be investigated to determine if a longer injection point would result in a larger ZOI.

Bibliography

Acomb, L.J., D. McKay, P. Currier, S.T. Berglund, T.V. Sherhart, and C.V. Benedicktsson. 1995. Neutron Probe Measurements of Air Saturation Near an Air Sparging Well. In *In Situ Aeration: Air Sparging, Bioventing, and Related Remediation Processes*. Columbus, Ohio: Battelle Press. Pp. 47-61.

Ahlfeld, D.P., A. Dahmani, and W. Ji. 1994. A Conceptual Model of Field Behavior of Air Sparging and Its Implications for Application. *Ground Water Monitoring and Remediation. 14(4)*:132-139.

Bass, D.H., N.A. Hastings, and R.A. Brown. 2000. Performance of Air Sparging Systems: A Review of Case Studies. *Journal of Hazardous Materials 72*:101-119.

Ellis, V. 1987. *Well Logging for Earth Scientists*. New York, NY: Elsevier. Pp. 532.

Fetter, C.W. 1994. *Applied Hydrogeology Third Edition*. New York, NY: Macmillan College Publishing Company. Pp. 99.

Freeze, R.A. and J.A. Cherry. 1979. *Groundwater*. Englewood Cliffs, NJ: Prentice Hall.

Jackson, M.J. and D.R. Tweeton. 1993. *Migratom – Geophysical tomography using wavefront migration and fuzzy constraints.* Report on Investigations, 9497, United States Department of the Interior, Bureau of Mines, Pp. 35.

Ji, W., A. Dahmani, D. Ahlfeld, J.D. Lin, and E. Hill III. 1993. Laboratory Study of Air Sparging: Air Flow Visualization. *Ground Water Monitoring and Remediation.* 23, no. 4: 115-126.

Johnson, P.C. 1998. Assessment of Contributions of Volatilization and Biodegradation to In Situ Air Sparging Performance. *Environmental Science and Technology 32(2):* 276-281.

Johnson, P.C., R.L. Johnson, C.L. Bruce, and A. Leeson. 2001. Advances in In Situ Air Sparging/Biosparging. *Bioremediation Journal 5(4)*:251-266.

Johnson, P.C., C.C. Stanley, M.W. Kemblowski, D.L. Byers, and J.D. Colthart. 1990. A Practical Approach to the Design, Operation, and Monitoring of In Situ Soil-Venting Systems. *Ground Water Monitoring and Remediation. 10(2):*159-178.

Kearey, P. and M. Brooks. 1991. *An Introduction to Geophysical Exploration Second Edition.* Oxford: Blackwell Scientific Publications.

Kueper, B.H. and E.O. Frind. 1991. Two-phase flow in heterogeneous porous media: 2. Model application. *Journal of Contaminant Hydrology* 2: 95-110.

Leeson, A. and R.E. Hinchee. 1996. *Soil Bioventing*. Boca Raton: CRC Press.

Leeson, A., R.E. Hinchee, G.L. Headington, and C.M. Vogel. 1995. Air Channel Distribution During Air Sparging: A Field Experiment. In *In Situ Aeration: Air Sparging, Bioventing, and Related Remediation Processes*. Columbus, Ohio: Battelle Press. Pp. 215-222.

Leeson, A., P.C. Johnson, R.L. Johnson, C.M. Vogel, R.E. Hinchee, M. Marley, T. Peargin, C.L. Bruce, I. L. Amerson, C.T. Coonfare, R.D. Gillespie, and D.B. McWhorter. 2002. *Air Sparging Design Paradigm.* Columbus, Ohio: Battelle Press.

Li, T.M.W. 2004. *Recovery of Source Non-Aqueous Phase Liquids from Groundwater Using Supersaturated Water Injection*. M.A.Sc. Thesis. University of Waterloo.

Lundegard, P.D. and D.J. LaBrecque. 1995. Air Sparging in a Sandy Aquifer (Florence, Oregon, USA): Actual and Apparent Radius of Influence. *Journal of Contaminant Hydrology. 19(1)*:1-27.

Lundegard, P.D. and D.J. LaBrecque. 1998. Geophysical and Hydrologic Monitoring of Air Sparging Flow Behavior: Comparison of Two Extreme Sites. *Remediation. Summer*: 59-71.

MacKay, D.M., D.L. Freyburg, P.V. Roberts, and J.A. Cherry. 1986. A Natural Gradient Experiment on Solute Transport in a Sand Aquifer: 1. Approach and Overview of Plume Movement. *Water Resources Research 22(13):*2017-2029.

Piggott, S. D. 2003. *Moisture content monitoring of water infiltration experiments in a landfill cover using horizontal cross-borehole ground penetrating radar, Brampton St. Landfill – Hamilton Ontario.* Environmental Geophysics Facility, University of Waterloo.

Piggott, S.D. 2006. *Personal Communication.*

Reddy, K.R. and J.A. Adams. 2001. Effects of Soil Heterogeneity on Airflow Patterns and Hydrocarbon Removal during In Situ Air Sparging. *Journal of Geotechnical and Geoenvironmental Engineering. 127(3)*:234-247.

Semer, R., J.A. Adams, and K.R. Reddy. 1998. An Experimental Investigation of Air Flow Patterns in Saturated Soils during Air Sparging. *Geotechnical and Geological Engineering. 16(1)*:59-75.

Sensors & Software Inc. 1997. *pulseEKKO crosshole data acquisition & EKKO_IMAGE processing, User's guide version 1.0 (Technical Manual 28)*.

Tomlinson, D.W., N.R. Thomson, R.L. Johnson, and J.D. Redman. 2003. Air Distribution in the Borden Aquifer during In Situ Air Sparging. *Journal of Contaminant Hydrology 67*:113-132.

Topp, G.C., Davis, J.L., Annan, A.P., 1980. Electromagnetic Determination of Soil Water Content: Measurements in Coaxial Transmission Lines, *Water Resources Research.* 16(3):574-582.

Unger, A.J.A., E.A. Sudicky, and P.A. Forsyth. 1995. Mechanisms Controlling Vacuum Extraction Coupled with Air Sparging for Remediation of Heterogeneous Formations Contaminated by Dense Nonaqueous Phase Liquids. *Water Resources Research. 31(8)*:1913-1925.

APPENDICES

Appendix A
Injection Point Design

Figure A.1
Injection Point Testing Summary

Slot/Holes	Size of Slot/Holes (inches)	Number of Slot/Holes	Pressure (psi)	Pressure (kPa)	Flow Rate (lpm)
Slot	0.01	1	56	386	3.95 4.21 4.30
Slots	0.01	2	40	276	11.15 11.13 10.56
Slots	0.01	2	56	386	3.51 3.47 3.51
Slots	0.01	3	44	303	9.00 8.80 9.60
Holes	3/64	4	56	386	5.32 5.62 5.48
Holes	3/64	8	40	276	12.27 13.07 11.93
Holes	1/16	4	42	290	10.77 10.89 10.99
Holes	3/32	4	24	165	17.50 16.00 16.53
Holes	1/32	4	58	400	3.23 3.18 3.12
Holes	1/32	5	58	400	4.14 4.16 4.03
Holes	1/32	6	58	400	3.93 4.12 4.05

Figure A.1
Injection Point Testing Summary

Slot/Holes	Size of Slot/Holes (inches)	Number of Slot/Holes	Pressure (psi)	Pressure (kPa)	Flow Rate (lpm)
Holes	1/32	8	54	372	6.30
					6.07
					6.44
Holes	1/32	9	53	365	6.64
					6.89
					6.71
Holes	1/32	10	52	359	6.96
					7.25
					7.12
Holes	1/32	12	48	331	8.96
					9.09
					8.84
Holes	1/32	9	43	296	6.69
			43	296	6.49
			50	345	6.51
			50	345	6.34
			54	372	6.53
			56	386	6.56
			75	517	8.20
			75	517	7.63
			78	538	7.55
Holes	1/32	4	58	400	3.05
			80	552	3.02
			70	483	3.34
Holes	1/32	5	70	483	4.34
			62	427	4.24
Holes	1/32	6	64	441	4.37
Holes	1/32	8	58	400	6.55
			58	400	6.84
			58	400	6.62
			49	338	6.30
			49	338	6.20
			49	338	6.02
			35	241	5.52
			30	207	5.11

Figure A.1
Injection Point Testing Summary

Slot/Holes	Size of Slot/Holes (inches)	Number of Slot/Holes	Pressure (psi)	Pressure (kPa)	Flow Rate (lpm)
Holes	1/32	10	30	207	5.84
			40	276	6.81
			50	345	7.59
			60	414	7.96
			60	414	8.15
Holes	1/32	12	58	400	9.49
			40	276	8.17
Holes	3/64	4	58	400	5.32
			35	241	3.92

Appendix B
Process Data

Table B.1
Process Data for Passive Injection Experiment

Date	Day	Time	Water Flow Rate (lpm)	Pressure after Pump (psi)	Pressure after Pump (kPa)	Pressure at GI (psi)	Pressure at GI (kPa)	Pressure @ IP-4 (psi)	Pressure @ IP-4 (kPa)	Gas Pressure @ Regulator 1 (psi)
May 10, 2005	0	14:05	NotAvail	NotAvail	NotAvail	NotAvail	NotAvail	NotAvail	NotAvail	NotAvail
May 10, 2005	0	14:10	6	69	476	55	379	55	379	112
May 10, 2005	0	15:05	6	67	462	55	379	55	379	112
May 10, 2005	0	16:45	6.5	69	476	55	379	56	386	110
May 12, 2005	2	3:30	NotAvail	NotAvail	NotAvail	NotAvail	NotAvail	56	NotAvail	110
May 12, 2005	2	9:35	NotAvail	NotAvail	NotAvail	NotAvail	NotAvail	NotAvail	NotAvail	50
May 12, 2005	2	9:45	NotAvail	NotAvail	NotAvail	NotAvail	NotAvail	NotAvail	NotAvail	NotAvail
May 12, 2005	2	9:55	6.5	70	483	60	414	60	414	110
May 12, 2005	2	13:00	6.5	70	483	58	400	60	414	100
May 12, 2005	2	18:35	6.5	72	496	60	414	60	414	100
May 13, 2005	3	9:05	6.5	72	496	60	414	60	414	100
May 13, 2005	3	11:45	NotAvail	NotAvail	NotAvail	NotAvail	NotAvail	NotAvail	NotAvail	NotAvail
May 13, 2005	3	13:25	8.5	62	427	50	345	50	345	100
May 13, 2005	3	14:20	8	62	427	48	331	48	331	100
May 14, 2005	4	9:25	8	64	441	50	345	50	345	100
May 14, 2005	4	20:45	NotAvail	NotAvail	NotAvail	NotAvail	NotAvail	NotAvail	NotAvail	NotAvail
May 15, 2005	5	9:40	NotAvail	NotAvail	NotAvail	NotAvail	NotAvail	NotAvail	NotAvail	NotAvail
May 15, 2005	5	9:45	8	60	414	48	331	46	317	
May 16, 2005	6	8:55	8	62	427	50	345	50	345	110
May 16, 2005	6	17:15	8	62	427	50	345	50	345	120
May 17, 2005	7	14:25	8	62	427	50	345	50	345	110
May 19, 2005	9	9:35	8	62	427	50	345	50	345	110
May 19, 2005	9	18:10	8.5	60	414	48	331	48	331	110
May 20, 2005	10	14:30	8	64	441	50	345	50	345	110

Table B.1
Process Data for Passive Injection Experiment

Date	Day	Time	Water Flow Rate (lpm)	Pressure after Pump (psi)	Pressure after Pump (kPa)	Pressure at GI (psi)	Pressure at GI (kPa)	Pressure @ IP-4 (psi)	Pressure @ IP-4 (kPa)	Gas Pressure @ Regulator 1 (psi)
May 22, 2005	12	8:05	8	62	427	50	345	50	345	110
May 23, 2005	13	10:20	8	62	427	50	345	50	345	110
May 24, 2005	14	13:45	8	64	441	50	345	50	345	110
May 25, 2005	15	6:00	NotAvail	NotAvail	NotAvail	NotAvail	NotAvail	NotAvail	NotAvail	NotAvail
May 25, 2005	15	16:30	NotAvail	NotAvail	NotAvail	NotAvail	NotAvail	NotAvail	NotAvail	NotAvail
May 25, 2005	15	20:15	8	58	400	50	345	50	345	110
May 26, 2005	16	10:35	8	58	400	50	345	50	345	110
May 26, 2005	16	18:00	NotAvail	NotAvail	NotAvail	NotAvail	NotAvail	NotAvail	NotAvail	NotAvail
May 27, 2005	17	8:50	NotAvail	NotAvail	NotAvail	NotAvail	NotAvail	NotAvail	NotAvail	NotAvail
May 27, 2005	17	9:00	5	68	469	58	400	58	400	110
May 27, 2005	17	12:30	5	68	469	58	400	58	400	110
May 28, 2005	18	2:45	NotAvail	NotAvail	NotAvail	NotAvail	NotAvail	NotAvail	NotAvail	NotAvail
May 29, 2005	19	13:00	NotAvail	NotAvail	NotAvail	NotAvail	NotAvail	NotAvail	NotAvail	NotAvail
May 29, 2005	19	13:10	4.5	71	490	58	400	58	400	110
May 30, 2005	20	12:10	3.8	70	483	62	427	62	427	110
May 30, 2005	20	12:20	NotAvail	NotAvail	NotAvail	NotAvail	NotAvail	NotAvail	NotAvail	NotAvail
May 30, 2005	20	12:45	8	62	427	48	331	48	331	110
May 31, 2005	21	12:50	8	62	427	48	331	48	331	110
June 2, 2005	23	13:06	8	62	427	48	331	48	331	110
June 2, 2005	23	17:30	NotAvail	NotAvail	NotAvail	NotAvail	NotAvail	NotAvail	NotAvail	NotAvail

Notes:

NotAvail - Not available.

NonAppl - Not applicable.

Table B.1
Process Data for Passive Injection Experiment

Date	Day	Time	Gas Pressure @ Regulator 1 (kPa)	Gas Pressure - Tank 1 (psi)	Gas Pressure - Tank 1 (kPa)	Amount in Tank 1	Gas Pressure @ Regulator 2 (psi)	Gas Pressure @ Regulator 2 (kPa)	Gas Pressure - Tank 2 (psi)
May 10, 2005	0	14:05	NotAvail	NotAvail	NotAvail	NotAvail	NonAppl	NonAppl	NonAppl
May 10, 2005	0	14:10	772	NotAvail	NotAvail	NotAvail	NonAppl	NonAppl	NonAppl
May 10, 2005	0	15:05	772	NotAvail	NotAvail	NotAvail	NonAppl	NonAppl	NonAppl
May 10, 2005	0	16:45	758	NotAvail	NotAvail	NotAvail	NonAppl	NonAppl	NonAppl
May 12, 2005	2	3:30	NotAvail	NotAvail	NotAvail	NotAvail	NonAppl	NonAppl	NonAppl
May 12, 2005	2	9:35	NotAvail	NotAvail	NotAvail	1/4	NonAppl	NonAppl	NonAppl
May 12, 2005	2	9:45	NotAvail	NotAvail	NotAvail	NotAvail	NonAppl	NonAppl	NonAppl
May 12, 2005	2	9:55	758	280	1931	Full	NonAppl	NonAppl	NonAppl
May 12, 2005	2	13:00	689	250	1724	Full	NonAppl	NonAppl	NonAppl
May 12, 2005	2	18:35	689	245	1689	Full	NonAppl	NonAppl	NonAppl
May 13, 2005	3	9:05	689	230	1586	<3/4	NonAppl	NonAppl	NonAppl
May 13, 2005	3	11:45	NotAvail	NotAvail	NotAvail	NotAvail	NonAppl	NonAppl	NonAppl
May 13, 2005	3	13:25	689	230	1586	1/2	100	689	350
May 13, 2005	3	14:20	689	230	1586	1/2	100	689	350
May 14, 2005	4	9:25	689	200	1379	<1/2	100	689	350
May 14, 2005	4	20:45	NotAvail	NotAvail	NotAvail	NotAvail	NotAvail	NotAvail	NotAvail
May 15, 2005	5	9:40	NotAvail	NotAvail	NotAvail	NotAvail	NotAvail	NotAvail	NotAvail
May 15, 2005	5	9:45	0	60	414	Empty	110	758	300
May 16, 2005	6	8:55	758	60	414	Empty	110	758	150
May 16, 2005	6	17:15	827	490	3378	>Full	110	758	170
May 17, 2005	7	14:25	758	220	1517	Full	110	758	250
May 19, 2005	9	9:35	758	210	1448	1/2	110	758	310
May 19, 2005	9	18:10	758	220	1517	1/2	110	758	200
May 20, 2005	10	14:30	758	320	2206	2/3	110	758	200

Table B.1
Process Data for Passive Injection Experiment

Date	Day	Time	Gas Pressure @ Regulator 1 (kPa)	Gas Pressure - Tank 1 (psi)	Gas Pressure - Tank 1 (kPa)	Amount in Tank 1	Gas Pressure @ Regulator 2 (psi)	Gas Pressure @ Regulator 2 (kPa)	Gas Pressure - Tank 2 (psi)
May 22, 2005	12	8:05	758	280	1931	1/4	110	758	500
May 23, 2005	13	10:20	758	280	1931	1/4	110	758	440
May 24, 2005	14	13:45	758	340	2344	1/4	110	758	250
May 25, 2005	15	6:00	NotAvail	NotAvail	NotAvail	NotAvail	NotAvail	NotAvail	NotAvail
May 25, 2005	15	16:30	NotAvail	NotAvail	NotAvail	NotAvail	NotAvail	NotAvail	NotAvail
May 25, 2005	15	20:15	758	340	2344	1/4	110	758	200
May 26, 2005	16	10:35	758	320	2206	1/5	110	758	450
May 26, 2005	16	18:00	NotAvail	NotAvail	NotAvail	NotAvail	NotAvail	NotAvail	NotAvail
May 27, 2005	17	8:50	NotAvail	NotAvail	NotAvail	NotAvail	NotAvail	NotAvail	NotAvail
May 27, 2005	17	9:00	758	270	1862	Broken gauge	110	758	290
May 27, 2005	17	12:30	758	270	1862	Broken gauge	110	758	290
May 28, 2005	18	2:45	NotAvail	NotAvail	NotAvail	NotAvail	NotAvail	NotAvail	NotAvail
May 29, 2005	19	13:00	NotAvail	NotAvail	NotAvail	NotAvail	NotAvail	NotAvail	NotAvail
May 29, 2005	19	13:10	758	120	827	<1/4	110	758	300
May 30, 2005	20	12:10	758	130	896	<1/4	110	758	280
May 30, 2005	20	12:20	NotAvail	NotAvail	NotAvail	NotAvail	NotAvail	NotAvail	NotAvail
May 30, 2005	20	12:45	758	130	896	<1/4	110	758	280
May 31, 2005	21	12:50	758	190	1310	>Full	110	758	240
June 2, 2005	23	13:06	758	170	1172	Full	110	758	240
June 2, 2005	23	17:30	NotAvail	NotAvail	NotAvail	NotAvail	NotAvail	NotAvail	NotAvail

Notes:

NotAvail - Not available.

NonAppl - Not applicable.

Table B.1
Process Data for Passive Injection Experiment

Date	Day	Time	Gas Pressure - Tank 2 (kPa)	Amount in Tank 2	Gas Flow Rate	Temperature (˚C)	Notes
May 10, 2005	0	14:05	NonAppl	NonAppl	NotAvail	NotAvail	Started injection
May 10, 2005	0	14:10	NonAppl	NonAppl	2	NotAvail	
May 10, 2005	0	15:05	NonAppl	NonAppl	2	NotAvail	
May 10, 2005	0	16:45	NonAppl	NonAppl	2.5 - 3.0	NotAvail	
May 12, 2005	2	3:30	NonAppl	NonAppl	NotAvail	NotAvail	Stopped. Ran out of CO2.
May 12, 2005	2	9:35	NonAppl	NonAppl	NotAvail	NotAvail	Experiment not running - ran out of CO2
May 12, 2005	2	9:45	NonAppl	NonAppl	NotAvail	NotAvail	Restarted experiment.
May 12, 2005	2	9:55	NonAppl	NonAppl	2.8	NotAvail	
May 12, 2005	2	13:00	NonAppl	NonAppl	3.6	NotAvail	
May 12, 2005	2	18:35	NonAppl	NonAppl	3.5	8	
May 13, 2005	3	9:05	NonAppl	NonAppl	3 - 4	10	
May 13, 2005	3	11:45	NonAppl	NonAppl	NotAvail	NotAvail	Stopped. Added second tank
May 13, 2005	3	13:25	2413	>Full	2 - 2.5	NotAvail	Restarted experiment
May 13, 2005	3	14:20	2413	>Full	2.5 - 3.0	NotAvail	
May 14, 2005	4	9:25	2413	>Full	2.5 - 3.0	NotAvail	
May 14, 2005	4	20:45	NotAvail	NotAvail	NotAvail	NotAvail	Stopped. Problem with 2nd gas tank.
May 15, 2005	5	9:40	NotAvail	NotAvail	NotAvail	15	Experiment not running - problem with 2nd gas tank
May 15, 2005	5	9:45	2068	>Full	2 - 3	15	Restarted experiment
May 16, 2005	6	8:55	1034	>Full	2 - 3	7	
May 16, 2005	6	17:15	1172	>Full	2 - 3	10	
May 17, 2005	7	14:25	1724	>Full	2 - 3	16	Added new tank 1
May 19, 2005	9	9:35	2137	>Full	2 - 3	NotAvail	
May 19, 2005	9	18:10	1379	Full	2 - 3	19	
May 20, 2005	10	14:30	1379	Full	2 - 3	22	Added new tank 1

Table B.1
Process Data for Passive Injection Experiment

Date	Day	Time	Gas Pressure - Tank 2 (kPa)	Amount in Tank 2	Gas Flow Rate	Temperature (˚C)	Notes
May 22, 2005	12	8:05	3447	Full	2 - 3	NotAvail	Added new tank 2
May 23, 2005	13	10:20	3034	Full	2 - 3	NotAvail	
May 24, 2005	14	13:45	1724	Full	2 - 3	18	Added new tank 2
May 25, 2005	15	6:00	NotAvail	NotAvail	NotAvail	NotAvail	Stopped. No H2O.
May 25, 2005	15	16:30	NotAvail	NotAvail	NotAvail	NotAvail	Notified that experiment is not running - ran out of H_2O.
May 25, 2005	15	20:15	1379	3/4	2 - 3	NotAvail	Restarted experiment
May 26, 2005	16	10:35	3103	1/2	2 - 3	25	
May 26, 2005	16	18:00	NotAvail	NotAvail	NotAvail	NotAvail	Stopped. Ran out of CO2.
May 27, 2005	17	8:50	NotAvail	NotAvail	NotAvail	NotAvail	Experiment not running - ran out of CO2
May 27, 2005	17	9:00	1999	1/2	2 - 2.5	24	Restarted. Added two new tanks. Lower flow rate.
May 27, 2005	17	12:30	1999	1/2	2 - 2.5	24	
May 28, 2005	18	2:45	NotAvail	NotAvail	NotAvail	NotAvail	Stopped. Problem with CO2 gauge.
May 29, 2005	19	13:00	NotAvail	NotAvail	NotAvail	NotAvail	Experiment not running - problem with tanks
May 29, 2005	19	13:10	2068	1/2	2 - 3	20	Restarted. Tank 1 gauge might be broken because it is a new tank. Lower flow rate.
May 30, 2005	20	12:10	1931	1/2	2 - 3	20	
May 30, 2005	20	12:20	NotAvail	NotAvail	NotAvail	NotAvail	Stopped experiment to redevelop IP-4
May 30, 2005	20	12:45	1931	1/2	2 - 3	20	Restarted experiment
May 31, 2005	21	12:50	1655	<1/4	2 - 3	25	Added new tank 1
June 2, 2005	23	13:06	1655	<1/4	2 - 3	NotAvail	
June 2, 2005	23	17:30	NotAvail	NotAvail	NotAvail	NotAvail	First experiment finished

Notes:

NotAvail - Not available.
NonAppl - Not applicable.

Table B.2
Process Data for Active Injection Experiment

Date	Day	Time	Water Flow Rate (lpm)	Pressure after Pump (psi)	Pressure after Pump (kPa)	Pressure at GI (psi)	Pressure at GI (kPa)	Pressure @ IP-4 (psi)	Pressure @ IP-4 (kPa)	Gas Pressure @ Regulator 1 (psi)	Gas Pressure @ Regulator 1 (kPa)
June 23, 2005	2	11:30	8	56	386	42	290	42	290	110	758
June 24, 2005	3	9:00	NotAvail	NotAvail	NotAvail	NotAvail	NotAvail	NotAvail	NotAvail	NotAvail	NotAvail
June 24, 2005	3	9:40	8	58	400	43	296	43	296	110	758
June 24, 2005	3	10:50	8	58	400	43	296	43	296	110	758
June 26, 2005	5	12:08	8	60	414	45	310	45	310	110	758
June 27, 2005	6	9:00	8	60	414	44	303	44	303	110	758
June 27, 2005	6	11:00	8	60	414	44	303	44	303	110	758
June 28, 2005	7	11:25	8	60	414	45	310	45	310	110	758
June 29, 2005	8	9:10	8	61	421	46	317	46	317	110	758
June 29, 2005	8	9:55	8	61	421	46	317	46	317	115	793
June 30, 2005	9	14:40	8	58	400	42	290	42	290	105	724
July 2, 2005	11	9:30	8	58	400	44	303	44	303	105	724
July 4, 2005	13	12:45	8	60	414	44	303	44	303	105	724
July 6, 2005	15	10:20	8	60	414	44	303	44	303	90	621
July 7, 2005	16	11:50	8	60	414	44	303	44	303	90	621
July 7, 2005	16	13:30	NonAppl	NonAppl	NonAppl	NonAppl	NonAppl	NonAppl	NonAppl	NonAppl	NonAppl

Notes:

NotAvail - Not available.
NonAppl - Not applicable.

Table B.2
Process Data for Active Injection Experiment

Date	Day	Time	Gas Pressure - Tank 1 (psi)	Gas Pressure - Tank 1 (kPa)	Amount in Tank 1	Gas Pressure @ Regulator 2 (psi)	Gas Pressure @ Regulator 2 (kPa)	Amount in Tank 2	Gas Flow Rate	Temperature (deg C)	EW-5 (Hz)
June 23, 2005	2	11:30	300	2068	Full	NotAvail	NotAvail	NotAvail	2 - 3	NotAvail	95
June 24, 2005	3	9:00	NotAvail	NotAvail	NotAvail	NotAvail	NotAvail	NotAvail	NotAvail	NotAvail	NotAvail
June 24, 2005	3	9:40	480	3309	>Full	110	758	3/4	2 - 3	NotAvail	
June 24, 2005	3	10:50	480	3309	>Full	110	758	3/4	2 - 3	NotAvail	95
June 26, 2005	5	12:08	415	2861	<Full	110	758	3/4	2 - 3	NotAvail	95
June 27, 2005	6	9:00	400	2758	<1/2	110	758	3/4	2 - 3	NotAvail	100
June 27, 2005	6	11:00	400	2758	<1/2	110	758	3/4	2 - 3	NotAvail	100
June 28, 2005	7	11:25	300	2068	>Empty	110	758	>1/2	2 - 3	NotAvail	82
June 29, 2005	8	9:10	300	2068	>Empty	110	758	<1/2	2 - 3	NotAvail	82
June 29, 2005	8	9:55	1000	6895		110	758	<1/2	2 - 3	NotAvail	82
June 30, 2005	9	14:40	300	2068	<Full	130	896	<Full	2 - 3	NotAvail	92
July 2, 2005	11	9:30	300	2068	<Full	125	862	<Full	2 - 3	NotAvail	92
July 4, 2005	13	12:45	120	827	Broken gauge?	115	793	>1/2	2 - 3	NotAvail	94
July 6, 2005	15	10:20	200	1379	3/4	130	896	<1/2	2 - 3	NotAvail	94
July 7, 2005	16	11:50	200	1379	<1/2	130	896	<1/2	2 - 3	NotAvail	94
July 7, 2005	16	13:30	NonAppl	NonAppl	NonAppl	NonAppl	NonAppl	NonAppl	NonAppl	NonAppl	NonAppl

Notes:

NotAvail - Not available.
NonAppl - Not applicable.

Table B.2
Process Data for Active Injection Experiment

Date	Day	Time	EW-6 (Hz)	Extraction Rate (lpm)	Notes
June 23, 2005	2	11:30	95	8	
June 24, 2005	3	9:00	NotAvail	NotAvail	Experiment not running - the tank is full, but unable to build pressure
June 24, 2005	3	9:40	95	4	Restarted experiment. Two new tanks of gas. Pump in EW-5 had an error message.
June 24, 2005	3	10:50	95	8	Pump at EW-5 working again.
June 26, 2005	5	12:08	95	8	
June 27, 2005	6	9:00	100	8	Increased pumping rate
June 27, 2005	6	11:00	100	8	
June 28, 2005	7	11:25	82	8	Problem with pump in EW-5. It didn't appear to be working, so it was adjusted.
June 29, 2005	8	9:10	82	8	
June 29, 2005	8	9:55	82	8	Changed to T size tank.
June 30, 2005	9	14:40	92	8	Added two new tanks. Increased pumping rate.
July 2, 2005	11	9:30	92	8	
July 4, 2005	13	12:45	94	8	Increased pumping rate
July 6, 2005	15	10:20	94	8	
July 7, 2005	16	11:50	94	8	
July 7, 2005	16	13:30	NonAppl	NonAppl	Second experiment finished.

Notes:

NotAvail - Not available.
NonAppl - Not applicable.

Appendix C
Groundwater Quality Data

Table C.1
CO_2 Concentrations and Partial Pressures

Monitoring Well	Collection Date	Collection Time	Experiment	Water Concentration (mg/L)	Water Concentration (mols/L)	pH	Partial Pressure (atm)	Exceeds Applicable Hydrostatic Pressure
MW-10-D	5/5/2005	1:57:00 PM	Background	405.20	9.21E-03	7.06	0.035	No
MW-10-D	5/12/2005	4:27:00 PM	No Hydraulic Control	263.88	6.00E-03	7.10	0.021	No
MW-10-D	5/16/2005	3:27:00 PM	No Hydraulic Control	227.70	5.17E-03	7.12	0.018	No
MW-10-D	5/20/2005	12:41:00 PM	No Hydraulic Control	359.84	8.18E-03	7.07	0.030	No
MW-10-D	5/24/2005	11:25:00 AM	No Hydraulic Control	2005.95	4.56E-02	6.56	0.382	No
MW-10-D	5/27/2005	11:14:00 AM	No Hydraulic Control	2065.39	4.69E-02	6.18	0.578	No
MW-10-D	5/30/2005	10:48:00 AM	No Hydraulic Control	1754.16	3.99E-02	5.79	0.614	No
MW-10-D	6/2/2005	11:30:00 AM	No Hydraulic Control	2918.07	6.63E-02	6.08	0.877	No
MW-10-D	6/21/2005	1:10:00 PM	Between	303.95	6.91E-03	7.09	0.025	No
MW-10-D	6/23/2005	9:43:00 AM	With Hydraulic Control	340.39	7.74E-03	7.08	0.028	No
MW-10-D	6/27/2005	9:43:00 AM	With Hydraulic Control	304.07	6.91E-03	7.09	0.025	No
MW-10-D	6/28/2005	9:34:00 AM	With Hydraulic Control	470.28	1.07E-02	7.04	0.042	No
MW-10-D	6/30/2005	9:34:00 AM	With Hydraulic Control	763.38	1.73E-02	6.94	0.081	No
MW-10-D	7/7/2005	10:37:00 AM	With Hydraulic Control	2664.01	6.05E-02	6.36	0.634	No
MW-10-S	5/5/2005	1:48:00 PM	Background	330.72	7.52E-03	7.08	0.027	No
MW-10-S	5/12/2005	4:22:00 PM	No Hydraulic Control	281.39	6.40E-03	7.10	0.023	No
MW-10-S	5/16/2005	3:25:00 PM	No Hydraulic Control	268.83	6.11E-03	7.10	0.021	No
MW-10-S	5/20/2005	12:36:00 PM	No Hydraulic Control	601.18	1.37E-02	6.99	0.059	No
MW-10-S	5/24/2005	11:20:00 AM	No Hydraulic Control	1897.36	4.31E-02	6.59	0.347	No
MW-10-S	5/27/2005	11:28:00 AM	No Hydraulic Control	2121.06	4.82E-02	6.12	0.620	No
MW-10-S	5/30/2005	10:50:00 AM	No Hydraulic Control	2086.96	4.74E-02	5.98	0.667	No
MW-10-S	6/2/2005	11:28:00 AM	No Hydraulic Control	2279.14	5.18E-02	6.10	0.676	No
MW-10-S	6/21/2005	1:05:00 PM	Between	273.05	6.21E-03	7.10	0.022	No
MW-10-S	6/23/2005	9:38:00 AM	With Hydraulic Control	296.63	6.74E-03	7.09	0.024	No
MW-10-S	6/27/2005	9:35:00 AM	With Hydraulic Control	248.52	5.65E-03	7.11	0.020	No
MW-10-S	6/28/2005	9:29:00 AM	With Hydraulic Control	241.15	5.48E-03	7.11	0.019	No
MW-10-S	6/30/2005	9:29:00 AM	With Hydraulic Control	296.35	6.74E-03	7.09	0.024	No
MW-10-S	7/7/2005	10:32:00 AM	With Hydraulic Control	352.06	8.00E-03	7.08	0.030	No
MW-11-D	5/5/2005	2:30:00 PM	Background	339.83	7.72E-03	7.08	0.028	No

Table C.1
CO_2 Concentrations and Partial Pressures

Monitoring Well	Collection Date	Collection Time	Experiment	Water Concentration (mg/L)	Water Concentration (mols/L)	pH	Partial Pressure (atm)	Exceeds Applicable Hydrostatic Pressure
MW-11-D	5/12/2005	5:40:00 PM	No Hydraulic Control	227.98	5.18E-03	7.12	0.018	No
MW-11-D	5/16/2005	3:55:00 PM	No Hydraulic Control	217.48	4.94E-03	7.12	0.017	No
MW-11-D	5/20/2005	1:16:00 PM	No Hydraulic Control	283.62	6.45E-03	7.10	0.023	No
MW-11-D	5/24/2005	12:17:00 PM	No Hydraulic Control	1037.72	2.36E-02	6.86	0.128	No
MW-11-D	5/27/2005	11:20:00 AM	No Hydraulic Control	1624.46	3.69E-02	6.20	0.447	No
MW-11-D	5/30/2005	11:08:00 AM	No Hydraulic Control	1801.05	4.09E-02	6.32	0.446	No
MW-11-D	6/2/2005	12:05:00 PM	No Hydraulic Control	3322.30	7.55E-02	6.06	1.012	No
MW-11-D	6/21/2005	1:32:00 PM	Between	1702.12	3.87E-02	6.65	0.287	No
MW-11-D	6/23/2005	10:10:00 AM	With Hydraulic Control	2467.62	5.61E-02	6.42	0.553	No
MW-11-D	6/27/2005	10:03:00 AM	With Hydraulic Control	3335.19	7.58E-02	6.17	0.942	No
MW-11-D	6/28/2005	10:00:00 AM	With Hydraulic Control	3562.87	8.10E-02	6.10	1.055	No
MW-11-D	6/30/2005	9:58:00 AM	With Hydraulic Control	3242.98	7.37E-02	6.19	0.898	No
MW-11-D	7/7/2005	10:55:00 AM	With Hydraulic Control	3580.48	8.14E-02	6.10	1.064	No
MW-11-S	5/5/2005	2:34:00 PM	Background	323.72	7.36E-03	7.08	0.027	No
MW-11-S	5/12/2005	5:35:00 PM	No Hydraulic Control	234.09	5.32E-03	7.11	0.018	No
MW-11-S	5/16/2005	3:50:00 PM	No Hydraulic Control	293.78	6.68E-03	7.09	0.024	No
MW-11-S	5/20/2005	1:07:00 PM	No Hydraulic Control	364.44	8.28E-03	7.07	0.031	No
MW-11-S	5/24/2005	12:12:00 PM	No Hydraulic Control	1565.48	3.56E-02	6.69	0.249	No
MW-11-S	5/27/2005	11:18:00 AM	No Hydraulic Control	3578.52	8.13E-02	6.08	1.076	No
MW-11-S	5/30/2005	11:10:00 AM	No Hydraulic Control	4159.84	9.45E-02	6.18	1.164	Yes
MW-11-S	6/2/2005	12:00:00 PM	No Hydraulic Control	4060.30	9.23E-02	5.99	1.291	Yes
MW-11-S	6/21/2005	1:27:00 PM	Between	2615.86	5.95E-02	6.38	0.614	No
MW-11-S	6/23/2005	10:05:00 AM	With Hydraulic Control	2955.56	6.72E-02	6.28	0.763	No
MW-11-S	6/27/2005	9:58:00 AM	With Hydraulic Control	2831.91	6.44E-02	6.31	0.707	No
MW-11-S	6/28/2005	9:55:00 AM	With Hydraulic Control	3315.51	7.54E-02	6.17	0.933	No
MW-11-S	6/30/2005	9:53:00 AM	With Hydraulic Control	3856.52	8.76E-02	6.02	1.204	Yes
MW-11-S	7/7/2005	10:52:00 AM	With Hydraulic Control	2703.63	6.14E-02	6.35	0.651	No
MW-12-D	5/5/2005	2:05:00 PM	Background	316.79	7.20E-03	7.09	0.026	No
MW-12-D	5/12/2005	5:15:00 PM	No Hydraulic Control	257.95	5.86E-03	7.11	0.020	No

Table C.1
CO_2 Concentrations and Partial Pressures

Monitoring Well	Collection Date	Collection Time	Experiment	Water Concentration (mg/L)	Water Concentration (mols/L)	pH	Partial Pressure (atm)	Exceeds Applicable Hydrostatic Pressure
MW-12-D	5/16/2005	3:43:00 PM	No Hydraulic Control	333.72	7.58E-03	7.08	0.028	No
MW-12-D	5/20/2005	1:05:00 PM	No Hydraulic Control	318.43	7.24E-03	7.09	0.026	No
MW-12-D	5/24/2005	11:37:00 AM	No Hydraulic Control	1115.41	2.54E-02	6.83	0.143	No
MW-12-D	5/27/2005	11:00:00 AM	No Hydraulic Control	1470.84	3.34E-02	6.32	0.364	No
MW-12-D	5/30/2005	10:55:00 AM	No Hydraulic Control	964.59	2.19E-02	6.09	0.288	No
MW-12-D	6/2/2005	11:54:00 AM	No Hydraulic Control	2095.35	4.76E-02	6.20	0.577	No
MW-12-D	6/21/2005	1:21:00 PM	Between	364.33	8.28E-03	7.07	0.031	No
MW-12-D	6/23/2005	9:58:00 AM	With Hydraulic Control	505.04	1.15E-02	7.03	0.047	No
MW-12-D	6/27/2005	9:53:00 AM	With Hydraulic Control	890.08	2.02E-02	6.90	0.102	No
MW-12-D	6/28/2005	9:45:00 AM	With Hydraulic Control	884.93	2.01E-02	6.90	0.101	No
MW-12-D	6/30/2005	9:45:00 AM	With Hydraulic Control	1627.75	3.70E-02	6.67	0.266	No
MW-12-D	7/7/2005	10:47:00 AM	With Hydraulic Control	2839.61	6.45E-02	6.31	0.711	No
MW-12-S	5/5/2005	2:02:00 PM	Background	477.92	1.09E-02	7.03	0.043	No
MW-12-S	5/12/2005	5:10:00 PM	No Hydraulic Control	352.41	8.01E-03	7.08	0.030	No
MW-12-S	5/16/2005	3:38:00 PM	No Hydraulic Control	935.04	2.13E-02	6.89	0.109	No
MW-12-S	5/20/2005	12:57:00 PM	No Hydraulic Control	1621.94	3.69E-02	6.67	0.264	No
MW-12-S	5/24/2005	11:35:00 AM	No Hydraulic Control	4094.50	9.31E-02	5.96	1.327	Yes
MW-12-S	5/27/2005	10:55:00 AM	No Hydraulic Control	4119.14	9.36E-02	6.04	1.271	Yes
MW-12-S	5/30/2005	11:03:00 AM	No Hydraulic Control	4049.77	9.20E-02	6.32	1.003	No
MW-12-S	6/2/2005	11:49:00 AM	No Hydraulic Control	4215.41	9.58E-02	5.98	1.348	Yes
MW-12-S	6/21/2005	1:16:00 PM	Between	2289.20	5.20E-02	6.47	0.483	No
MW-12-S	6/23/2005	9:53:00 AM	With Hydraulic Control	2464.31	5.60E-02	6.42	0.552	No
MW-12-S	6/27/2005	9:48:00 AM	With Hydraulic Control	2800.72	6.37E-02	6.32	0.693	No
MW-12-S	6/28/2005	9:40:00 AM	With Hydraulic Control	3196.97	7.27E-02	6.21	0.875	No
MW-12-S	6/30/2005	9:40:00 AM	With Hydraulic Control	2624.13	5.96E-02	6.37	0.617	No
MW-12-S	7/7/2005	10:45:00 AM	With Hydraulic Control	2063.83	4.69E-02	6.54	0.402	No
MW-1-D	5/5/2005	11:58:00 AM	Background	271.16	6.16E-03	7.10	0.022	No
MW-1-D	5/12/2005	2:38:00 PM	No Hydraulic Control	291.79	6.63E-03	7.10	0.024	No
MW-1-D	5/16/2005	4:57:00 PM	No Hydraulic Control	250.05	5.68E-03	7.11	0.020	No

Table C.1
CO_2 Concentrations and Partial Pressures

Monitoring Well	Collection Date	Collection Time	Experiment	Water Concentration (mg/L)	Water Concentration (mols/L)	pH	Partial Pressure (atm)	Exceeds Applicable Hydrostatic Pressure
MW-1-D	5/20/2005	2:25:00 PM	No Hydraulic Control	266.77	6.06E-03	7.10	0.021	No
MW-1-D	5/24/2005	1:25:00 PM	No Hydraulic Control	277.56	6.31E-03	7.10	0.022	No
MW-1-D	5/27/2005	11:59:00 AM	No Hydraulic Control	360.23	8.19E-03	6.78	0.050	No
MW-1-D	5/30/2005	11:58:00 AM	No Hydraulic Control	1248.04	2.84E-02	6.41	0.282	No
MW-1-D	6/2/2005	1:06:00 PM	No Hydraulic Control	1158.74	2.63E-02	6.46	0.248	No
MW-1-D	6/21/2005	2:42:00 PM	Between	3168.98	7.20E-02	6.21	0.862	No
MW-1-D	6/23/2005	11:03:00 AM	With Hydraulic Control	3480.99	7.91E-02	6.13	1.014	No
MW-1-D	6/27/2005	10:58:00 AM	With Hydraulic Control	3556.02	8.08E-02	6.10	1.051	No
MW-1-D	6/28/2005	10:56:00 AM	With Hydraulic Control	2801.58	6.37E-02	6.32	0.694	No
MW-1-D	6/30/2005	10:55:00 AM	With Hydraulic Control	2079.79	4.73E-02	6.53	0.408	No
MW-1-D	7/7/2005	11:38:00 AM	With Hydraulic Control	2866.07	6.51E-02	6.30	0.722	No
MW-1-S	5/5/2005	11:50:00 AM	Background	276.78	6.29E-03	7.10	0.022	No
MW-1-S	5/12/2005	2:28:00 PM	No Hydraulic Control	291.73	6.63E-03	7.10	0.024	No
MW-1-S	5/16/2005	4:55:00 PM	No Hydraulic Control	212.85	4.84E-03	7.12	0.016	No
MW-1-S	5/20/2005	2:20:00 PM	No Hydraulic Control	356.13	8.09E-03	7.07	0.030	No
MW-1-S	5/24/2005	1:20:00 PM	No Hydraulic Control	1860.23	4.23E-02	6.60	0.335	No
MW-1-S	5/27/2005	11:45:00 AM	No Hydraulic Control	3557.64	8.09E-02	5.93	1.169	Yes
MW-1-S	5/30/2005	11:55:00 AM	No Hydraulic Control	4377.31	9.95E-02	6.07	1.325	Yes
MW-1-S	6/2/2005	1:03:00 PM	No Hydraulic Control	3701.31	8.41E-02	6.11	1.090	No
MW-1-S	6/21/2005	2:48:00 PM	Between	3970.73	9.02E-02	5.99	1.263	Yes
MW-1-S	6/23/2005	10:57:00 AM	With Hydraulic Control	3539.32	8.04E-02	6.11	1.043	No
MW-1-S	6/27/2005	10:53:00 AM	With Hydraulic Control	3716.03	8.45E-02	6.06	1.132	No
MW-1-S	6/28/2005	10:53:00 AM	With Hydraulic Control	3280.24	7.46E-02	6.18	0.915	No
MW-1-S	6/30/2005	10:50:00 AM	With Hydraulic Control	3289.06	7.48E-02	6.18	0.920	No
MW-1-S	7/7/2005	11:35:00 AM	With Hydraulic Control	2514.86	5.72E-02	6.40	0.572	No
MW-2-D	5/5/2005	11:56:00 AM	Background	286.95	6.52E-03	7.10	0.023	No
MW-2-D	5/12/2005	2:20:00 PM	No Hydraulic Control	277.62	6.31E-03	7.10	0.022	No
MW-2-D	5/16/2005	2:00:00 PM	No Hydraulic Control	235.21	5.35E-03	7.11	0.018	No
MW-2-D	5/20/2005	11:33:00 AM	No Hydraulic Control	279.15	6.34E-03	7.10	0.022	No

Table C.1
CO_2 Concentrations and Partial Pressures

Monitoring Well	Collection Date	Collection Time	Experiment	Water Concentration (mg/L)	Water Concentration (mols/L)	pH	Partial Pressure (atm)	Exceeds Applicable Hydrostatic Pressure
MW-2-D	5/24/2005	9:55:00 AM	No Hydraulic Control	255.67	5.81E-03	7.11	0.020	No
MW-2-D	5/27/2005	9:45:00 AM	No Hydraulic Control	321.73	7.31E-03	7.02	0.030	No
MW-2-D	5/30/2005	10:15:00 AM	No Hydraulic Control	318.49	7.24E-03	7.25	0.019	No
MW-2-D	6/2/2005	10:45:00 AM	No Hydraulic Control	330.91	7.52E-03	6.92	0.037	No
MW-2-D	6/21/2005	12:00:00 PM	Between	278.23	6.32E-03	7.10	0.022	No
MW-2-D	6/23/2005	9:10:00 AM	With Hydraulic Control	294.81	6.70E-03	7.09	0.024	No
MW-2-D	6/27/2005	9:21:00 AM	With Hydraulic Control	228.83	5.20E-03	7.12	0.018	No
MW-2-D	6/28/2005	8:45:00 AM	With Hydraulic Control	235.78	5.36E-03	7.11	0.018	No
MW-2-D	6/30/2005	9:35:00 AM	With Hydraulic Control	233.73	5.31E-03	7.11	0.018	No
MW-2-D	7/7/2005	9:50:00 AM	With Hydraulic Control	354.49	8.06E-03	7.07	0.030	No
MW-2-S	5/5/2005	11:48:00 AM	Background	269.02	6.11E-03	7.10	0.022	No
MW-2-S	5/12/2005	2:10:00 PM	No Hydraulic Control	273.27	6.21E-03	7.10	0.022	No
MW-2-S	5/16/2005	1:50:00 PM	No Hydraulic Control	252.42	5.74E-03	7.11	0.020	No
MW-2-S	5/20/2005	11:30:00 AM	No Hydraulic Control	278.97	6.34E-03	7.10	0.022	No
MW-2-S	5/24/2005	9:45:00 AM	No Hydraulic Control	296.51	6.74E-03	7.09	0.024	No
MW-2-S	5/27/2005	9:50:00 AM	No Hydraulic Control	571.36	1.30E-02	7.08	0.048	No
MW-2-S	5/30/2005	10:05:00 AM	No Hydraulic Control	314.53	7.15E-03	7.12	0.024	No
MW-2-S	6/2/2005	10:40:00 AM	No Hydraulic Control	270.16	6.14E-03	6.74	0.040	No
MW-2-S	6/21/2005	11:55:00 AM	Between	263.14	5.98E-03	7.10	0.021	No
MW-2-S	6/23/2005	9:00:00 AM	With Hydraulic Control	282.00	6.41E-03	7.10	0.023	No
MW-2-S	6/27/2005	9:15:00 AM	With Hydraulic Control	243.39	5.53E-03	7.11	0.019	No
MW-2-S	6/28/2005	8:35:00 AM	With Hydraulic Control	252.07	5.73E-03	7.11	0.020	No
MW-2-S	6/30/2005	9:25:00 AM	With Hydraulic Control	237.22	5.39E-03	7.11	0.019	No
MW-2-S	7/7/2005	9:53:00 AM	With Hydraulic Control	269.51	6.13E-03	7.10	0.022	No
MW-3-D	5/5/2005	12:58:00 PM	Background	285.53	6.49E-03	7.10	0.023	No
MW-3-D	5/12/2005	2:50:00 PM	No Hydraulic Control	228.27	5.19E-03	7.12	0.018	No
MW-3-D	5/16/2005	4:34:00 PM	No Hydraulic Control	207.81	4.72E-03	7.12	0.016	No
MW-3-D	5/20/2005	2:13:00 PM	No Hydraulic Control	1600.31	3.64E-02	6.68	0.258	No
MW-3-D	5/24/2005	1:10:00 PM	No Hydraulic Control	4332.72	9.85E-02	5.89	1.451	Yes

Table C.1
CO_2 Concentrations and Partial Pressures

Monitoring Well	Collection Date	Collection Time	Experiment	Water Concentration (mg/L)	Water Concentration (mols/L)	pH	Partial Pressure (atm)	Exceeds Applicable Hydrostatic Pressure
MW-3-D	5/27/2005	12:21:00 PM	No Hydraulic Control	4123.38	9.37E-02	5.86	1.401	Yes
MW-3-D	5/30/2005	11:45:00 AM	No Hydraulic Control	4493.67	1.02E-01	5.94	1.468	Yes
MW-3-D	6/2/2005	12:35:00 PM	No Hydraulic Control	3832.19	8.71E-02	6.05	1.175	No
MW-3-D	6/21/2005	2:30:00 PM	Between	3381.90	7.69E-02	6.15	0.965	No
MW-3-D	6/23/2005	10:51:00 AM	With Hydraulic Control	2674.37	6.08E-02	6.36	0.639	No
MW-3-D	6/27/2005	10:48:00 AM	With Hydraulic Control	3769.11	8.57E-02	6.05	1.159	No
MW-3-D	6/28/2005	10:45:00 AM	With Hydraulic Control	3200.46	7.27E-02	6.21	0.877	No
MW-3-D	6/30/2005	10:40:00 AM	With Hydraulic Control	2910.50	6.61E-02	6.29	0.742	No
MW-3-D	7/7/2005	11:24:00 AM	With Hydraulic Control	2881.94	6.55E-02	6.30	0.729	No
MW-3-S	5/5/2005	1:10:00 PM	Background	365.68	8.31E-03	7.07	0.031	No
MW-3-S	5/12/2005	2:45:00 PM	No Hydraulic Control	353.45	8.03E-03	7.08	0.030	No
MW-3-S	5/16/2005	4:36:00 PM	No Hydraulic Control	297.44	6.76E-03	7.09	0.024	No
MW-3-S	5/20/2005	2:10:00 PM	No Hydraulic Control	287.39	6.53E-03	7.10	0.023	No
MW-3-S	5/24/2005	1:05:00 PM	No Hydraulic Control	1130.67	2.57E-02	6.83	0.146	No
MW-3-S	5/27/2005	12:18:00 PM	No Hydraulic Control	3910.83	8.89E-02	5.86	1.329	Yes
MW-3-S	5/30/2005	11:40:00 AM	No Hydraulic Control	3925.41	8.92E-02	6.06	1.196	Yes
MW-3-S	6/2/2005	12:48:00 PM	No Hydraulic Control	3978.78	9.04E-02	6.03	1.235	Yes
MW-3-S	6/21/2005	2:20:00 PM	Between	3361.80	7.64E-02	6.16	0.955	No
MW-3-S	6/23/2005	10:50:00 AM	With Hydraulic Control	3373.56	7.67E-02	6.16	0.961	No
MW-3-S	6/27/2005	10:43:00 AM	With Hydraulic Control	3347.46	7.61E-02	6.16	0.948	No
MW-3-S	6/28/2005	10:43:00 AM	With Hydraulic Control	3123.29	7.10E-02	6.23	0.841	No
MW-3-S	6/30/2005	10:38:00 AM	With Hydraulic Control	2536.56	5.76E-02	6.40	0.581	No
MW-3-S	7/7/2005	11:23:00 AM	With Hydraulic Control	3272.77	7.44E-02	6.19	0.912	No
MW-4-D	5/5/2005	1:32:00 PM	Background	224.83	5.11E-03	7.12	0.017	No
MW-4-D	5/12/2005	4:10:00 PM	No Hydraulic Control	295.75	6.72E-03	7.09	0.024	No
MW-4-D	5/16/2005	2:10:00 PM	No Hydraulic Control	219.69	4.99E-03	7.12	0.017	No
MW-4-D	5/20/2005	12:27:00 PM	No Hydraulic Control	260.24	5.91E-03	7.11	0.021	No
MW-4-D	5/24/2005	9:57:00 AM	No Hydraulic Control	305.51	6.94E-03	7.09	0.025	No
MW-4-D	5/27/2005	10:37:00 AM	No Hydraulic Control	702.50	1.60E-02	6.63	0.122	No

Table C.1
CO_2 Concentrations and Partial Pressures

Monitoring Well	Collection Date	Collection Time	Experiment	Water Concentration (mg/L)	Water Concentration (mols/L)	pH	Partial Pressure (atm)	Exceeds Applicable Hydrostatic Pressure
MW-4-D	5/30/2005	10:27:00 AM	No Hydraulic Control	614.99	1.40E-02	6.82	0.080	No
MW-4-D	6/2/2005	11:20:00 AM	No Hydraulic Control	1096.97	2.49E-02	7.04	0.098	No
MW-4-D	6/21/2005	12:47:00 PM	Between	290.85	6.61E-03	7.10	0.024	No
MW-4-D	6/23/2005	9:17:00 AM	With Hydraulic Control	243.46	5.53E-03	7.11	0.019	No
MW-4-D	6/27/2005	9:29:00 AM	With Hydraulic Control	339.94	7.73E-03	7.08	0.028	No
MW-4-D	6/28/2005	9:13:00 AM	With Hydraulic Control	364.54	8.28E-03	7.07	0.031	No
MW-4-D	6/30/2005	9:10:00 AM	With Hydraulic Control	918.48	2.09E-02	6.89	0.106	No
MW-4-D	7/7/2005	10:19:00 AM	With Hydraulic Control	2895.74	6.58E-02	6.29	0.736	No
MW-4-S	5/5/2005	1:34:00 PM	Background	262.59	5.97E-03	7.10	0.021	No
MW-4-S	5/12/2005	4:05:00 PM	No Hydraulic Control	288.23	6.55E-03	7.10	0.023	No
MW-4-S	5/16/2005	2:05:00 PM	No Hydraulic Control	227.11	5.16E-03	7.12	0.018	No
MW-4-S	5/20/2005	12:25:00 PM	No Hydraulic Control	288.85	6.56E-03	7.10	0.023	No
MW-4-S	5/24/2005	10:03:00 AM	No Hydraulic Control	273.20	6.21E-03	7.10	0.022	No
MW-4-S	5/27/2005	10:56:00 AM	No Hydraulic Control	240.73	5.47E-03	7.07	0.020	No
MW-4-S	5/30/2005	10:23:00 AM	No Hydraulic Control	316.51	7.19E-03	7.04	0.028	No
MW-4-S	6/2/2005	11:22:00 AM	No Hydraulic Control	310.65	7.06E-03	6.50	0.063	No
MW-4-S	6/21/2005	12:42:00 PM	Between	265.07	6.02E-03	7.10	0.021	No
MW-4-S	6/23/2005	9:15:00 AM	With Hydraulic Control	236.22	5.37E-03	7.11	0.019	No
MW-4-S	6/27/2005	9:25:00 AM	With Hydraulic Control	233.95	5.32E-03	7.11	0.018	No
MW-4-S	6/28/2005	9:08:00 AM	With Hydraulic Control	246.33	5.60E-03	7.11	0.019	No
MW-4-S	6/30/2005	9:05:00 AM	With Hydraulic Control	262.75	5.97E-03	7.10	0.021	No
MW-4-S	7/7/2005	10:17:00 AM	With Hydraulic Control	267.11	6.07E-03	7.10	0.021	No
MW-5-D	5/5/2005	1:23:00 PM	Background	255.98	5.82E-03	7.11	0.020	No
MW-5-D	5/12/2005	3:00:00 PM	No Hydraulic Control	3593.58	8.17E-02	6.09	1.070	No
MW-5-D	5/16/2005	4:25:00 PM	No Hydraulic Control	4444.50	1.01E-01	5.86	1.510	Yes
MW-5-D	5/20/2005	1:58:00 PM	No Hydraulic Control	3332.66	7.57E-02	6.17	0.941	No
MW-5-D	5/24/2005	12:53:00 PM	No Hydraulic Control	3916.84	8.90E-02	6.00	1.235	No
MW-5-D	5/27/2005	12:07:00 PM	No Hydraulic Control	3178.86	7.22E-02	6.02	0.993	No
MW-5-D	5/30/2005	11:33:00 AM	No Hydraulic Control	3901.68	8.87E-02	6.02	1.219	No

Table C.1
CO_2 Concentrations and Partial Pressures

Monitoring Well	Collection Date	Collection Time	Experiment	Water Concentration (mg/L)	Water Concentration (mols/L)	pH	Partial Pressure (atm)	Exceeds Applicable Hydrostatic Pressure
MW-5-D	6/2/2005	12:27:00 PM	No Hydraulic Control	3745.64	8.51E-02	5.98	1.198	No
MW-5-D	6/21/2005	2:05:00 PM	Between	2972.45	6.76E-02	6.27	0.770	No
MW-5-D	6/23/2005	10:43:00 AM	With Hydraulic Control	3213.31	7.30E-02	6.20	0.883	No
MW-5-D	6/27/2005	10:35:00 AM	With Hydraulic Control	2883.35	6.55E-02	6.30	0.730	No
MW-5-D	6/28/2005	10:32:00 AM	With Hydraulic Control	2686.89	6.11E-02	6.35	0.644	No
MW-5-D	6/30/2005	10:30:00 AM	With Hydraulic Control	3209.93	7.30E-02	6.20	0.882	No
MW-5-D	7/7/2005	11:16:00 AM	With Hydraulic Control	2528.89	5.75E-02	6.40	0.578	No
MW-5-S	5/5/2005	1:35:00 PM	Background	414.26	9.41E-03	7.06	0.036	No
MW-5-S	5/12/2005	2:55:00 PM	No Hydraulic Control	309.69	7.04E-03	7.09	0.025	No
MW-5-S	5/16/2005	4:23:00 PM	No Hydraulic Control	3999.10	9.09E-02	5.98	1.277	Yes
MW-5-S	5/20/2005	1:55:00 PM	No Hydraulic Control	4456.76	1.01E-01	5.86	1.517	Yes
MW-5-S	5/24/2005	12:50:00 PM	No Hydraulic Control	3354.78	7.62E-02	6.16	0.952	No
MW-5-S	5/27/2005	12:02:00 PM	No Hydraulic Control	3601.83	8.19E-02	5.84	1.235	Yes
MW-5-S	5/30/2005	11:35:00 AM	No Hydraulic Control	3769.98	8.57E-02	6.01	1.185	Yes
MW-5-S	6/2/2005	12:22:00 PM	No Hydraulic Control	3420.43	7.77E-02	6.02	1.068	No
MW-5-S	6/21/2005	2:11:00 PM	Between	3048.96	6.93E-02	6.25	0.806	No
MW-5-S	6/23/2005	10:38:00 AM	With Hydraulic Control	2719.07	6.18E-02	6.34	0.658	No
MW-5-S	6/27/2005	10:30:00 AM	With Hydraulic Control	2376.99	5.40E-02	6.45	0.517	No
MW-5-S	6/28/2005	10:31:00 AM	With Hydraulic Control	2182.11	4.96E-02	6.50	0.444	No
MW-5-S	6/30/2005	10:27:00 AM	With Hydraulic Control	3126.17	7.10E-02	6.23	0.842	No
MW-5-S	7/7/2005	11:17:00 AM	With Hydraulic Control	2155.73	4.90E-02	6.51	0.434	No
MW-6-D	5/5/2005	12:58:00 PM	Background	503.83	1.15E-02	7.03	0.046	No
MW-6-D	5/12/2005	3:52:00 PM	No Hydraulic Control	2726.87	6.20E-02	6.34	0.661	No
MW-6-D	5/16/2005	2:40:00 PM	No Hydraulic Control	4015.43	9.13E-02	5.98	1.286	No
MW-6-D	5/20/2005	12:12:00 PM	No Hydraulic Control	4191.09	9.53E-02	5.93	1.377	Yes
MW-6-D	5/24/2005	10:27:00 AM	No Hydraulic Control	3489.99	7.93E-02	6.12	1.018	No
MW-6-D	5/27/2005	10:30:00 AM	No Hydraulic Control	3246.54	7.38E-02	5.98	1.038	No
MW-6-D	5/30/2005	10:17:00 AM	No Hydraulic Control	4189.70	9.52E-02	6.15	1.199	No
MW-6-D	6/2/2005	11:15:00 AM	No Hydraulic Control	3499.38	7.95E-02	5.94	1.143	No

Table C.1
CO_2 Concentrations and Partial Pressures

Monitoring Well	Collection Date	Collection Time	Experiment	Water Concentration (mg/L)	Water Concentration (mols/L)	pH	Partial Pressure (atm)	Exceeds Applicable Hydrostatic Pressure
MW-6-D	6/21/2005	12:32:00 PM	Between	1795.71	4.08E-02	6.62	0.315	No
MW-6-D	6/23/2005	9:11:00 AM	With Hydraulic Control	3380.25	7.68E-02	6.15	0.964	No
MW-6-D	6/27/2005	9:10:00 AM	With Hydraulic Control	2829.71	6.43E-02	6.31	0.706	No
MW-6-D	6/28/2005	8:46:00 AM	With Hydraulic Control	2402.63	5.46E-02	6.44	0.527	No
MW-6-D	6/30/2005	9:57:00 AM	With Hydraulic Control	3064.92	6.97E-02	6.24	0.813	No
MW-6-D	7/7/2005	9:57:00 AM	With Hydraulic Control	2223.54	5.05E-02	6.49	0.459	No
MW-6-S	5/5/2005	12:50:00 PM	Background	589.39	1.34E-02	7.00	0.057	No
MW-6-S	5/12/2005	3:50:00 PM	No Hydraulic Control	787.02	1.79E-02	6.94	0.085	No
MW-6-S	5/16/2005	2:30:00 PM	No Hydraulic Control	4503.16	1.02E-01	5.84	1.541	Yes
MW-6-S	5/20/2005	12:10:00 PM	No Hydraulic Control	3278.48	7.45E-02	6.18	0.915	No
MW-6-S	5/24/2005	11:00:00 AM	No Hydraulic Control	3435.73	7.81E-02	6.14	0.991	No
MW-6-S	5/27/2005	10:25:00 AM	No Hydraulic Control	3398.78	7.72E-02	6.02	1.062	No
MW-6-S	5/30/2005	10:25:00 AM	No Hydraulic Control	3991.72	9.07E-02	6.02	1.247	Yes
MW-6-S	6/2/2005	11:10:00 AM	No Hydraulic Control	3691.80	8.39E-02	5.97	1.187	Yes
MW-6-S	6/21/2005	12:30:00 PM	Between	2803.62	6.37E-02	6.32	0.695	No
MW-6-S	6/23/2005	9:01:00 AM	With Hydraulic Control	2497.31	5.68E-02	6.41	0.565	No
MW-6-S	6/27/2005	9:00:00 AM	With Hydraulic Control	2693.75	6.12E-02	6.35	0.647	No
MW-6-S	6/28/2005	8:46:00 AM	With Hydraulic Control	2495.90	5.67E-02	6.41	0.564	No
MW-6-S	6/30/2005	9:55:00 AM	With Hydraulic Control	3120.46	7.09E-02	6.23	0.839	No
MW-6-S	7/7/2005	9:55:00 AM	With Hydraulic Control	2279.77	5.18E-02	6.47	0.480	No
MW-7-D	5/5/2005	2:00:00 PM	Background	298.92	6.79E-03	7.09	0.024	No
MW-7-D	5/12/2005	5:50:00 PM	No Hydraulic Control	1818.08	4.13E-02	6.61	0.322	No
MW-7-D	5/16/2005	4:05:00 PM	No Hydraulic Control	4046.36	9.20E-02	5.97	1.302	Yes
MW-7-D	5/20/2005	1:20:00 PM	No Hydraulic Control	3591.90	8.16E-02	6.09	1.069	No
MW-7-D	5/24/2005	12:40:00 PM	No Hydraulic Control	3441.60	7.82E-02	6.14	0.994	No
MW-7-D	5/27/2005	11:35:00 AM	No Hydraulic Control	3855.66	8.76E-02	5.90	1.286	No
MW-7-D	5/30/2005	11:18:00 AM	No Hydraulic Control	3906.45	8.88E-02	5.99	1.242	No
MW-7-D	6/2/2005	12:38:00 PM	No Hydraulic Control	3730.60	8.48E-02	6.02	1.165	No
MW-7-D	6/21/2005	1:54:00 PM	Between	3272.75	7.44E-02	6.19	0.912	No

Table C.1
CO_2 Concentrations and Partial Pressures

Monitoring Well	Collection Date	Collection Time	Experiment	Water Concentration (mg/L)	Water Concentration (mols/L)	pH	Partial Pressure (atm)	Exceeds Applicable Hydrostatic Pressure
MW-7-D	6/23/2005	10:30:00 AM	With Hydraulic Control	1670.63	3.80E-02	6.66	0.278	No
MW-7-D	6/27/2005	10:23:00 AM	With Hydraulic Control	2772.27	6.30E-02	6.33	0.681	No
MW-7-D	6/28/2005	10:21:00 AM	With Hydraulic Control	2733.83	6.21E-02	6.34	0.664	No
MW-7-D	6/30/2005	9:14:00 AM	With Hydraulic Control	3114.58	7.08E-02	6.23	0.836	No
MW-7-D	7/7/2005	11:11:00 AM	With Hydraulic Control	1942.39	4.41E-02	6.58	0.361	No
MW-7-S	5/5/2005	1:50:00 PM	Background	456.67	1.04E-02	7.04	0.041	No
MW-7-S	5/12/2005	5:45:00 PM	No Hydraulic Control	627.39	1.43E-02	6.99	0.062	No
MW-7-S	5/16/2005	4:00:00 PM	No Hydraulic Control	4486.18	1.02E-01	5.85	1.532	Yes
MW-7-S	5/20/2005	1:22:00 PM	No Hydraulic Control	3422.08	7.78E-02	6.14	0.985	No
MW-7-S	5/24/2005	12:37:00 PM	No Hydraulic Control	3707.51	8.43E-02	6.06	1.128	No
MW-7-S	5/27/2005	11:30:00 AM	No Hydraulic Control	3843.94	8.74E-02	5.92	1.269	Yes
MW-7-S	5/30/2005	11:20:00 AM	No Hydraulic Control	3717.19	8.45E-02	6.04	1.147	Yes
MW-7-S	6/2/2005	12:33:00 PM	No Hydraulic Control	3305.27	7.51E-02	6.03	1.026	No
MW-7-S	6/21/2005	1:49:00 PM	Between	3302.64	7.51E-02	6.18	0.926	No
MW-7-S	6/23/2005	10:27:00 AM	With Hydraulic Control	2646.89	6.02E-02	6.37	0.627	No
MW-7-S	6/27/2005	10:18:00 AM	With Hydraulic Control	2315.02	5.26E-02	6.46	0.493	No
MW-7-S	6/28/2005	10:16:00 AM	With Hydraulic Control	2383.15	5.42E-02	6.44	0.520	No
MW-7-S	6/30/2005	9:17:00 AM	With Hydraulic Control	3050.38	6.93E-02	6.25	0.806	No
MW-7-S	7/7/2005	11:08:00 AM	With Hydraulic Control	1529.91	3.48E-02	6.70	0.239	No
MW-8-D	5/5/2005	2:22:00 PM	Background	354.81	8.06E-03	7.07	0.030	No
MW-8-D	5/12/2005	4:45:00 PM	No Hydraulic Control	3522.64	8.01E-02	6.11	1.035	No
MW-8-D	5/16/2005	3:00:00 PM	No Hydraulic Control	4598.78	1.05E-01	5.82	1.591	Yes
MW-8-D	5/20/2005	12:51:00 PM	No Hydraulic Control	3492.91	7.94E-02	6.12	1.020	No
MW-8-D	5/24/2005	11:10:00 AM	No Hydraulic Control	3425.33	7.78E-02	6.14	0.986	No
MW-8-D	5/27/2005	10:40:00 AM	No Hydraulic Control	3792.84	8.62E-02	6.06	1.156	No
MW-8-D	5/30/2005	10:40:00 AM	No Hydraulic Control	3651.91	8.30E-02	6.98	0.365	No
MW-8-D	6/2/2005	11:43:00 AM	No Hydraulic Control	3419.21	7.77E-02	5.96	1.105	No
MW-8-D	6/21/2005	12:58:00 PM	Between	3426.92	7.79E-02	6.14	0.987	No
MW-8-D	6/23/2005	9:30:00 AM	With Hydraulic Control	2882.95	6.55E-02	6.30	0.730	No

Table C.1
CO_2 Concentrations and Partial Pressures

Monitoring Well	Collection Date	Collection Time	Experiment	Water Concentration (mg/L)	Water Concentration (mols/L)	pH	Partial Pressure (atm)	Exceeds Applicable Hydrostatic Pressure
MW-8-D	6/27/2005	9:28:00 AM	With Hydraulic Control	3533.83	8.03E-02	6.11	1.040	No
MW-8-D	6/28/2005	9:23:00 AM	With Hydraulic Control	2429.17	5.52E-02	6.43	0.538	No
MW-8-D	6/30/2005	9:23:00 AM	With Hydraulic Control	2646.25	6.01E-02	6.37	0.627	No
MW-8-D	7/7/2005	10:27:00 AM	With Hydraulic Control	2099.52	4.77E-02	6.53	0.414	No
MW-8-S	5/5/2005	2:17:00 PM	Background	431.65	9.81E-03	7.05	0.038	No
MW-8-S	5/12/2005	4:40:00 PM	No Hydraulic Control	1544.88	3.51E-02	6.70	0.243	No
MW-8-S	5/16/2005	2:55:00 PM	No Hydraulic Control	4384.08	9.96E-02	5.88	1.478	Yes
MW-8-S	5/20/2005	12:46:00 PM	No Hydraulic Control	3651.39	8.30E-02	6.08	1.099	No
MW-8-S	5/24/2005	11:08:00 AM	No Hydraulic Control	3013.00	6.85E-02	6.26	0.789	No
MW-8-S	5/27/2005	10:42:00 AM	No Hydraulic Control	3593.35	8.17E-02	5.95	1.168	Yes
MW-8-S	5/30/2005	10:42:00 AM	No Hydraulic Control	3755.50	8.54E-02	6.83	0.483	No
MW-8-S	6/2/2005	11:38:00 AM	No Hydraulic Control	3409.67	7.75E-02	5.97	1.096	No
MW-8-S	6/21/2005	12:53:00 PM	Between	3195.78	7.26E-02	6.21	0.875	No
MW-8-S	6/23/2005	9:25:00 AM	With Hydraulic Control	2720.15	6.18E-02	6.34	0.658	No
MW-8-S	6/27/2005	9:23:00 AM	With Hydraulic Control	2575.02	5.85E-02	6.39	0.597	No
MW-8-S	6/28/2005	9:18:00 AM	With Hydraulic Control	2824.75	6.42E-02	6.31	0.704	No
MW-8-S	6/30/2005	9:18:00 AM	With Hydraulic Control	3167.77	7.20E-02	6.22	0.862	No
MW-8-S	7/7/2005	10:25:00 AM	With Hydraulic Control	2633.61	5.99E-02	6.37	0.621	No
MW-9-D	5/5/2005	2:15:00 PM	Background	388.04	8.82E-03	7.06	0.033	No
MW-9-D	5/12/2005	6:11:00 PM	No Hydraulic Control	318.07	7.23E-03	7.09	0.026	No
MW-9-D	5/16/2005	4:17:00 PM	No Hydraulic Control	350.39	7.96E-03	7.08	0.029	No
MW-9-D	5/20/2005	1:47:00 PM	No Hydraulic Control	316.96	7.20E-03	7.09	0.026	No
MW-9-D	5/24/2005	12:30:00 PM	No Hydraulic Control	315.90	7.18E-03	7.09	0.026	No
MW-9-D	5/27/2005	11:55:00 AM	No Hydraulic Control	1643.83	3.74E-02	8.13	0.015	No
MW-9-D	5/30/2005	11:25:00 AM	No Hydraulic Control	3231.90	7.35E-02	6.04	0.997	No
MW-9-D	6/2/2005	12:15:00 PM	No Hydraulic Control	3436.66	7.81E-02	6.02	1.074	No
MW-9-D	6/21/2005	1:43:00 PM	Between	3495.26	7.94E-02	6.12	1.021	No
MW-9-D	6/23/2005	10:20:00 AM	With Hydraulic Control	3381.25	7.68E-02	6.15	0.965	No
MW-9-D	6/27/2005	10:13:00 AM	With Hydraulic Control	3131.23	7.12E-02	6.23	0.844	No

Table C.1
CO_2 Concentrations and Partial Pressures

Monitoring Well	Collection Date	Collection Time	Experiment	Water Concentration (mg/L)	Water Concentration (mols/L)	pH	Partial Pressure (atm)	Exceeds Applicable Hydrostatic Pressure
MW-9-D	6/28/2005	10:10:00 AM	With Hydraulic Control	3599.12	8.18E-02	6.09	1.073	No
MW-9-D	6/30/2005	10:10:00 AM	With Hydraulic Control	3183.17	7.23E-02	6.21	0.869	No
MW-9-D	7/7/2005	11:02:00 AM	With Hydraulic Control	2514.07	5.71E-02	6.40	0.572	No
MW-9-S	5/5/2005	2:25:00 PM	Background	331.66	7.54E-03	7.08	0.028	No
MW-9-S	5/12/2005	6:07:00 PM	No Hydraulic Control	373.79	8.50E-03	7.07	0.032	No
MW-9-S	5/16/2005	4:12:00 PM	No Hydraulic Control	2299.88	5.23E-02	6.47	0.488	No
MW-9-S	5/20/2005	1:42:00 PM	No Hydraulic Control	2385.15	5.42E-02	6.44	0.520	No
MW-9-S	5/24/2005	12:25:00 PM	No Hydraulic Control	3652.90	8.30E-02	6.08	1.100	No
MW-9-S	5/27/2005	11:50:00 AM	No Hydraulic Control	3877.81	8.81E-02	5.91	1.287	Yes
MW-9-S	5/30/2005	11:27:00 AM	No Hydraulic Control	4497.19	1.02E-01	6.07	1.361	Yes
MW-9-S	6/2/2005	12:10:00 PM	No Hydraulic Control	3364.49	7.65E-02	6.09	1.005	No
MW-9-S	6/21/2005	1:38:00 PM	Between	3070.56	6.98E-02	6.24	0.816	No
MW-9-S	6/23/2005	10:15:00 AM	With Hydraulic Control	3498.32	7.95E-02	6.12	1.023	No
MW-9-S	6/27/2005	10:08:00 AM	With Hydraulic Control	2975.78	6.76E-02	6.27	0.772	No
MW-9-S	6/28/2005	10:05:00 AM	With Hydraulic Control	3166.22	7.20E-02	6.22	0.861	No
MW-9-S	6/30/2005	10:05:00 AM	With Hydraulic Control	3628.36	8.25E-02	6.08	1.088	No
MW-9-S	7/7/2005	11:00:00 AM	With Hydraulic Control	2971.50	6.75E-02	6.27	0.770	No

Notes:
1. Equations are provided in Chapter 3.1.2
2. Applicable hydrostatic pressures:
   Shallow wells - 1.145 atm
   Deep wells - 1.290 atm

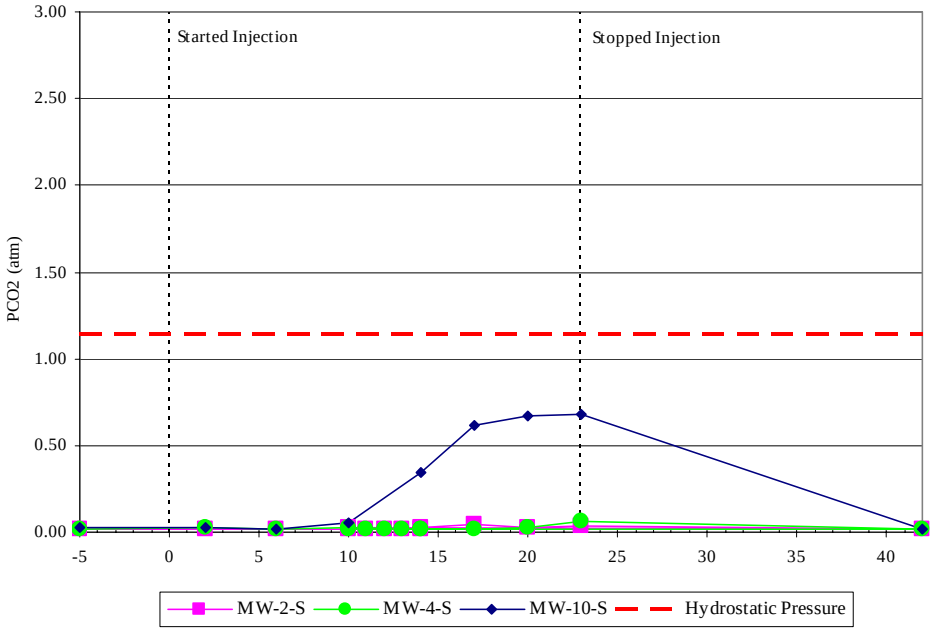

(a)

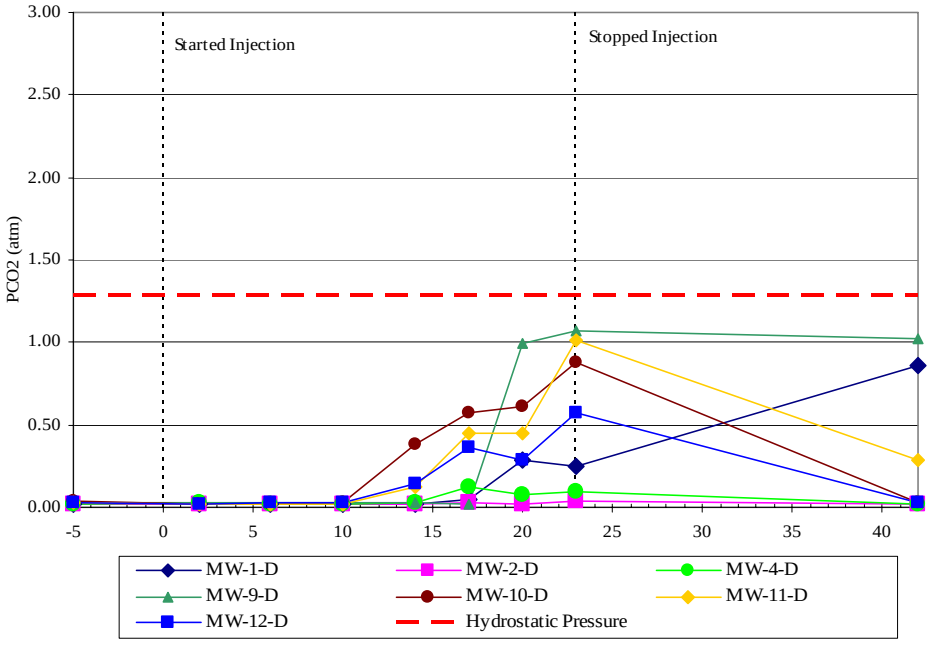

(b)

Figure C.1 – p_{CO_2} below the hydrostatic pressure for the passive injection experiment in (a) shallow wells screened at 2.5 m bgs and (b) deep wells screened at 4.0 m bgs.

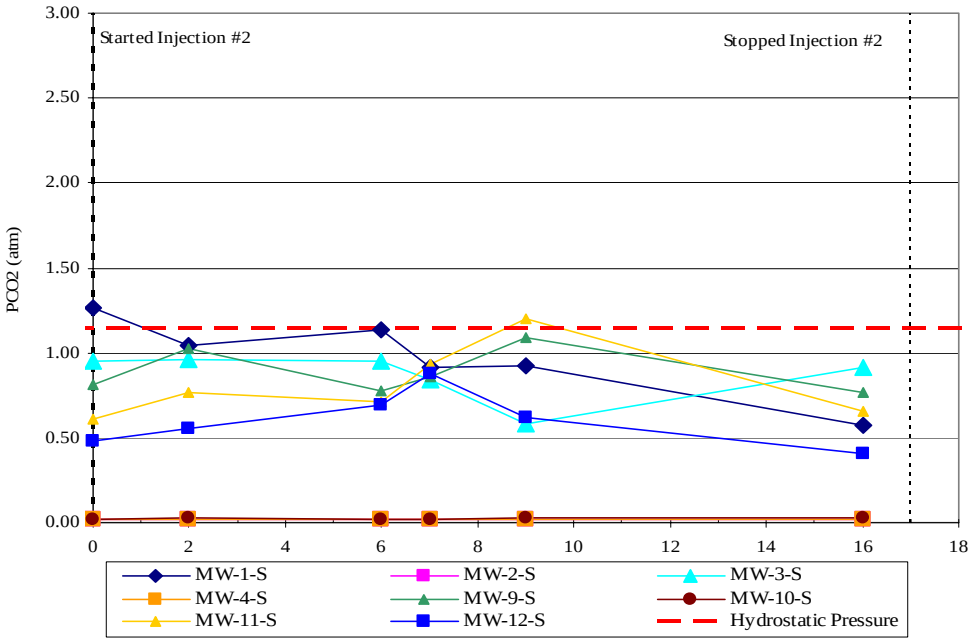

(a)

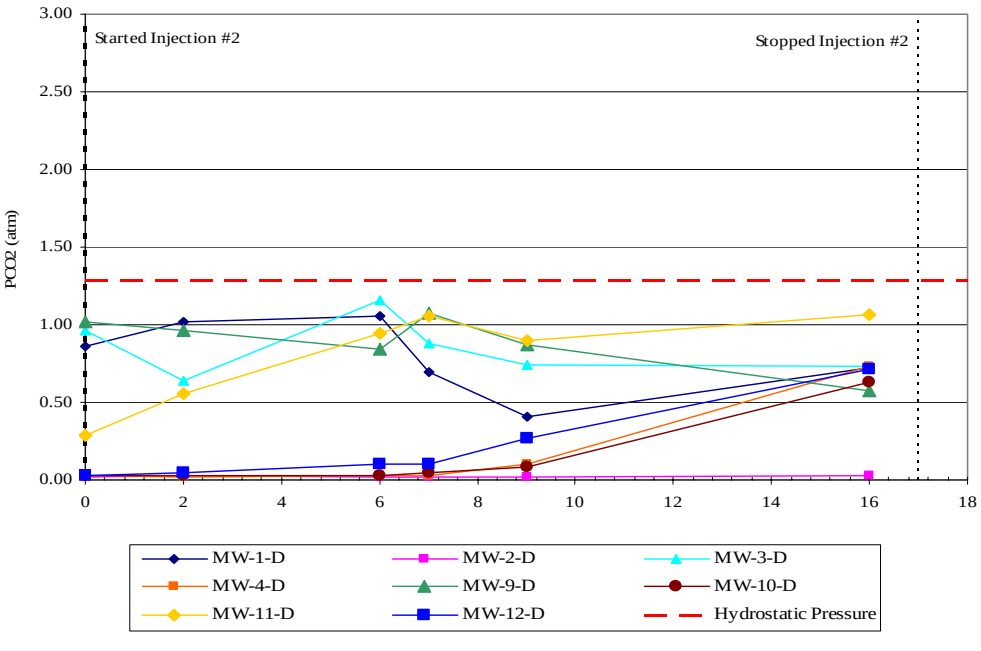

(b)

Figure C.2 – p_{CO_2} in the monitoring wells located ~ 5 – 5.5 m from IP-4 (a) shallow wells screened at 2.5 m bgs and (b) deep wells screened at 4.0 m bgs.

Appendix D
Hydraulic Monitoring Data

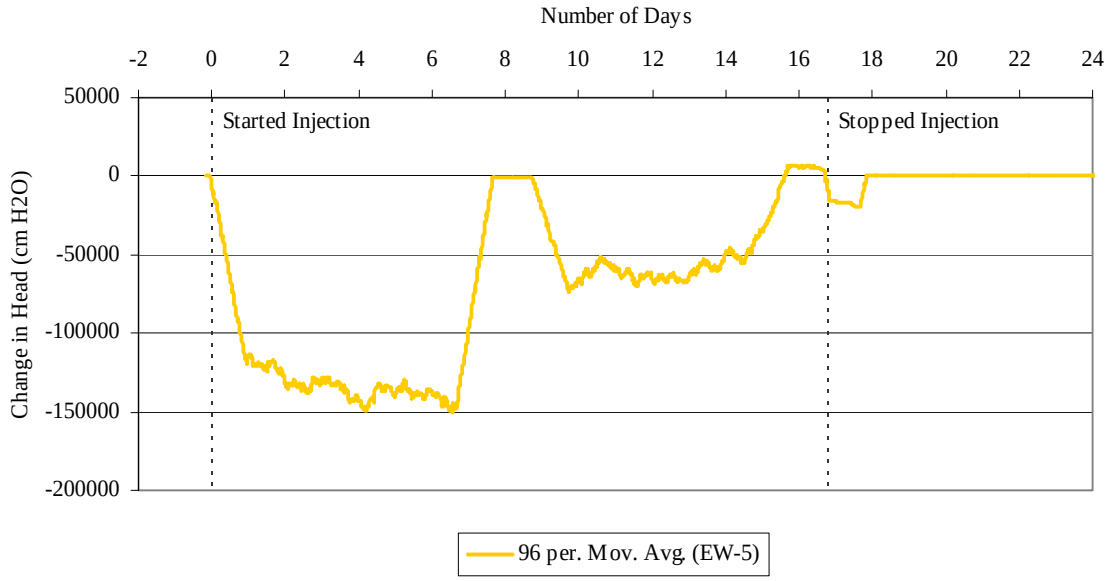

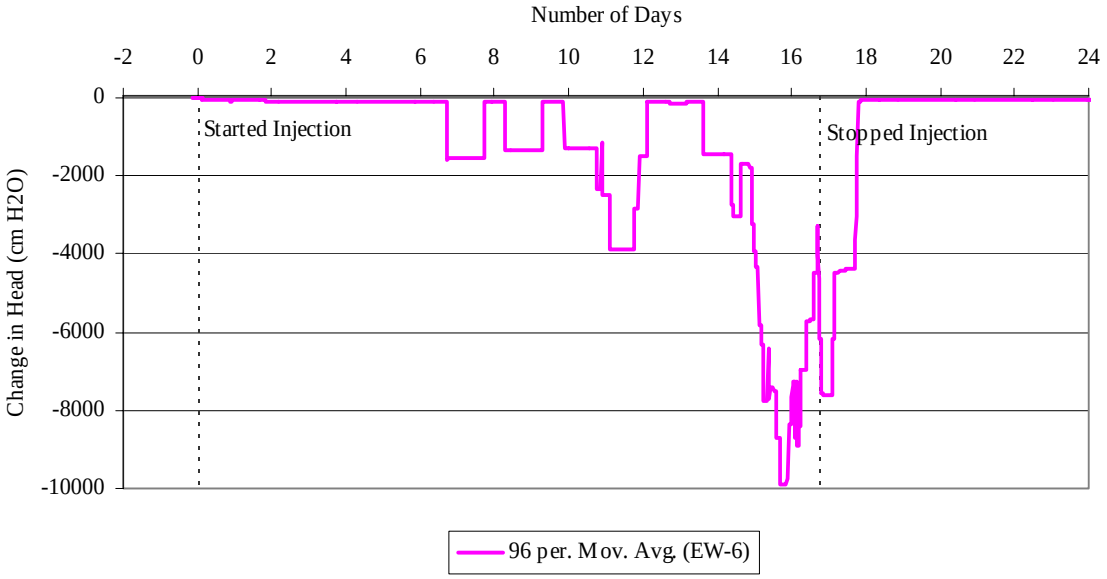

Figure D.1 – Hydraulic monitoring data from extraction wells for experiment with hydraulic control.

Appendix E
Surface GPR Data

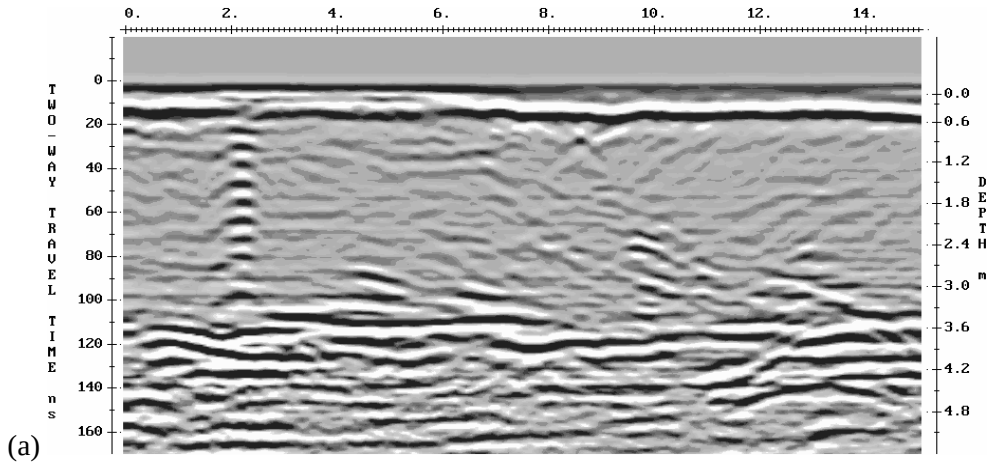

(a)

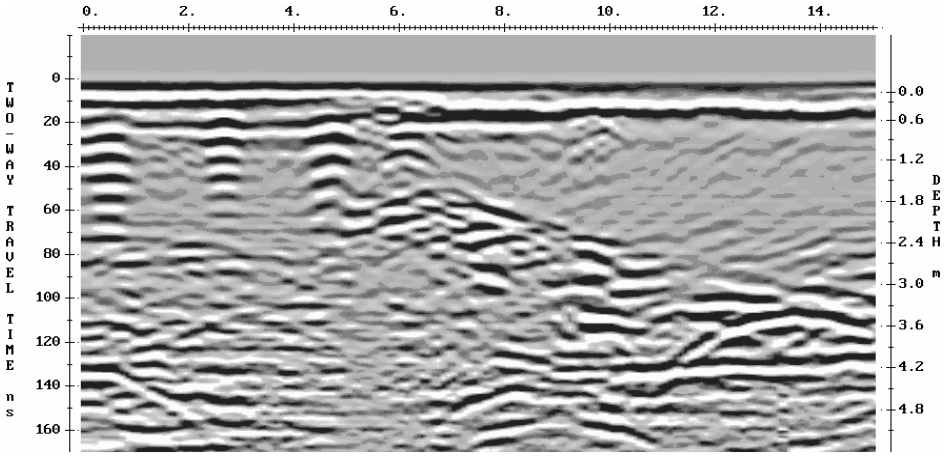

(b)

Figure E.1 – Ground penetrating radar survey at 200 mHz for (a) line 1a2 (near access tubes GP-13 to GP-15) and (b) line 1a3 (near access tubes GP-7 to GP-12) prior to geophysical access tube installations. A spherical spreading, exponential compensation (SEC) gain function (maximum gain 3000 and attenuation 2.7 db/min) was used to process the GPR data.

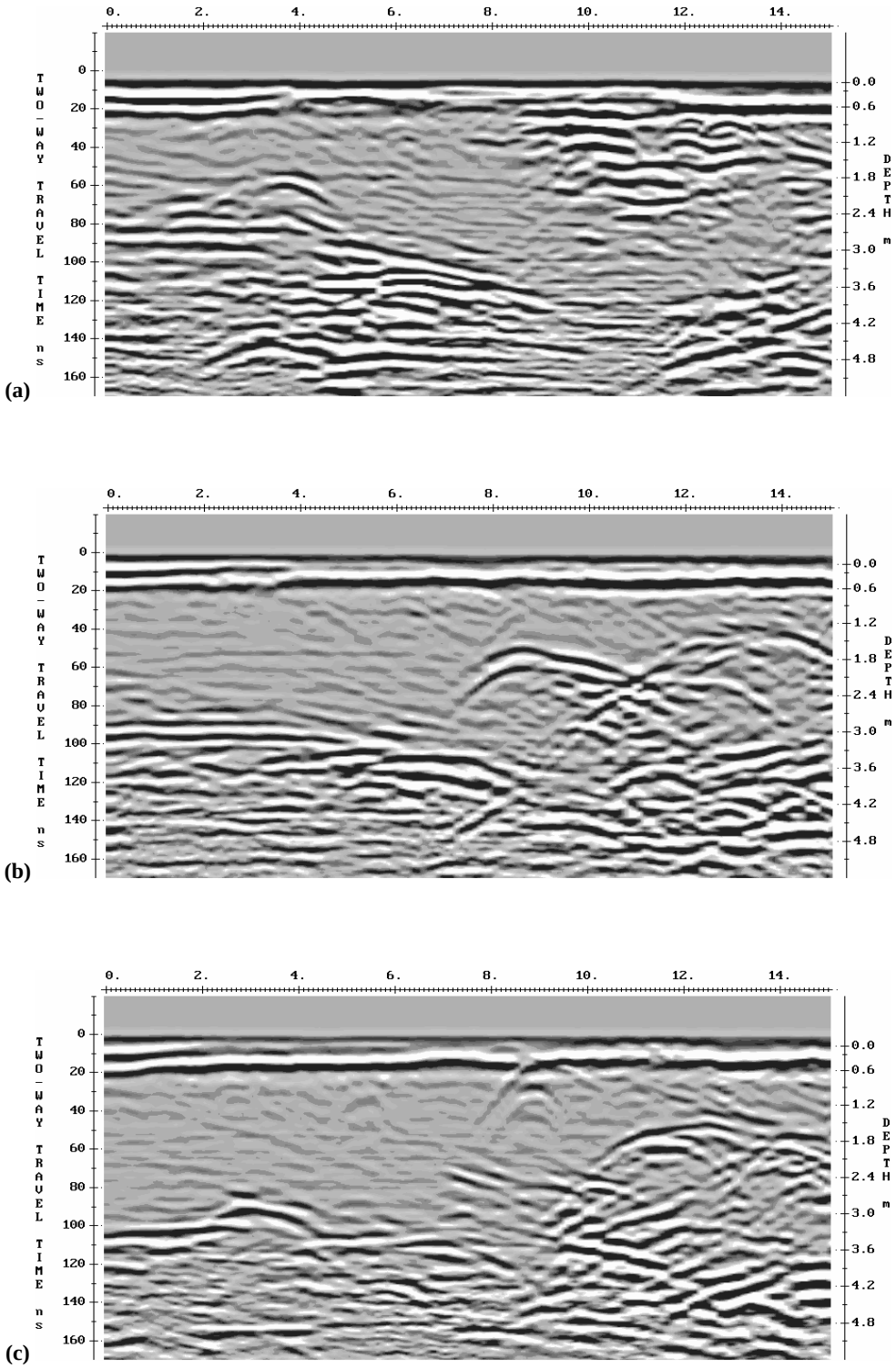

Figure E.2 – Ground penetrating radar survey at 200 mHz for (a) line 1a4 (near access tubes GP-13 to GP-4), (b) line 1a5 (near access tubes GP-17 to GP-10), and (c) line 1a6 (near access tubes GP-18 to GP-3) prior to geophysical access tube installations. A spherical spreading, exponential compensation (SEC) gain function (maximum gain 3000 and attenuation 2.7 db/min) was used to process the GPR data.

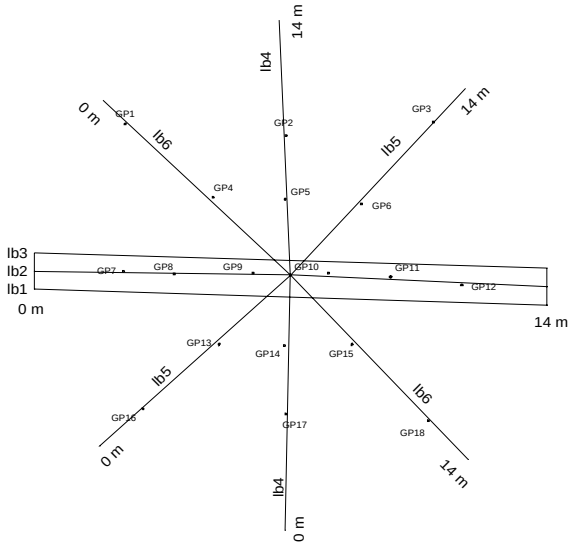

Figure E.3 – Diagram of October 9, 2004 surface GPR survey lines relative to GP access tubes

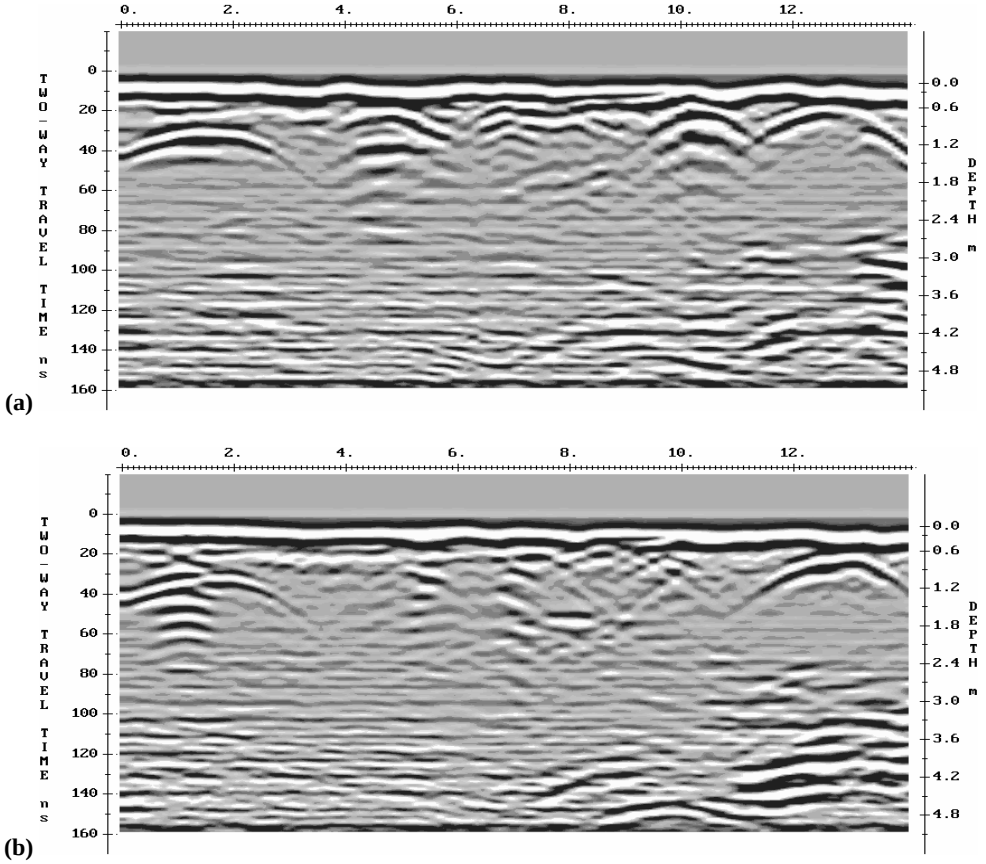

Figure E.4 – Ground penetrating radar survey at 200 mHz for (a) line 1b1 and (b) line 1b3 subsequent to geophysical access tube installations, but prior to injection of CO_2-supersaturated water. A SEC gain function (maximum gain 500 and attenuation 2.7 db/min) was used to process the GPR data.

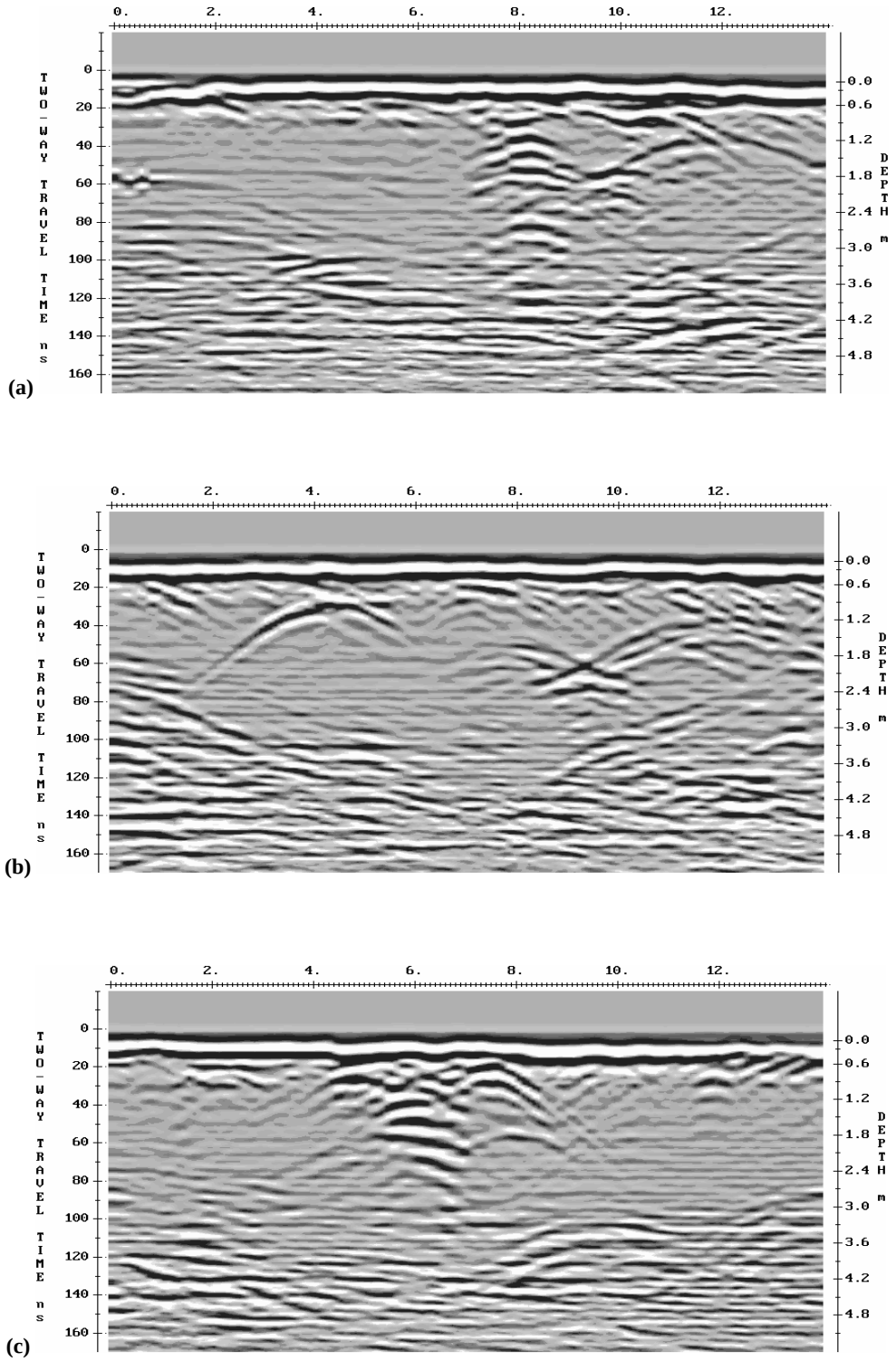

Figure E.5 – Ground penetrating radar survey at 200 mHz for (a) line 1b4, (b) line 1b5, and (c) line 1b6 subsequent to geophysical access tube installations, but prior to injection of CO_2-supersaturated water. A SEC gain function (maximum gain 500 and attenuation 2.7 db/min) was used to process the GPR data.

.

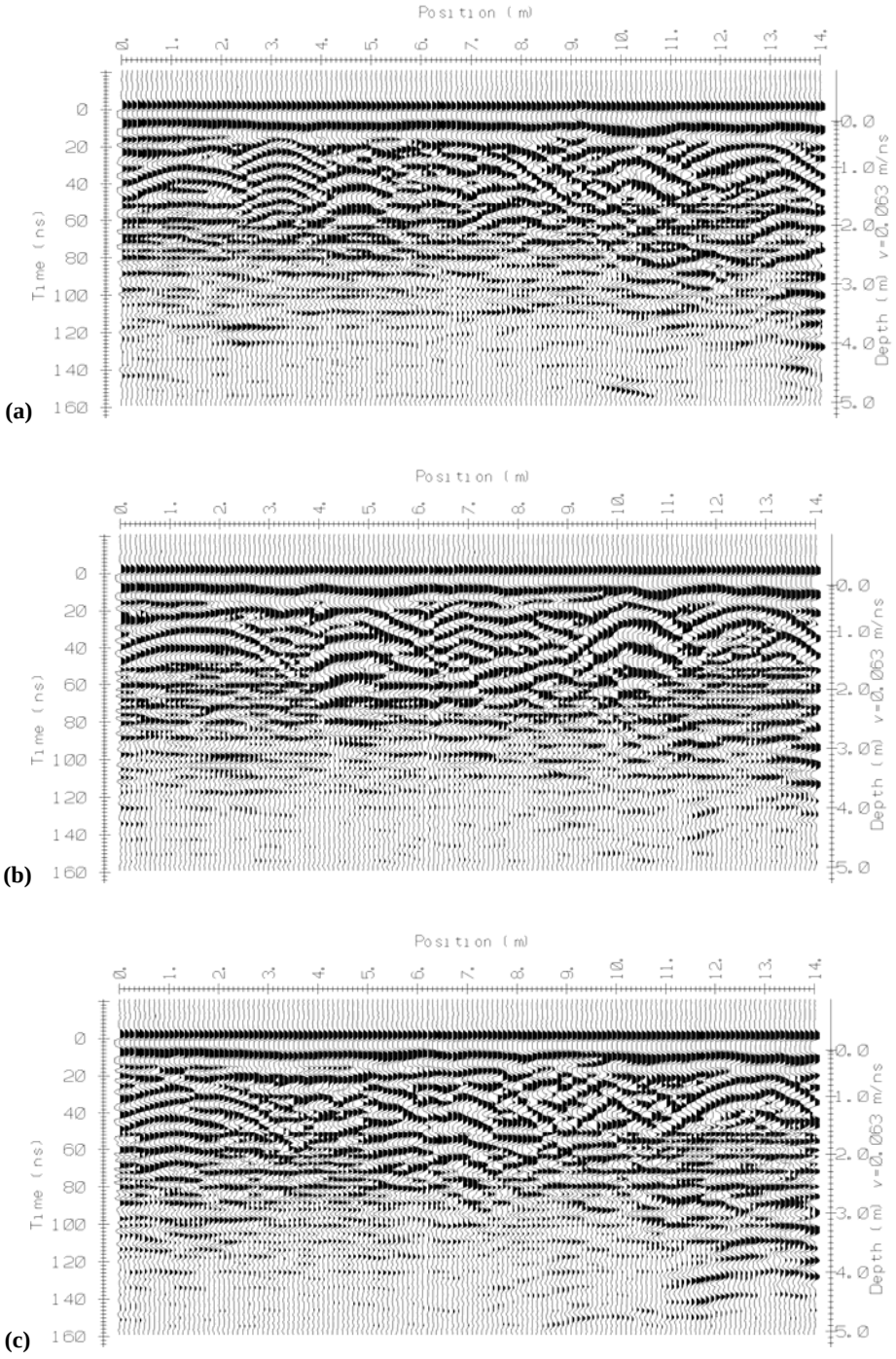

Figure E.6 – Ground penetrating radar survey at 200 mHz for (a) line 1b1, (b) line 1b2 and (c) line 1b3 subsequent to geophysical access tube installations, but prior to injection of CO_2-supersaturated water. An automatic gain control (AGC) function (maximum gain 500 and window 1.0) was used to process the GPR data.

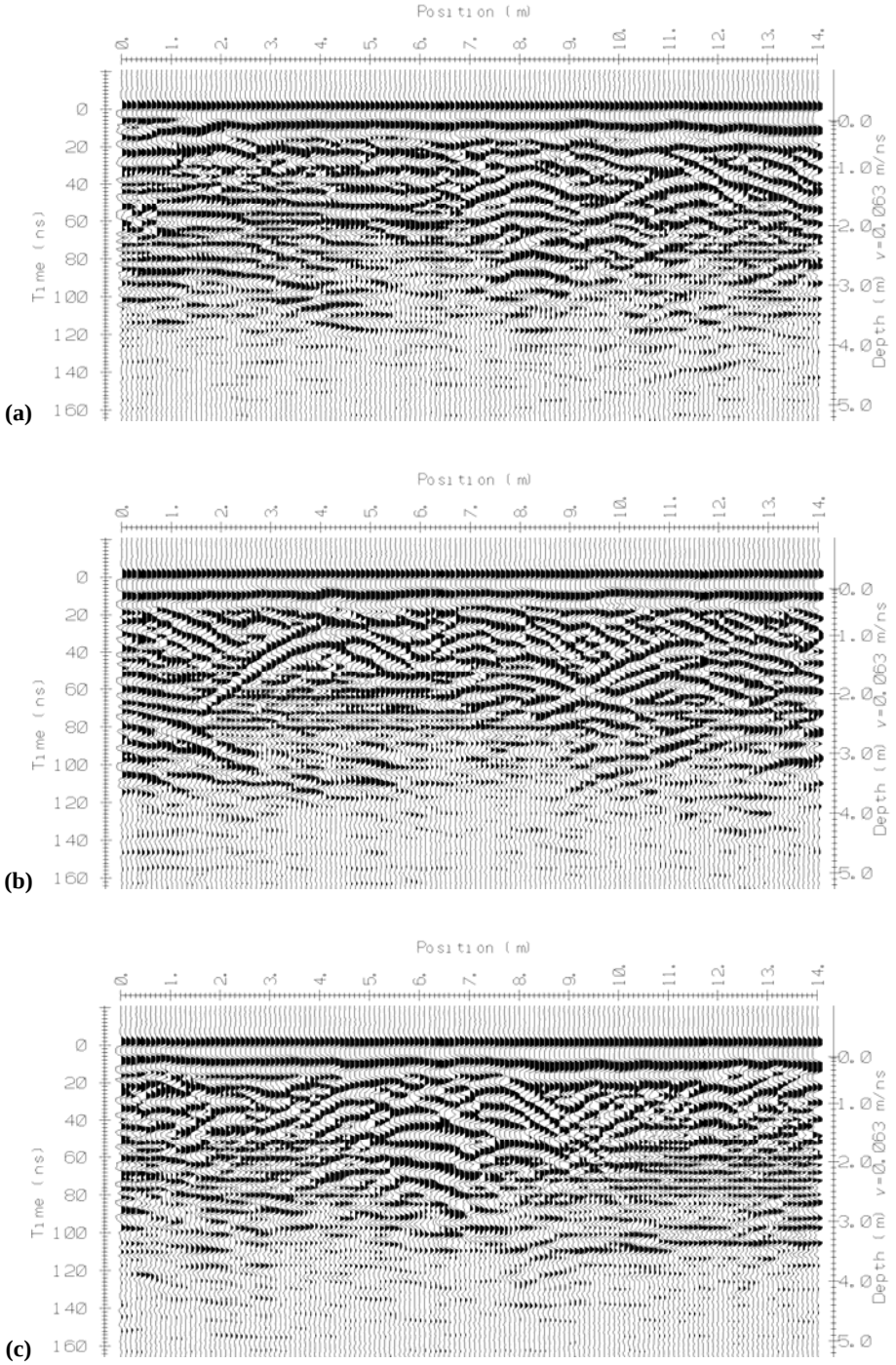

Figure E.7 – Ground penetrating radar survey at 200 mHz for (a) line 1b4, (b) line 1b5, and (c) line 1b6 subsequent to geophysical access tube installations, but prior to injection of CO_2-supersaturated water. An automatic gain control (AGC) function (maximum gain 500 and window 1.0) was used to process the GPR data.

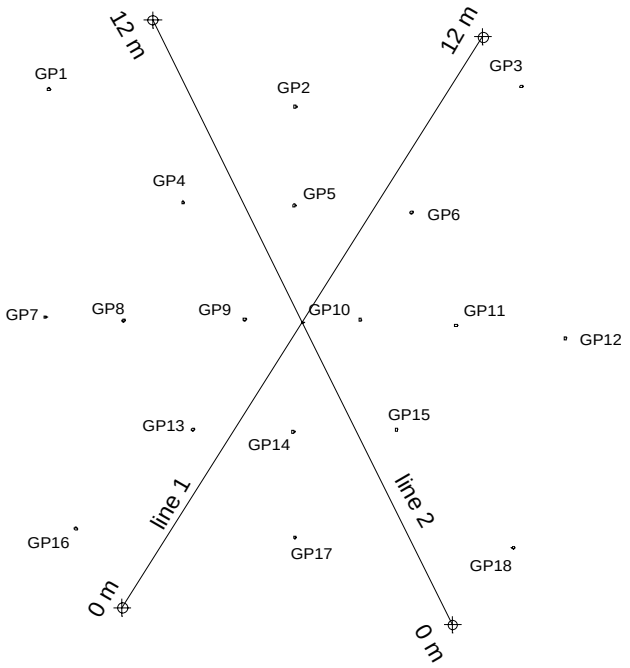

Figure E.8 – Diagram of April to July, 2005 surface GPR survey lines relative to GP access tubes.

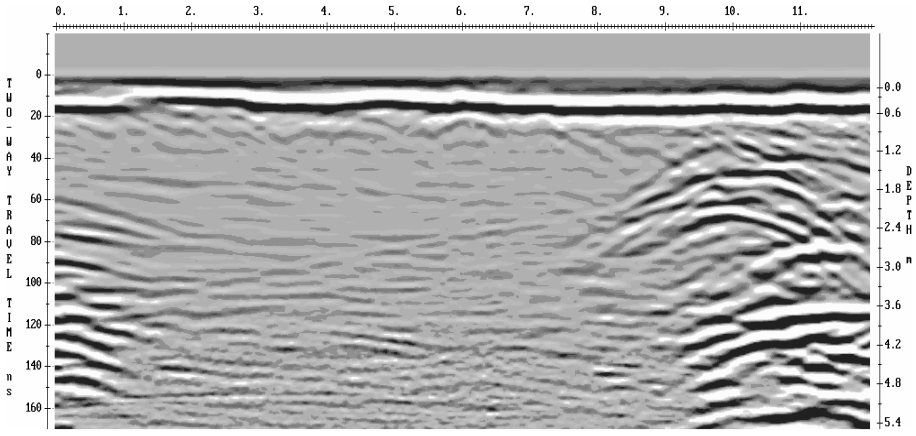

Figure E.9– Ground penetrating radar survey at 200 mHz for line 1 (diagonal from near GP-16 to GP-3) on May 19, 2005 (9 days after injection without hydraulic control commenced). A SEC gain function (maximum gain 3000 and attenuation 2.7 db/min) was used to process the GPR data.

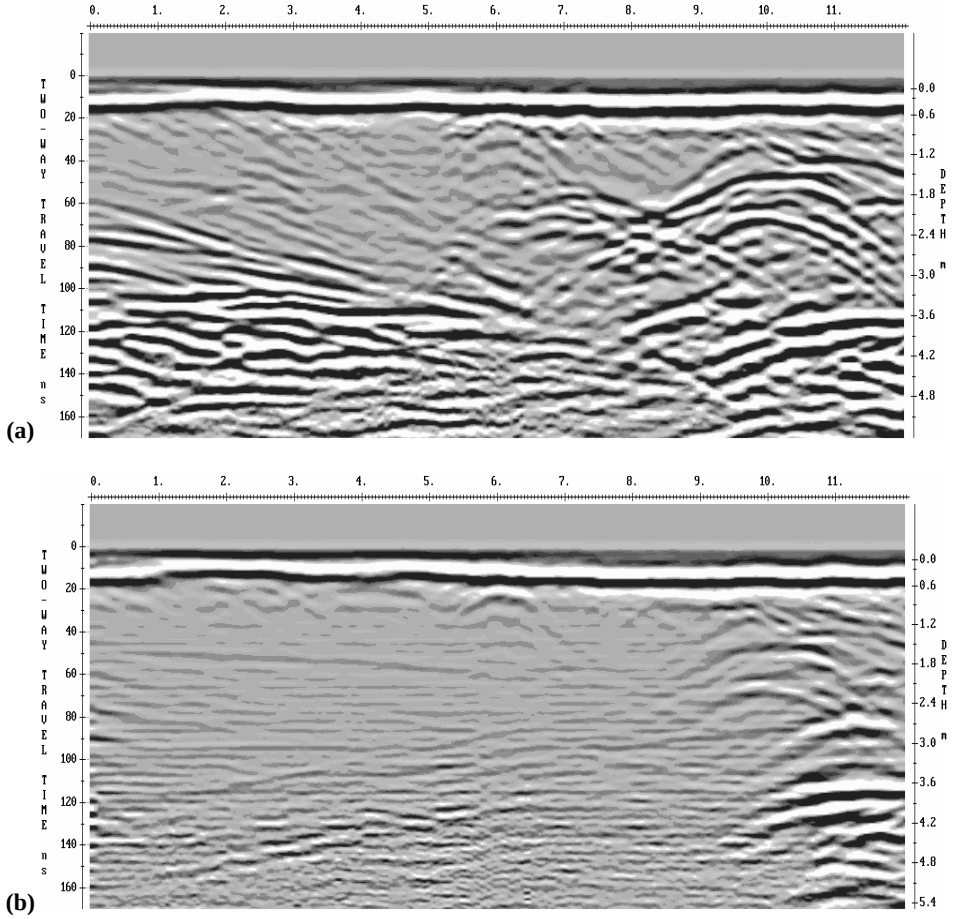

Figure E.10 – Ground penetrating radar survey at 200 mHz for line 1 (diagonal from near GP-16 to GP-3) showing attenuation of reflections for passive injection experiment between (a) April 21, 2005 (background), (b) May 30, 2005 (20 days after initiation of injection). A SEC gain function (maximum gain 3000 and attenuation 2.7 db/min) was used to process the GPR data.

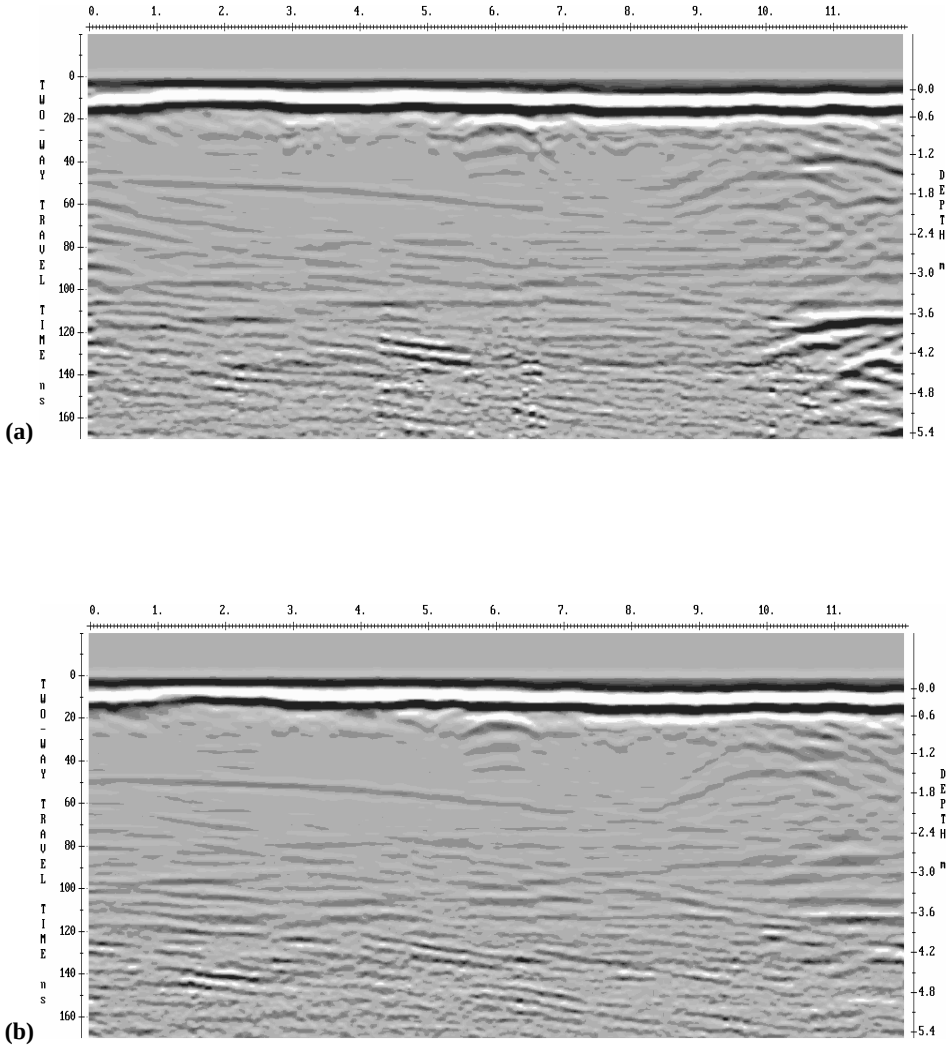

Figure E.11 – Ground penetrating radar survey at 200 mHz for line 1 (diagonal from near GP-16 to GP-3) showing attenuation of reflections between (a) June 17, 2005 (between experiments) and (b) July 6, 2005 (15 days after initiation of injection). A SEC gain function (maximum gain 3000 and attenuation 2.7 db/min) was used to process the GPR data.

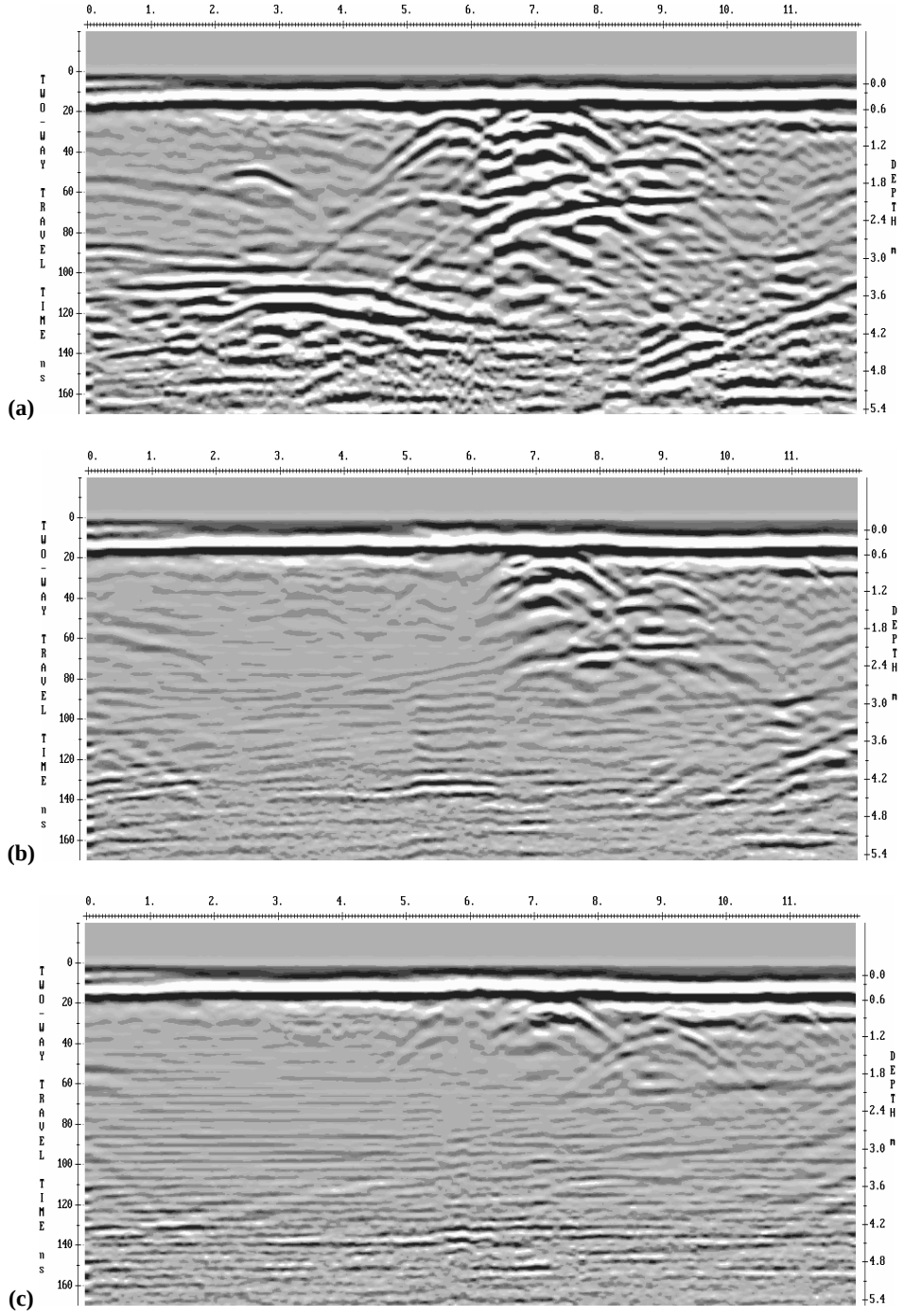

Figure E.12 – Ground penetrating radar survey at 200 mHz for line 2 (diagonal from near GP-16 to GP-3) showing attenuation of reflections for passive injection experiment between (a) April 21, 2005 (background), (b) May 19, 2005 (9 days after initiation of injection), and (c) May 30, 2005 (20 days after initiation of injection). A SEC gain function (maximum gain 3000 and attenuation 2.7 db/min) was used to process the GPR data.

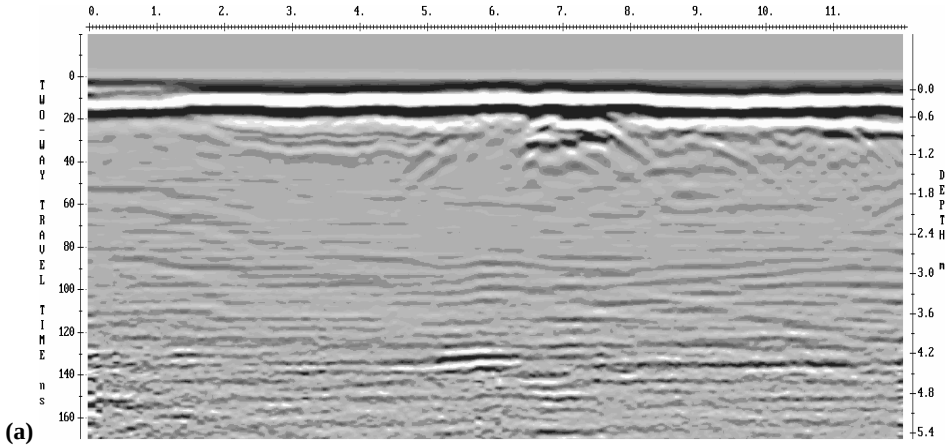

(a)

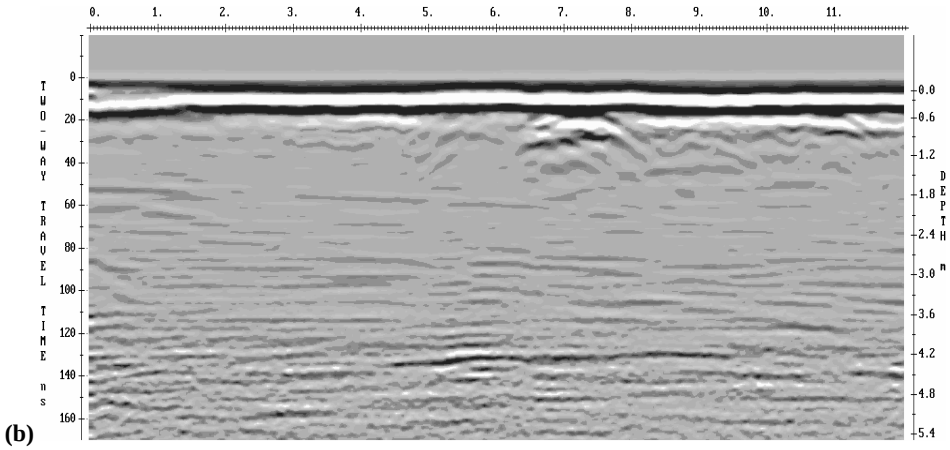

(b)

Figure E.13 – Ground penetrating radar survey at 200 mHz for line 2 (diagonal from near GP-16 to GP-3) showing attenuation of reflections between (a) June 17, 2005 (between experiments) and (b) July 6, 2005 (15 days after initiation of injection). A SEC gain function (maximum gain 3000 and attenuation 2.7 db/min) was used to process the GPR data.

Appendix F

Cross-borehole GPR – ZOP Data

Table F.1
Borehole GPR (ZOP Mode) Sampling Summary
Listed by Well Pair

Antenna Locations			
Transmitter	**Receiver**	**Date**	**Comments**
2	1	7-Oct-04	
2	1	19-May-05	
2	1	27-May-05	
2	1	30-May-05	
3	2	7-Oct-04	
3	2	19-May-05	
3	2	27-May-05	
3	2	30-May-05	
4	1	7-Oct-04	
4	1	14-Jun-05	
4	1	6-Jul-05	
5	2	7-Oct-04	
5	2	16-May-05	
5	2	14-Jun-05	
5	2	6-Jul-05	
5	4	4-May-05	
5	4	19-May-05	
5	4	24-May-05	
5	4	27-May-05	
5	4	30-May-05	
5	4	2-Jun-05	
5	4	14-Jun-05	
5	4	27-Jun-05	
5	4	28-Jun-05	
5	4	30-Jun-05	
5	4	4-Jul-05	
6	3	10-Aug-04	
6	3	14-Jun-05	
6	3	6-Jul-05	Problem with data. Not used.
6	5	4-May-05	
6	5	19-May-05	
6	5	24-May-05	
6	5	27-May-05	
6	5	30-May-05	
6	5	2-Jun-05	
6	5	14-Jun-05	
6	5	27-Jun-05	
6	5	28-Jun-05	

Table F.1
Borehole GPR (ZOP Mode) Sampling Summary
Listed by Well Pair

Antenna Locations			
Transmitter	**Receiver**	**Date**	**Comments**
6	5	30-Jun-05	
6	5	4-Jul-05	
7	1	10-Aug-04	
7	1	19-May-05	
7	1	24-May-05	
7	1	27-May-05	
7	1	30-May-05	
7	1	14-Jun-05	
7	1	6-Jul-05	
8	4	4-May-05	
8	4	19-May-05	
8	4	24-May-05	
8	4	27-May-05	
8	4	30-May-05	
8	4	2-Jun-05	
8	4	14-Jun-05	
8	4	27-Jun-05	
8	4	28-Jun-05	
8	4	30-Jun-05	
8	4	4-Jul-05	
8	7	21-Apr-05	
8	7	12-May-05	
8	7	16-May-05	
8	7	16-Jun-05	
8	7	23-Jun-05	
8	7	27-Jun-05	
8	7	28-Jun-05	
8	7	30-Jun-05	
8	7	4-Jul-05	
9	4	7-Oct-04	
9	4	4-May-05	
9	4	14-Jun-05	
9	4	16-Jun-05	
9	4	5-Jul-05	
9	5	4-May-05	
9	5	12-May-05	
9	5	16-May-05	
9	5	2-Jun-05	
9	5	14-Jun-05	

Table F.1
Borehole GPR (ZOP Mode) Sampling Summary
Listed by Well Pair

Antenna Locations			
Transmitter	**Receiver**	**Date**	**Comments**
9	5	23-Jun-05	
9	5	27-Jun-05	
9	5	28-Jun-05	
9	5	30-Jun-05	
9	5	5-Jul-05	
9	8	21-Apr-05	
9	8	12-May-05	
9	8	16-May-05	
9	8	2-Jun-05	
9	8	16-Jun-05	
9	8	23-Jun-05	
9	8	27-Jun-05	
9	8	28-Jun-05	
9	8	30-Jun-05	
9	8	4-Jul-05	
10	5	4-May-05	
10	5	12-May-05	
10	5	16-May-05	
10	5	2-Jun-05	
10	5	14-Jun-05	
10	5	23-Jun-05	
10	5	27-Jun-05	
10	5	28-Jun-05	
10	5	30-Jun-05	
10	5	5-Jul-05	
10	6	4-May-05	
10	6	14-Jun-05	
10	6	16-Jun-05	
10	6	5-Jul-05	
10	9	21-Apr-05	
10	9	12-May-05	
10	9	16-May-05	
10	9	2-Jun-05	
10	9	16-Jun-05	
10	9	23-Jun-05	
10	9	27-Jun-05	
10	9	28-Jun-05	
10	9	30-Jun-05	
10	9	4-Jul-05	

Table F.1
Borehole GPR (ZOP Mode) Sampling Summary
Listed by Well Pair

Antenna Locations			
Transmitter	**Receiver**	**Date**	**Comments**
11	6	4-May-05	
11	6	19-May-05	
11	6	24-May-05	
11	6	27-May-05	
11	6	30-May-05	
11	6	2-Jun-05	
11	6	14-Jun-05	
11	6	27-Jun-05	
11	6	28-Jun-05	
11	6	30-Jun-05	
11	6	4-Jul-05	
11	10	21-Apr-05	
11	10	12-May-05	
11	10	16-May-05	
11	10	2-Jun-05	
11	10	16-Jun-05	
11	10	23-Jun-05	
11	10	27-Jun-05	
11	10	28-Jun-05	
11	10	30-Jun-05	
11	10	4-Jul-05	
12	3	10-Aug-04	
12	3	19-May-05	
12	3	27-May-05	
12	3	30-May-05	
12	3	14-Jun-05	
12	3	28-Jun-05	Problem with data. Not used.
12	3	6-Jul-05	Problem with data. Not used.
12	11	5-May-05	
12	11	12-May-05	
12	11	16-May-05	
12	11	16-Jun-05	
12	11	23-Jun-05	
12	11	27-Jun-05	
12	11	28-Jun-05	
12	11	30-Jun-05	
12	11	4-Jul-05	
13	8	7-Oct-04	
13	8	4-May-05	Problem with data. Not used.

Table F.1
Borehole GPR (ZOP Mode) Sampling Summary
Listed by Well Pair

Antenna Locations			
Transmitter	**Receiver**	**Date**	**Comments**
13	8	19-May-05	
13	8	24-May-05	
13	8	27-May-05	
13	8	30-May-05	
13	8	2-Jun-05	
13	8	14-Jun-05	
13	8	27-Jun-05	
13	8	28-Jun-05	
13	8	30-Jun-05	
13	8	4-Jul-05	
13	9	7-Oct-04	
13	9	14-Jun-05	
13	9	5-Jul-05	
14	9	21-Apr-05	
14	9	12-May-05	
14	9	16-May-05	
14	9	2-Jun-05	
14	9	14-Jun-05	
14	9	23-Jun-05	
14	9	27-Jun-05	
14	9	28-Jun-05	
14	9	30-Jun-05	
14	9	5-Jul-05	
14	10	21-Apr-05	
14	10	12-May-05	
14	10	16-May-05	
14	10	2-Jun-05	
14	10	14-Jun-05	
14	10	23-Jun-05	
14	10	27-Jun-05	
14	10	28-Jun-05	
14	10	30-Jun-05	
14	10	5-Jul-05	
14	13	7-Oct-04	
14	13	19-May-05	
14	13	24-May-05	
14	13	27-May-05	
14	13	30-May-05	
14	13	2-Jun-05	
14	13	14-Jun-05	

Table F.1
Borehole GPR (ZOP Mode) Sampling Summary
Listed by Well Pair

Antenna Locations			
Transmitter	**Receiver**	**Date**	**Comments**
14	13	27-Jun-05	
14	13	28-Jun-05	
14	13	30-Jun-05	
14	13	4-Jul-05	
15	10	4-May-05	
15	10	14-Jun-05	
15	10	16-Jun-05	
15	10	5-Jul-05	
15	11	4-May-05	
15	11	19-May-05	
15	11	24-May-05	
15	11	27-May-05	
15	11	30-May-05	
15	11	2-Jun-05	
15	11	14-Jun-05	
15	11	27-Jun-05	
15	11	28-Jun-05	
15	11	30-Jun-05	
15	11	4-Jul-05	
15	14	4-May-05	
15	14	19-May-05	
15	14	24-May-05	
15	14	27-May-05	
15	14	30-May-05	
15	14	2-Jun-05	
15	14	14-Jun-05	
15	14	27-Jun-05	
15	14	28-Jun-05	
15	14	30-Jun-05	
15	14	4-Jul-05	
16	7	10-Aug-04	
16	7	19-May-05	
16	7	24-May-05	
16	7	27-May-05	
16	7	30-May-05	
16	7	14-Jun-05	
16	7	6-Jul-05	Problem with data. Not used.
16	13	7-Oct-04	
16	13	14-Jun-05	

Table F.1
Borehole GPR (ZOP Mode) Sampling Summary
Listed by Well Pair

Antenna Locations			
Transmitter	**Receiver**	**Date**	**Comments**
16	13	6-Jul-05	
17	14	10-Aug-04	
17	14	12-May-05	
17	14	16-May-05	
17	14	14-Jun-05	
17	14	6-Jul-05	
17	16	10-Aug-04	
17	16	19-May-05	
17	16	24-May-05	
17	16	27-May-05	
17	16	30-May-05	
18	12	10-Aug-04	
18	12	19-May-05	
18	12	24-May-05	
18	12	27-May-05	
18	12	30-May-05	
18	12	14-Jun-05	
18	12	28-Jun-05	Problem with data. Not used.
18	12	6-Jul-05	
18	15	6-Oct-04	
18	15	14-Jun-05	
18	15	6-Jul-05	
18	17	10-Aug-04	
18	17	19-May-05	
18	17	24-May-05	
18	17	27-May-05	
18	17	30-May-05	

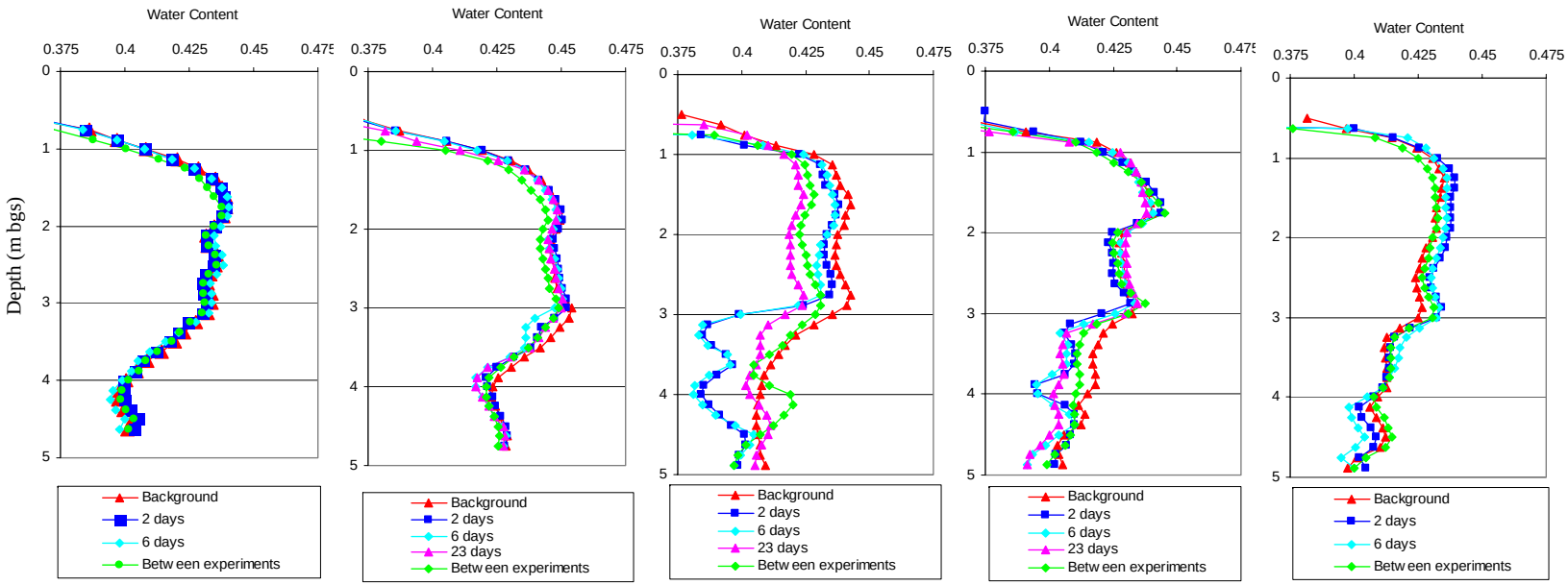

Figure F.1 – Passive injection experiment water content profiles between GP-7 and GP-12 showing induced CO_2-gas inferred from cross-borehole GPR (ZOP mode) data.

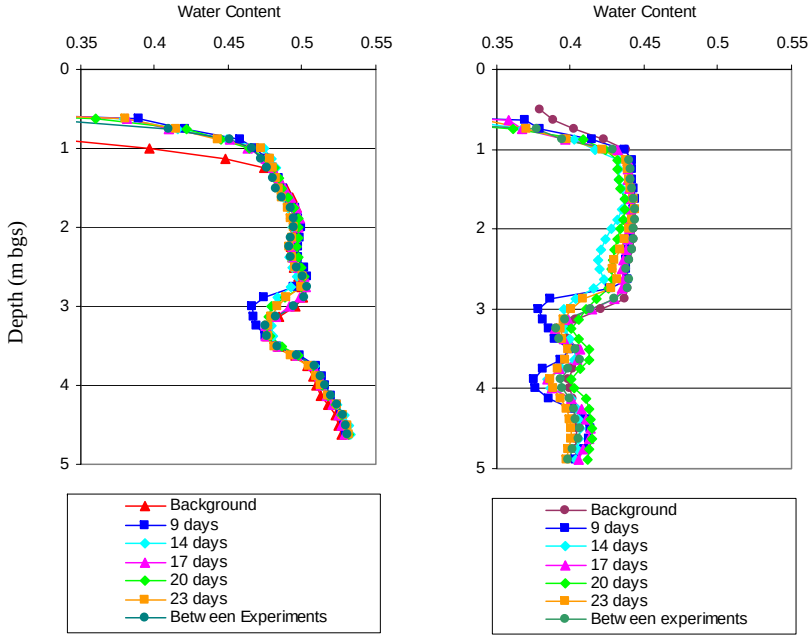

Figure F.2 – Passive injection experiment water content profiles between GP-13 and GP-15 showing induced CO_2-gas inferred from cross-borehole GPR (ZOP mode) data.

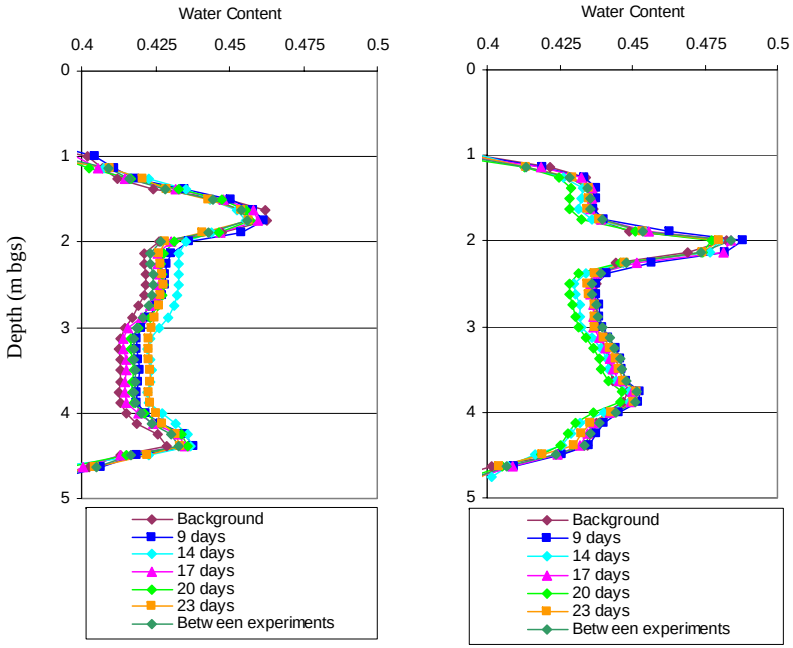

Figure F.3 – Passive injection experiment water content profiles between GP-4 and GP-6 showing induced CO_2-gas inferred from cross-borehole GPR (ZOP mode) data.

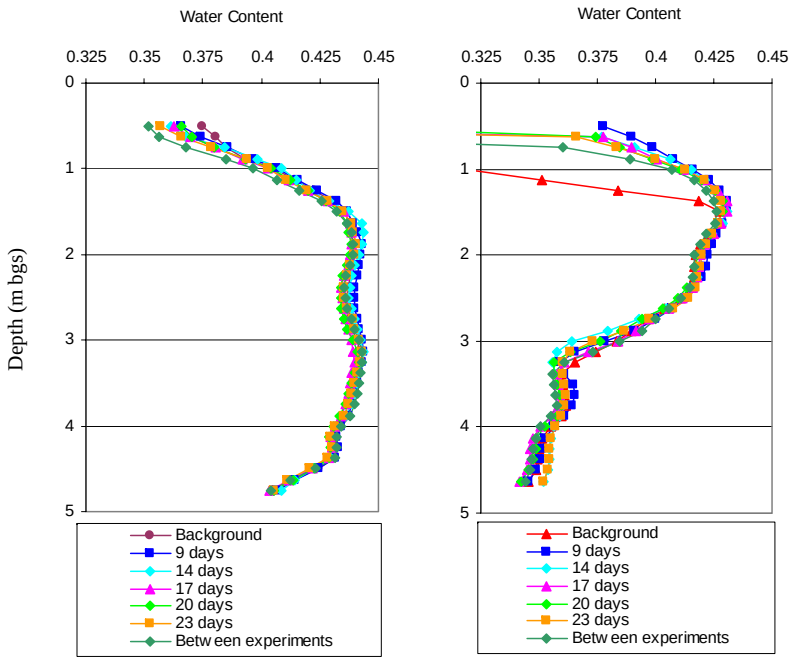

Figure F.4 – Passive injection experiment water content profiles between GP-4 and GP-13 showing induced CO_2-gas inferred from cross-borehole GPR (ZOP mode) data.

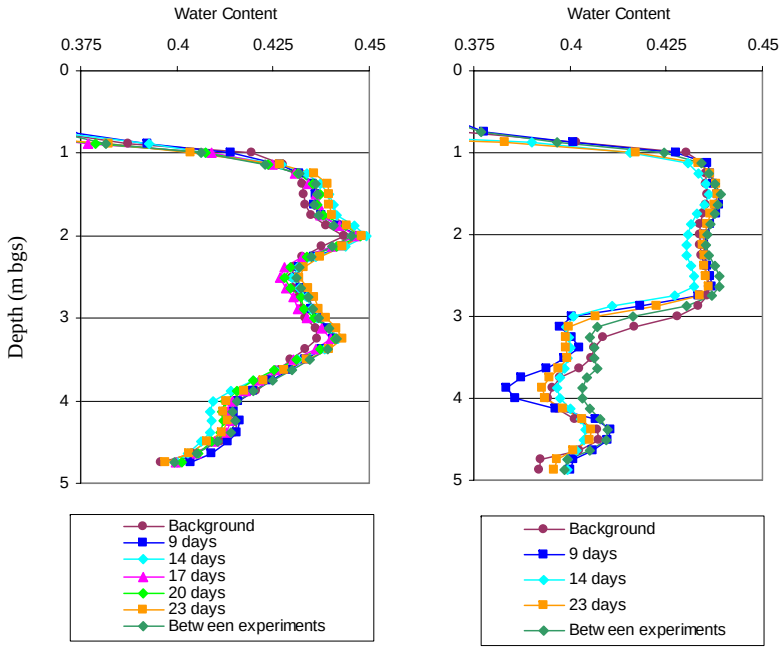

Figure F.5 - Passive injection experiment water content profiles between GP-6 and GP-15 showing induced CO_2-gas inferred from cross-borehole GPR (ZOP mode) data.

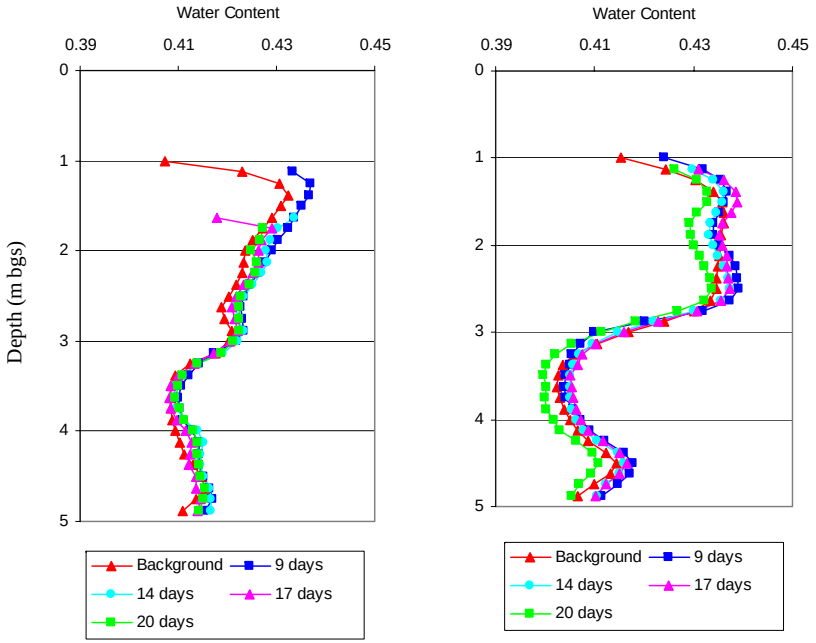

Figure F.6 – Passive injection experiment water content profiles between GP-16 and GP-18 showing induced CO_2-gas inferred from cross-borehole GPR (ZOP mode) data.

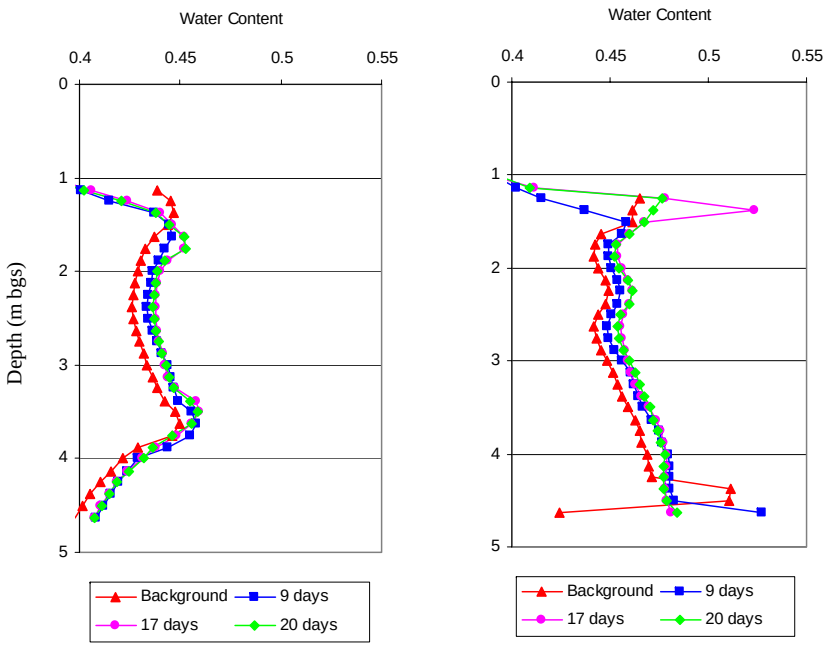

Figure F.7 – Passive injection experiment water content profiles between GP-1 and GP-3 showing induced CO_2-gas inferred from cross-borehole GPR (ZOP mode) data.

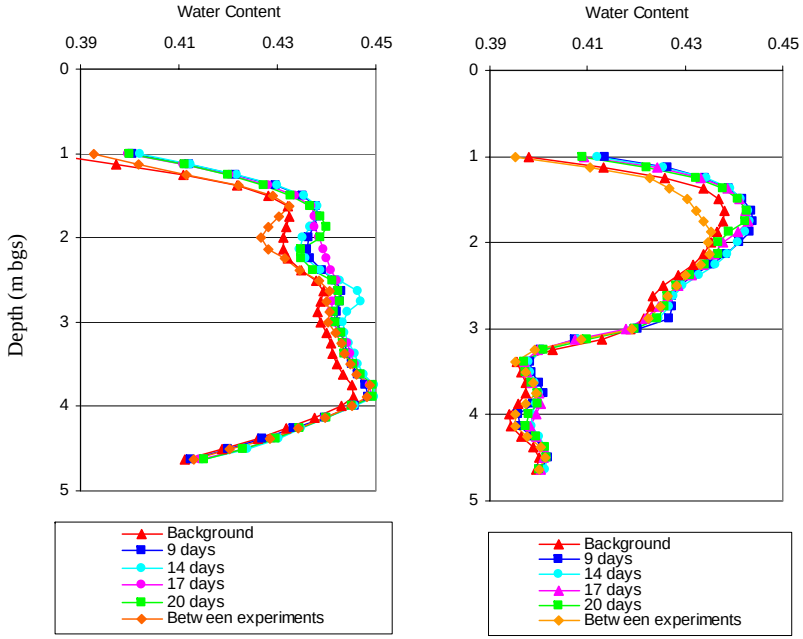

Figure F.8 – Passive injection experiment water content profiles between GP-1 and GP-16 showing induced CO_2-gas inferred from cross-borehole GPR (ZOP mode) data.

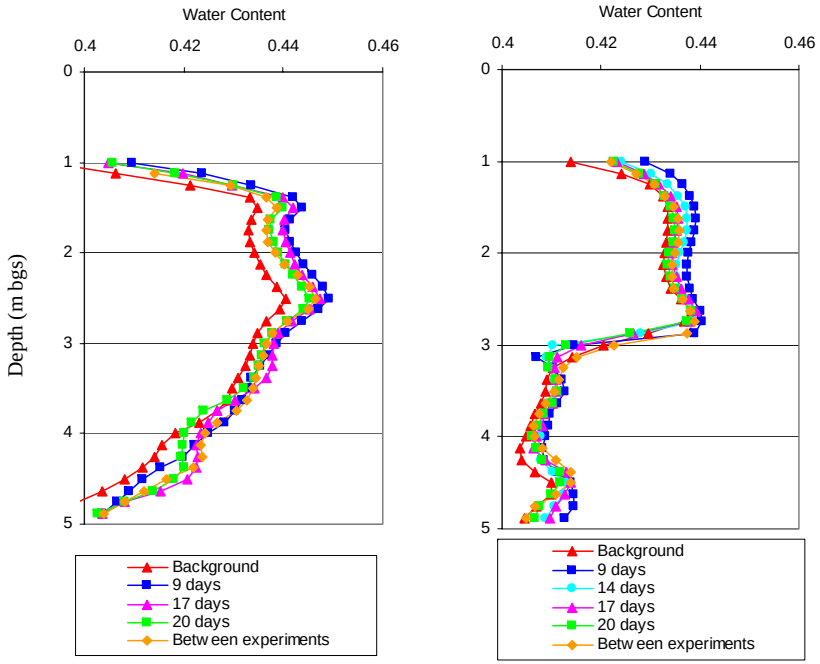

Figure F.9 – Passive injection experiment water content profiles between GP-3 and GP-18 showing induced CO_2-gas inferred from cross-borehole GPR (ZOP mode) data.

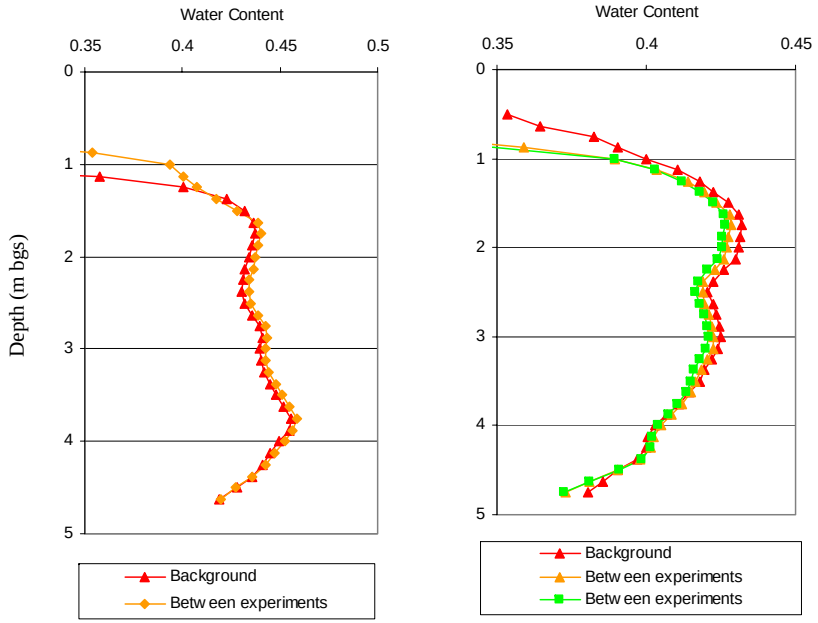

Figure F.10 – Passive injection experiment water content profiles between GP-1 and GP-9 showing induced CO_2-gas inferred from cross-borehole GPR (ZOP mode) data.

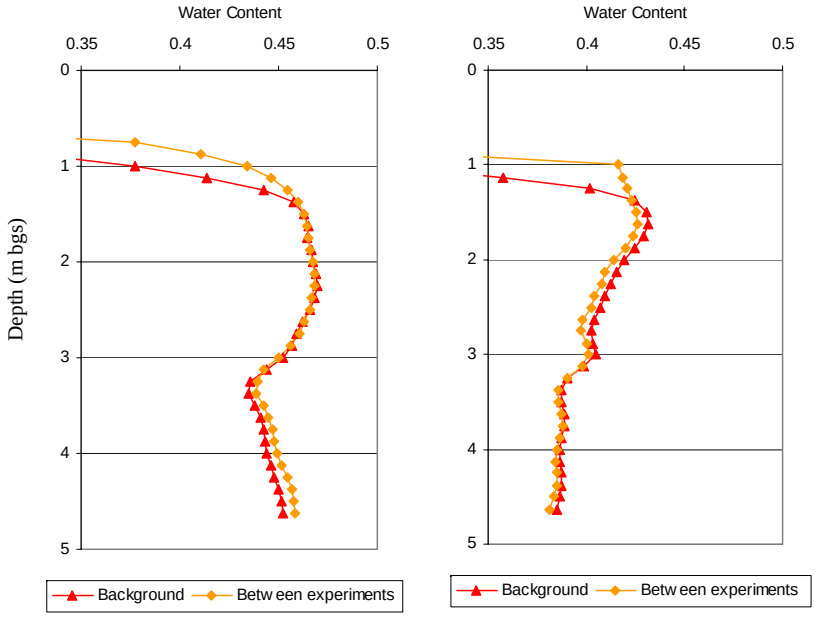

Figure F.11 – Passive injection experiment water content profiles between GP-9 and GP-16 showing induced CO_2-gas inferred from cross-borehole GPR (ZOP mode) data.

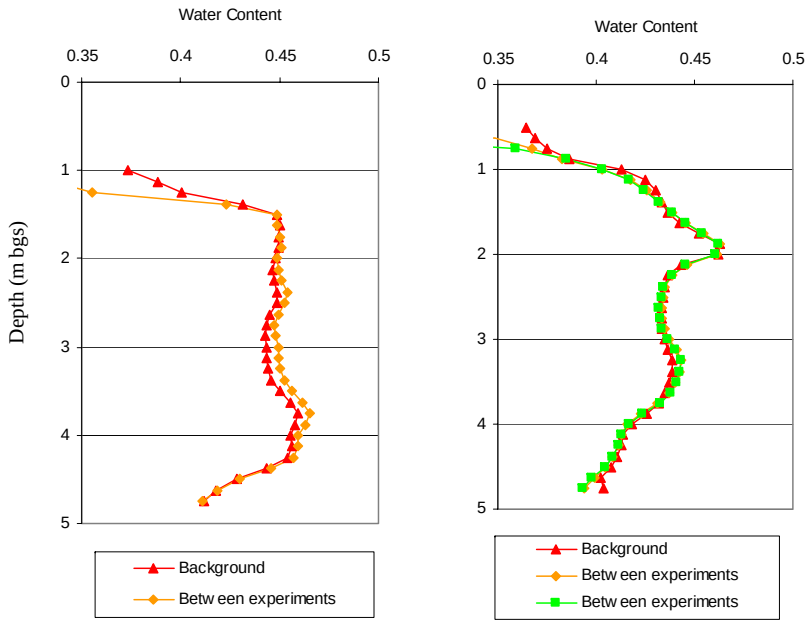

Figure F.12 – Passive injection experiment water content profiles between GP-3 and GP-10 showing induced CO_2-gas inferred from cross-borehole GPR (ZOP mode) data.

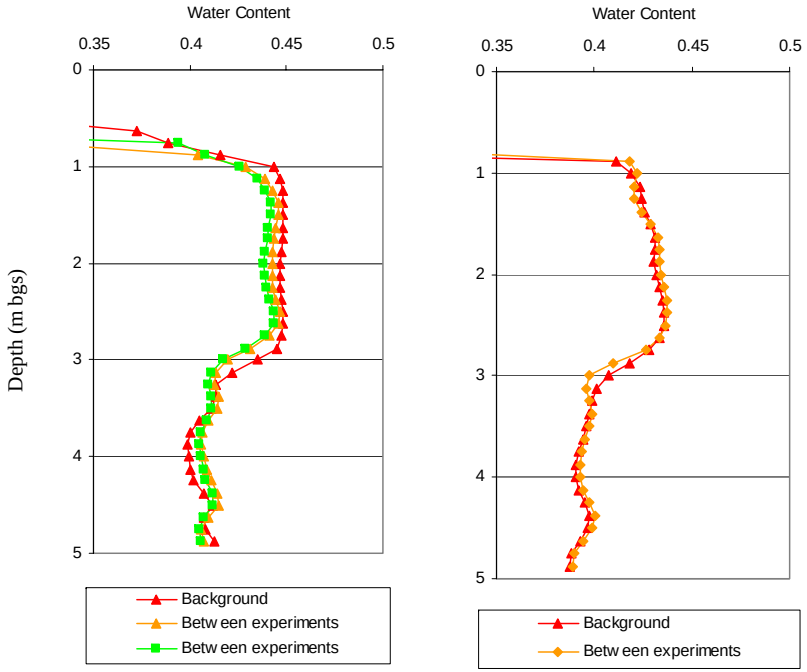

Figure F.13 – Passive injection experiment water content profiles between GP-10 and GP-18 showing induced CO_2-gas inferred from cross-borehole GPR (ZOP mode) data.

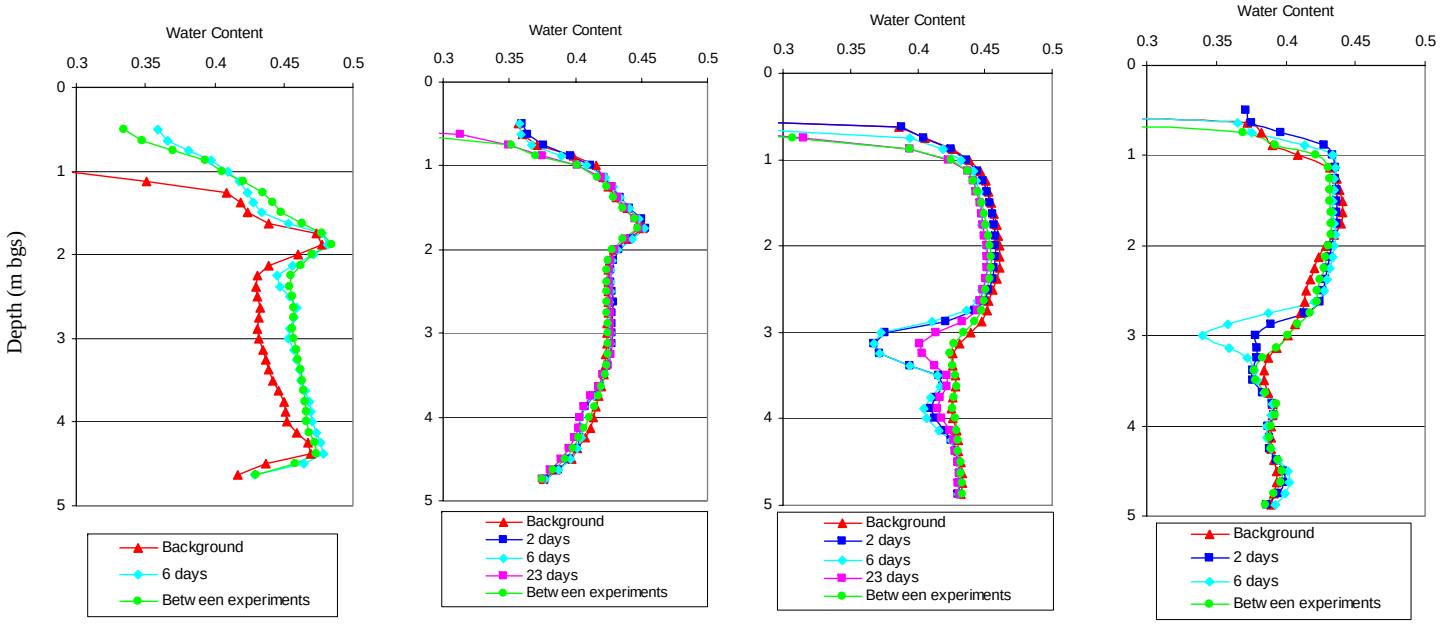

Figure F.14 – Passive injection experiment water content profiles between GP-2 and GP-17 showing induced CO_2-gas inferred from cross-borehole GPR (ZOP mode) data.

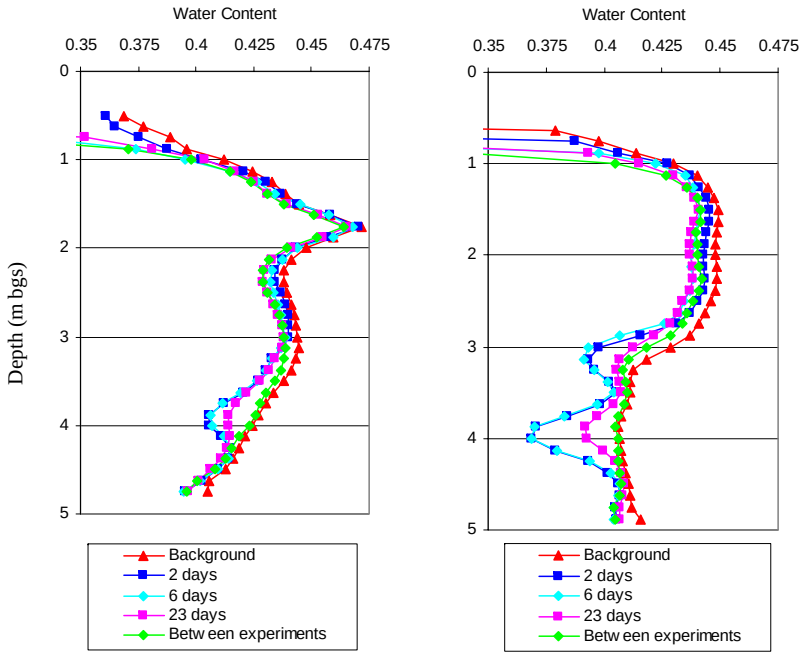

Figure F.15 – Passive injection experiment water content profiles between GP-5 and GP-14 showing induced CO_2-gas inferred from cross-borehole GPR (ZOP mode) data.

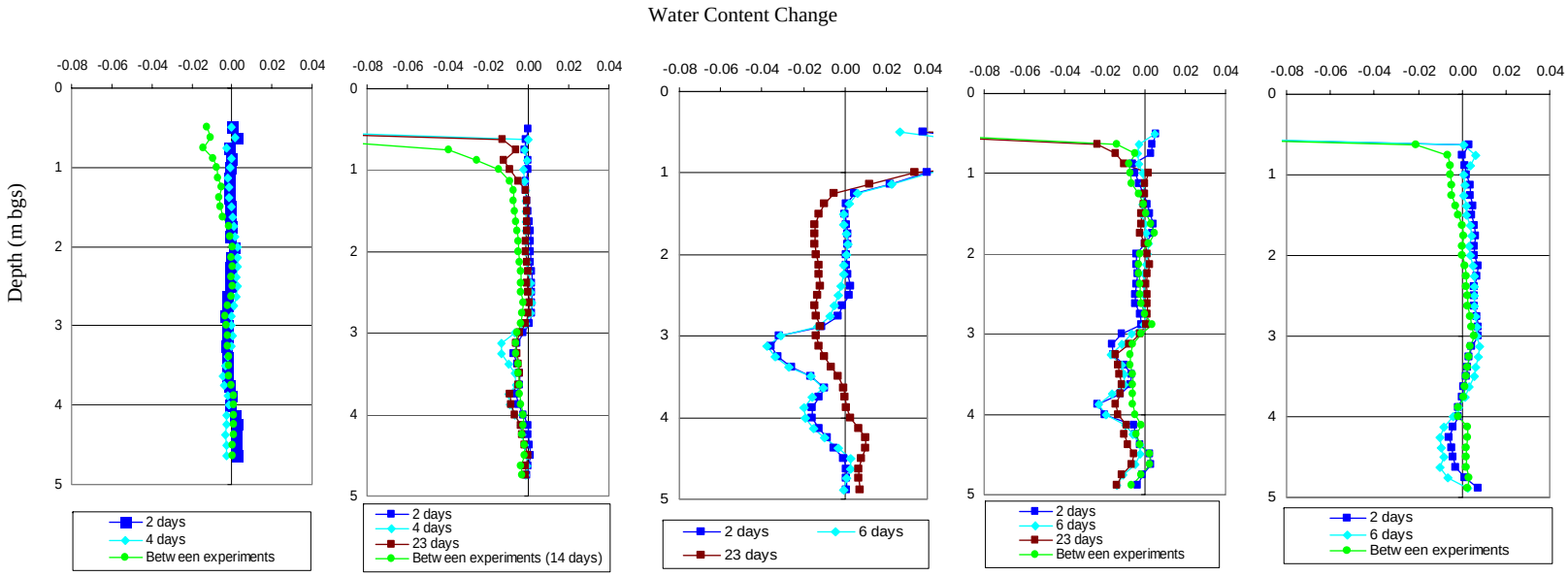

Figure F.16 – Passive injection experiment water content change profiles between GP-7 and GP-12 showing induced CO_2-gas inferred from cross-borehole GPR (ZOP mode) data.

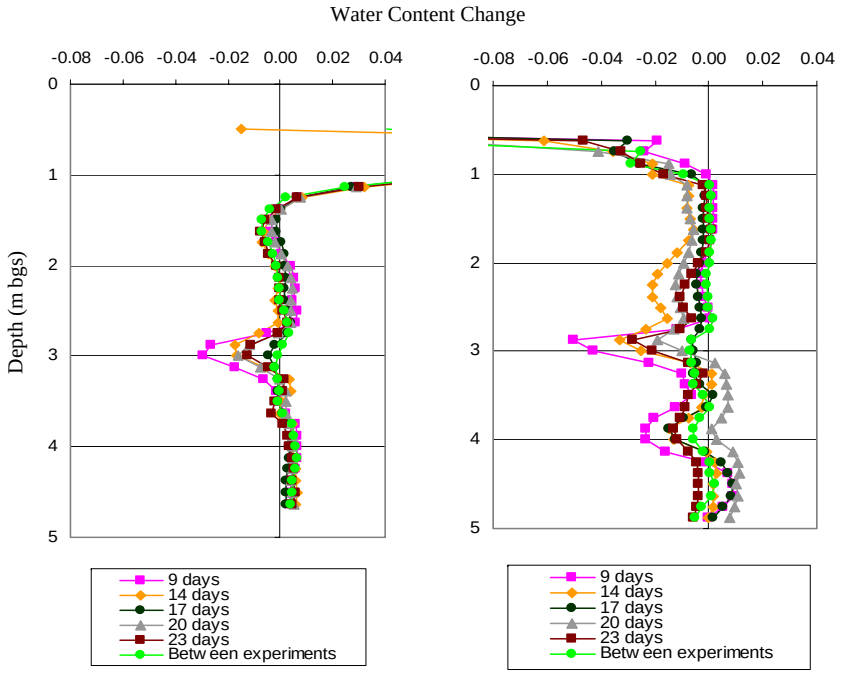

Figure F.17 – Passive injection experiment water content change profiles between GP-13 and GP-15 showing induced CO_2-gas inferred from cross-borehole GPR (ZOP mode) data.

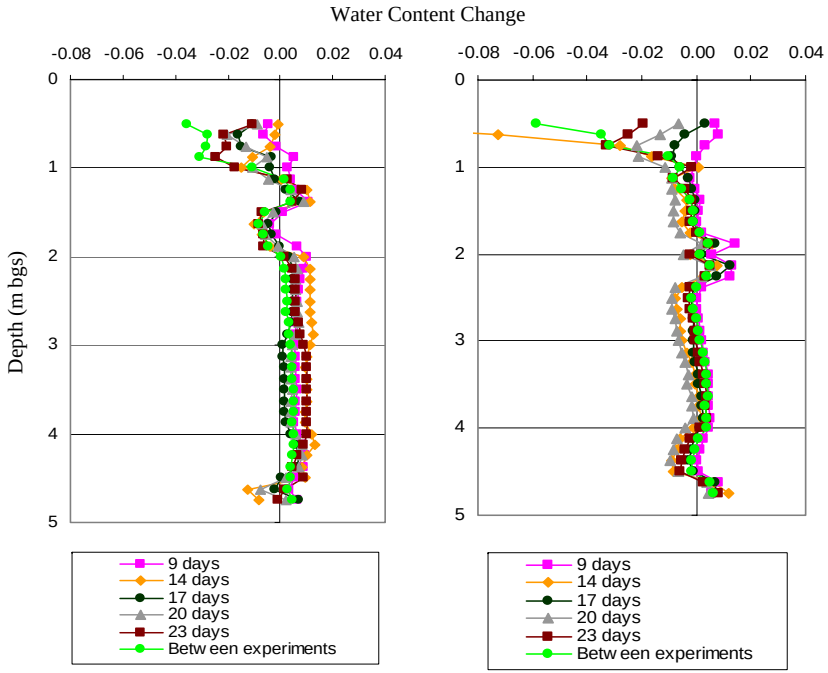

Figure F.18 – Passive injection experiment water content change profiles between GP-4 and GP-6 showing induced CO_2-gas inferred from cross-borehole GPR (ZOP mode) data.

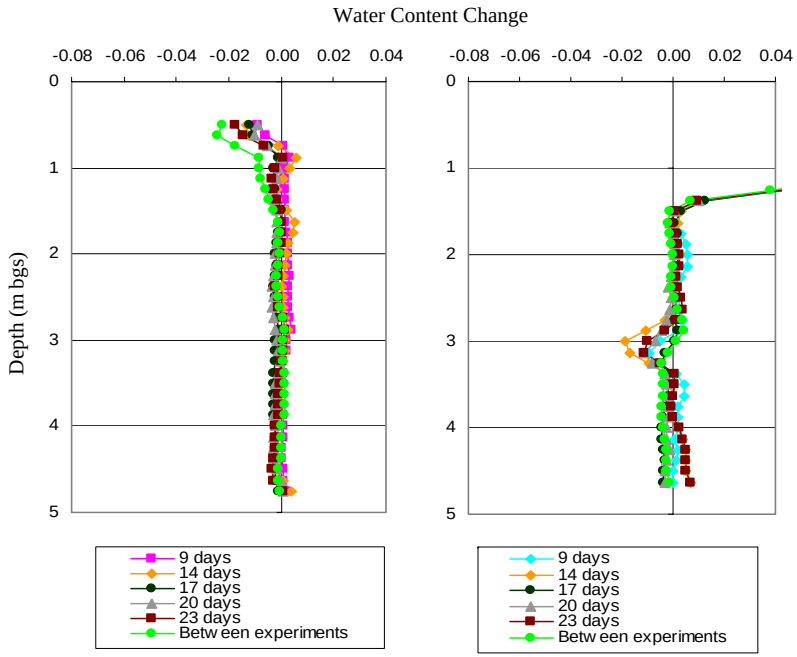

Figure F.19 – Passive injection experiment water content change profiles between GP-4 and GP-13 showing induced CO_2-gas inferred from cross-borehole GPR (ZOP mode) data.

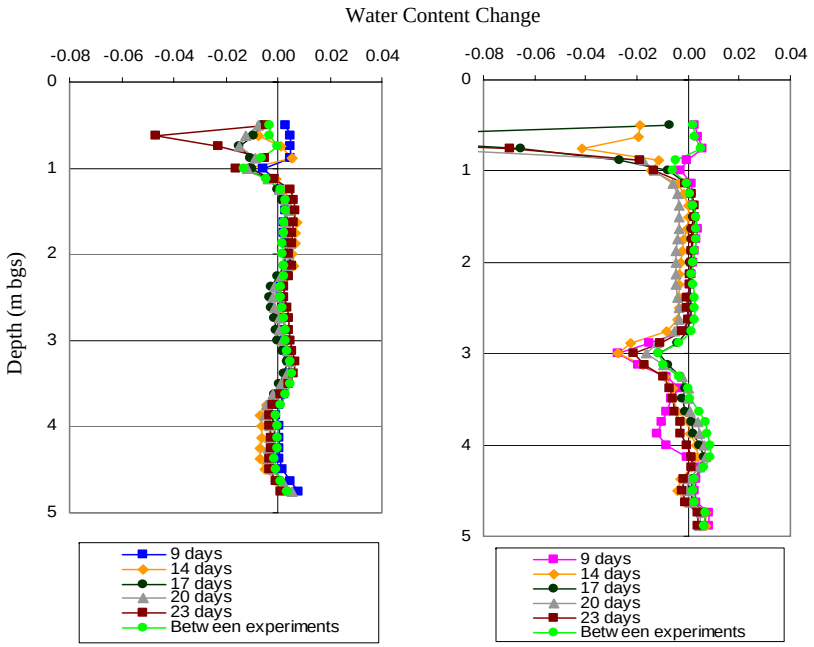

Figure F.20 – Passive injection experiment water content change profiles between GP-6 and GP-15 showing induced CO_2-gas inferred from cross-borehole GPR (ZOP mode) data.

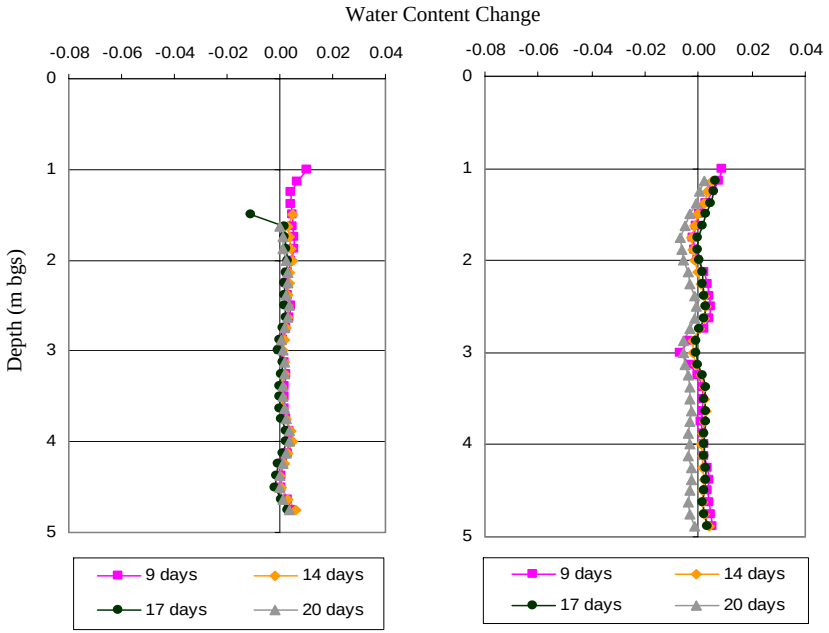

Figure F.21 – Passive injection experiment water content change profiles between GP-16 and GP-18 showing induced CO_2-gas inferred from cross-borehole GPR (ZOP mode) data.

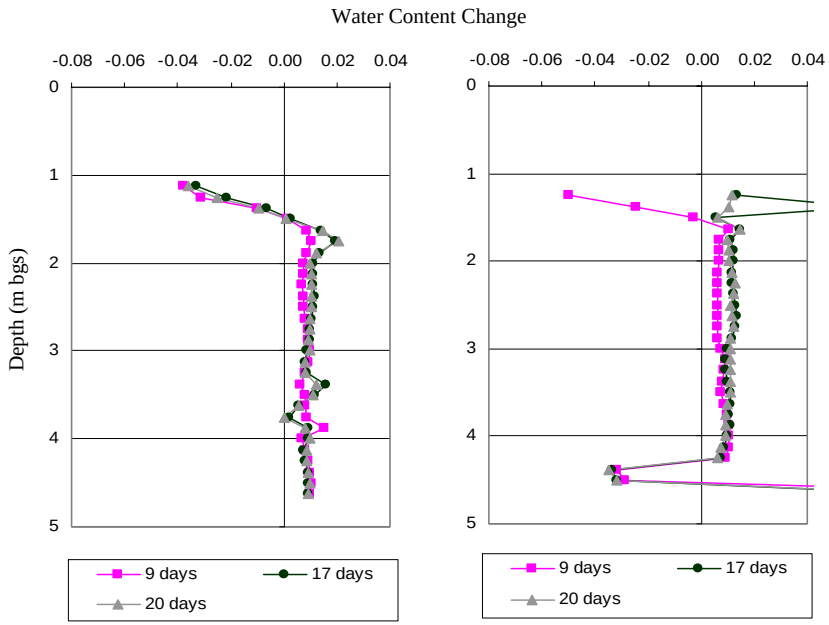

Figure F.22 – Passive injection experiment water content change profiles between GP-1 and GP-3 showing induced CO_2-gas inferred from cross-borehole GPR (ZOP mode) data.

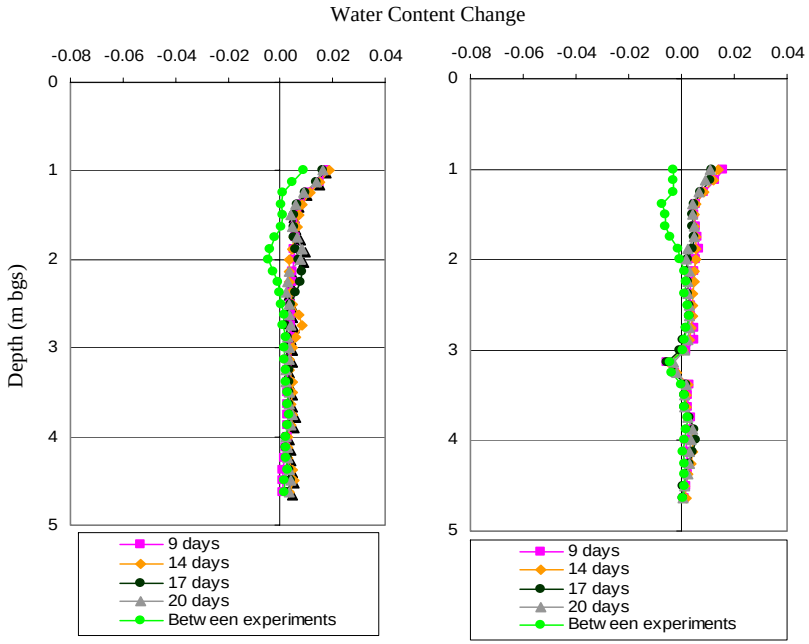

Figure F.23 – Passive injection experiment water content change profiles between GP-1 and GP-16 showing induced CO_2-gas inferred from cross-borehole GPR (ZOP mode) data.

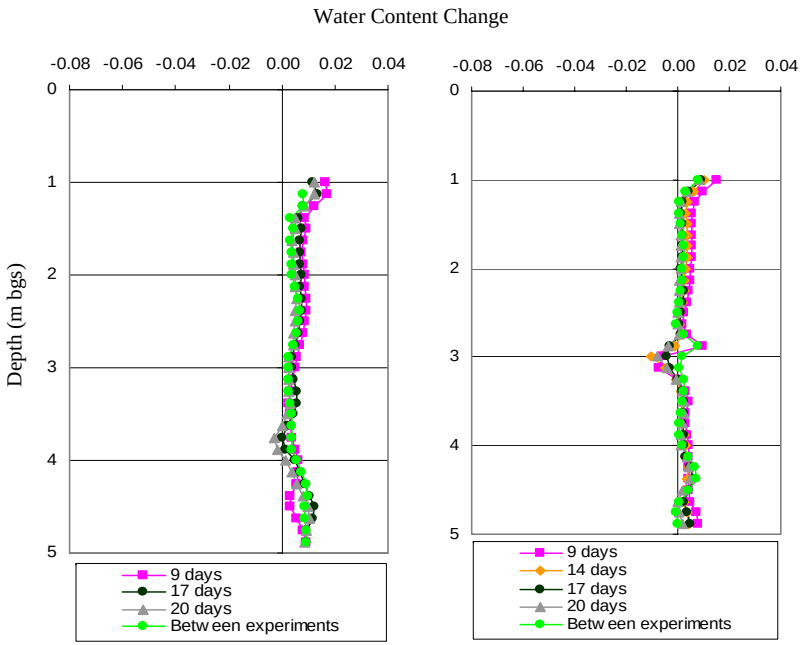

Figure F.24 – Passive injection experiment water content change profiles between GP-3 and GP-18 showing induced CO_2-gas inferred from cross-borehole GPR (ZOP mode) data.

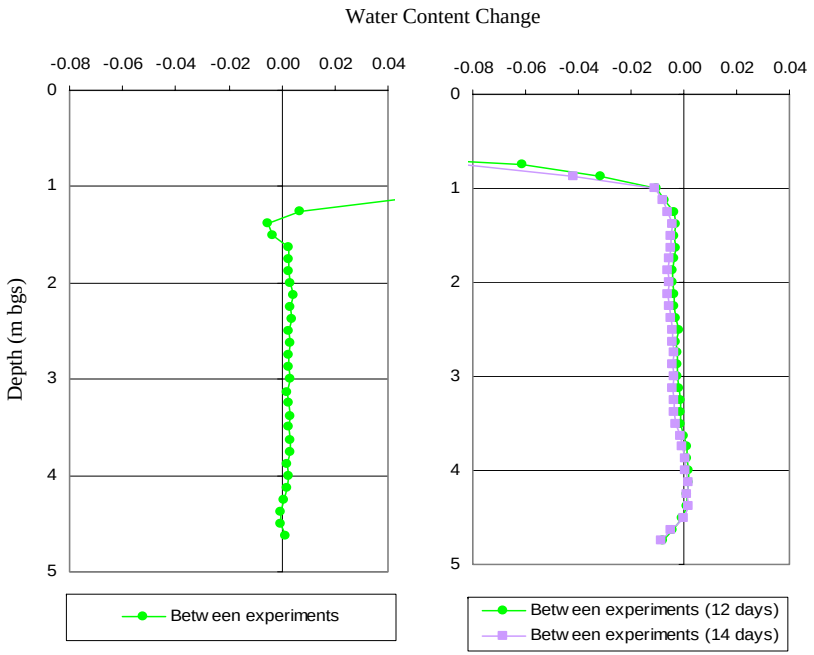

Figure F.25 – Passive injection experiment water content change profiles between GP-1 and GP-9 showing induced CO_2-gas inferred from cross-borehole GPR (ZOP mode) data.

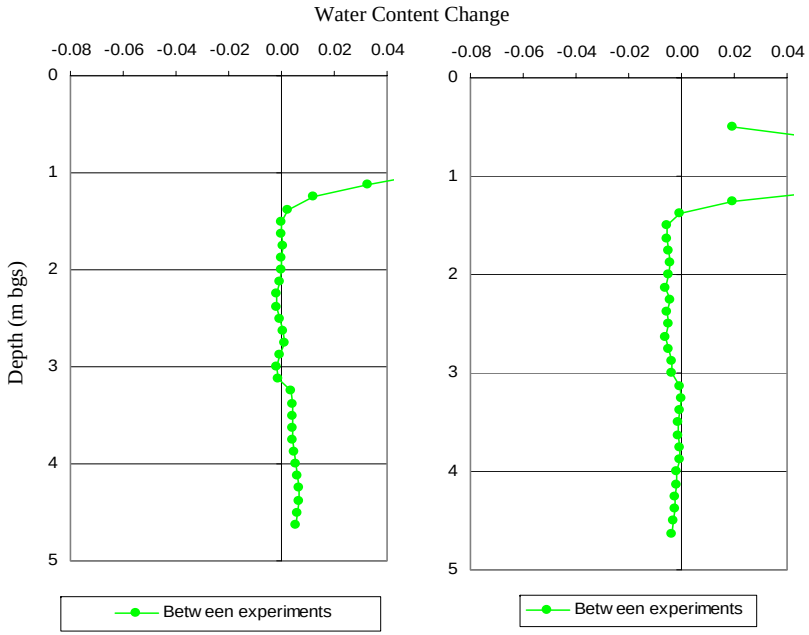

Figure F.26 – Passive injection experiment water content change profiles between GP-9 and GP-16 showing induced CO_2-gas inferred from cross-borehole GPR (ZOP mode) data.

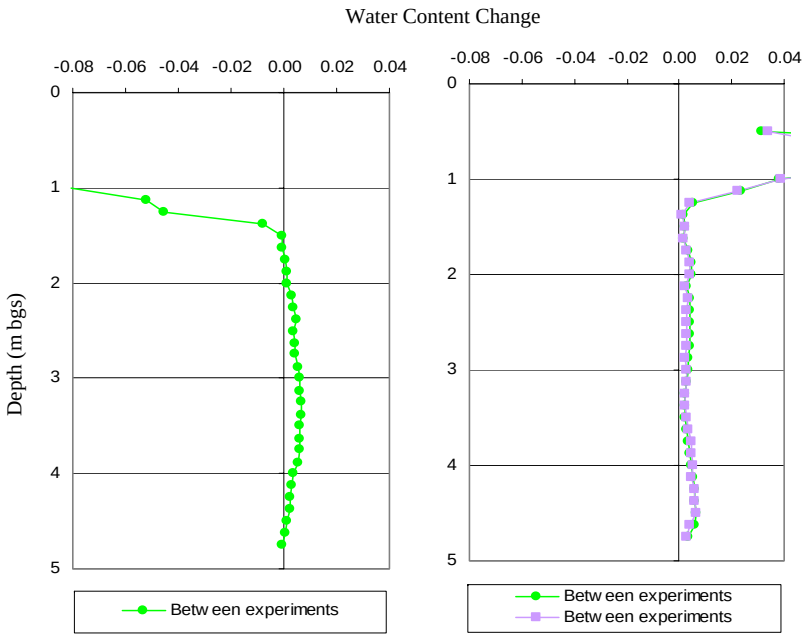

Figure F.27 – Passive injection experiment water content change profiles between GP-3 and GP-10 showing induced CO_2-gas inferred from cross-borehole GPR (ZOP mode) data.

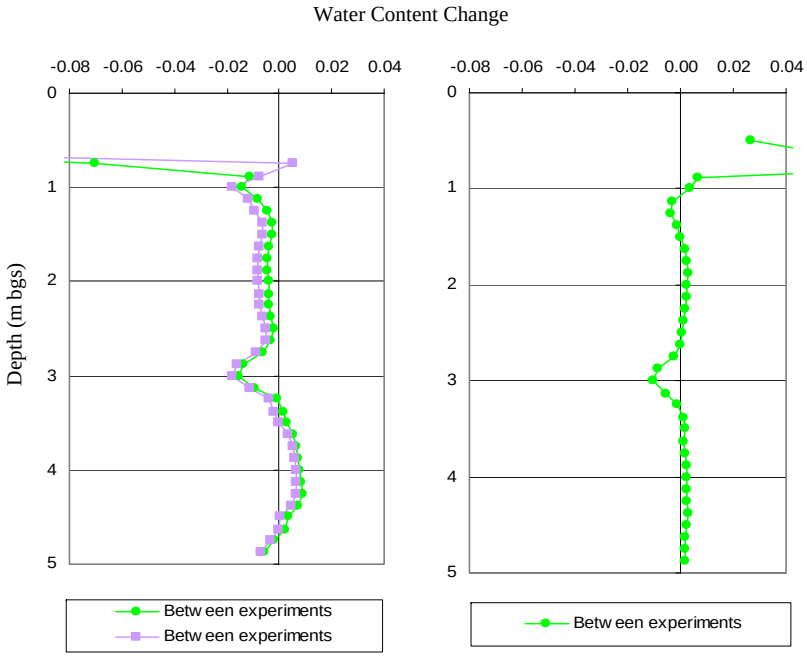

Figure F.28 – Passive injection experiment water content change profiles between GP-10 and GP-18 showing induced CO_2-gas inferred from cross-borehole GPR (ZOP mode) data.

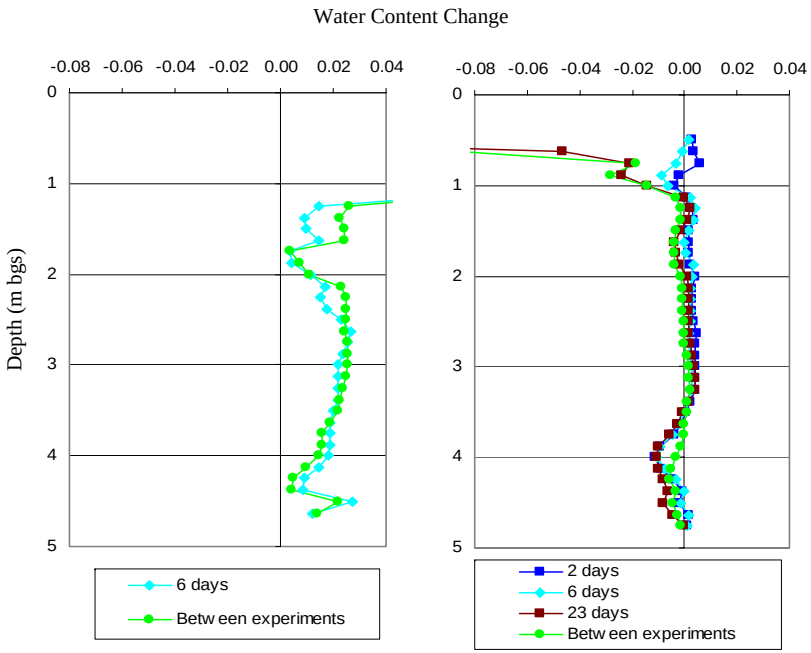

Figure F.29 – Passive injection experiment water content change profiles between GP-2 and GP-9 showing induced CO_2-gas inferred from cross-borehole GPR (ZOP mode) data.

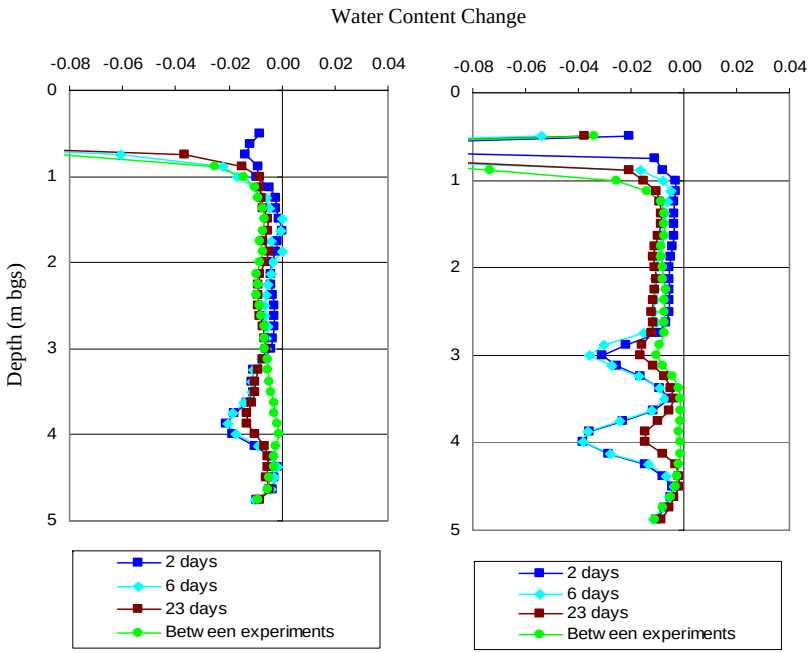

Figure F.30 – Passive injection experiment water content change profiles between GP-5 and GP-14 showing induced CO_2-gas inferred from cross-borehole GPR (ZOP mode) data.

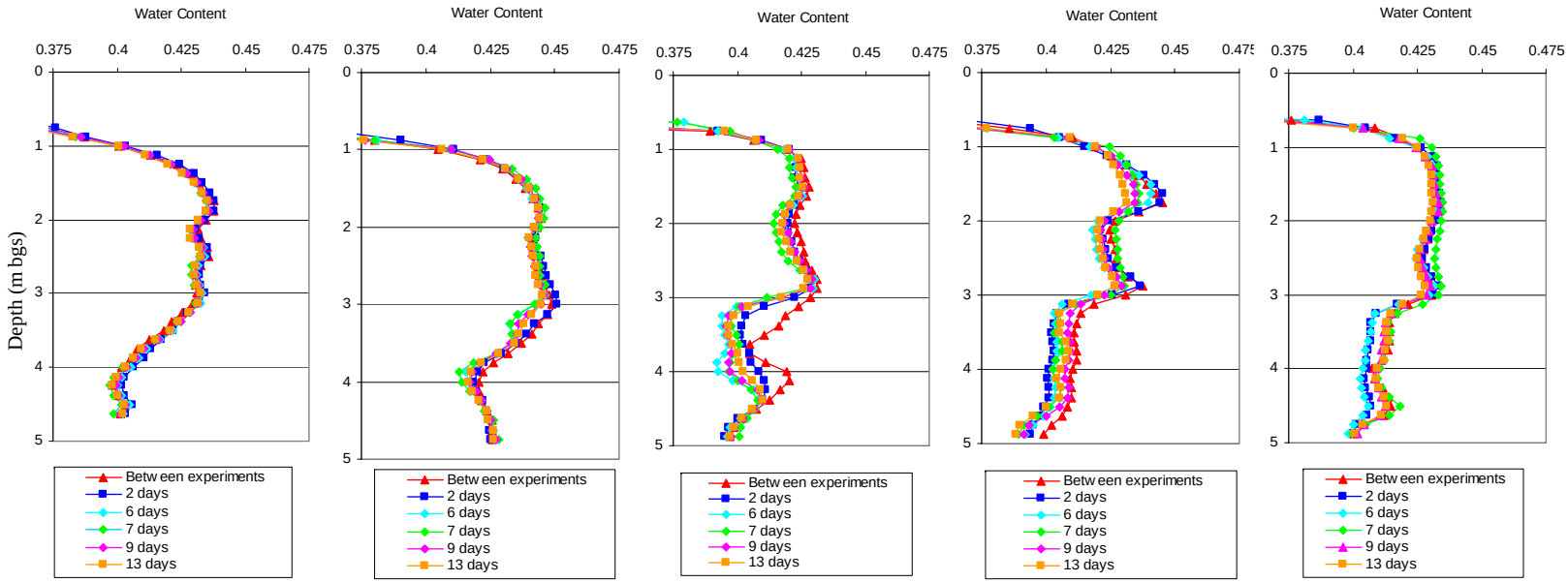

Figure F.31 – Active injection experiment water content change profiles between GP-7 and GP-12 showing induced CO_2-gas inferred from cross-borehole GPR (ZOP mode) data.

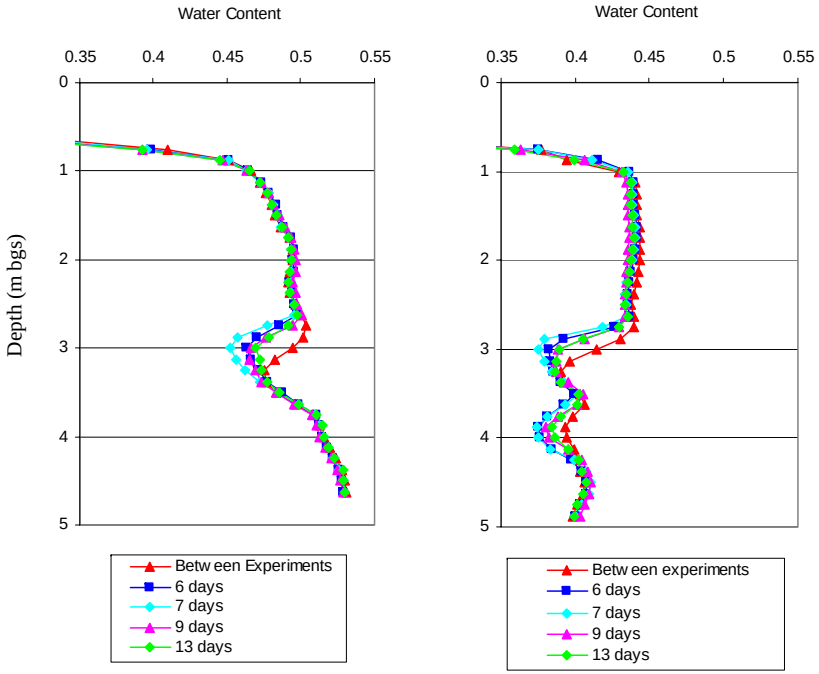

Figure F.32 – Active injection experiment water content profiles between GP-13 and GP-15 showing induced CO_2-gas inferred from cross-borehole GPR (ZOP mode) data.

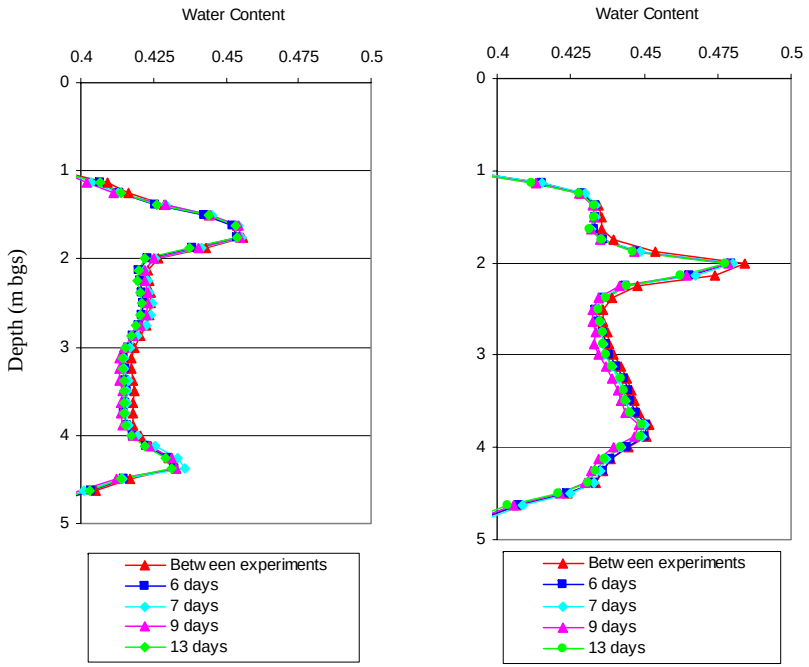

Figure F.33 – Active injection experiment water content profiles between GP-4 and GP-6 showing induced CO_2-gas inferred from cross-borehole GPR (ZOP mode) data.

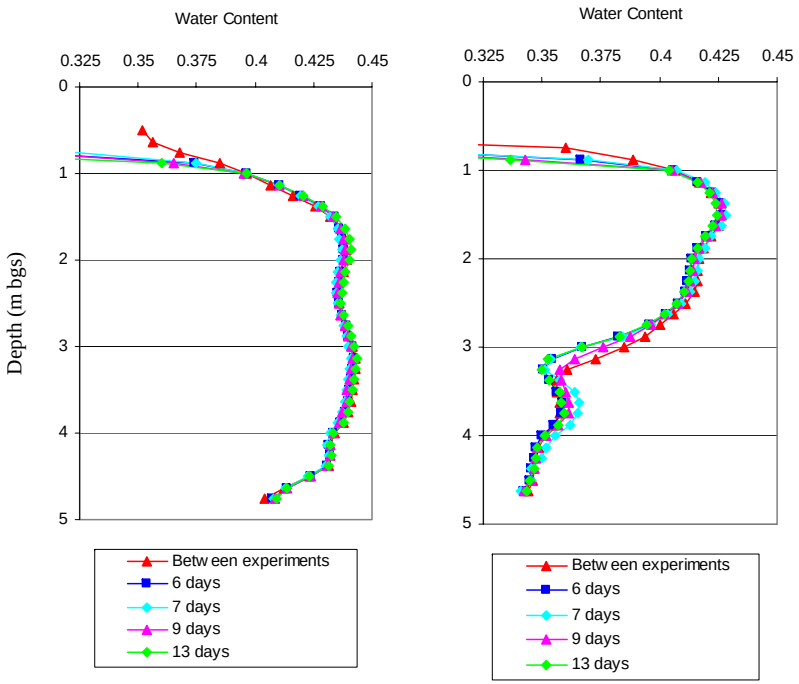

Figure F.34 – Active injection experiment water content profiles between GP-4 and GP-13 showing induced CO_2-gas inferred from cross-borehole GPR (ZOP mode) data.

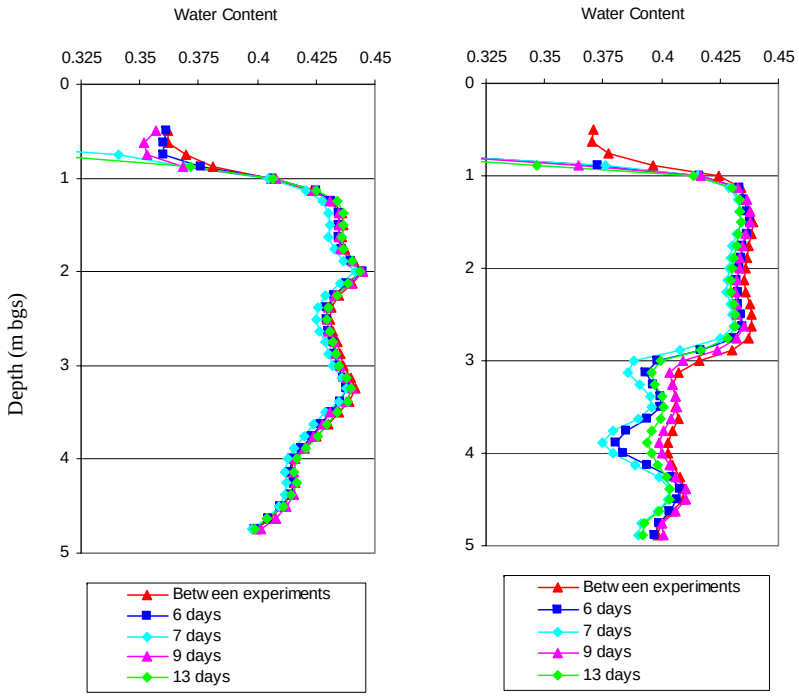

Figure F.35 - Active injection experiment water content profiles between GP-6 and GP-15 showing induced CO_2-gas inferred from cross-borehole GPR (ZOP mode) data.

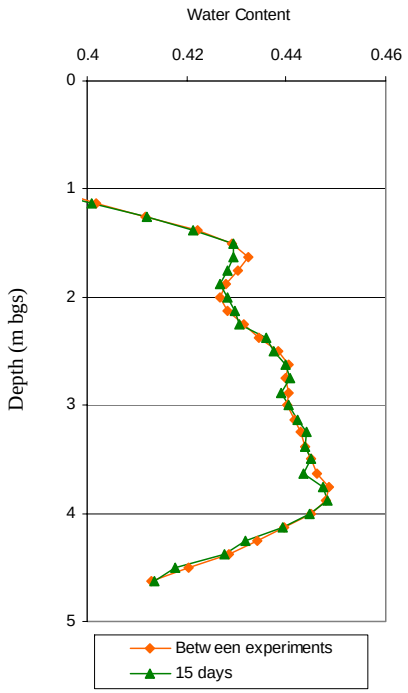

Figure F.36 – Active injection experiment water content profiles between GP-1 and GP-7 showing induced CO_2-gas inferred from cross-borehole GPR (ZOP mode) data.

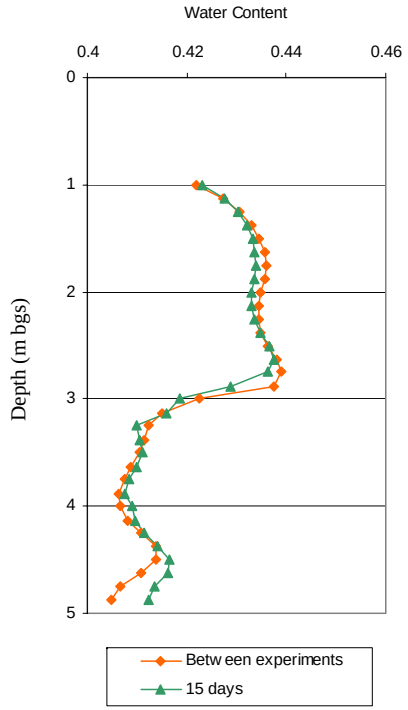

Figure F.37 – Active injection experiment water content profiles between GP-12 and GP-18 showing induced CO_2-gas inferred from cross-borehole GPR (ZOP mode) data.

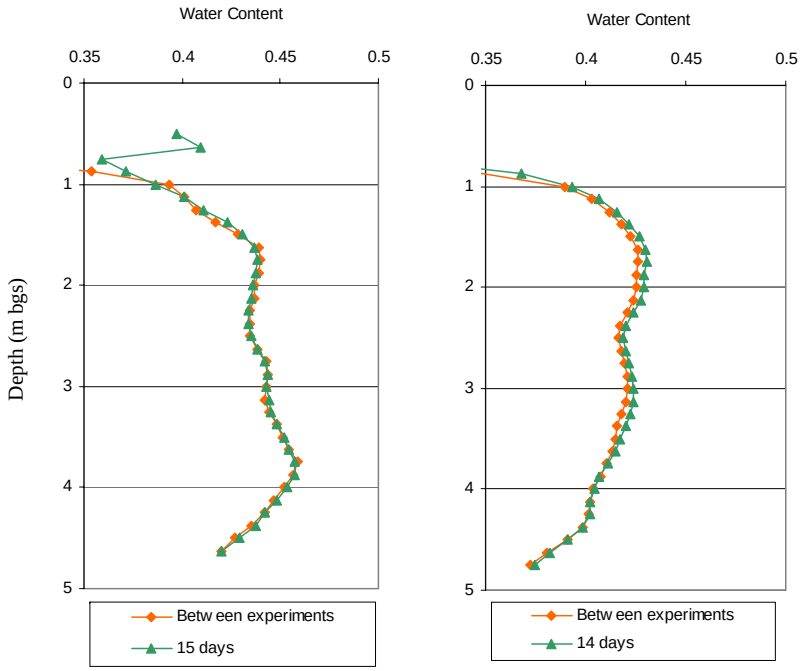

Figure F.38 – Active injection experiment water content profiles between GP-1 and GP-9 showing induced CO_2-gas inferred from cross-borehole GPR (ZOP mode) data.

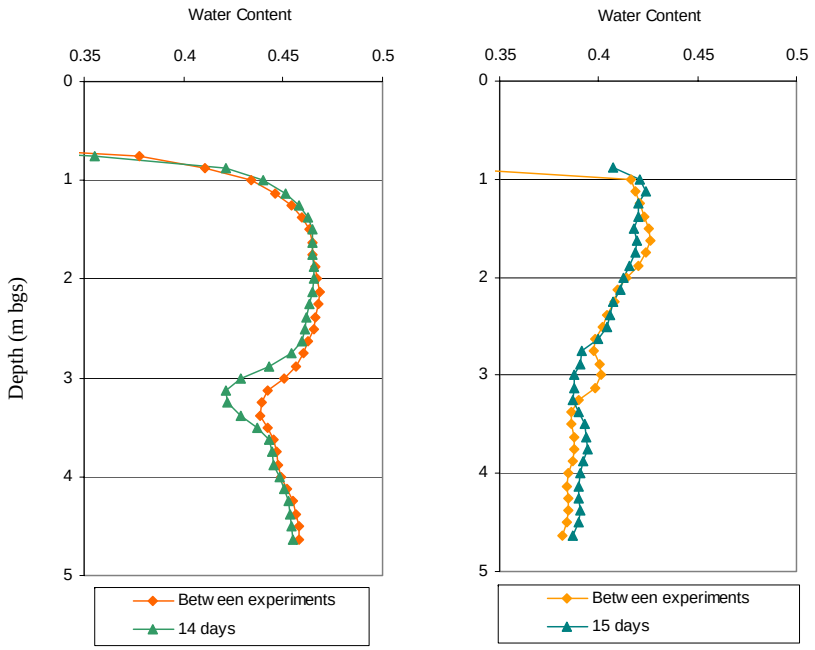

Figure F.11 – Passive injection experiment water content profiles between GP-9 and GP-16 showing induced CO_2-gas inferred from cross-borehole GPR (ZOP mode) data.

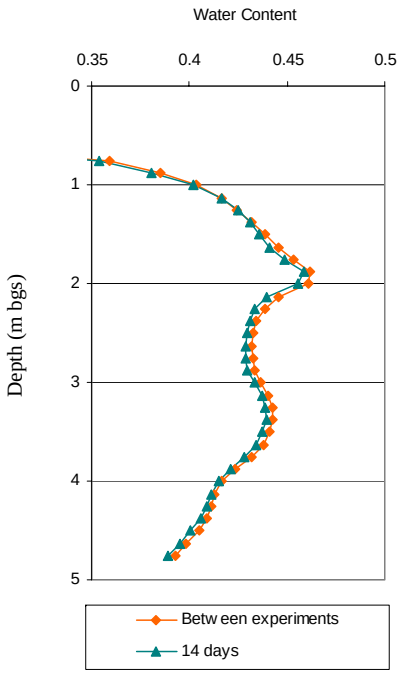

Figure F.40 – Active injection experiment water content profiles between GP-6 and GP-10 showing induced CO_2-gas inferred from cross-borehole GPR (ZOP mode) data.

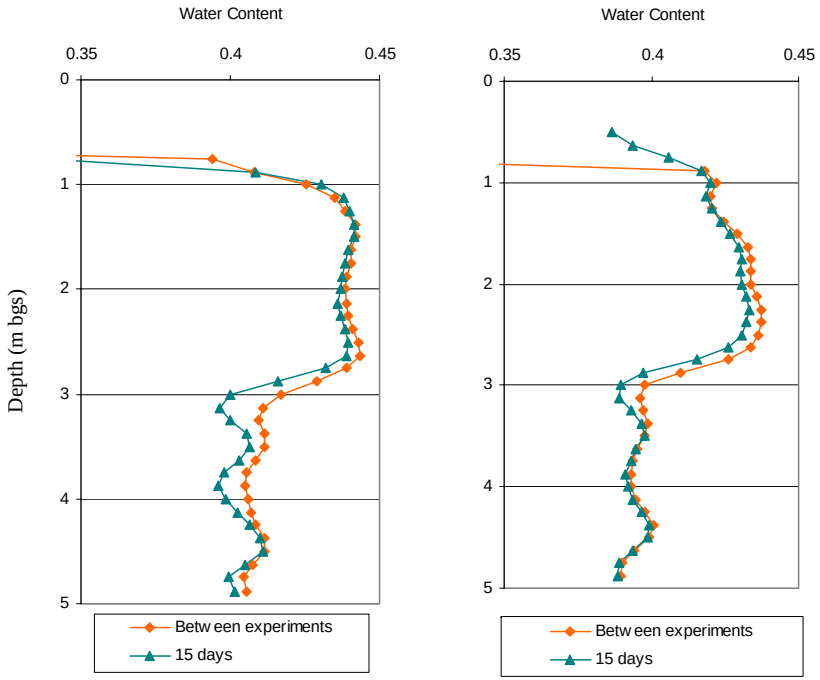

Figure F.41 – Active injection experiment water content profiles between GP-10 and GP-18 showing induced CO_2-gas inferred from cross-borehole GPR (ZOP mode) data.

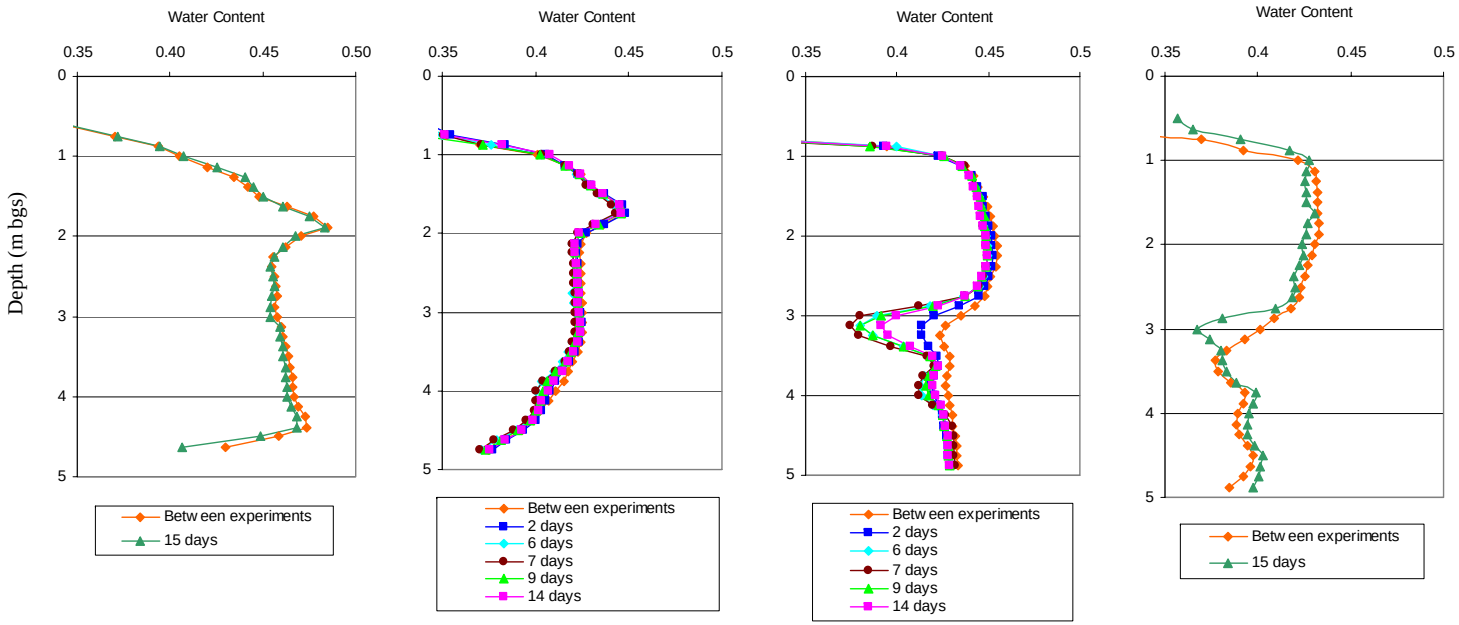

Figure F. 42 – Active injection experiment water content profiles between GP-2 and GP-17 showing induced CO_2-gas inferred from cross-borehole GPR (ZOP mode) data.

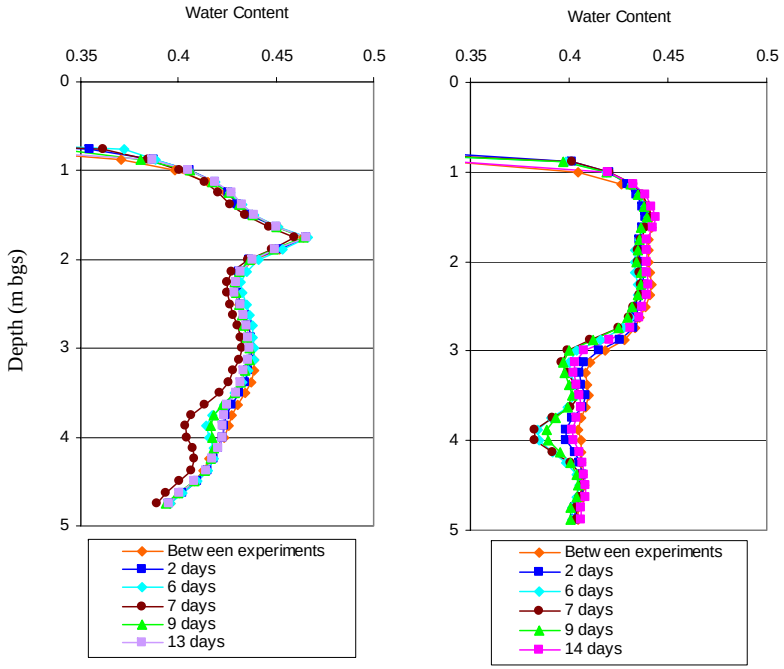

Figure F.43 – Active injection experiment water content profiles between GP-5 and GP-14 showing induced CO_2-gas inferred from cross-borehole GPR (ZOP mode) data.

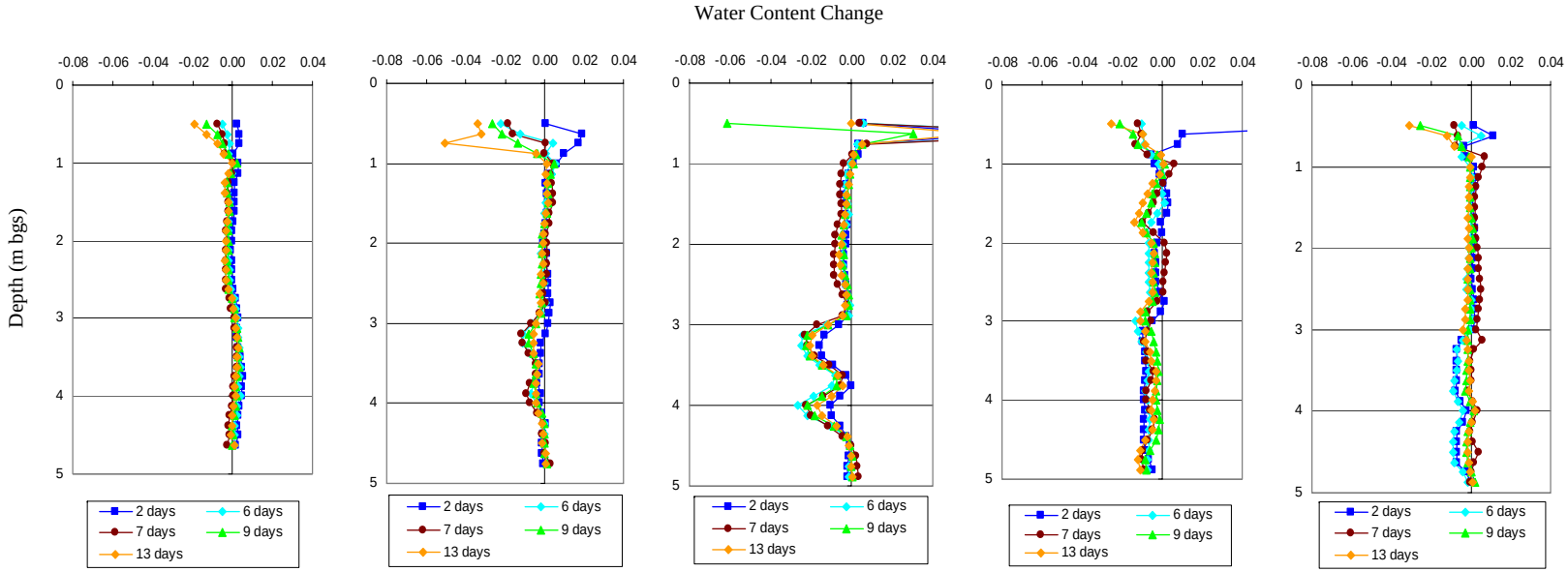

Figure F.44 – Active injection experiment water content change profiles between GP-7 and GP-12 showing induced CO_2-gas inferred from cross-borehole GPR (ZOP mode) data.

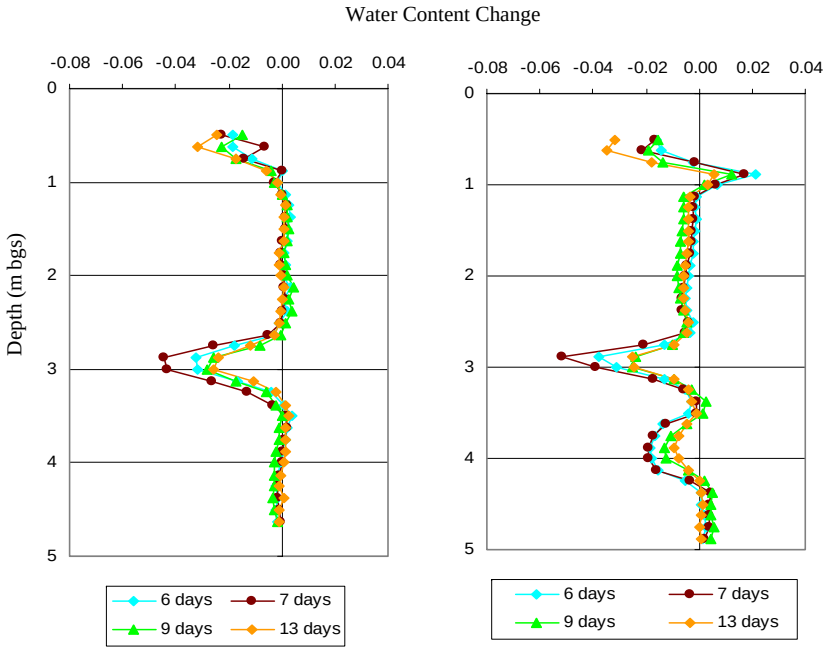

Figure F.45 – Active injection experiment water content change profiles between GP-13 and GP-15 showing induced CO_2-gas inferred from cross-borehole GPR (ZOP mode) data.

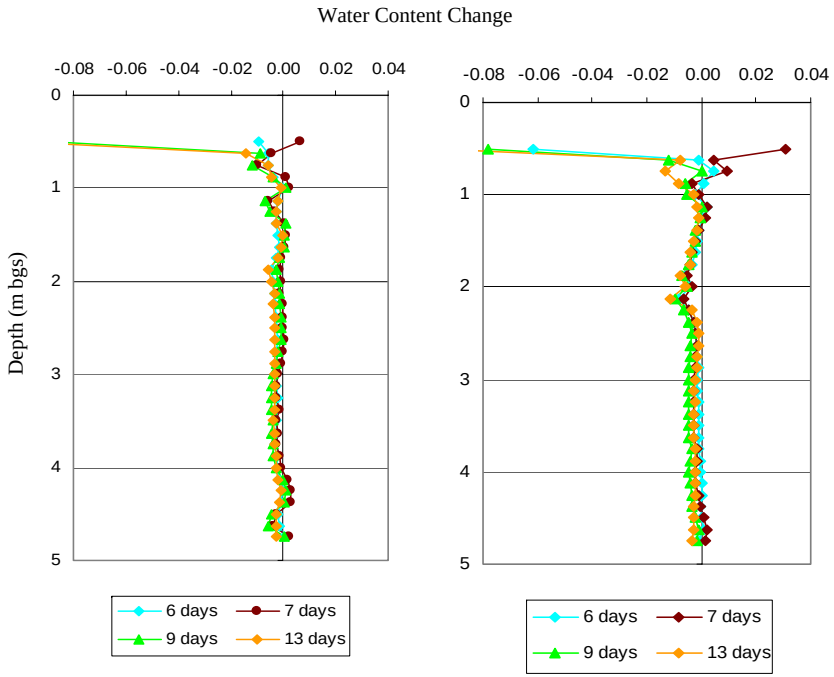

Figure F.46 – Active injection experiment water content change profiles between GP-4 and GP-6 showing induced CO_2-gas inferred from cross-borehole GPR (ZOP mode) data.

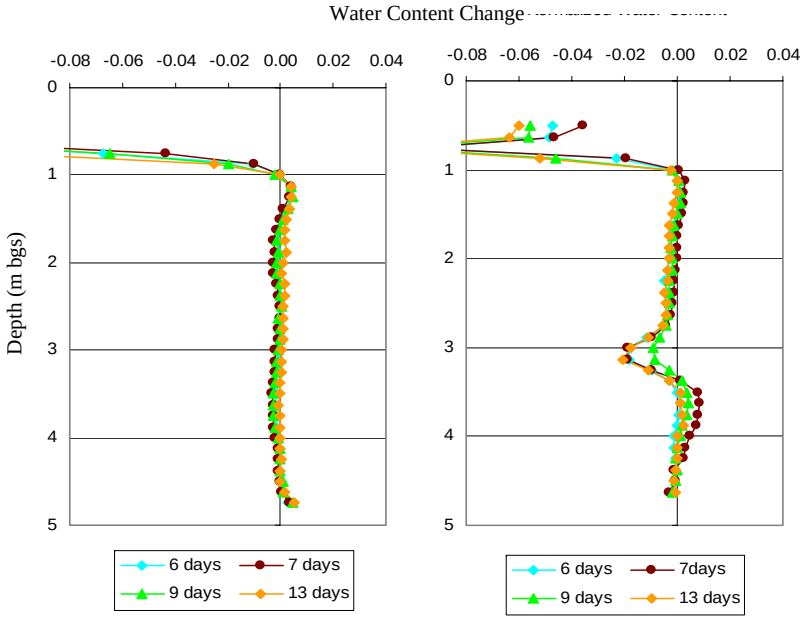

Figure F.47 – Active injection experiment water content change profiles between GP-4 and GP-13 showing induced CO_2-gas inferred from cross-borehole GPR (ZOP mode) data.

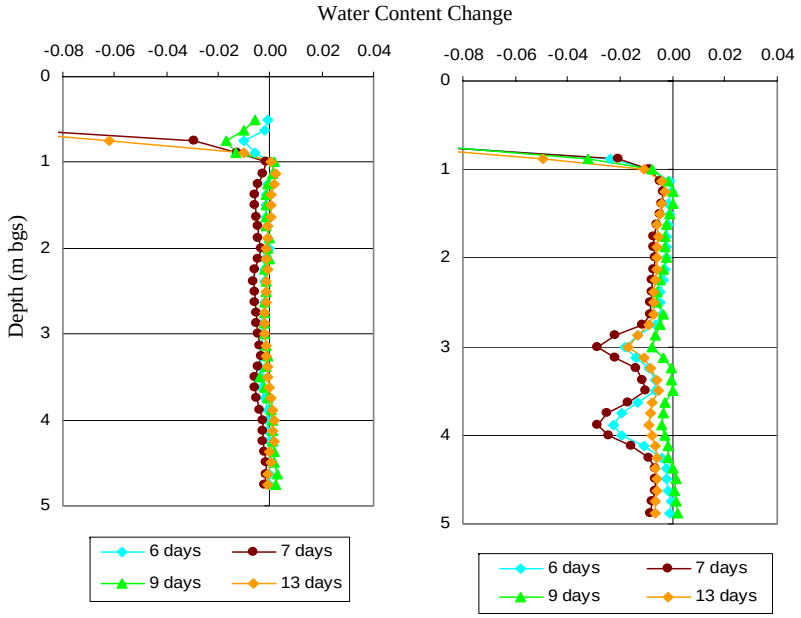

Figure F.48 – Active injection experiment water content change profiles between GP-6 and GP-15 showing induced CO_2-gas inferred from cross-borehole GPR (ZOP mode) data.

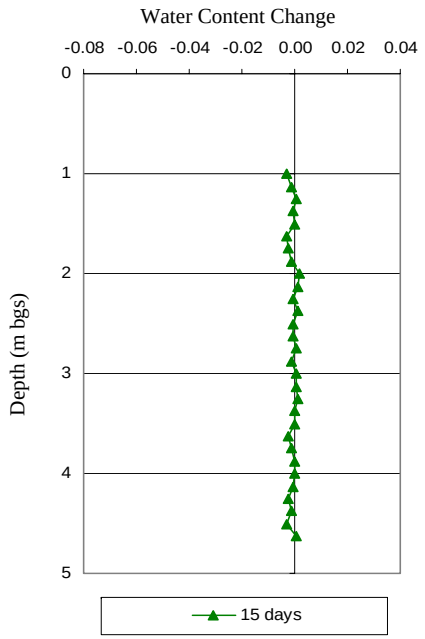

Figure F.49 – Active injection experiment water content change profiles between GP-1 and GP-7 showing induced CO_2-gas inferred from cross-borehole GPR (ZOP mode) data.

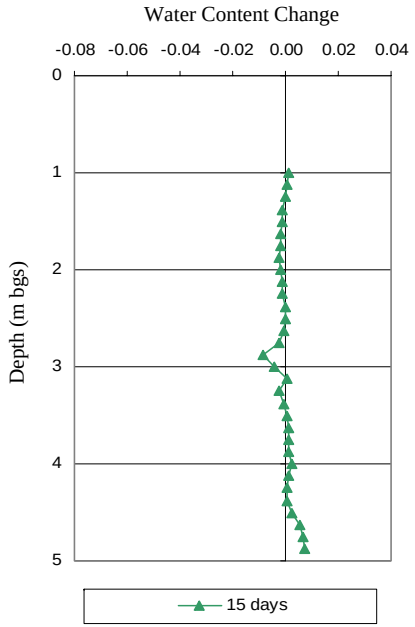

Figure F.50 – Active injection experiment water content change profiles between GP-12 and GP-18 showing induced CO_2-gas inferred from cross-borehole GPR (ZOP mode) data.

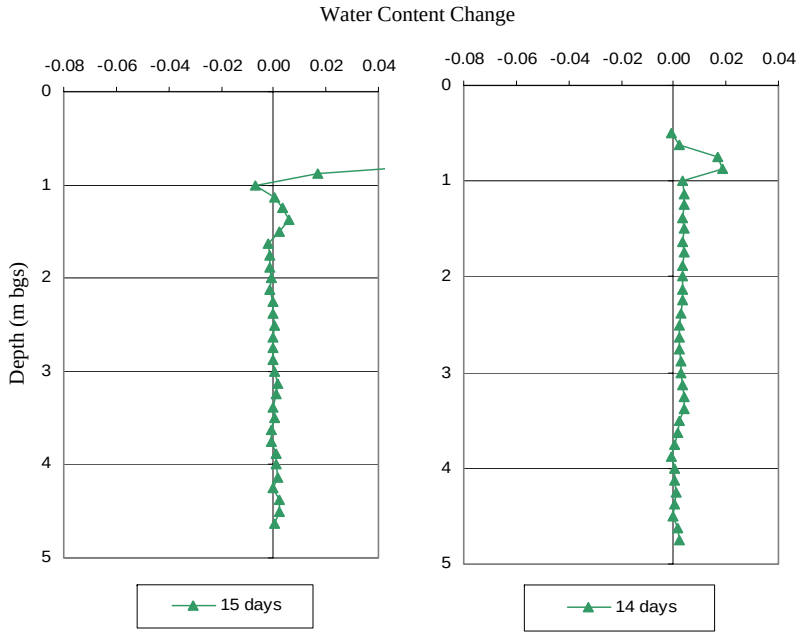

Figure F.51 – Active injection experiment water content change profiles between GP-1 and GP-9 showing induced CO_2-gas inferred from cross-borehole GPR (ZOP mode) data.

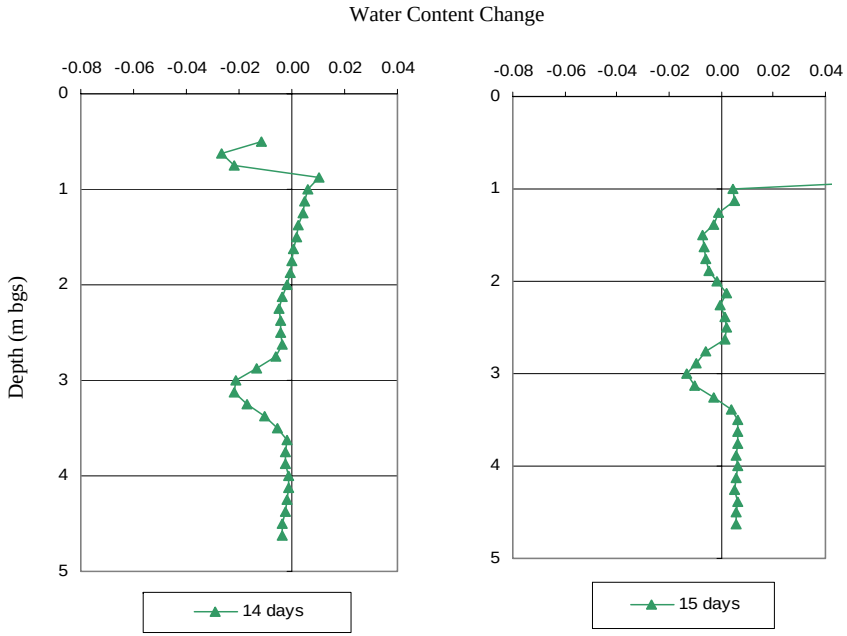

Figure F.52 – Active injection experiment water content change profiles between GP-9 and GP-16 showing induced CO_2-gas inferred from cross-borehole GPR (ZOP mode) data.

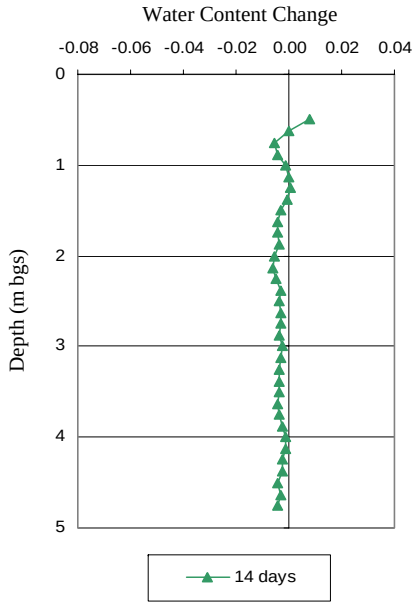

Figure F.53 – Active injection experiment water content change profiles between GP-6 and GP-10 showing induced CO_2-gas inferred from cross-borehole GPR (ZOP mode) data.

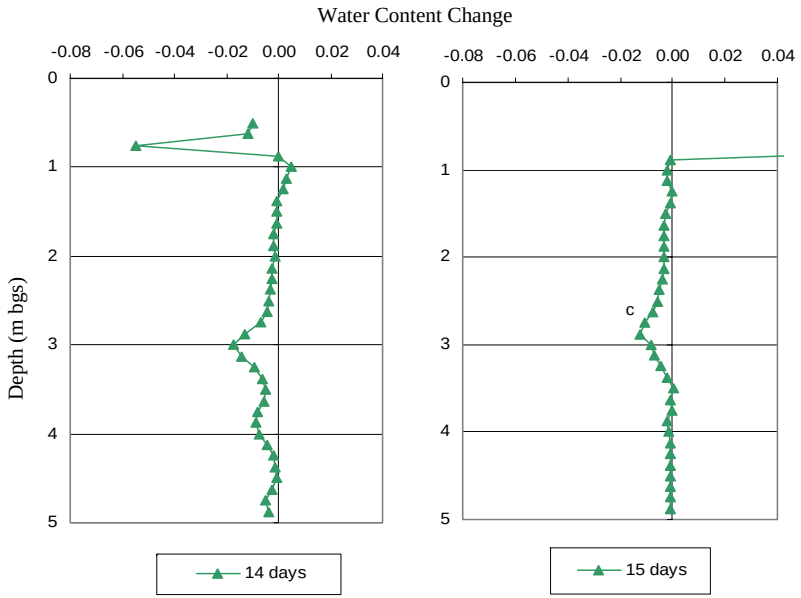

Figure F.54 – Active injection experiment water content change profiles between GP-10 and GP-18 showing induced CO_2-gas inferred from cross-borehole GPR (ZOP mode) data.

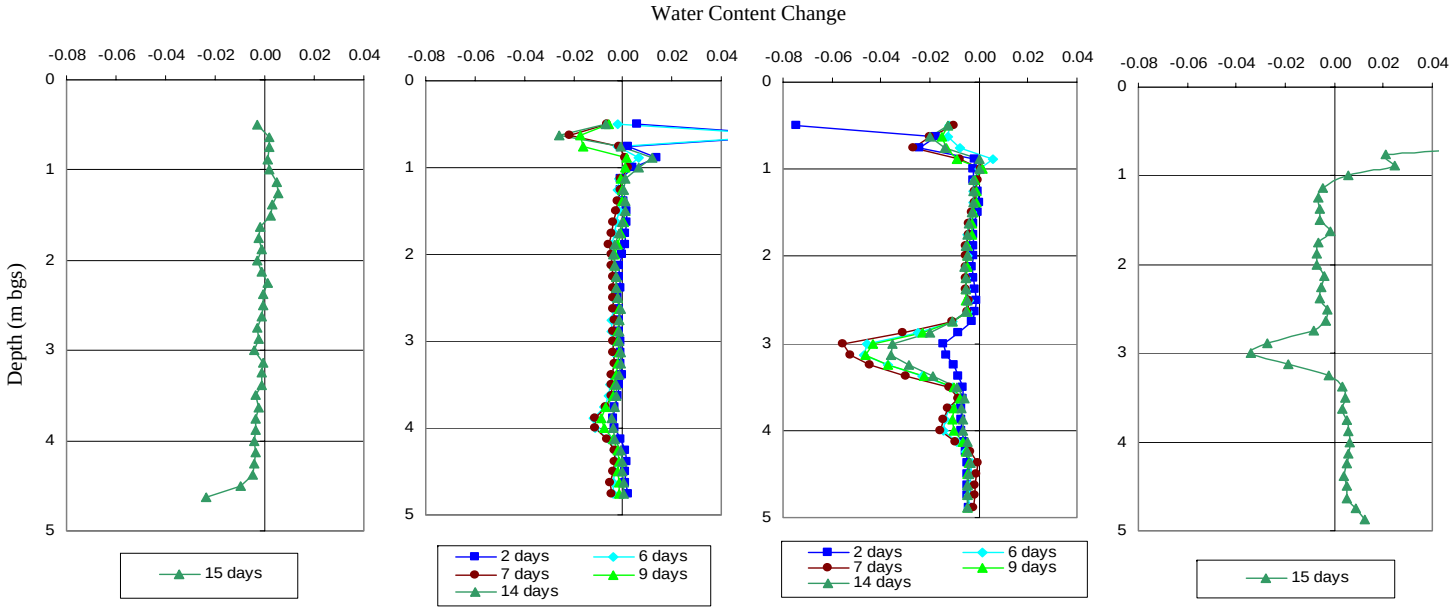

Figure F.55 – Active injection experiment water content change profiles between GP-2 and GP-9 showing induced CO_2-gas inferred from cross-borehole GPR (ZOP mode) data.

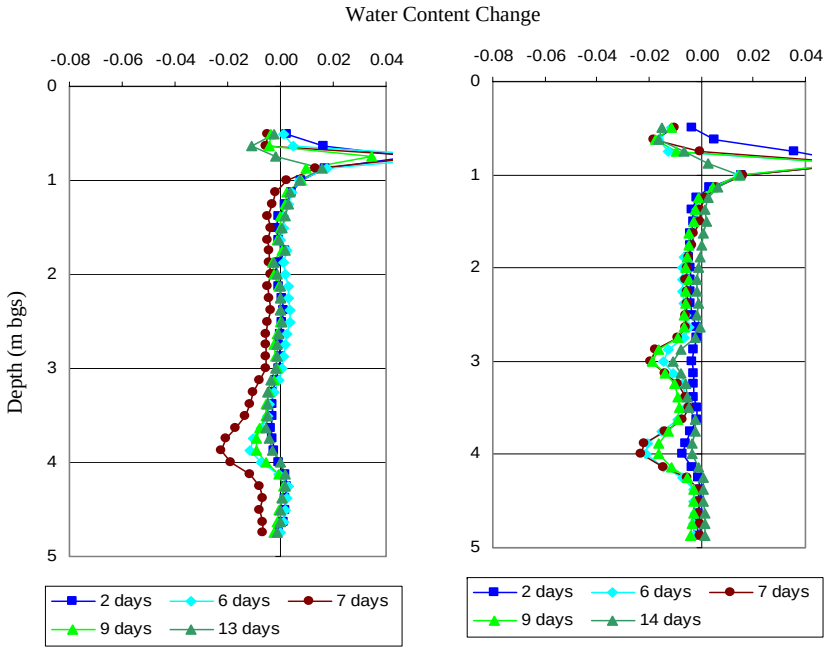

Figure F.56 – Active injection experiment water content change profiles between GP-5 and GP-14 showing induced CO_2-gas inferred from cross-borehole GPR (ZOP mode) data.

Appendix G
Cross-borehole GPR – MOG Data

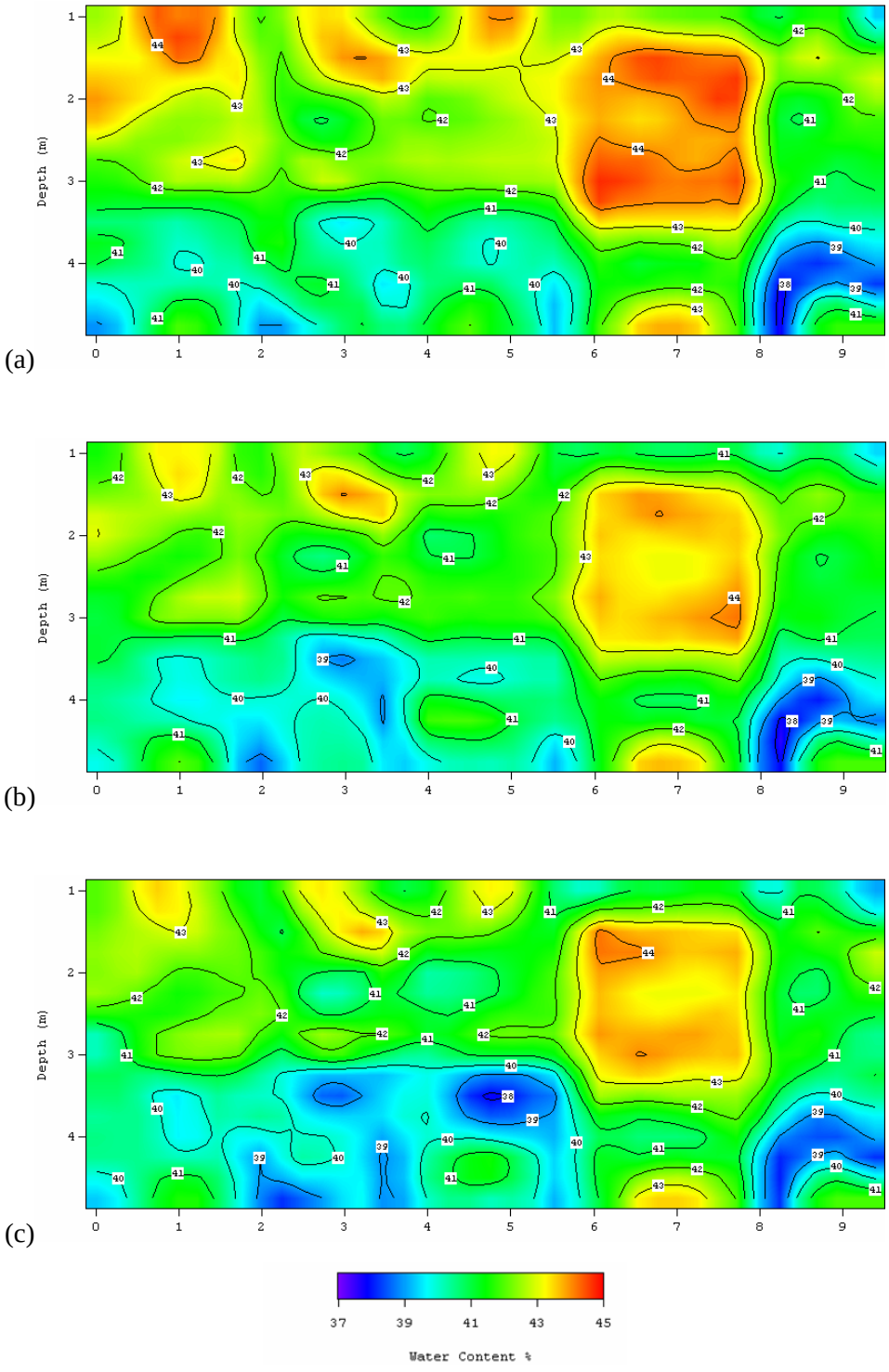

Figure G.1 – Water content obtained between GP-12 and GP-7 from cross-borehole GPR (MOG) data for (a) May 5, 2005 (background), (b) June 15, 2005 (between experiments), and (c) July 4, 2005 (13 days after initiation of hydraulic control experiment).

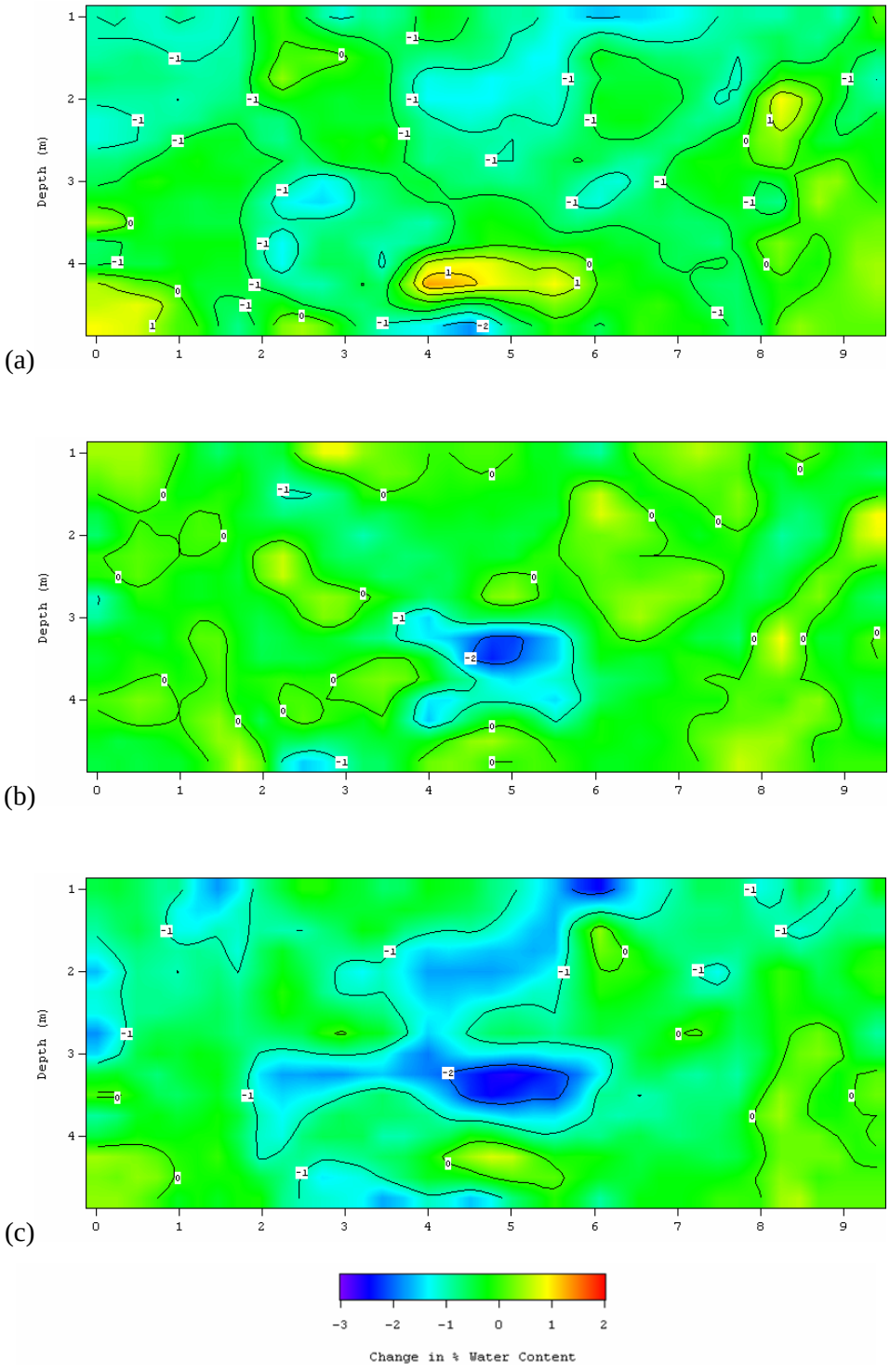

Figure G.2 – Water content changes obtained between GP-12 and GP-7 from cross-borehole GPR (MOG) data for (a) May 5, 2005 and June 15, 2005, (b) June 15, 2005 and July 4, 2005, and (c) May 5, 2005 and July 4, 2005.

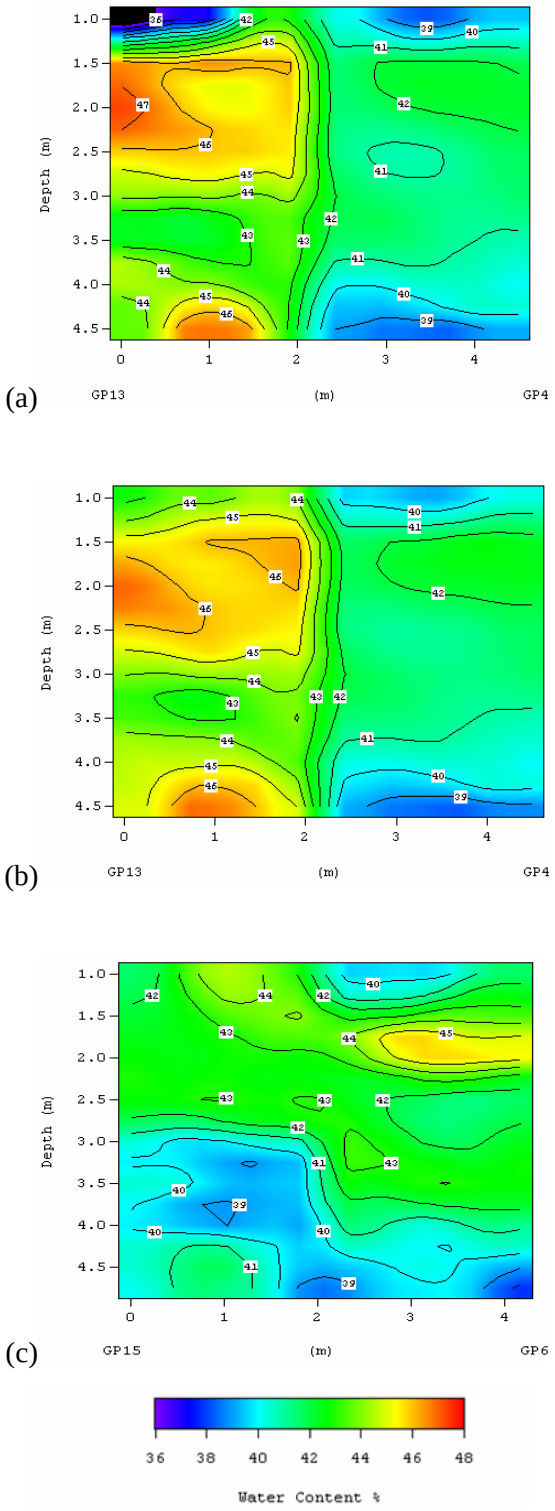

Figure G.3 – Water content obtained between GP-15 and GP-6 from cross-borehole GPR (MOG) data for (a) October 6, 2004 (background), (b) June 17, 2005 (between experiments), and (c) July 5, 2005 (14 days after initiation of hydraulic control experiment).

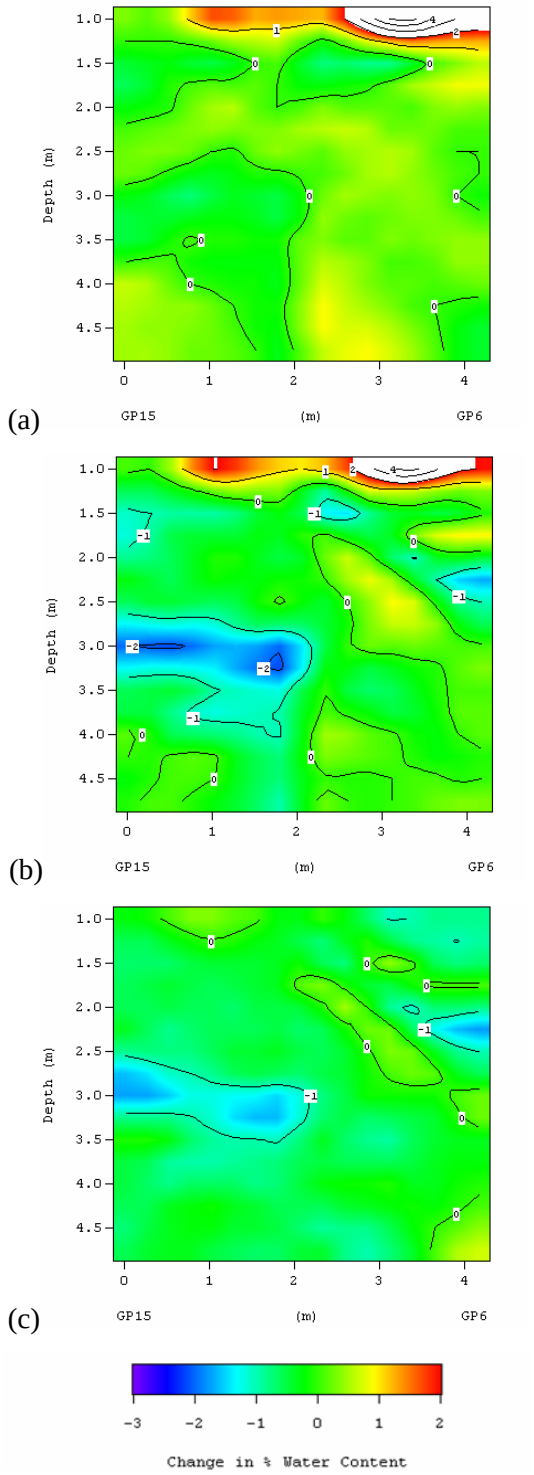

Figure G.4 – Water content changes obtained between GP-12 and GP-7 from cross-borehole GPR (MOG) data for (a) October 6, 2004 and June 17, 2005, (b) October 6, 2004 and July 4, 2005, and (c) June 17, 2005 and July 5, 2005.

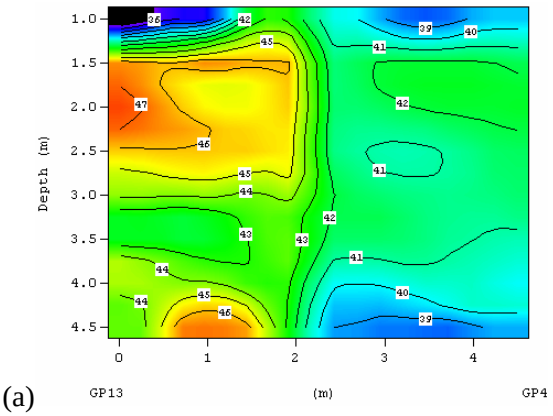

(a)

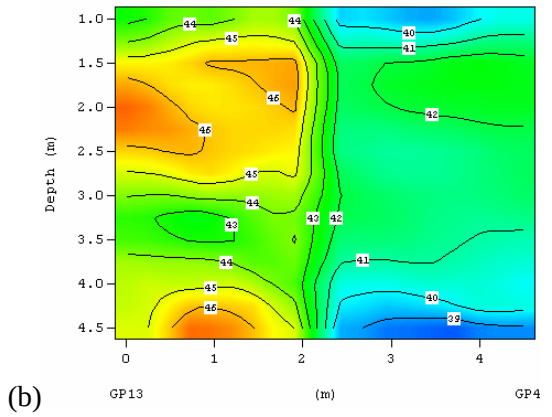

(b)

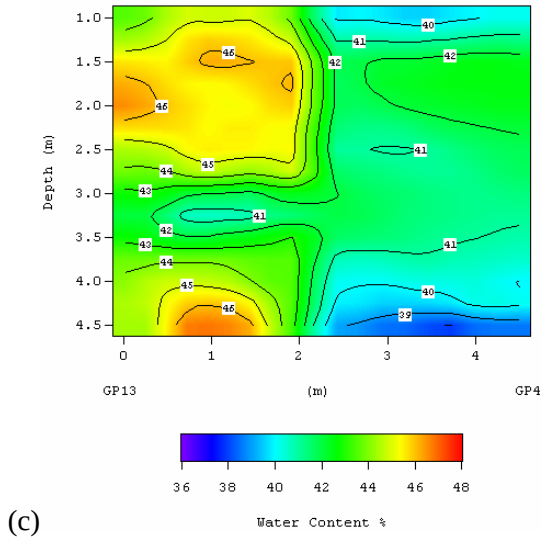

(c)

Figure G.5 – Water content obtained between GP-13 and GP-4 from cross-borehole GPR (MOG) data for (a) October 6, 2004 (background), (b) June 17, 2005 (between experiments), and (c) July 5, 2005 (14 days after initiation of hydraulic control experiment).

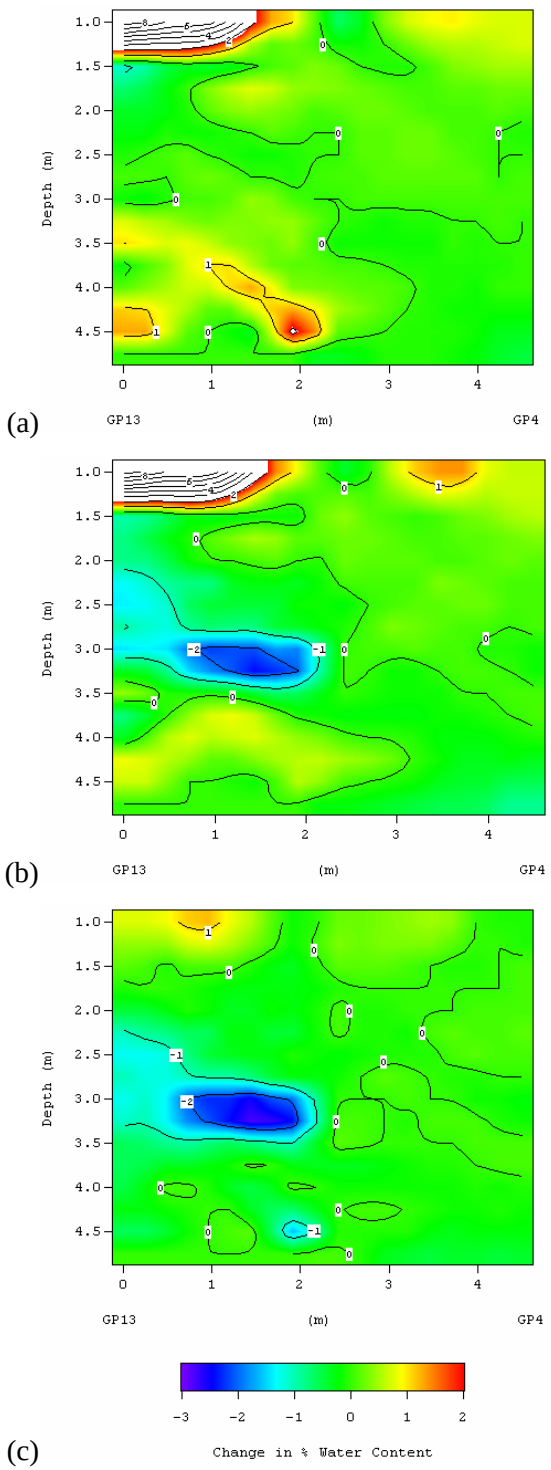

(a)

(b)

(c)

Figure G.6 – Water content changes obtained between GP-13 and GP-4 from cross-borehole GPR (MOG) data for (a) October 6, 2004 and June 17, 2005, (b) October 6, 2004 and July 4, 2005, and (c) June 17, 2005 and July 5, 2005.

Appendix H
Neutron Data

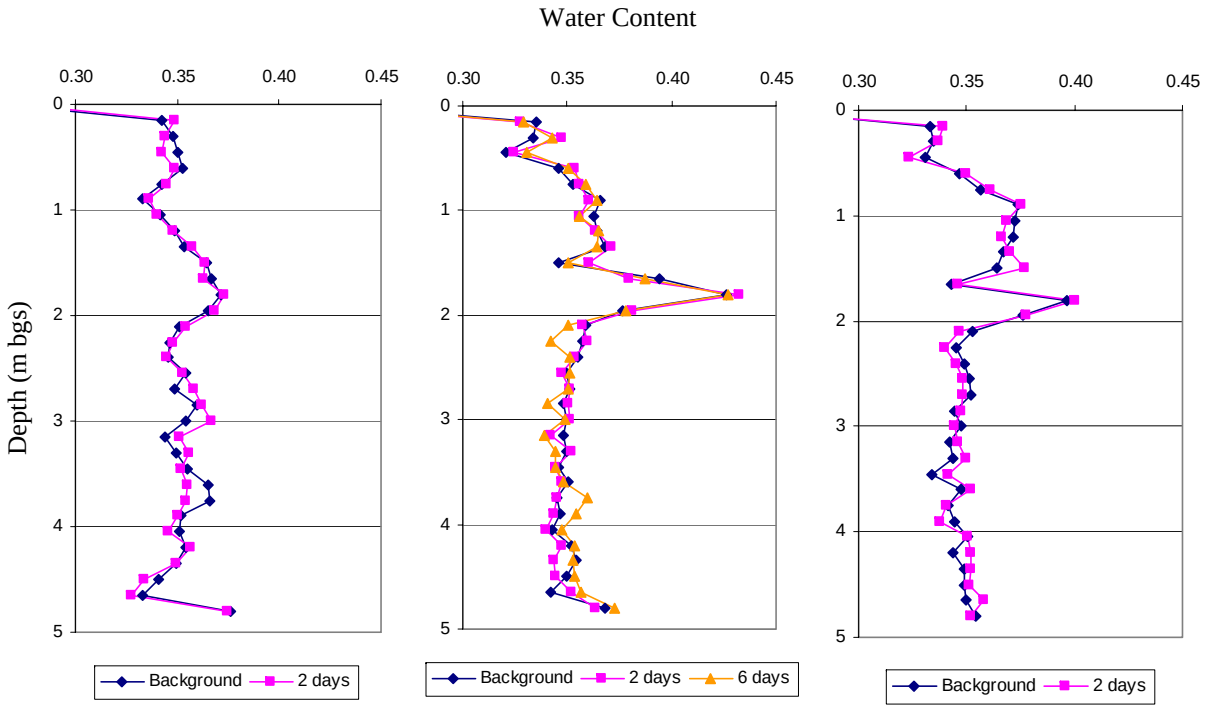

Figure H.1 – Passive injection experiment water content profiles between GP-4 and GP-6 showing induced CO_2-gas inferred from CPN neutron data.

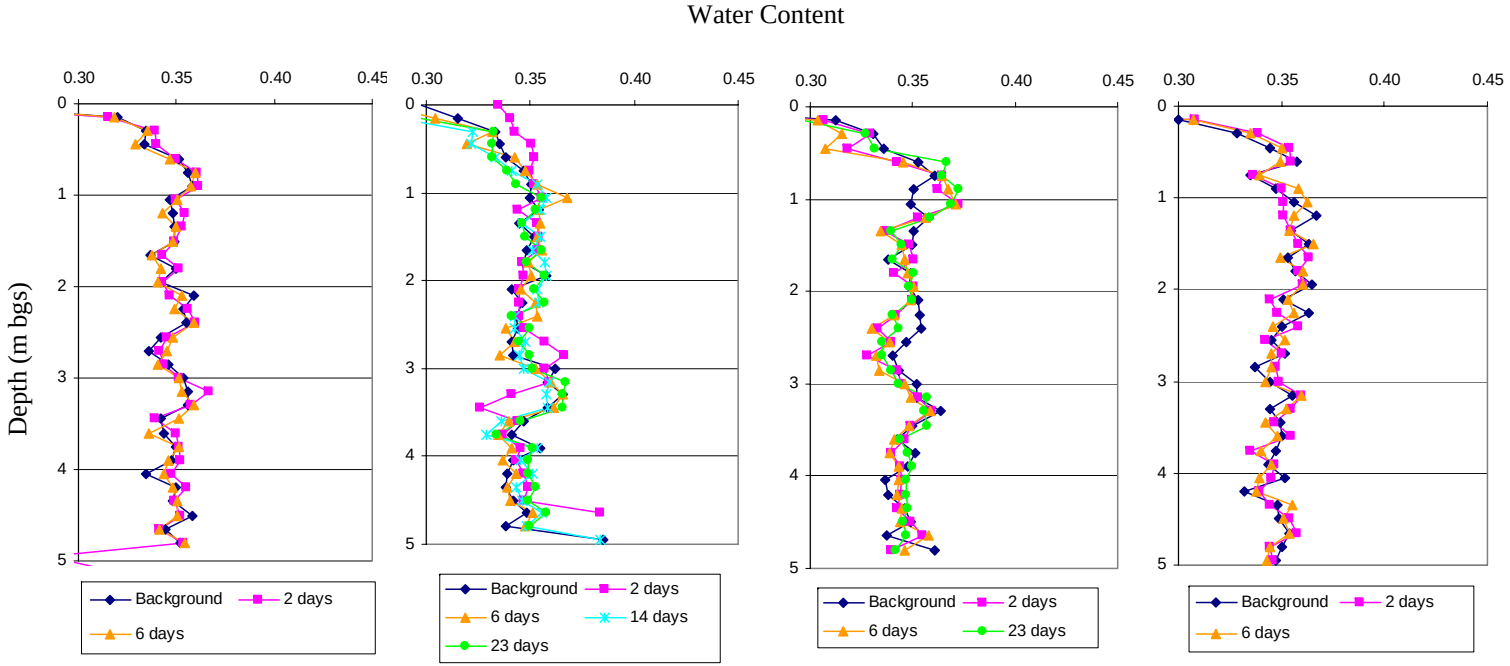

Figure H.2 – Passive injection experiment water content profiles between GP-8 and GP-11 showing induced CO_2-gas inferred from CPN neutron data.

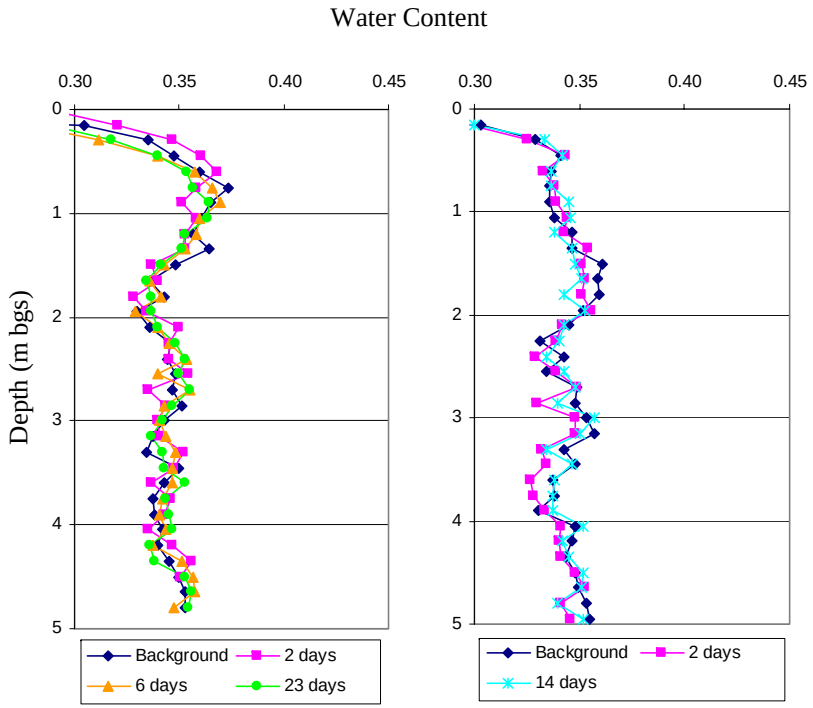

Figure H.3 – Passive injection experiment water content profiles between GP-14 and GP-15 showing induced CO_2-gas inferred from CPN neutron data.

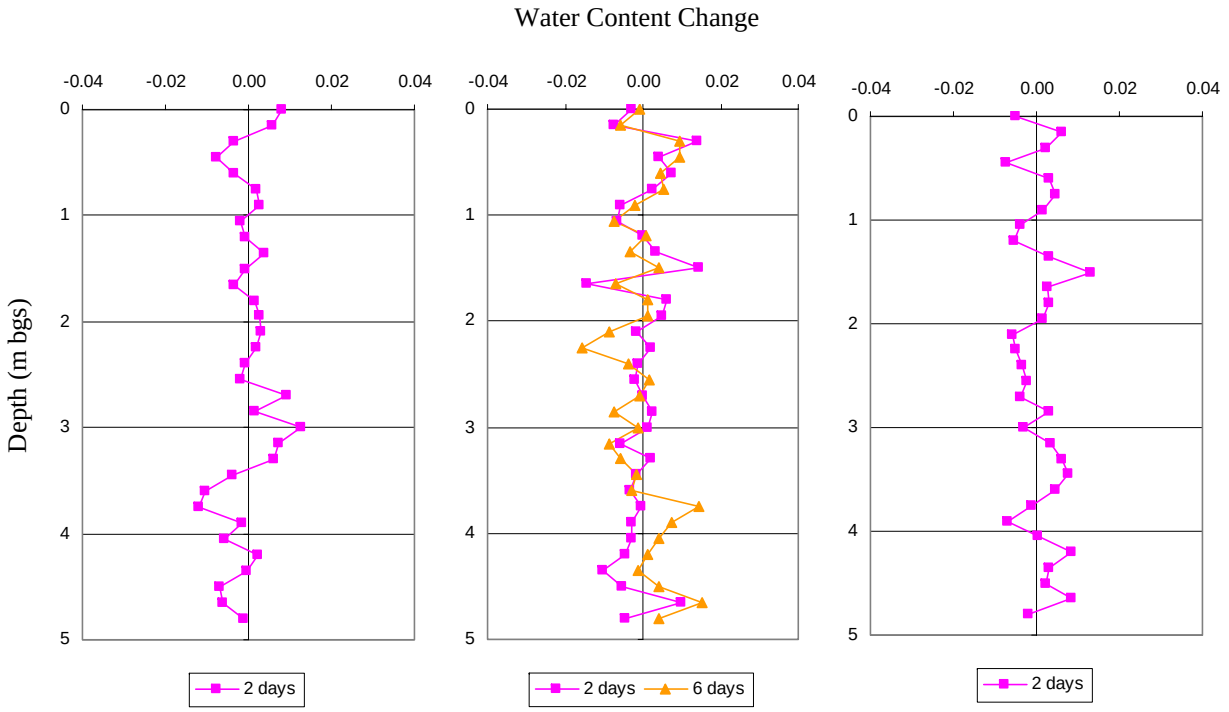

Figure H.4 – Passive injection experiment water content change profiles between GP-4 and GP-6 showing induced CO_2-gas inferred from CPN neutron data.

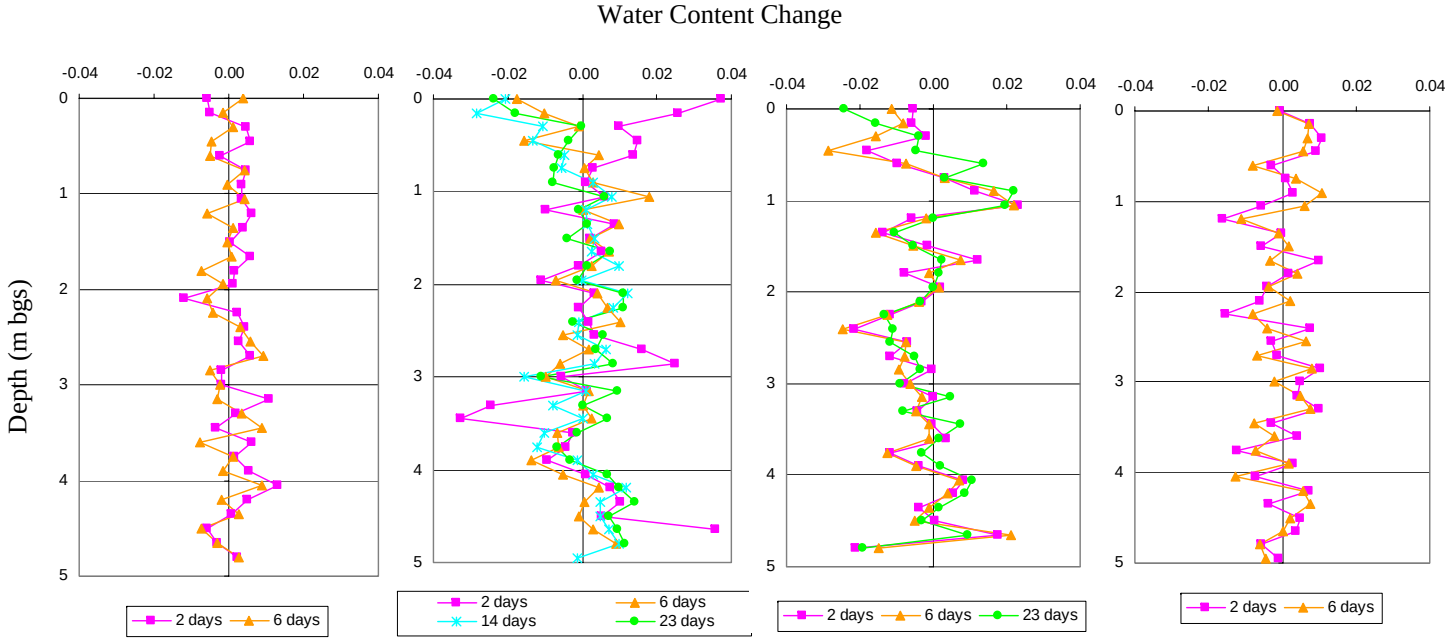

Figure H.5 – Passive injection experiment water content change profiles between GP-8 and GP-11 showing induced CO_2-gas inferred from CPN neutron data.

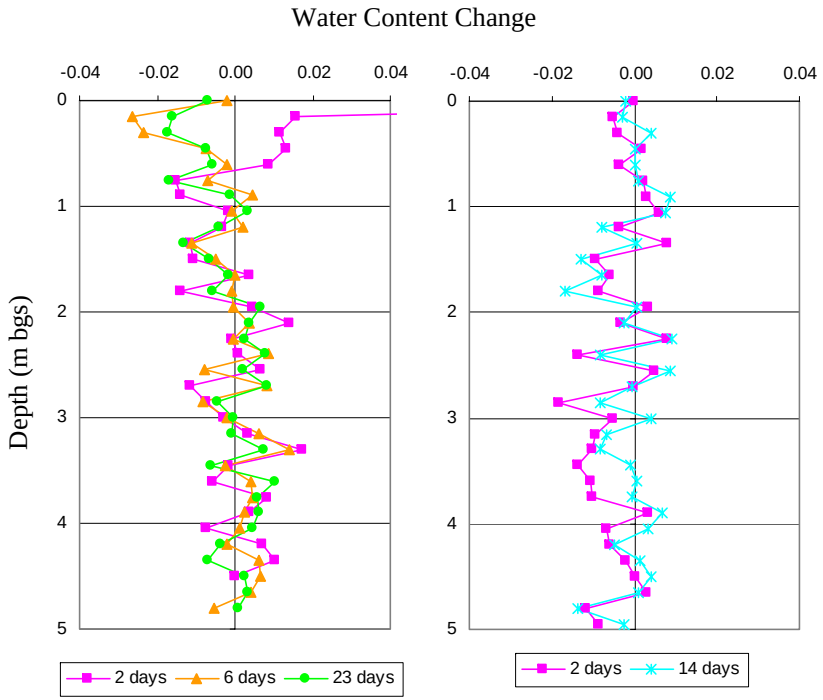

Figure H.6 – Passive injection experiment water content change profiles between GP-14 and GP-15 showing induced CO_2-gas inferred from CPN neutron data.

Appendix I

Hydraulic Conductivity Data

Table I.1
Summary of Hydraulic Conductivities
from Falling-Head Permeameter Tests

Boring ID	Top Depth of Sample Interval (mm bgs)	Bottom Depth of Sample Interval (mm bgs)	Geometric Mean K (cm/s)	Minimum K (cm/s)	Maximum K (cm/s)
B-1	1524.00	1581.74	1.65E-02	1.53E-02	1.78E-02
B-1	1870.42	1928.16	7.59E-03	4.76E-03	1.09E-02
B-1	2101.37	2159.10	8.77E-03	2.89E-03	2.02E-02
B-1	2390.05	2447.79	1.17E-02	4.17E-03	2.22E-02
B-1	2678.73	2736.47	7.55E-03	4.64E-03	9.99E-03
B-1	2967.42	3025.15	1.09E-02	4.91E-03	2.00E-02
B-1	3048.00	3098.00	1.00E-02	4.94E-03	1.71E-02
B-1	3298.00	3348.00	9.42E-03	4.98E-03	1.61E-02
B-1	3348.00	3398.00	1.27E-02	4.86E-03	3.01E-02
B-1	3548.00	3598.00	1.87E-02	1.66E-02	1.96E-02
B-1	3798.00	3848.00	7.17E-03	4.59E-03	9.03E-03
B-1	4048.00	4098.00	5.74E-03	4.46E-03	6.50E-03
B-1	4298.00	4348.00	8.56E-03	4.61E-03	1.68E-02
B-2	1524.00	1582.62	7.43E-03	4.42E-03	1.12E-02
B-2	1817.08	1875.70	7.16E-03	4.34E-03	1.07E-02
B-2	2110.17	2168.78	6.28E-03	4.86E-03	8.06E-03
B-2	2403.25	2461.87	1.09E-02	4.63E-03	1.70E-02
B-2	2696.33	2754.95	8.68E-03	4.65E-03	1.38E-02
B-2	2989.42	3048.03	1.24E-02	4.54E-03	2.11E-02
B-2	3048.00	3098.00	7.72E-03	1.64E-03	1.63E-02
B-2	3298.00	3348.00	9.83E-03	4.12E-03	2.23E-02
B-2	3548.00	3598.00	6.89E-03	3.58E-03	1.32E-02
B-2	3798.00	3848.00	5.46E-03	4.68E-03	6.13E-03
B-2	4048.00	4098.00	7.71E-03	4.78E-03	1.03E-02
B-6	1524.00	1579.62	8.18E-03	4.90E-03	1.48E-02
B-6	1802.09	1857.70	7.37E-03	4.87E-03	1.14E-02
B-6	2080.17	1579.62	6.71E-03	4.10E-03	1.00E-02
B-6	2358.26	2413.88	6.04E-03	5.02E-03	7.74E-03
B-6	2636.35	2691.96	9.54E-03	4.78E-03	1.42E-02
B-6	2914.43	2970.05	5.80E-03	3.66E-03	7.33E-03
B-6	3048.00	3102.23	4.66E-03	4.19E-03	5.29E-03
B-6	3319.15	3373.38	7.35E-03	4.83E-03	9.46E-03
B-6	3590.30	3644.53	6.07E-03	4.42E-03	7.74E-03
B-6	3861.45	3915.68	6.14E-03	4.67E-03	7.14E-03
B-6	4132.60	4186.83	6.70E-03	4.59E-03	8.51E-03
B-6	4403.75	4457.98	7.61E-03	4.39E-03	1.02E-02
B-4	1524.00	1574.00	5.41E-03	3.37E-03	8.05E-03
B-4	2024.00	2083.00	5.33E-03	3.45E-03	6.80E-03
B-4	2524.00	2574.00	6.17E-03	3.87E-03	7.88E-03
B-4	3048.00	3115.20	6.47E-03	4.75E-03	7.68E-03
B-4	3693.99	3758.59	7.17E-03	4.70E-03	8.87E-03
B-4	4339.99	4404.59	6.57E-03	4.08E-03	9.37E-03

Table I.1
Summary of Hydraulic Conductivities
from Falling-Head Permeameter Tests

Boring ID	Top Depth of Sample Interval (mm bgs)	Bottom Depth of Sample Interval (mm bgs)	Geometric Mean K (cm/s)	Minimum K (cm/s)	Maximum K (cm/s)
B-5	1524.00	1574.00	1.06E-02	4.65E-03	1.62E-02
B-5	1985.07	2024.00	6.60E-03	4.72E-03	8.01E-03
B-5	2087.52	2124.00	4.99E-03	3.88E-03	6.65E-03
B-5	2343.67	2374.00	6.47E-03	4.33E-03	8.27E-03
B-5	2425.64	2454.00	5.03E-03	4.66E-03	5.28E-03
B-5	2804.74	2824.00	4.04E-03	3.64E-03	4.79E-03
B-3	1524.00	1578.64	6.05E-03	2.57E-03	9.34E-03
B-3	2070.45	2616.90	8.20E-03	4.60E-03	1.12E-02
B-3	2616.90	2671.54	6.57E-03	4.49E-03	8.46E-03
B-3	2890.12	2944.77	9.77E-03	4.49E-03	1.46E-02
B-3	3048.00	3098.00	6.27E-03	4.66E-03	7.47E-03
B-3	3298.00	3348.00	8.94E-03	4.81E-03	1.26E-02
B-3	3548.00	3598.00	6.56E-03	4.58E-03	7.92E-03
B-3	4048.00	4098.00	5.16E-03	4.20E-03	5.83E-03

Notes:
K = Hydraulic Conductivity

Table I.2
Grain Size Analysis Data

Boring	Run	Run (mm)	Depth (mm bgs)	Depth - bottom (mm bgs)	Sieve	Sieve Size (mm)	Actual Weight (g)	Percent Retained	Percent Passing
B-2	5	1524	2126.41	2186.65	18	1	0	0.00%	100.00%
B-2	5	1524	2126.41	2186.65	35	0.5	0.03	0.06%	99.94%
B-2	5	1524	2126.41	2186.65	60	0.25	0.89	1.85%	98.09%
B-2	5	1524	2126.41	2186.65	80	0.18	6.78	14.10%	83.98%
B-2	5	1524	2126.41	2186.65	100	0.15	8.42	17.52%	66.47%
B-2	5	1524	2126.41	2186.65	120	0.125	11.24	23.38%	43.08%
B-2	5	1524	2126.41	2186.65	140	0.106	8.54	17.77%	25.32%
B-2	5	1524	2126.41	2186.65	170	0.09	6.08	12.65%	12.67%
B-2	5	1524	2126.41	2186.65	200	0.075	2.1	4.37%	8.30%
B-2	5	1524	2126.41	2186.65	230	0.063	2.56	5.33%	2.97%
B-2	5	1524	2126.41	2186.65	450	0.032	1.29	2.68%	0.29%
B-2	5	1524	2126.41	2186.65	Tray		0.14	0.29%	0.00%
B-2	5	1524	2754.95	2813.57	18	1	0.01	0.01%	99.99%
B-2	5	1524	2754.95	2813.57	35	0.5	0.15	0.16%	99.83%
B-2	5	1524	2754.95	2813.57	60	0.25	4.59	4.88%	94.95%
B-2	5	1524	2754.95	2813.57	80	0.18	19.02	20.24%	74.71%
B-2	5	1524	2754.95	2813.57	100	0.15	15.74	16.75%	57.96%
B-2	5	1524	2754.95	2813.57	120	0.125	18.41	19.59%	38.37%
B-2	5	1524	2754.95	2813.57	140	0.106	12.85	13.67%	24.70%
B-2	5	1524	2754.95	2813.57	170	0.09	10.83	11.52%	13.17%
B-2	5	1524	2754.95	2813.57	230	0.063	8.73	9.29%	3.88%
B-2	5	1524	2754.95	2813.57	450	0.032	3.24	3.45%	0.44%
					Tray		0.41	0.44%	0.00%

Table I.2
Grain Size Analysis Data

Boring	Run	Run (mm)	Depth (mm bgs)	Depth - bottom (mm bgs)	Sieve	Sieve Size (mm)	Actual Weight (g)	Percent Retained	Percent Passing
B-2	5	1524	2813.57	2872.18	18	1	0.03	0.03%	99.97%
B-2	5	1524	2813.57	2872.18	35	0.5	0.21	0.20%	99.77%
B-2	5	1524	2813.57	2872.18	60	0.25	7.73	7.28%	92.50%
B-2	5	1524	2813.57	2872.18	80	0.18	26.37	24.83%	67.66%
B-2	5	1524	2813.57	2872.18	100	0.15	18.74	17.65%	50.02%
B-2	5	1524	2813.57	2872.18	120	0.125	23.29	21.93%	28.09%
B-2	5	1524	2813.57	2872.18	140	0.106	12.37	11.65%	16.44%
B-2	5	1524	2813.57	2872.18	170	0.09	8.36	7.87%	8.57%
B-2	5	1524	2813.57	2872.18	230	0.063	6.22	5.86%	2.71%
B-2	5	1524	2813.57	2872.18	450	0.032	2.53	2.38%	0.33%
					Tray		0.35	0.33%	0.00%
B-2	5	1524	2872.18	2930.80	18	1	0	0.00%	100.00%
B-2	5	1524	2872.18	2930.80	35	0.5	0.09	0.09%	99.91%
B-2	5	1524	2872.18	2930.80	60	0.25	6.3	6.49%	93.42%
B-2	5	1524	2872.18	2930.80	80	0.18	24.12	24.84%	68.58%
B-2	5	1524	2872.18	2930.80	100	0.15	18.9	19.46%	49.11%
B-2	5	1524	2872.18	2930.80	120	0.125	22.23	22.89%	26.22%
B-2	5	1524	2872.18	2930.80	140	0.106	11.12	11.45%	14.77%
B-2	5	1524	2872.18	2930.80	170	0.09	8.18	8.42%	6.34%
B-2	5	1524	2872.18	2930.80	230	0.063	4.18	4.30%	2.04%
B-2	5	1524	2872.18	2930.80	450	0.032	1.75	1.80%	0.24%
					Tray		0.23	0.24%	0.00%

Table I.2
Grain Size Analysis Data

Boring	Run	Run (mm)	Depth (mm bgs)	Depth - bottom (mm bgs)	Sieve	Sieve Size (mm)	Actual Weight (g)	Percent Retained	Percent Passing
B-2	5	1524	2930.80	2989.42	18	1	0.54	0.49%	99.51%
B-2	5	1524	2930.80	2989.42	35	0.5	1.89	1.73%	97.77%
B-2	5	1524	2930.80	2989.42	60	0.25	13.29	12.18%	85.59%
B-2	5	1524	2930.80	2989.42	80	0.18	25.08	22.99%	62.60%
B-2	5	1524	2930.80	2989.42	100	0.15	17.91	16.42%	46.19%
B-2	5	1524	2930.80	2989.42	120	0.125	19.19	17.59%	28.60%
B-2	5	1524	2930.80	2989.42	140	0.106	14.2	13.02%	15.58%
B-2	5	1524	2930.80	2989.42	170	0.09	8.76	8.03%	7.55%
B-2	5	1524	2930.80	2989.42	200	0.075	2.66	2.44%	5.11%
B-2	5	1524	2930.80	2989.42	230	0.063	-0.43	-0.39%	5.51%
B-2	5	1524	2930.80	2989.42	450	0.032	2.04	1.87%	3.64%
					Tray		3.97	3.64%	0.00%
B-2	5	1524	2989.42	3048.03	18	1	0.35	0.38%	99.62%
B-2	5	1524	2989.42	3048.03	35	0.5	1.91	2.08%	97.54%
B-2	5	1524	2989.42	3048.03	60	0.25	23.6	25.65%	71.89%
B-2	5	1524	2989.42	3048.03	80	0.18	32.03	34.81%	37.08%
B-2	5	1524	2989.42	3048.03	100	0.15	13.07	14.20%	22.88%
B-2	5	1524	2989.42	3048.03	120	0.125	9.54	10.37%	12.51%
B-2	5	1524	2989.42	3048.03	140	0.106	5.33	5.79%	6.72%
B-2	5	1524	2989.42	3048.03	170	0.09	3.11	3.38%	3.34%
B-2	5	1524	2989.42	3048.03	200	0.075	0.82	0.89%	2.45%
B-2	5	1524	2989.42	3048.03	230	0.063	1.22	1.33%	1.12%
B-2	5	1524	2989.42	3048.03	450	0.032	0.86	0.93%	0.18%
B-2	5	1524	2989.42	3048.03	Tray		0.17	0.18%	0.00%

Table I.2
Grain Size Analysis Data

Boring	Run	Run (mm)	Depth (mm bgs)	Depth - bottom (mm bgs)	Sieve	Sieve Size (mm)	Actual Weight (g)	Percent Retained	Percent Passing
B-2	10	3048	3048.00	3098.00	18	1	0.37	0.96%	99.04%
B-2	10	3048	3048.00	3098.00	35	0.5	2.11	5.47%	93.57%
B-2	10	3048	3048.00	3098.00	60	0.25	11.4	29.56%	64.01%
B-2	10	3048	3048.00	3098.00	80	0.18	11.23	29.12%	34.90%
B-2	10	3048	3048.00	3098.00	100	0.15	4.97	12.89%	22.01%
B-2	10	3048	3048.00	3098.00	120	0.125	3.57	9.26%	12.76%
B-2	10	3048	3048.00	3098.00	140	0.106	1.92	4.98%	7.78%
B-2	10	3048	3048.00	3098.00	170	0.09	1.1	2.85%	4.93%
B-2	10	3048	3048.00	3098.00	200	0.075	0.42	1.09%	3.84%
B-2	10	3048	3048.00	3098.00	230	0.063	0.57	1.48%	2.36%
B-2	10	3048	3048.00	3098.00	450	0.032	0.57	1.48%	0.88%
					Tray		0.34	0.88%	0.00%
B-2	10	3048	3098.00	3148.00	18	1	0.39	0.42%	99.58%
B-2	10	3048	3098.00	3148.00	35	0.5	2.96	3.20%	96.38%
B-2	10	3048	3098.00	3148.00	60	0.25	26.47	28.63%	67.74%
B-2	10	3048	3098.00	3148.00	80	0.18	29.39	31.79%	35.95%
B-2	10	3048	3098.00	3148.00	100	0.15	12.47	13.49%	22.46%
B-2	10	3048	3098.00	3148.00	120	0.125	9.11	9.86%	12.60%
B-2	10	3048	3098.00	3148.00	140	0.106	4.83	5.23%	7.38%
B-2	10	3048	3098.00	3148.00	170	0.09	2.74	2.96%	4.41%
B-2	10	3048	3098.00	3148.00	200	0.075	0.9	0.97%	3.44%
B-2	10	3048	3098.00	3148.00	230	0.063	1.44	1.56%	1.88%
B-2	10	3048	3098.00	3148.00	450	0.032	1.45	1.57%	0.31%
					Tray		0.29	0.31%	0.00%

Table I.2
Grain Size Analysis Data

Boring	Run	Run (mm)	Depth (mm bgs)	Depth - bottom (mm bgs)	Sieve	Sieve Size (mm)	Actual Weight (g)	Percent Retained	Percent Passing
B-2	10	3048	3148.00	3198.00	18	1	0.64	0.61%	99.39%
B-2	10	3048	3148.00	3198.00	35	0.5	5.25	5.02%	94.37%
B-2	10	3048	3148.00	3198.00	60	0.25	31.62	30.23%	64.14%
B-2	10	3048	3148.00	3198.00	80	0.18	32.17	30.76%	33.38%
B-2	10	3048	3148.00	3198.00	100	0.15	12.76	12.20%	21.19%
B-2	10	3048	3148.00	3198.00	120	0.125	9.73	9.30%	11.88%
B-2	10	3048	3148.00	3198.00	140	0.106	5	4.78%	7.10%
B-2	10	3048	3148.00	3198.00	170	0.09	2.86	2.73%	4.37%
B-2	10	3048	3148.00	3198.00	200	0.075	1.16	1.11%	3.26%
B-2	10	3048	3148.00	3198.00	230	0.063	1.55	1.48%	1.78%
B-2	10	3048	3148.00	3198.00	450	0.032	1.46	1.40%	0.38%
					Tray		0.4	0.38%	0.00%
B-2	10	3048	3298.00	3348.00	18	1	1.99	3.60%	96.40%
B-2	10	3048	3298.00	3348.00	35	0.5	4.11	7.44%	88.96%
B-2	10	3048	3298.00	3348.00	60	0.25	16.12	29.18%	59.78%
B-2	10	3048	3298.00	3348.00	80	0.18	14.51	26.26%	33.52%
B-2	10	3048	3298.00	3348.00	100	0.15	6.33	11.46%	22.06%
B-2	10	3048	3298.00	3348.00	120	0.125	5.31	9.61%	12.45%
B-2	10	3048	3298.00	3348.00	140	0.106	3.03	5.48%	6.97%
B-2	10	3048	3298.00	3348.00	170	0.09	1.94	3.51%	3.46%
B-2	10	3048	3298.00	3348.00	200	0.075	0.51	0.92%	2.53%
B-2	10	3048	3298.00	3348.00	230	0.063	0.72	1.30%	1.23%
B-2	10	3048	3298.00	3348.00	450	0.032	0.58	1.05%	0.18%
B-2	10	3048	3298.00	3348.00	Tray		0.1	0.18%	0.00%

Table I.2
Grain Size Analysis Data

Boring	Run	Run (mm)	Depth (mm bgs)	Depth - bottom (mm bgs)	Sieve	Sieve Size (mm)	Actual Weight (g)	Percent Retained	Percent Passing
B-2	10	3048	3548.00	3598.00	18	1	0.47	0.97%	99.03%
B-2	10	3048	3548.00	3598.00	35	0.5	0.86	1.77%	97.26%
B-2	10	3048	3548.00	3598.00	60	0.25	4.4	9.05%	88.21%
B-2	10	3048	3548.00	3598.00	80	0.18	8.58	17.65%	70.56%
B-2	10	3048	3548.00	3598.00	100	0.15	7.76	15.96%	54.60%
B-2	10	3048	3548.00	3598.00	120	0.125	8.77	18.04%	36.56%
B-2	10	3048	3548.00	3598.00	140	0.106	6.4	13.17%	23.39%
B-2	10	3048	3548.00	3598.00	170	0.09	4.68	9.63%	13.76%
B-2	10	3048	3548.00	3598.00	200	0.075	1.93	3.97%	9.79%
B-2	10	3048	3548.00	3598.00	230	0.063	2.73	5.62%	4.18%
B-2	10	3048	3548.00	3598.00	450	0.032	1.85	3.81%	0.37%
B-2	10	3048	3548.00	3598.00	Tray		0.18	0.37%	0.00%
B-2	10	3048	4048.00	4098.00	18	1	0.54	0.95%	99.05%
B-2	10	3048	4048.00	4098.00	35	0.5	1.22	2.14%	96.92%
B-2	10	3048	4048.00	4098.00	60	0.25	5.5	9.63%	87.29%
B-2	10	3048	4048.00	4098.00	80	0.18	9.39	16.44%	70.85%
B-2	10	3048	4048.00	4098.00	100	0.15	7.4	12.96%	57.90%
B-2	10	3048	4048.00	4098.00	120	0.125	8.2	14.36%	43.54%
B-2	10	3048	4048.00	4098.00	140	0.106	6.36	11.13%	32.41%
B-2	10	3048	4048.00	4098.00	170	0.09	6.19	10.84%	21.57%
B-2	10	3048	4048.00	4098.00	200	0.075	1.99	3.48%	18.08%
B-2	10	3048	4048.00	4098.00	230	0.063	4.74	8.30%	9.79%
B-2	10	3048	4048.00	4098.00	450	0.032	4.93	8.63%	1.16%
B-2	10	3048	4048.00	4098.00	Tray		0.66	1.16%	0.00%

Table I.2
Grain Size Analysis Data

Boring	Run	Run (mm)	Depth (mm bgs)	Depth - bottom (mm bgs)	Sieve	Sieve Size (mm)	Actual Weight (g)	Percent Retained	Percent Passing
B-6	5	1524	2080.17	2135.79	18	1	0.01	0.02%	99.98%
B-6	5	1524	2080.17	2135.79	35	0.5	0.04	0.06%	99.92%
B-6	5	1524	2080.17	2135.79	60	0.25	1	1.53%	98.39%
B-6	5	1524	2080.17	2135.79	80	0.18	12.75	19.53%	78.87%
B-6	5	1524	2080.17	2135.79	100	0.15	16.17	24.76%	54.10%
B-6	5	1524	2080.17	2135.79	120	0.125	18.41	28.19%	25.91%
B-6	5	1524	2080.17	2135.79	140	0.106	9.12	13.97%	11.94%
B-6	5	1524	2080.17	2135.79	170	0.09	4.2	6.43%	5.51%
B-6	5	1524	2080.17	2135.79	200	0.075	1.33	2.04%	3.48%
B-6	5	1524	2080.17	2135.79	230	0.063	1.03	1.58%	1.90%
B-6	5	1524	2080.17	2135.79	450	0.032	0.86	1.32%	0.58%
					Tray		0.38	0.58%	0.00%
B-6	5	1524	2636.35	2691.96	18	1	0.01	0.02%	99.98%
B-6	5	1524	2636.35	2691.96	35	0.5	0.01	0.02%	99.96%
B-6	5	1524	2636.35	2691.96	60	0.25	2.67	5.40%	94.56%
B-6	5	1524	2636.35	2691.96	80	0.18	12.66	25.59%	68.97%
B-6	5	1524	2636.35	2691.96	100	0.15	12.27	24.80%	44.17%
B-6	5	1524	2636.35	2691.96	120	0.125	10.47	21.16%	23.00%
B-6	5	1524	2636.35	2691.96	140	0.106	5.36	10.83%	12.17%
B-6	5	1524	2636.35	2691.96	170	0.09	3.26	6.59%	5.58%
B-6	5	1524	2636.35	2691.96	200	0.075	0.84	1.70%	3.88%
B-6	5	1524	2636.35	2691.96	230	0.063	1.08	2.18%	1.70%
B-6	5	1524	2636.35	2691.96	450	0.032	0.7	1.41%	0.28%
B-6	5	1524	2636.35	2691.96	Tray		0.14	0.28%	0.00%

Table I.2
Grain Size Analysis Data

Boring	Run	Run (mm)	Depth (mm bgs)	Depth - bottom (mm bgs)	Sieve	Sieve Size (mm)	Actual Weight (g)	Percent Retained	Percent Passing
B-6	5	1524	2914.43	2970.05	18	1	0	0.00%	100.00%
B-6	5	1524	2914.43	2970.05	35	0.5	0.17	0.27%	99.73%
B-6	5	1524	2914.43	2970.05	60	0.25	3.14	4.99%	94.74%
B-6	5	1524	2914.43	2970.05	80	0.18	15.68	24.91%	69.83%
B-6	5	1524	2914.43	2970.05	100	0.15	15.15	24.07%	45.76%
B-6	5	1524	2914.43	2970.05	120	0.125	13.22	21.00%	24.75%
B-6	5	1524	2914.43	2970.05	140	0.106	6.75	10.72%	14.03%
B-6	5	1524	2914.43	2970.05	170	0.09	4.35	6.91%	7.12%
B-6	5	1524	2914.43	2970.05	200	0.075	1.42	2.26%	4.86%
B-6	5	1524	2914.43	2970.05	230	0.063	1.38	2.19%	2.67%
B-6	5	1524	2914.43	2970.05	450	0.032	1.13	1.80%	0.87%
B-6	5	1524	2914.43	2970.05	Tray		0.55	0.87%	0.00%
B-6	10	3048	3048.00	3102.23	18	1	0.09	0.11%	99.89%
B-6	10	3048	3048.00	3102.23	35	0.5	0.57	0.71%	99.18%
B-6	10	3048	3048.00	3102.23	60	0.25	5.04	6.25%	92.93%
B-6	10	3048	3048.00	3102.23	80	0.18	15.55	19.30%	73.63%
B-6	10	3048	3048.00	3102.23	100	0.15	17.01	21.11%	52.52%
B-6	10	3048	3048.00	3102.23	120	0.125	17.32	21.49%	31.03%
B-6	10	3048	3048.00	3102.23	140	0.106	10.25	12.72%	18.30%
B-6	10	3048	3048.00	3102.23	170	0.09	7	8.69%	9.62%
B-6	10	3048	3048.00	3102.23	200	0.075	2.6	3.23%	6.39%
B-6	10	3048	3048.00	3102.23	230	0.063	2.85	3.54%	2.85%
B-6	10	3048	3048.00	3102.23	450	0.032	1.71	2.12%	0.73%
B-6	10	3048	3048.00	3102.23	Tray		0.59	0.73%	0.00%

Table I.2
Grain Size Analysis Data

Boring	Run	Run (mm)	Depth (mm bgs)	Depth - bottom (mm bgs)	Sieve	Sieve Size (mm)	Actual Weight (g)	Percent Retained	Percent Passing
B-6	10	3048	3319.15	3373.38	18	1	0.07	0.15%	99.85%
B-6	10	3048	3319.15	3373.38	35	0.5	0.13	0.27%	99.58%
B-6	10	3048	3319.15	3373.38	60	0.25	1.53	3.21%	96.37%
B-6	10	3048	3319.15	3373.38	80	0.18	6.76	14.19%	82.18%
B-6	10	3048	3319.15	3373.38	100	0.15	8.95	18.79%	63.39%
B-6	10	3048	3319.15	3373.38	120	0.125	10.81	22.69%	40.70%
B-6	10	3048	3319.15	3373.38	140	0.106	7.83	16.44%	24.27%
B-6	10	3048	3319.15	3373.38	170	0.09	5.76	12.09%	12.17%
B-6	10	3048	3319.15	3373.38	200	0.075	1.5	3.15%	9.03%
B-6	10	3048	3319.15	3373.38	230	0.063	2.57	5.39%	3.63%
B-6	10	3048	3319.15	3373.38	450	0.032	1.48	3.11%	0.52%
B-6	10	3048	3319.15	3373.38	Tray		0.25	0.52%	0.00%
B-6	10	3048	4132.60	4186.83	18	1	0.1	0.13%	99.87%
B-6	10	3048	4132.60	4186.83	35	0.5	0.34	0.46%	99.41%
B-6	10	3048	4132.60	4186.83	60	0.25	3.59	4.81%	94.61%
B-6	10	3048	4132.60	4186.83	80	0.18	7.99	10.69%	83.91%
B-6	10	3048	4132.60	4186.83	100	0.15	8.9	11.91%	72.00%
B-6	10	3048	4132.60	4186.83	120	0.125	14.08	18.85%	53.15%
B-6	10	3048	4132.60	4186.83	140	0.106	11.71	15.67%	37.48%
B-6	10	3048	4132.60	4186.83	170	0.09	10.29	13.77%	23.70%
B-6	10	3048	4132.60	4186.83	200	0.075	4.75	6.36%	17.35%
B-6	10	3048	4132.60	4186.83	230	0.063	5.93	7.94%	9.41%
B-6	10	3048	4132.60	4186.83	450	0.032	6.18	8.27%	1.14%
					Tray		0.85	1.14%	0.00%

Table I.2
Grain Size Analysis Data

Boring	Run	Run (mm)	Depth (mm bgs)	Depth - bottom (mm bgs)	Sieve	Sieve Size (mm)	Actual Weight (g)	Percent Retained	Percent Passing
B-3	5	1524	2070.45	2125.09	18	1	0.01	0.01%	99.99%
B-3	5	1524	2070.45	2125.09	35	0.5	0	0.00%	99.99%
B-3	5	1524	2070.45	2125.09	60	0.25	4	4.54%	95.44%
B-3	5	1524	2070.45	2125.09	80	0.18	29.7	33.74%	61.71%
B-3	5	1524	2070.45	2125.09	100	0.15	21.39	24.30%	37.41%
B-3	5	1524	2070.45	2125.09	120	0.125	17.26	19.61%	17.80%
B-3	5	1524	2070.45	2125.09	140	0.106	7.82	8.88%	8.92%
B-3	5	1524	2070.45	2125.09	170	0.09	4.32	4.91%	4.01%
B-3	5	1524	2070.45	2125.09	200	0.075	1.19	1.35%	2.66%
B-3	5	1524	2070.45	2125.09	230	0.063	1.34	1.52%	1.14%
B-3	5	1524	2070.45	2125.09	450	0.032	0.8	0.91%	0.23%
B-3	5	1524	2070.45	2125.09	Tray		0.2	0.23%	0.00%
B-3	5	1524	2616.90	2671.54	18	1	0.03	0.04%	99.96%
B-3	5	1524	2616.90	2671.54	35	0.5	0.01	0.01%	99.95%
B-3	5	1524	2616.90	2671.54	60	0.25	2.08	2.70%	97.25%
B-3	5	1524	2616.90	2671.54	80	0.18	16.63	21.60%	75.65%
B-3	5	1524	2616.90	2671.54	100	0.15	16.63	21.60%	54.05%
B-3	5	1524	2616.90	2671.54	120	0.125	17.23	22.38%	31.68%
B-3	5	1524	2616.90	2671.54	140	0.106	10.31	13.39%	18.29%
B-3	5	1524	2616.90	2671.54	170	0.09	7.09	9.21%	9.08%
B-3	5	1524	2616.90	2671.54	200	0.075	2.73	3.55%	5.53%
B-3	5	1524	2616.90	2671.54	230	0.063	2.56	3.32%	2.21%
B-3	5	1524	2616.90	2671.54	450	0.032	1.45	1.88%	0.32%
B-3	5	1524	2616.90	2671.54	Tray		0.25	0.32%	0.00%

Table I.2
Grain Size Analysis Data

Boring	Run	Run (mm)	Depth (mm bgs)	Depth - bottom (mm bgs)	Sieve	Sieve Size (mm)	Actual Weight (g)	Percent Retained	Percent Passing
B-3	5	1524	2890.12	2944.77	18	1	0.02	0.03%	99.97%
B-3	5	1524	2890.12	2944.77	35	0.5	0	0.00%	99.97%
B-3	5	1524	2890.12	2944.77	60	0.25	2.62	4.30%	95.66%
B-3	5	1524	2890.12	2944.77	80	0.18	22.96	37.72%	57.94%
B-3	5	1524	2890.12	2944.77	100	0.15	12.02	19.75%	38.20%
B-3	5	1524	2890.12	2944.77	120	0.125	10.98	18.04%	20.16%
B-3	5	1524	2890.12	2944.77	140	0.106	5.7	9.36%	10.79%
B-3	5	1524	2890.12	2944.77	170	0.09	3.6	5.91%	4.88%
B-3	5	1524	2890.12	2944.77	200	0.075	1.52	2.50%	2.38%
B-3	5	1524	2890.12	2944.77	230	0.063	1.01	1.66%	0.72%
B-3	5	1524	2890.12	2944.77	450	0.032	0.39	0.64%	0.08%
B-3	5	1524	2890.12	2944.77	Tray		0.05	0.08%	0.00%
B-3	10	3048	3048.00	3098.00	18	1	0.1	0.28%	99.72%
B-3	10	3048	3048.00	3098.00	35	0.5	0.58	1.60%	98.13%
B-3	10	3048	3048.00	3098.00	60	0.25	5.63	15.49%	82.64%
B-3	10	3048	3048.00	3098.00	80	0.18	8.39	23.09%	59.55%
B-3	10	3048	3048.00	3098.00	100	0.15	6.06	16.68%	42.87%
B-3	10	3048	3048.00	3098.00	120	0.125	5.95	16.37%	26.50%
B-3	10	3048	3048.00	3098.00	140	0.106	3.93	10.81%	15.69%
B-3	10	3048	3048.00	3098.00	170	0.09	2.78	7.65%	8.04%
B-3	10	3048	3048.00	3098.00	200	0.075	1.07	2.94%	5.09%
B-3	10	3048	3048.00	3098.00	230	0.063	0.99	2.72%	2.37%
B-3	10	3048	3048.00	3098.00	450	0.032	0.78	2.15%	0.22%
B-3	10	3048	3048.00	3098.00	Tray		0.08	0.22%	0.00%

Table I.2
Grain Size Analysis Data

Boring	Run	Run (mm)	Depth (mm bgs)	Depth - bottom (mm bgs)	Sieve	Sieve Size (mm)	Actual Weight (g)	Percent Retained	Percent Passing
B-3	10	3048	3298.00	3348.00	18	1	0.85	1.86%	98.14%
B-3	10	3048	3298.00	3348.00	35	0.5	2.78	6.08%	92.06%
B-3	10	3048	3298.00	3348.00	60	0.25	14.21	31.09%	60.97%
B-3	10	3048	3298.00	3348.00	80	0.18	10.39	22.73%	38.24%
B-3	10	3048	3298.00	3348.00	100	0.15	5.53	12.10%	26.14%
B-3	10	3048	3298.00	3348.00	120	0.125	4.98	10.89%	15.25%
B-3	10	3048	3298.00	3348.00	140	0.106	2.8	6.13%	9.12%
B-3	10	3048	3298.00	3348.00	170	0.09	1.92	4.20%	4.92%
B-3	10	3048	3298.00	3348.00	200	0.075	0.74	1.62%	3.30%
B-3	10	3048	3298.00	3348.00	230	0.063	0.84	1.84%	1.47%
B-3	10	3048	3298.00	3348.00	450	0.032	0.61	1.33%	0.13%
B-3	10	3048	3298.00	3348.00	Tray		0.06	0.13%	0.00%
B-3	10	3048	3548.00	3598.00	18	1	0.15	0.31%	99.69%
B-3	10	3048	3548.00	3598.00	35	0.5	0.86	1.75%	97.94%
B-3	10	3048	3548.00	3598.00	60	0.25	6.85	13.97%	83.97%
B-3	10	3048	3548.00	3598.00	80	0.18	11.19	22.82%	61.15%
B-3	10	3048	3548.00	3598.00	100	0.15	8.82	17.99%	43.17%
B-3	10	3048	3548.00	3598.00	120	0.125	8.41	17.15%	26.02%
B-3	10	3048	3548.00	3598.00	140	0.106	5.14	10.48%	15.54%
B-3	10	3048	3548.00	3598.00	170	0.09	3.51	7.16%	8.38%
B-3	10	3048	3548.00	3598.00	200	0.075	1.31	2.67%	5.71%
B-3	10	3048	3548.00	3598.00	230	0.063	1.5	3.06%	2.65%
B-3	10	3048	3548.00	3598.00	450	0.032	1.11	2.26%	0.39%
B-3	10	3048	3548.00	3598.00	Tray		0.19	0.39%	0.00%

Table I.2
Grain Size Analysis Data

Boring	Run	Run (mm)	Depth (mm bgs)	Depth - bottom (mm bgs)	Sieve	Sieve Size (mm)	Actual Weight (g)	Percent Retained	Percent Passing
B-3	10	3048	4048.00	4098.00	18	1	0.39	1.04%	98.96%
B-3	10	3048	4048.00	4098.00	35	0.5	0.3	0.80%	98.16%
B-3	10	3048	4048.00	4098.00	60	0.25	4.16	11.12%	87.04%
B-3	10	3048	4048.00	4098.00	80	0.18	9.55	25.53%	61.51%
B-3	10	3048	4048.00	4098.00	100	0.15	7.55	20.18%	41.33%
B-3	10	3048	4048.00	4098.00	120	0.125	6.78	18.12%	23.20%
B-3	10	3048	4048.00	4098.00	140	0.106	3.75	10.02%	13.18%
B-3	10	3048	4048.00	4098.00	170	0.09	2.3	6.15%	7.03%
B-3	10	3048	4048.00	4098.00	200	0.075	0.92	2.46%	4.57%
B-3	10	3048	4048.00	4098.00	230	0.063	0.91	2.43%	2.14%
B-3	10	3048	4048.00	4098.00	450	0.032	0.67	1.79%	0.35%
B-3	10	3048	4048.00	4098.00	Tray		0.13	0.35%	0.00%

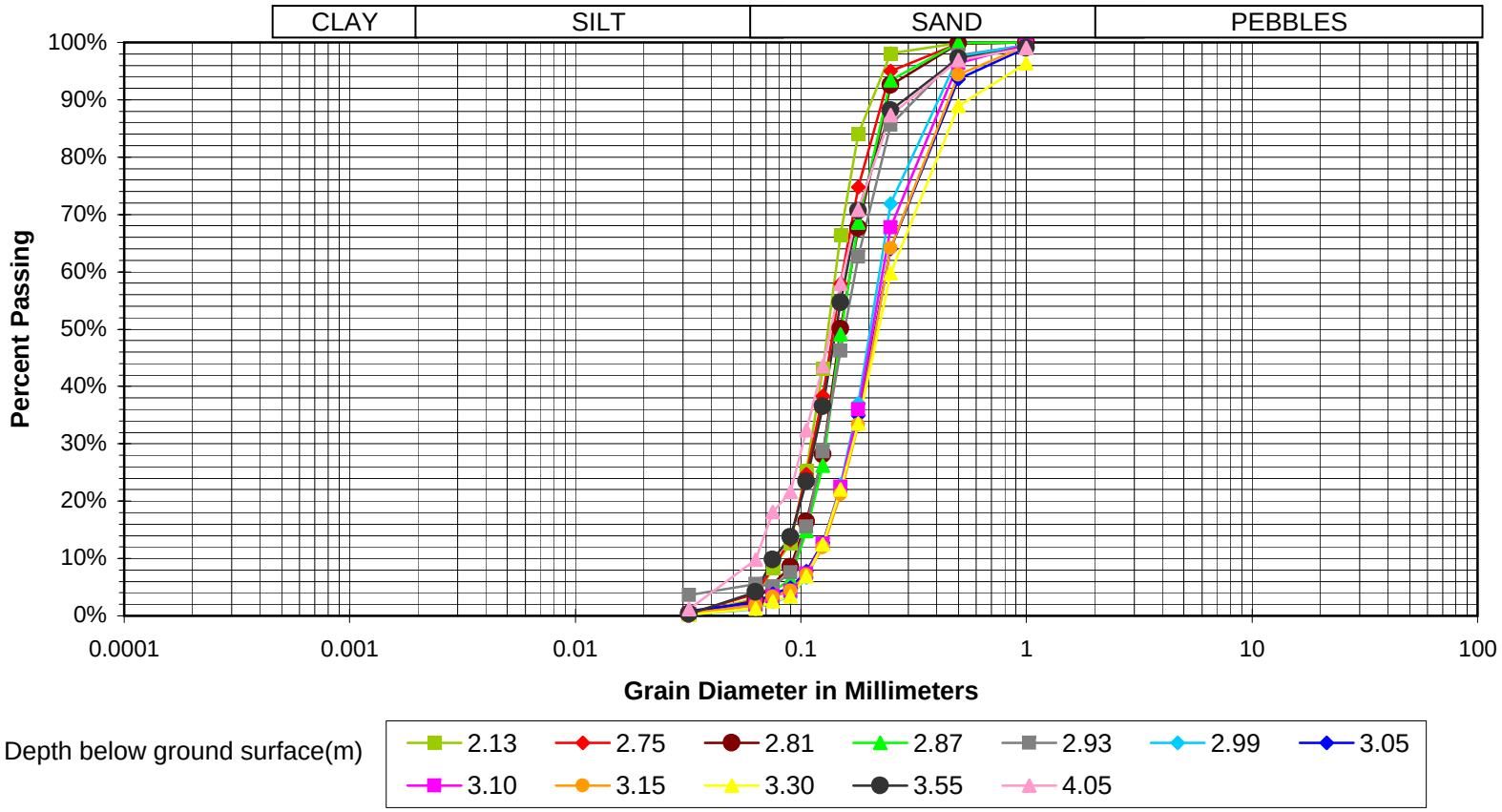

Figure I.1 - Grain Size Cumulative Distribution Curve for B-2 (Between GP-14 and GP-15)

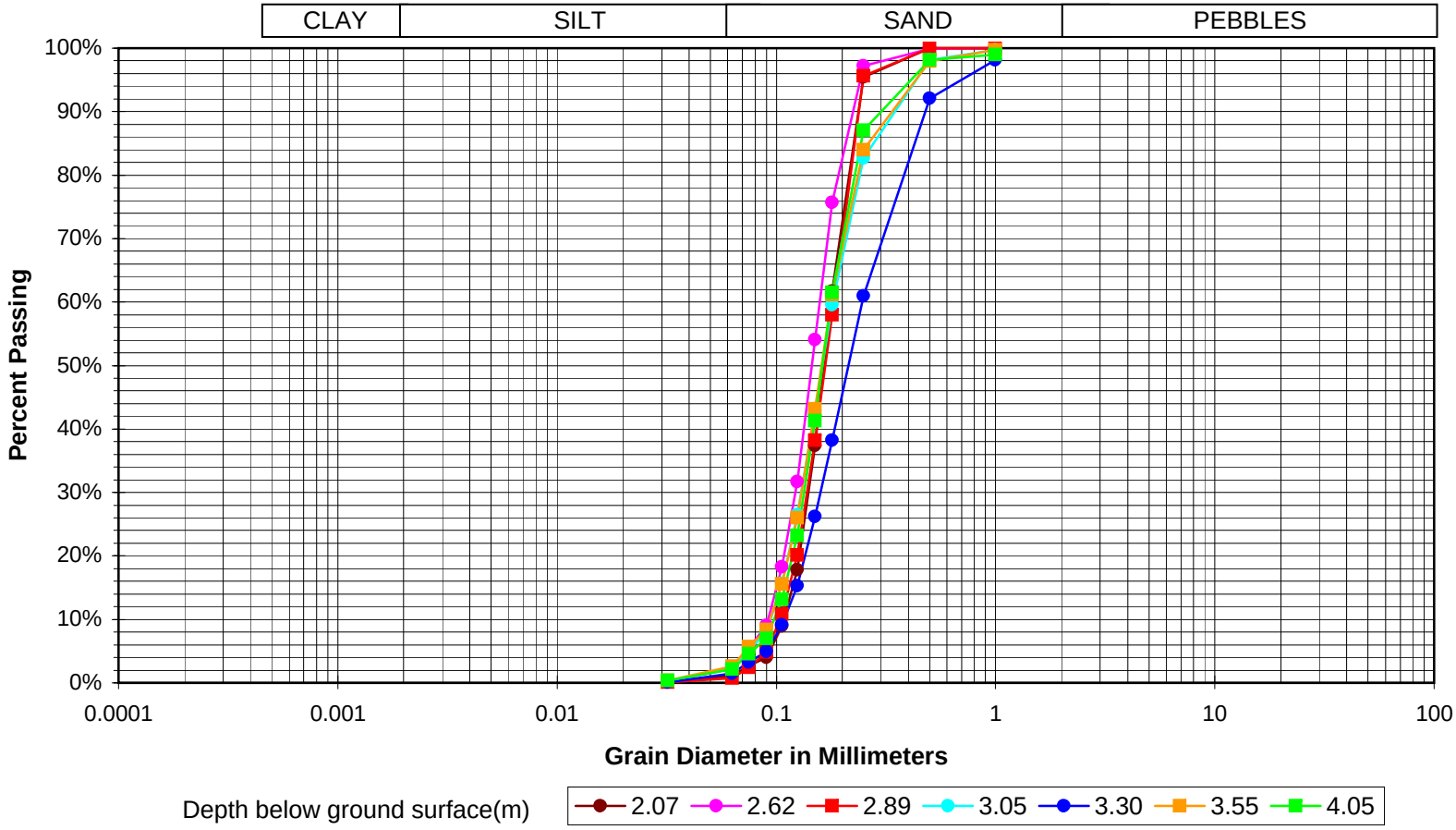

Figure I.2 - Grain Size Cumulative Distribution Curve for B-3 (Between GP-13 and GP-8)

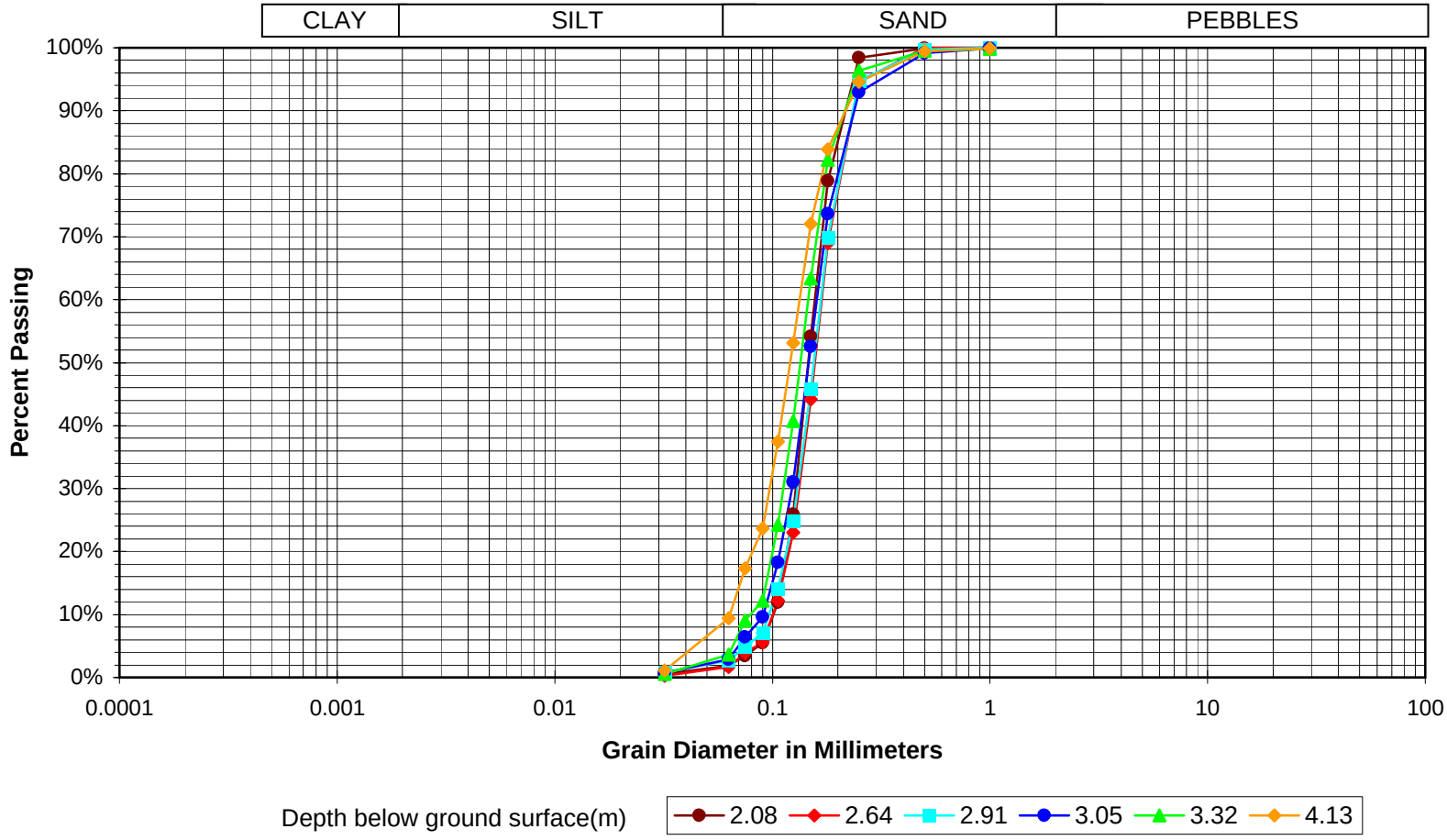

Figure I.3 - Grain Size Cumulative Distribution Curve for B-6 (Between GP-6 and GP-11)